

Copyright
by
Mahdy Shirdel
2010

**The Thesis Committee for Mahdy Shirdel
Certifies that this is the approved version of the following thesis:**

**Development of a Coupled Wellbore-Reservoir Compositional
Simulator for Horizontal Wells**

**APPROVED BY
SUPERVISING COMMITTEE:**

Supervisor:

Kamy Sepehrnoori

Paulo Roberto Ribeiro

**Development of a Coupled Wellbore-Reservoir Compositional
Simulator for Horizontal Wells**

by

Mahdy Shirdel, B.Sc.

Thesis

Presented to the Faculty of the Graduate School of

The University of Texas at Austin

in Partial Fulfillment

of the Requirements

for the Degree of

Master of Science in Engineering

The University of Texas at Austin

December 2010

To

my parents

Abolhassan and Goldaneh

without their support none of this would be possible

Acknowledgments

I am extremely grateful to my supervisor, Dr. Kamy Sepehrnoori for his support during this research. I am also thankful to Dr Paulo Ribeiro for the review of the text and the suggestions. This work was financially supported by the Reservoir Simulation Joint Industry Project at the Center for Petroleum and Geosystems Engineering of The University of Texas at Austin.

December 2010

Abstract

Development of a Coupled Wellbore-Reservoir Compositional Simulator for Horizontal Wells

Mahdy Shirdel, M.S.E.

The University of Texas at Austin, 2010

Supervisor: Kamy Sepehrnoori

Two-phase flow occurs during the production of oil and gas in the wellbores. Modeling this phenomenon is important for monitoring well productivity and designing surface facilities. Since the transient time period in the wellbore is usually shorter than reservoir time steps, stabilized flow is assumed in the wellbore. As such, semi-steady state models are used for modeling wellbore flow dynamics. However, in the case that flow variations happen in a short period of time (*i.e.*, a gas kick during drilling) the use of a transient two-phase model is crucial.

Over the last few years, a number of numerical and analytical wellbore simulators have been developed to mimic wellbore-reservoir interaction. However, some issues still remain a concern in these studies. The main issues surrounding a comprehensive wellbore model consist of fluid property calculations, such as black-oil or compositional

models, governing equations, such as mechanistic or correlation-based models, effect of temperature variation and non-isothermal assumption, and methods for coupling the wellbore to the reservoir. In most cases, only standalone wellbore models for blackoil have been used to simulate reservoir and wellbore dynamic interactions. Those models are based on simplified assumptions that lead to an unrealistic estimation of pressure and temperature distributions inside the well. In addition, most reservoir simulators use rough estimates for the perforation pressure as a coupling condition between the wellbore and the reservoir, neglecting pressure drops in the horizontal section.

In this study, we present an implementation of a compositional, pseudo steady-state, non-isothermal, coupled wellbore-reservoir simulator for fluid flow in wellbores with a vertical section and a horizontal section embedded on the producing reservoir. In addition, we present the implementation of a pseudo-compositional, fully implicit, transient two-fluid model for two-phase flow in wellbores.

In this model, we solve gas/liquid mass balance, gas/liquid momentum balance, and two-phase energy equations in order to obtain the five primary variables: liquid velocity, gas velocity, pressure, holdup and temperature. In our simulation, we compared stratified, bubbly, intermittent flow effects on pressure and temperature distributions in either a transient or steady-state condition. We found that flow geometry variation in different regimes can significantly affect the flow parameters. We also observed that there are significant differences in flow rate prediction between a coupled wellbore-reservoir simulator and a stand-alone reservoir simulator, at the early stages of production.

The outcome of this research leads to a more accurate and reliable simulation of multiphase flow in the wellbore, which can be applied to surface facility design, well performance optimization, and wellbore damage estimation.

Table of Contents

List of Tables	xii
List of Figures.....	xiii
Chapter 1: Introduction.....	1
Chapter 2: Background and Literature Review.....	4
2.1 Multiphase Flow Simulation of a Producing Wellbore	4
2.2 Coupled Wellbore-Reservoir Simulation	6
2.3 Compositional Wellbore Simulation.....	10
2.4 Transient Wellbore Simulation.....	11
2.5 Multiphase Flow Horizontal Well Simulation.....	12
2.6 Objectives of the Research	14
Chapter 3: Pseudo-Compositional, Standalone, Wellbore Model	16
3.1 Multiphase Flow Main Parameters Definition	16
3.1.1 Mass and Volumetric Flow Rates	16
3.1.2 Liquid Holdup	17
3.1.3 Superficial Velocity.....	17
3.1.4 Actual Velocity	18
3.1.5 Mixture Velocity	18
3.1.6 Slip Velocity	18
3.1.7 Drift Velocity	19
3.1.8 Average Fluid Properties	19
3.2 Flow Patterns Definition in a Horizontal Well	20
3.2.1 Flow Patterns	20
3.2.1.1 Stratified Flow	20
3.2.1.2 Intermittent Flow	21
3.2.1.3 Annular Flow	21
3.2.1.4 Dispersed-Bubbly Flow	21
3.2.2 Flow Pattern Prediction	21

3.3	Fluid Properties Calculation	24
3.4	Flow Equations in the Wellbore	25
3.4.1	Liquid Mass Balance	25
3.4.2	Gas Mass Balance	28
3.4.3	Liquid Momentum Balance	29
3.4.4	Gas Momentum Balance	34
3.4.5	Total Energy Balance	35
3.5	Solution Procedure.....	38
3.6	Results	41
3.6.1	Case 1: Constant Pressure at Outlet, No Flow at Inlet	42
3.6.2	Case 2: Constant Pressure at Outlet, Constant Flow Rate at Inlet	42
3.6.3	Case 3: Constant Pressure at Outlet, Cold Fluid Influx	43
Chapter 4: Coupled Wellbore-Reservoir Compositional Model		61
4.1	Flow Patterns	61
4.1.1	Bubble Flow	61
4.1.2	Slug Flow	61
4.1.3	Churn Flow.....	62
4.1.4	Annular Flow.....	62
4.1.5	Dispersed-Bubble Flow	62
4.1.6	Flow regimes transition.....	62
4.2	Flow Equations for the Wellbore.....	64
4.2.1	Components Mass Balance	65
4.2.2	Momentum Balance	67
4.2.2.1	Stratified and Annular-Mist Flow Momentum Equation	67
4.2.2.2	Bubbly Flow Momentum Equation	70
4.2.2.3	Intermittent Flow Momentum Equation	72
4.2.3	Energy Balance	73
4.2.4	Phase-Equilibrium Equation	77
4.3	Coupling of the Wellbore to the Reservoir	78
4.4	Solution Procedure.....	79

4.5	Results	80
Chapter 5: Transient Pseudo-Compositional Thermal Wellbore Model		99
5.1	Flow Equations in the Wellbore	99
5.1.1	Liquid Mass Balance	100
5.1.2	Gas Mass Balance	101
5.1.3	Liquid Momentum Balance	103
5.1.4	Gas Momentum Balance	104
5.1.5	Mixture Momentum Balance	106
5.1.6	Total Energy Balance	107
5.2	Solution Procedure.....	109
5.3	Results	109
5.3.1	Case 1: Constant Flow Rate Injection, Constant Outlet Pressure..	110
5.3.2	Case 2: Cold Fluid Injection in the Inlet and Middle of Pipe ...	111
Chapter 6: Comparisons of Models and the Investigation of the Sensitivity of Model Parameters.....		129
6.1	Spatial Discretization	129
6.2	Time-Step Size.....	130
6.3	Comparison of Steady-State and Transient Solutions.....	132
6.4	Comparison between the Pseudo-Compositional and the Compositional Models.....	132
6.5	Comparison between THE NUMERICAL and the Analytical Solutions	133
6.6	Validation of the Transient Model with Experimental Data	134
Chapter 7: Summary, Conclusions and Recommendations		160
7.1	Summary	160
7.2	Conclusions	161
7.3	Recommendations.....	162
Appendix A: Fluid Properties Calculation		164
A.1	Compressibility Factor Calculation	164
A.2	Phase Equilibrium Calculation	167

A.3	Density Calculation.....	167
A.4	Viscosity Calculation	169
Appendix B: Unit Conversion.....		177
Appendix C: Wellbore Boundary Conditions		178
C.1	Constant Flow Rate Inlet and Constant Pressure Outlet	178
C.2	No Flow Inlet and Constant Pressure Inlet.....	178
C.3	No Flow Inlet and Constant Pressure Outlet	179
C.4	No Flow Inlet and Constant Flow Rate Outlet	179
Appendix D: Sample Input Data		180
D.1	Sample Input Data for the Standalone Wellbore Case.....	180
D.2	Sample Input Data for the Coupled Wellbore/Reservoir Case	182
Appendix E: Reservoir Simulation Model (GPAS).....		186
E.1	Governing Equations.....	186
E.2	Solution Procedure.....	187
Glossary		190
References.....		194
Vita		201

List of Tables

Table 3.1	Hydrocarbon fluid components data.....	45
Table 3.2	Hydrocarbon fluid components enthalpy coefficient data (Appendix A)	45
Table 4.1	Input parameters for the base case	83
Table 4.2	Components critical values and pertinent data	83
Table 4.3	Gas and liquid phase compositions at different places for the base case	84
Table 5.1	Wellbore geometry and fluid data	113
Table 6.1	Wellbore geometry and fluid data for water and air flow in horizontal pipe.....	136
Table 6.2	Comparison between the results for different mesh sizes, maximum difference respect to fine mesh size ($dz = 5$ ft).....	136
Table 6.3	CPU time comparison for the segments variation study (1.8 GHz processor and 2038 MB of RAM)	136
Table 6.4	CPU time comparison for the time-step variation study (1.8 GHz processor and 2038 MB of RAM)	137
Table 6.5	Comparison between the results for different time-step sizes, maximum difference respect to smallest time-step size ($dt = 0.1$ sec)	137
Table 6.6	Wellbore geometry and fluid data for the compositional model	137
Table A.1	Fluid properties calculation for a mixture of 50% C1 and 50% NC10 at 100 °F and 1000 psi.....	175

List of Figures

Figure 3.1	Dominant flow regimes and acting forces in horizontal tubular sections	46
Figure 3.2	Flow pattern map in horizontal pipes (Baker, 1954)	46
Figure 3.3	Flow pattern map in horizontal pipes (Mandhane et al., 1974)	47
Figure 3.4	Flow pattern map in horizontal pipes, gas/oil system (Ouyang, 1998)	47
Figure 3.5	Procedure to select appropriate flow regimes (Ouyang, 1998)	48
Figure 3.6	Schematic view of wellbore segments for nodal calculation	48
Figure 3.7	Schematic view of wellbore segments for fluid transfer	49
Figure 3.8	Schematic view of flow cross section in the pipe for stratified flow	49
Figure 3.9	Numerical calculation procedure, using Newton method	50
Figure 3.10	Oil formation volume factor for six-component fluid <i>versus</i> pressure for different temperatures	51
Figure 3.11	Oil viscosity for six-component fluid <i>versus</i> pressure for different temperatures	51
Figure 3.12	Oil enthalpy for six-component fluid <i>versus</i> pressure for different temperatures	52
Figure 3.13	Solution gas ratio for six-component fluid <i>versus</i> pressure for different temperatures	52
Figure 3.14	Gas formation volume factor for six-component fluid <i>versus</i> pressure for different temperatures	53
Figure 3.15	Gas viscosity for six-component fluid <i>versus</i> pressure for different temperatures	53

Figure 3.16	Gas enthalpy for six-component fluid <i>versus</i> pressure for different temperatures.....	54
Figure 3.17	Schematic view of wellbore, reservoir and surface facility connection	55
Figure 3.18	Schematic view of pipe and the setup in Case1	55
Figure 3.19	Pressure and temperature distributions along the well, Case 1	56
Figure 3.20	liquid and gas superficial velocity distribution, Case 1	56
Figure 3.21	Liquid holdup distribution, Case 1.....	57
Figure 3.22	Pressure and temperature distribution along the well, Case 2	57
Figure 3.23	Liquid and gas superficial velocity distribution, Case 2	58
Figure 3.24	Holdup distribution, Case 2	58
Figure 3.25	Pressure and temperature distribution, Case 3.....	59
Figure 3.26	Liquid and gas superficial velocities, Case 3	59
Figure 3.27	Holdup and flow regimes variations in the pipe, (1: bubbly, 2: intermittent, 3: annular, 4: stratified flow)	60
Figure 4.1	Different flow regimes in vertical flow.....	84
Figure 4.2	Procedure to select appropriate flow regimes for vertical inclination	85
Figure 4.3	Schematic views of wellbore, reservoir and surface wellhead connection and flow domains	86
Figure 4.4	Intermittent flow regime.....	87
Figure 4.5	Schematic views of phases equilibrium	87
Figure 4.6	Schematic view of wellbore segments and reservoir gridblocks	88
Figure 4.7	Solution procedure by marching algorithm.....	89
Figure 4.8	Pressure distribution from the toe to the surface	90

Figure 4.9	Temperature distribution from the toe to the surface.....	90
Figure 4.10	Temperature and pressure distribution in the horizontal section	91
Figure 4.11	Holdup distribution and flow regime changes from the toe to the surface (1: bubbly, 2: stratified, 3: annular mist, 4: intermittent flow)	91
Figure 4.12	Phase velocity distribution from the toe to the surface	92
Figure 4.13	Flow rates from toe to the surface.....	92
Figure 4.14	Gas phase composition at different sections of the wellbore (1: toe, 2: heel, 3: wellhead, 4: standard condition).....	93
Figure 4.15	Oil phase composition at different sections of the wellbore (1: toe, 2: heel, 3: wellhead, 4: standard condition).....	93
Figure 4.16	Comparison of gas flow rate with/without the wellbore simulation....	94
Figure 4.17	Comparison of oil flow rate with/without the wellbore simulation.	94
Figure 4.18	Comparison of water flow rate with/without the wellbore simulation	95
Figure 4.19	Gas flow rate estimation error	95
Figure 4.20	Oil flow rate estimation error	96
Figure 4.21	Water low rate estimation error	96
Figure 4.22	Pressure profile as a function of time for the horizontal section	97
Figure 4.23	Holdup profile as a function of time for the horizontal section.....	97
Figure 4.24	Flow regimes variation as a function of time for the horizontal section (1: bubbly, 2: stratified, 3: annular mist, 4: intermittent flow)	98
Figure 5.1	Numerical calculation procedure, using Newton method.....	114
Figure 5.2	Gas superficial velocity in the middle of the pipe <i>versus</i> time for	

Case 1	115
Figure 5.3 Liquid superficial velocity in the middle of the pipe <i>versus</i> time for Case 1	115
Figure 5.4 Pressure in the middle of the pipe <i>versus</i> time for Case 1	116
Figure 5.5 Holdup in the middle of the pipe <i>versus</i> time for Case 1	116
Figure 5.7 Liquid superficial velocity profile for different times for Case 1...	118
Figure 5.8 Pressure profile for different times for Case 1.....	119
Figure 5.9 Holdup profile for different times for Case 1	120
Figure 5.10 Gas superficial velocity in the middle of the pipe <i>versus</i> time for Case 2	121
Figure 5.11 Liquid superficial velocity in the middle of the pipe <i>versus</i> time for Case 2	121
Figure 5.12 Pressure in the middle of the pipe <i>versus</i> time for Case 2	122
Figure 5.13 Holdup in the middle of the pipe <i>versus</i> time for Case 2.....	122
Figure 5.14 Temperature in the middle of the pipe <i>versus</i> time for Case 2.....	123
Figure 5.15 Gas superficial velocity profile for different times for Case 2	124
Figure 5.16 Liquid superficial velocity profile for different times for Case 2...	125
Figure 5.17 Pressure profile for different times for Case 2.....	126
Figure 5.18 Holdup profile for different times for Case 2	127
Figure 5.19 Temperature profile for different times for Case 2.....	128
Figure 6.1 Pressure profile for different mesh sizes after 4000 sec.....	138
Figure 6.2 Holdup profile for different mesh sizes after 4000 sec	139
Figure 6.3 Liquid superficial velocity profile for different mesh sizes after 4000 sec	140

Figure 6.4	Gas superficial velocity profile for different mesh sizes after 4000 sec	141
Figure 6.5	Pressure profile for different time-step sizes after 4000 sec	142
Figure 6.6	Holdup profile for different time-step sizes after 4000 sec	143
Figure 6.7	Liquid superficial velocity profile for different time-step sizes after 4000 sec	144
Figure 6.8	Gas superficial velocity for different time-step sizes after 4000 sec	145
Figure 6.9	Pressure profile comparison between transient and steady-state solutions.....	146
Figure 6.10	Holdup profile comparison between transient and steady-state solutions.....	147
Figure 6.11	Liquid superficial velocity profile comparison between transient and steady-state solutions	148
Figure 6.12	Gas superficial velocity profile comparison between transient and steady-state solutions	149
Figure 6.13	Pressure profile comparison between the compositional/explicit and pseudo-compositional/fully implicit calculation methods	150
Figure 6.14	Holdup profile comparison between the compositional/explicit and pseudo-compositional/fully implicit calculation methods	151
Figure 6.15	Flow Regimes profile comparison between the compositional/explicit and pseudo-compositional/fully implicit calculation methods (1: bubbly, 2: intermittent, 3: annular, 4: stratified flow)	152
Figure 6.16	Liquid superficial velocity profile comparison between the compositional/ explicit and pseudo-compositional/fully implicit calculation methods.....	153

Figure 6.17	Liquid superficial velocity profile comparison between the compositional /explicit and pseudo-compositional/fully implicit calculation methods.....	154
Figure 6.18	Pressure profile comparison between the numerical and analytical calculations	155
Figure 6.19	Schematic view of experimental setup, Minami and Shoham (1994)	156
Figure 6.20	Comparison between experimental data (Minami and Shoham, 1994) and the stratified flow regime model results for gas/liquid inlet and outlet flow rates <i>versus</i> time	157
Figure 6.21	Comparison between experimental data (Minami and Shoham, 1994) and the stratified flow regime model results for pressure <i>versus</i> time in station 1 and station 2.....	157
Figure 6.22	Comparison between experimental data (Minami and Shoham, 1994) and the stratified flow regime model results for holdup in station 2 and station 4	158
Figure 6.23	Comparison between experimental data (Minami and Shoham, 1994) and the bubbly flow regime model results for gas/liquid inlet and outlet flow rates <i>versus</i> time.....	158
Figure 6.24	Comparison between experimental data (Minami and Shoham, 1994) and the bubbly flow regime model results for pressure <i>versus</i> time in station 1 and station 2.....	159
Figure 6.25	Comparison between experimental data (Minami and Shoham, 1994) and the bubbly flow regime model results for holdup in station 2 and station 4	159

Figure A.1	Oil phase enthalpy calculation and comparison with CMG for the mixture of 50% C1 and 50% NC10, at 100 °F	176
Figure A.2	Gas phase enthalpy calculation and comparison with CMG for the mixture of 50% C1 and 50% NC10, at 100 °F	176

Chapter 1: Introduction

Two-phase flow is a common phenomenon that occurs in different applications such as in the petroleum industry, chemical and process industry, geothermal energy plants, etc. Particularly in the petroleum industry, which deals with the oil and gas production from the wellbore and transportation through the pipeline system, multiphase flow is frequently encountered. Even in the under-saturated reservoirs, where the pressure is above bubble point, we might have two-phase flow in the pipelines. In fact, from the reservoir to the surface facility, we have a significant pressure decline which causes the appearance of the gas phase in the midst of the oil flow.

Hence, for the purpose of production and flow lines design and optimization, the development of a multiphase coupled wellbore-reservoir model is crucial. For instance, using a multiphase flow model can enhance designing artificial lift practices in case that well productivity is declined. A wellbore model also can be used for detecting damage in the wellbore as well as redesigning flow stream and remediation procedures. Over the past few years, researchers have also used coupled wellbore-reservoir models for well testing applications, such as to model wellbore storage and phase redistribution effect in pressure buildup tests.

Despite the extensive two-phase flow modeling since the 1950's, still some challenging issues remain in coupled wellbore-reservoir models. Introducing the new geometries for the flow such as horizontal and deviated wells, complex fluid models, fluid heat exchange coupled to the flow models, and different mathematical approaches for the flow models makes the development of more comprehensive wellbore models necessary.

Over the last decade, the application of horizontal wells for the oil and gas recovery in thin rims and offshore fields has been imperative. A considerable amount of analytical and experimental research contributions has been performed to model the dynamic interaction between a horizontal wells and the reservoir in order to study the productivity of these systems. For instance, transient two-phase flow models for the wellbore, as well as steady-state inflow models and productivity indexes estimation have been developed. Although the existing models provide good insight into the behavior of horizontal wells, the treatment of the compositional nature of the coupled wellbore-reservoir system is limited. A few published models consider the compositional simulation of coupled vertical wells to the reservoir (Pourafshary, 2009; Livescu 2009).

The primary objective of this study is to develop a comprehensive horizontal wellbore simulator coupled to a reservoir numerical simulator called GPAS (Wang et al., 1997, 1999; Han et al., 2007).

The wellbore simulator is a one-dimensional, staggered grid, explicit and fully implicit, compositional steady-state and pseudo-compositional transient that applies the finite volume method to compute pressure, temperature, phase velocities and holdup. The reservoir simulator is a parallel, three-dimensional, fully implicit, thermal equation of state, compositional model that applies Newton iteration numerical algorithms for solving very large, sparse linear systems (Varavei, 2009). The coupled wellbore-reservoir simulator can be applied to steady-state problems, such as the primary production of the reservoir as well as to transient problems, such as well test analysis. Fluid flow in the wellbore can also be modeled with the blackoil approach, which is not recommended for the complex fluid models, such as volatile oils.

The following paragraphs give a general overview of the material covered in the thesis.

Chapter 2 focuses on a literature review about the different approaches of modeling multiphase flow through pipes and wellbores. A discussion is also conducted on fluid flow in the vertical and horizontal wells, fluid properties calculation approaches (*i.e.*, blackoil and compositional), methods to couple wellbore to the reservoir and multiphase flow governing equations, such as mechanistic or correlation-based models.

Chapter 3 presents the pseudo-compositional, steady-state approach as well as a discussion on the model set-up and appropriate transport and fluid properties equations.

Chapter 4 describes the compositional approach for horizontal wells as well as the coupled wellbore-reservoir simulator. In this chapter, coupling horizontal well to the vertical well and applying the well condition in the wellhead is also presented.

Chapter 5 presents the pseudo-compositional, thermal, transient two-fluid model and explains the effect of the inter-phase momentum term, pointing out the flow regime effect in the transient model.

Chapter 6 presents the comparison and discussion of the different case studies for wellbore simulations and also the validation of the wellbore model.

Chapter 7 presents the summary, conclusions and recommendations for future work.

Chapter 2: Background and Literature Review

During oil production, the multiphase flow may occur in different sections of the flow line such as in the wellbore, the tubing, and surface equipment. Despite vast research efforts in the area, the complexity of multiphase flow still remains a challenging problem in the petroleum industry. Since the last couple of decades, complex drilling and completion methods, such as those applied to multilateral and horizontal wells, has added new challenges for realistic reservoir modeling.

In this chapter, we review different approaches to model fluid flow in the wellbore and discuss the most recently developed coupled wellbore-reservoir simulators. The closure of the chapter points out the objectives of the present work.

2.1 MULTIPHASE FLOW SIMULATION OF A PRODUCING WELLBORE

One of the simplest approaches to compute multiphase flow variables in the wellbore is using empirical correlation. This approach is based on experimental data obtained at certain range of liquid and gas velocities. In the literature there are different correlations for multiphase flow calculation. The most commonly used correlations are: Dukler and Cleveland (1964), Hagedorn and Brown (1965), for oil wells, and Orkiszewski (1967) for the gas wells with gas/liquid ratio above 50,000 scf/bbl. Other researchers, such as Duns and Ros (1963), Eaton and Brown (1967), Beggs and Brill (1973), and Mukherjee et al. (1983), have also introduced different experimental correlations for multiphase flow in vertical and inclined pipes. In most commercial reservoir simulators, these correlations are still used to calculate well flow performance. However, these correlations are fundamentally established based on the limited experimental conditions which are not valid for all cases.

Another approach to model multiphase flow is using fundamental and mechanistic transport equations. Since transport equations are based on the conservation of mass, momentum and energy, the results obtained from these equations are more reliable and more predictive. Yuan and Zhou (2009) compared correlation-based and mechanistic models with experimental data. As it is observed from Yuan and Zhou (2009) comparison, correlation-based models are valid only in a certain range of velocities. However, the mechanistic model gives acceptable results at a wide range of liquid and gas velocities.

The most famous mechanistic models introduced in the literature can be listed as follows: Taitel and Dukler (1976) and Taitel et al. (1980) pioneered in presenting mechanistic modeling by introducing different flow regimes and explaining the criteria for the transition between the flow regimes. Ozon et al. (1987), Hasan and Kabir (1988), Ansari et al. (1994), Petalas and Aziz (2000), and Gomez et al. (2000) also presented comprehensive mechanistic modeling of two-phase flow in vertical pipes.

One of the mechanistic models used to calculate multiphase flow variables is the homogeneous model. In this model, the mixture of fluids is assumed to be flowing with no slippage between the two phases and average bulk flow properties are incorporated into a pseudo-fluid. The homogenous model is simple to be implemented, but is inaccurate for high density and viscosity contrast fluid situations. For this reason, in order to improve the homogenous model, an auxiliary equation is applied to calculate the velocity difference between the moving phases. The homogenous model with slippage between phases upgrades to the drift flux model, where the mixture velocity is related to the gas and liquid velocities by a linear correlation. Despite the fact that the drift flux model considers slippage between phases more accurately than does the homogenous model, it still neglects the inter-phase momentum transfer in the momentum equation. In

fact, the momentum equation is solved for the bulk flow of the fluids. The inter-phase shear stress affects the flow of each phase significantly where the separate two-phase flow exists. This phenomenon is more accurately considered if separate flow momentum equations are used in the model. The inter-phase term in the momentum equation has an important role in the drag forces between the fluids.

Other mechanistic models which have been widely used in the multiphase flow literature are the two-fluid or multi-fluid model. In these models separate momentum equations for gas, liquid, and droplets are considered and a closure relationship for inter-phase drag forces are assumed, which incorporate the slippage between the phases. This approach has been applied in the commercial pipeline simulator OLGA (Bendiksen et al., 1991).

2.2 COUPLED WELLBORE-RESERVOIR SIMULATION

For a comprehensive reservoir production simulation the development and application of a coupled wellbore-reservoir simulator is essential. Nennie et al. (2007) emphasized the importance to model reservoir and well dynamics interactions for better understanding and control of smart wells.

A coupled wellbore-reservoir simulator can be applied to different problems in either the production or the reservoir engineering areas. For instance, in the well test analysis, wellbore damage simulation (*i.e.*, wellbore plugging by precipitates), well design (*i.e.*, smart wells application), well performance analysis and well control (*i.e.*, kick and blowout situation), a dynamic wellbore-reservoir simulator is required. Several researchers have recently introduced coupled wellbore-reservoir models using different mechanistic approaches. In this section, we review what we consider to be the most important published works.

Stone et al. (1989) presented a fully implicit, blackoil and three-dimensional reservoir simulator coupled to a blackoil and one-dimensional wellbore simulator. They mainly targeted a horizontal well for wellbore-reservoir system in their study. They also used two-fluid model considering different flow regimes for the wellbore model. Stone et al. (1989) solved oil, water and gas mass balance, liquid/gas momentum balance energy equation simultaneously with reservoir equations in their model. They also considered parallel flow in the inner tubing and outer annuli and slant angle effect. Stone et al. (1989) validated their model against field data and showed a good agreement between their model results and field data.

The other point that Stone et al. (1989) also discussed in their work was the stability of their model. They presented that in the high velocity condition where bubbly and slug flow were generated their model was less stable.

Almehaideb et al. (1989) presented an isothermal, blackoil wellbore model coupled to a blackoil reservoir simulator. In their study, the effect of phase segregation in the wellbore during concurrent water and gas injection and the effect of multiphase flow in a pressure build up test were investigated. They explained that the two-fluid model as well as a mixture momentum equation could be used for the wellbore model. Almehaideb et al. (1989) solved oil, water and gas mass balance equations and liquid/gas momentum balance equations simultaneously with reservoir equations. They calculated liquid and gas superficial velocities, wellbore pressure, free gas mass fraction and water mass fraction as the primary variables in their wellbore model. Almehaideb et al. (1989) showed how gas and water injection rate and gas quality vary in different layers of a reservoir, in lab scale test. They validated their model with some limited data points from experimental results. They also illustrated the gas solubility effect on pressure buildup and compared two-fluid model and mixture model results for a pressure buildup test.

Winterfeld (1989) explained the application of a wellbore-reservoir simulator for pressure build up test. In his study, a transient, isothermal wellbore model was fully coupled to a blackoil, two-dimensional (r-z) reservoir simulator. The wellbore mechanistic model was a two-fluid model with some simplifications in inter-phase closure relations. Winterfeld (1989) showed good agreement between model results and field data for bottom-hole pressure in build up test.

Hasan and Kabir (1996), and Hasan et al. (1997; 1998) presented a blackoil model for single and two-phase flow in wellbores coupled to the reservoir. They applied a hybrid numerical model for the wellbore and an analytical single-phase model for the reservoir. Material balances for each phase, one momentum balance equation for the mixture and energy balance were solved to obtain pressure, velocity, temperature, and fluid density in the wellbore. To calculate the liquid fraction (holdup) at each segment of the wellbore, Hasan et al. (1998) tracked the migration of gas bubbles throughout the wellbore. They used the wellbore-reservoir model for well test analysis application.

Likewise, Fan et al. (2000) developed a semi-analytical wellbore-reservoir simulator in which a single-phase analytical model for the reservoir was coupled to the wellbore. Fan et al. (2000) mainly targeted thermal effects in this study and they applied the simulator to a high-temperature gas well pressure buildup test.

Nennie et al. (2007) stated the importance of coupling the wellbores to the reservoir for modeling the dynamic and realistic phenomena that take place in the wellbore. They demonstrated explicit coupling of a standalone wellbore simulator (OLGA) to a standalone reservoir simulator (MoReS) to study the gas conning phenomena. They externally coupled these two domains by using MATLAB, programming software. Nennie et al. (2007) also compared the results for different cases as standalone wellbore model, standalone reservoir model and coupled wellbore-reservoir

model. They presented that the coupled wellbore-reservoir model results were significantly different than either the standalone wellbore or the standalone reservoir models.

Hence, from the works performed by different researchers we conclude that a coupled wellbore simulator is necessary for a realistic and comprehensive reservoir simulation. In the literature also two different approaches have been introduced for this purpose. One method is an iterative and explicit coupling, where the, wellbore and reservoir systems are solved separately. The other method is fully coupling the wellbore and reservoir systems.

In the iterative method the pressure results are conveyed to each system by well productivity index, until both systems converge, numerically. One of the advantages of the iterative coupling method is that the wellbore model can be coupled to any reservoir simulator. This approach would be more robust if the wellbore model was used in the steady-state condition. In addition in the iterative approach, different time steps is allowed for the two flow domains (wellbore and reservoir).

In fully coupled wellbore-reservoir simulations wellbore and reservoir models are simultaneously solved. Behie et al. (1985) explained the mathematical approach to solve a bordered jacobian matrix in the case where the well crosses multiple blocks of the reservoir grid. They did not present the wellbore model to calculate the perforation pressure. However, they showed the method how to implement a fully coupled wellbore-reservoir system. They claimed that the fully coupled method was more stable than an explicit wellbore pressure coupling.

2.3 COMPOSITIONAL WELLBORE SIMULATION

Since compositional simulation is computationally expensive and challenging this approach is not applied for fluid property calculations in the wellbore in most of the coupled wellbore reservoir simulators. However, different researchers have shown that in some specific cases of hydrocarbon reservoirs simulation, the application of a compositional model is crucial.

In 1979, Thomas L. Gould introduced the compositional fluid flow model in the pipelines. He explained that the blackoil model is simplified and unrealistic and is not valid for complicated fluid types, such as for the flow of volatile oils or gas condensates. Gould applied steady-state mass balance, momentum balance, and energy balance equations, neglecting the inter-phase shear force in the momentum equation to solve multiphase flow variables. In addition he computed the phase slippage effect by assuming local equilibrium in the segments of the pipe. He assumed that one portion of the slipping phase was in equilibrium with the other phase and the other portion with the same composition was not. Hence he computed the overall composition of each segments by considering mole fraction of phase-1, mole fraction of equilibrated phase-2, mole fraction of slipping phase-2 and holdup. In Chapter 4 we explain this calculation procedure with some modifications for compositional approach.

Recently, more comprehensive compositional wellbore-reservoir models have been introduced by different researchers. Pourafshary (2007) and Pourafshary et al. (2009) developed a thermal, blackoil wellbore simulator to model transient fluid flow and a thermal, compositional wellbore simulator to model semi-steady state flow. The model was applied for vertical wells and was explicitly coupled to a compositional reservoir simulator, General Purpose Adaptive Simulator (GPAS) (Wang et al., 1997; 1999; Han et al., 2007). Pourafshary (2007) applied the coupled wellbore-reservoir simulator for a

pressure build up test and showed the back flow, after flow phenomenon and phase segregation in the wellbore. He also compared his model results with field data and showed good agreement.

Pourafshary et al. (2009) presented development of thermal compositional coupled wellbore-reservoir simulator. He performed simulation on producing well with different case studies for crude oil, condensate gas and volatile oil. He demonstrated that the blackoil approach was not accurate for the representation of condensate and volatile oils flow in the wellbore.

Livescu et al. (2009) also developed a fully-coupled thermal compositional wellbore model. Mass conservation for each component, momentum conservation, and energy equation for the mixture of the fluids were solved to obtain pressure, temperature, and holdup profiles in the complete flow line. They used the drift-flux model to consider the slippage between the phases. In their study, different cases for thermal process and different well geometries were presented.

2.4 TRANSIENT WELLBORE SIMULATION

Since the time steps in the reservoir model are in the order of days, the producing wellbore system usually reaches steady-state long before the completion of a reservoir time step (In Chapter 5 where we explain the transient models it can be seen that transient time for a wellbore with 1000 ft long is in the order of several minutes). Therefore, steady-state equations are usually applied to the fluid flow model in the wellbore. This assumption also reduces computational time because the transient model using wellbore time-step for the reservoir increases the number of calculation steps for the reservoir to reach the final time. Thus, in steady-state mode wellbore simulation can be conducted with large time-steps on par with reservoir dynamics.

However, in case that the flow variations occur in a short period of time (*i.e.*, gas kick during drilling, Avelar et al., 2009) or in case that the countercurrent flow of gas and liquid occurs, the use of a transient two-phase model is essential.

Bendiksen et al. (1991) presented a standalone, extended two-fluid model, OLGA, with a pseudo-compositional approach for fluid properties calculation. Separated mass balance for gas, bulk liquid and liquid droplets, three momentum equations for the continuous bulk fluids and liquid droplet, and one energy equation for the mixture of fluid were solved. The steady-state pressure drop, liquid holdup phase velocities, and temperature were obtained from the equations. Different flow regimes such as stratified and annular mist (considered as separated flow), bubbly flow and slug flow (considered as distributed flow) were included in the calculation. Bendiksen et al. (1991) compared their model with SINTEF experimental data and showed good agreement between the model results and experimental data.

Other published works, which we previously explained, such as Winterfeld (1989), Almehaideb et al. (1989), Stone et al. (1989), Pourafshary (2007), also developed transient two-fluid models for gas and liquid continuous phases. Livescu et al. (2008; 2009) also developed a drift-flux transient model.

2.5 MULTIPHASE FLOW HORIZONTAL WELL SIMULATION

Since in this thesis we studied a horizontal wellbore model, we introduce some of the works performed by previous researchers in this particular well configuration. Changing the inclination of the well from vertical to horizontal has significant effects on

the flow regimes that occur in the two-phase flow system. In addition, having perforations along the well, or an open-hole horizontal well, influences the wall shear stress due to radial influx/outflux which is different than the case in a vertical well. Hence, in the wellbore simulation, a horizontal well is distinguished from the vertical and deviated wells (the treatment of a deviated well is as complex or maybe more than a horizontal well).

In a horizontal well, we have tighter dynamic interaction between the reservoir and the wellbore and considering the effect of multiphase flow inside the well is highly influential.

Islam and Chakma (1990) addressed the physical and mathematical modeling of a horizontal wellbore coupled to a compositional reservoir simulator. In their study, a series of numerical tests were performed to show the effect of pressure drops in the wellbore on the performance of a horizontal well.

Ouyang and Aziz (1999) explained some fundamental issues on the development of a wellbore model for horizontal wells. They covered modeling steady-state and transient wellbore flow and coupling wellbore flow with reservoir inflow. Ouyang (1998) showed that there were significant differences between fluid flow in the wellbore where radial influx through the perforation occurred and the fluid flow in a regular pipe. In the wellbore model reservoir inflow affect the boundary layer, kinetic energy and flow pattern transition which cause primary differences compared to a pipe model. He also discussed the flow regimes available in a horizontal well and explained the flow pattern transition criteria. In the transient model, Ouyang (1998) solved pressure and two-phase velocity as the primary variables and used analytical reservoir influx model for modeling wellbore-reservoir interaction.

Vicente and Ertekin (2006) and Vicente (2000) developed a three-dimensional fully-implicit blackoil reservoir model which was coupled to a horizontal wellbore model. They solved conservation of mass and Darcy's law for the reservoir, and conservation of mass and momentum in the wellbore simultaneously. Vicente et al. (2006) applied a homogenous and an isothermal model for the wellbore simulation. They used their model for transient pressure and flow rate behavior of horizontal well at early times. They also compared their model results with Eclipse 100 and semi-analytical solutions and showed good agreement between them.

Gui et al. (2007) also developed a homogenous two-phase flow model for a horizontal well which was fully coupled to a blackoil reservoir model. They investigated the transient flow behavior of the horizontal well at early time of production and showed a sensitivity analysis for different reservoir parameters. They discussed reservoir permeability and initial gas saturation effect on well productivity.

2.6 OBJECTIVES OF THE RESEARCH

Different approaches have been introduced in the literature to calculate multiphase flow variables but still some challenging issues regarding accurate and robust calculation exists. Considering compositional phase behavior for complex fluid types, solving thermal equation for substantial temperature variations and using separated momentum equations for different flow regimes are crucial in multiphase flow.

For this purpose, in this study, we present an explicitly-coupled, mechanistic, semi-steady state, two-fluid model for a multi-component, horizontal wellbore-reservoir simulator. The wellbore model was coupled to a parallel multi-component reservoir simulator, General Purpose Adaptive Simulator - GPAS (Wang et al., 1997; 1999; Han et

al., 2007). The main objective for this development was to calculate different variables such as pressure, temperature, phase velocities, phase fractions, and compositions in the horizontal well in conjunction with a vertical well.

In addition, a comprehensive transient two-fluid model was developed to study transient two-phase flow more accurately. In this model separate gas and liquid momentum equations were used by association with appropriate inter-phase momentum transfer for different flow regimes. The model was compared against analytical solutions and experimental data

The present development was aimed to be used for different applications which mainly are for wellbore and reservoir dynamic interactions and for wellbore and near wellbore damage simulations.

Chapter 3: Pseudo-Compositional, Standalone, Wellbore Model

The fluid flow model for the wellbore has been well-established for single-phase flow. Introducing the second phase as a concurrent or counter-current gas/liquid flow led to flow models that are computationally more challenging. In this chapter, we introduce a mechanistic two-fluid model for the wellbore which can be coupled to a compositional reservoir simulator. We explain the governing equations, methods for calculating fluid properties and the different boundary conditions that can be imposed to the flow domain.

3.1 MULTIPHASE FLOW MAIN PARAMETERS DEFINITION

In this section, we describe the main variables of the two-phase flow model that have been introduced in multiphase flow equations. These variables are generally explained to incorporate liquid and gas phases in the equations.

3.1.1 Mass and Volumetric Flow Rates

Liquid and gas phases mass flow rates are defined as follows:

$$W_l = \frac{dm_l}{dt}, \quad (3.1)$$

$$W_g = \frac{dm_g}{dt}. \quad (3.2)$$

Using volume instead of mass we obtain the volumetric flow rate as follows:

$$q_l = \frac{dV_l}{dt}, \quad (3.3)$$

$$q_g = \frac{dV_g}{dt}. \quad (3.4)$$

3.1.2 Liquid Holdup

The fraction of the volume which is occupied by the liquid phase in a bulk of two-phase systems is called holdup. Similarly, the gas fraction can be defined for the gas phase. For the two-phase flow equations, either the holdup (H_L) or gas fraction (α) are used,

$$H_L = \frac{V_l}{V_l + V_g}, \quad (3.5)$$

$$\alpha = 1 - H_L. \quad (3.6)$$

There is also another holdup definition which is interpreted as the no-slip holdup. In case the slippage between the phases is neglected, the holdup value becomes the volumetric flow rate ratio of the liquid phase to the total volumetric flow rate. This parameter is defined as follows:

$$\lambda_l = \frac{q_l}{q_g + q_l}. \quad (3.7)$$

3.1.3 Superficial Velocity

The superficial velocity is defined as the volumetric flow rate of each phase divided by the pipe cross-section:

$$US_l = \frac{q_l}{A}, \quad (3.8)$$

$$US_g = \frac{q_g}{A}. \quad (3.9)$$

3.1.4 Actual Velocity

The actual velocity is defined as the volumetric flow rate of each phase divided by the respective phase cross-sectional area. Hence,

$$U_l = \frac{q_l}{A_l} = \frac{US_l}{H_l}, \quad (3.10)$$

$$U_g = \frac{q_g}{A_g} = \frac{US_g}{\alpha}. \quad (3.11)$$

3.1.5 Mixture Velocity

The summation of the superficial velocities of the phases or dividing the total volume flow rate by the pipe cross-sectional area yields to the mixture velocity,

$$U_m = \frac{q_g + q_l}{A}. \quad (3.12)$$

3.1.6 Slip Velocity

The difference between actual velocities of each phase is expressed as the slip velocity,

$$U_{slip} = U_g - U_l. \quad (3.13)$$

This velocity has a significant effect on the inter-phase shear stress magnitude.

3.1.7 Drift Velocity

Another definition that incorporates the slippage between the phases is the drift velocity. This reference velocity is defined as the difference between each phase velocity and the mixture velocity,

$$UD_l = U_l - U_m, \quad (3.14)$$

$$UD_g = U_g - U_m. \quad (3.15)$$

3.1.8 Average Fluid Properties

For the mixture of gas and liquid, the density and the viscosity are defined by arithmetic volumetric averaging. These values are used for the homogenous mixture approach or the drift flux approach in the fluid flow equations,

$$\rho_m = \rho_l H_l + \rho_g (1 - H_l), \quad (3.16)$$

$$\mu_m = \mu_l H_l + \mu_g (1 - H_l). \quad (3.17)$$

3.2 FLOW PATTERNS DEFINITION IN A HORIZONTAL WELL

In addition to the number of flow variables in two-phase fluid flow, different flow regimes are encountered in horizontal pipes. In fact, different flow patterns in a two-phase flow system imply the spatial configurations of gas and liquid phases in each segment of the flow line.

Different parameters such as liquid and gas velocity, flow line inclination and fluid density and viscosity establish the dominant flow pattern during the two-phase fluid flow. To determine these flow patterns and the criteria that derive the transition among them, a set of experimental tests should be performed. Since these experiments are sensitive to flow conditions and they are recognized by visual means, different flow regimes and transition maps might be observed and reported in the literature. Thus the flow regimes transition maps are not universal and it is recommended to test the experiment for particular condition. However, there are general definitions for flow patterns that have been accepted by many researchers. These flow pattern definitions can mainly be classified for horizontal and vertical inclinations.

3.2.1 Flow Patterns

For horizontal or near horizontal pipes, generally four flow patterns have been introduced (Shoham, 2005). Although, these flow patterns can be sub-divided to slightly different flow regimes, but to avoid more complex situations we only consider them as main flow configurations. Following are the main flow regimes that researchers have agreed upon for horizontal flow (Shoham, 2005).

3.2.1.1 Stratified Flow

Stratified flow occurs at low velocities of gas and liquid. Another terminology for this flow pattern is separated flow. In this flow regime, liquid flows in the bottom and gas

flows in the top of the pipe due to gravity segregation. Figure 3.1a shows the schematic view of the stratified flow.

3.2.1.2 Intermittent Flow

Figure 3.1b shows the schematic view of the intermittent flow. In this flow regime, a liquid slug combined with elongated gas bubbles occurs. At a high gas flow rates small gas bubbles can also be entrained in the liquid slugs.

3.2.1.3 Annular Flow

At a very high gas flow rate, the annular flow occurs. In this flow regime, gas containing small droplets of liquid moves in the core of the pipeline and liquid film is generated around the core. As Figure 3.1c shows annular spatial configuration is generated at this condition.

3.2.1.4 Dispersed-Bubbly Flow

Dispersed bubbly flow regime occurs at very high liquid flow rates. In this flow regime small gas bubbles are dispersed in the liquid continuous medium. Figure 3.1d shows the schematic view of the dispersed bubbly flow.

3.2.2 Flow Pattern Prediction

The main step in two-phase flow modeling is the flow pattern determination. In fact, the dominant flow regime characterizes the flow equation to be applied. In this section, we introduce several flow pattern maps that have been reported by different researchers.

Baker (1954) presented a flow pattern map for horizontal pipes that considers the following regimes, according to Figure 3.2: stratified smooth, stratified wavy, elongated bubble, dispersed bubble and annular flow. In the flow regime map, gas and liquid mass

flow rates (G_g, G_l) and other non-dimensional parameters $(\lambda = f(\rho_g, \rho_l), \psi = f(\sigma, \mu_l, \rho_l))$, are used in the coordination of the flow pattern map.

Mandhane et al. (1974) also reported a flow pattern map for horizontal pipes using a large data bank (the American Gas Association (AGA) - American Petroleum Institute (API) Data Bank). In this flow pattern map there are similar flow regimes to the ones defined by Baker (1954). However, superficial liquid gas velocities are used in the coordinates of the map, according to Figure 3.3.

Other researchers (Govier and Aziz (1972), Alves (1954), Eaton et al.(1967), Simpson et al.(1977)) also have presented different flow pattern maps for horizontal pipes using experimental data. Since these flow pattern maps have been developed for specific experimental condition they cannot be generalized where the data is not available. Hence, mechanistic models have been developed based on physical approaches to more universally predict the flow patterns.

For this purpose, Tatial and Dukler (1976) introduced the flow pattern maps using mechanistic approach. They used mechanistic momentum equations for liquid and gas and defined some non-dimensional variables to obtain liquid level. They performed stability analysis to determine flow regime transitions. In the mechanistic flow pattern transition analysis pipe diameter, pipe inclination, and friction factors are the main parameters that affect the shape of the map.

Recently more comprehensive models and computer programs have been developed based on Tatial and Dukler (1976) analysis to generate the flow pattern maps (Shoham, 2005). In this study we use a flow pattern map analysis, which was developed by Ouyang (1998). The fundamental approach in Ouyang's work (1998) is similar to Tatial and Dukler (1976). However, he generalized the flow pattern map for wellbore and considered the effect of inflow from surrounding by modifying the friction factors. Figure

3.4 shows the flow pattern map obtained by Ouyang (1998) approach and Figure 3.5 shows the corresponding flowchart for flow regime transition.

As can be seen in Figure 3.5 if the gas fraction is less than 0.52 and the bubble diameter is below the critical bubble diameter, then the bubbly flow is dominant. The critical bubble diameter can be obtained as follows:

$$\lambda_v = \frac{\mu_l}{\mu_g}, \quad (3.18)$$

$$Af = \frac{3\rho_l f_m U_m^2}{8(\rho_l - \rho_g)g \cos(\theta)}, \quad (3.19)$$

$$Bf = \frac{6\mu_l U_{lm} C_{id}}{(\rho_l - \rho_g)g \cos(\theta)} \frac{2\lambda_v}{\lambda_v + 1}, \quad (3.20)$$

$$d_{CB} = \frac{1}{2}(Af + \sqrt{Af^2 + 4Bf}). \quad (3.21)$$

If the condition for bubbly flow is not satisfied, then the other criterion for stratified flow is verified. The Kelvin-Helmholtz stability criterion (Taitel and Dukler, 1976) is used for transition from stratified to non-stratified flow. Hence, for non-stratified flow we obtain

$$UG > (1 - \frac{h_l}{D}) \left\{ \frac{A_g}{\frac{dA_l}{dh_l}} \left[\frac{\rho_l g \cos(\theta)}{\rho_g} + \frac{U_{lm} |U_{lm}|}{2h_g} \right] \right\}^{0.5}. \quad (3.22)$$

The next step is to check for the intermittent and annular flow regimes criterion. If liquid holdup is below 0.24, then annular mist flow is the dominant flow regime. Otherwise if the holdup is greater than 0.24, the intermittent flow should be chosen as the dominant flow regime.

3.3 FLUID PROPERTIES CALCULATION

During the oil and gas production from the reservoir to the surface facility, fluids flow a long path which has a wide range of pressure and temperature variations. In fact, the large change in the thermodynamic condition of the fluid influences the fluid properties such as the viscosity, density, interfacial tension, solution gas ratio, and formation volume factor. The effect of pressure and temperature in the fluid properties needs to be properly addressed in the two-phase model. There are two approaches for fluid property calculation: one is the blackoil model, which applies empirical correlations to obtain fluid properties; the other is the compositional model, which applies multiphase flash calculations.

In this study, we performed blackoil, pseudo compositional and compositional approaches for fluid properties calculation. We call the combined multiphase flash calculation with blackoil properties as the pseudo-compositional model. In pseudo-compositional approach, the variables that are defined in the blackoil models (*i.e.*, solution gas ratio and formation volume factor) are calculated by batch calculation with a compositional model, instead of empirical correlations. Since pseudo-compositional approach is more universal than correlations in blackoil model and less computationally challenging than fully compositional models it is desirable for fluid properties calculation. In this chapter we use pseudo-compositional approach for the fluid properties calculation. Calculation procedure details can be found in Appendix A.

3.4 FLOW EQUATIONS IN THE WELLBORE

In this study, we use the two-fluid model as the mechanistic approach to model the two-phase flow. We have five balance equations: liquid and gas mass, liquid and gas momentum, and mixture energy. Accordingly, we have liquid and gas velocities, pressure, holdup and temperature, as the primary flow variables.

We make the following general assumptions to derive the governing equations:

- one-dimensional flow;
- steady-state condition;
- the liquid phase is the oil/water mixture, in case that water exists in the flow (liquid properties are calculated by volumetric averaging between water and oil);
- the pseudo-compositional approach is applied to calculate the fluid properties;
- in addition to source or sink mass flow rate another term is also considered which is calculated by well indices values for each phase;
- interface shear force, wall shear force, and spatial geometry of flow are modified for different flow regimes;
- both gas and liquid phases have identical pressure and temperature;
- pressure and holdup are calculated in the center of the wellbore segments and temperature, liquid velocity, gas velocity and mixture velocity are calculated in the sides of the wellbore segments, according to Figure 3.6. To update the fluid properties temperature is also calculated in the segment center by interpolation.

3.4.1 Liquid Mass Balance

Figure 3.7 shows the schematic view of fluid transfer in a well segment. For this segment, liquid mass balance can be described by Equation (3.23):

$$(Mass_{in} - Mass_{out}) \pm (Source / Sink) = 0 . \quad (3.23)$$

Substituting the input mass rate, output mass rate, and the source and sinks terms we obtain:

$$Adt[H_l(i-1/2)\rho_l(i-1/2)U_l(i-1)] - Adt[H_l(i+1/2)\rho_l(i+1/2)U_l(i)] + dzdt[PI_o\rho_{ores} + PI_w\rho_{wres}](P_{res} - P(i)) \pm dz\dot{m}_l dt = 0. \quad (3.24)$$

In the above equation, i represents the segment index. $H_l(i)$, $\rho_l(i)$ and $P(i)$ are calculated in the segment center and $U_l(i)$ is obtained in the segment sides. In addition, oil density is applied for free oil as below:

$$\rho_{oil,free} = \rho_{oil}(P,T) - \frac{R_s(P,T)}{B_o(P,T)} \rho_{gsc}. \quad (3.25)$$

In Equation (3.23) source and sink terms can be either via reservoir influx, or by constant influx/outflux, \dot{m}_l . Reservoir influx is calculated by well index value and the pressure difference between reservoirs and wellbore. Constant influx/outflux is another option to include source or sink term which corresponds to injection to or production from the wellbore. This term is independent from reservoir coupling. We define both source/sink terms as mass flow rates per unit length.

Since we used staggered gridding in which density and holdup were defined in the segment center and velocity was defined in the segment side we used upstream weighting for numerical calculation. We performed the upstream weighting based on velocity sign. Hence, we categorized the mass conservation equation for different velocity signs as below:

$$\begin{aligned}
& 1. U_l(i) > 0, U_l(i-1) > 0, \\
& \left(\frac{1}{dz}\right)[H_l(i)\rho_l(i) \times U_l(i)] - \left(\frac{1}{dz}\right)[H_l(i-1)\rho_l(i-1) \times U_l(i-1)] \\
& + \left(\frac{1}{A}\right)[PI_o\rho_{ores} + PI_w\rho_{wres}](P(i) - P_{res}) \pm \left(\frac{\dot{m}_l}{A}\right) = 0.
\end{aligned} \tag{3.26}$$

$$\begin{aligned}
& 2. U_l(i) < 0, U_l(i-1) > 0, \\
& -\left(\frac{1}{dz}\right)[H_l(i+1)\rho_l(i+1) \times U_l(i)] - \left(\frac{1}{dz}\right)[H_l(i-1)\rho_l(i-1) \times U_l(i-1)] \\
& + \left(\frac{1}{A}\right)[PI_o\rho_{ores} + PI_w\rho_{wres}](P(i) - P_{res}) \pm \left(\frac{\dot{m}_l}{A}\right) = 0.
\end{aligned} \tag{3.27}$$

$$\begin{aligned}
& 3. U_l(i) < 0, U_l(i-1) < 0, \\
& -\left(\frac{1}{dz}\right)[H_l(i+1)\rho_l(i+1) \times U_l(i)] + \left(\frac{1}{dz}\right)[H_l(i)\rho_l(i) \times U_l(i-1)] \\
& + \left(\frac{1}{A}\right)[PI_o\rho_{ores} + PI_w\rho_{wres}](P(i) - P_{res}) \pm \left(\frac{\dot{m}_l}{A}\right) = 0.
\end{aligned} \tag{3.28}$$

$$\begin{aligned}
& 4. U_l(i) > 0, U_l(i-1) < 0, \\
& \left(\frac{1}{dz}\right)[H_l(i)\rho_l(i) \times U_l(i)] + \left(\frac{1}{dz}\right)[H_l(i)\rho_l(i) \times U_l(i-1)] \\
& + \left(\frac{1}{A}\right)[PI_o\rho_{ores} + PI_w\rho_{wres}](P(i) - P_{res}) \pm \left(\frac{\dot{m}_l}{A}\right) = 0.
\end{aligned} \tag{3.29}$$

Combining above conditions we can write the liquid mass conversation equation in the form as follows:

$$\begin{aligned}
& \left(\frac{1}{dz}\right)[H_l(i)\rho_l(i) \times \max(U_l(i), 0) - H_l(i+1)\rho_l(i+1) \times \max(-U_l(i), 0)] \\
& - \left(\frac{1}{dz}\right)[H_l(i-1)\rho_l(i-1) \times \max(U_l(i-1), 0) - H_l(i)\rho_l(i) \times \max(-U_l(i-1), 0)]
\end{aligned}$$

$$+(\frac{1}{A})[PI_o\rho_{ores} + PI_w\rho_{wres}](P(i) - P_{res}) \pm (\frac{\dot{m}_l}{A}) = 0 \quad (3.30)$$

Rearranging the coefficients and assuming small dz in Equation (3.24) we can obtain the partial differential equation for mass conservation. Hence, the final partial differential equation for liquid mass conservation can be written as

$$\frac{\partial[H_l\rho_l U_l]}{\partial z} + [\frac{PI_o\rho_{ores} + PI_w\rho_{wres}}{A}](P_{well} - P_{res}) \pm \frac{\dot{m}_l}{A} = 0. \quad (3.31)$$

3.4.2 Gas Mass Balance

Likewise, we write gas mass balance as:

$$(Mass_{in} - Mass_{out}) \pm (Source / Sink) = 0 \quad (3.32)$$

Substituting the input/output mass flow rates and gas influx we obtain:

$$\begin{aligned} & Adt[(1 - H_l(i - 1/2))\rho_g(i - 1/2)U_g(i - 1) + \frac{R_s(i - 1/2)}{B_o(i - 1/2)}\rho_{gsc}H_l(i - 1/2)U_l(i - 1/2)] \\ & - Adt[(1 - H_l(i + 1/2))\rho_g(i + 1/2)U_g(i) + \frac{R_s(i + 1/2)}{B_o(i + 1/2)}\rho_{gsc}H_l(i + 1/2)U_l(i)] \\ & + dzdt[PI_g(i)\rho_{gres}(i) + PI_o(i)\frac{R_{sres}}{B_{ores}}\rho_{gsc}](P_{res} - P(i)) \pm \dot{m}_g dzdt = 0. \end{aligned} \quad (3.33)$$

Input/output gas mass flows consist of two terms. First term, $\rho_g(i)(1 - H_l(i))U_g(i)$ is the free gas flow and the second term, $\frac{R_s(i)}{B_o(i)}\rho_{gsc}H_l(i)U_l(i)$ is the solution gas in the oil.

After rearranging the coefficients and applying upstream weighting based on velocity sign (likewise in liquid mass balance equation) we obtain:

$$\begin{aligned}
& \left(\frac{1}{dz}\right)[(1-H_l(i))\rho_g(i) \times \max(U_g(i), 0) - (1-H_l(i+1))\rho_g(i+1) \times \max(-U_g(i), 0) \\
& + \frac{R_s(i)}{B_o(i)}\rho_{gsc}H_l(i) \times \max(U_l(i), 0) - \frac{R_s(i+1)}{B_o(i+1)}\rho_{gsc}H_l(i+1) \times \max(-U_l(i), 0)] \\
& - \left(\frac{1}{dz}\right)[(1-H_l(i-1))\rho_g(i-1) \times \max(U_g(i-1), 0) - (1-H_l(i))\rho_g(i) \times \max(-U_g(i-1), 0) \\
& + \frac{R_s(i-1)}{B_o(i-1)}\rho_{gsc}H_l(i-1) \times \max(U_l(i-1), 0) - \frac{R_s(i)}{B_o(i)}\rho_{gsc}H_l(i) \times \max(-U_l(i-1), 0)] \\
& + \left(\frac{1}{A}\right)[PI_g(i)\rho_{gres}(i) + PI_o(i)\frac{R_{sres}}{B_{ores}}\rho_{gsc}](P(i) - P_{res}) \pm \left(\frac{\dot{m}_g}{A}\right) = 0 . \tag{3.34}
\end{aligned}$$

The final partial differential equation for gas mass conservation can be written as:

$$\begin{aligned}
& \frac{\partial[(1-H_l)\rho_g U_g + \frac{R_s}{B_o}\rho_{gsc}H_l U_l]}{\partial z} + \left[\frac{PI_g\rho_{gres} + PI_o(i)\frac{R_{sres}}{B_{ores}}\rho_{gsc}}{A}\right](P_{well} - P_{res}) \\
& \pm \frac{\dot{m}_g}{A} = 0 . \tag{3.35}
\end{aligned}$$

$\rho_g(i)$, $B_o(i)$ and $R_s(i)$ are calculated in the center of the well segment and $U_g(i)$ is obtained in the side of the well segment.

3.4.3 Liquid Momentum Balance

We write the momentum balance as follows:

$$(Momentum_{in} - Momentum_{out}) + (Forces) = 0 . \tag{3.36}$$

Figure 3.1 shows the forces that act on the phases in a control volume. Replacing input/output momentum in the center of the segments and body forces as gravity force, inter-phase shear force, F_{lg} , and wall shear force, τ_{wl} , we obtain:

$$\begin{aligned}
& Adt[H_l(i)\rho_l(i)(\frac{U_l(i)+U_l(i-1)}{2})^2 - H_l(i+1)\rho_l(i+1)(\frac{U_l(i)+U_l(i+1)}{2})^2] \\
& + Adt[H_l(i)\frac{R_s(i)}{B_o(i)}\rho_{gsc}(\frac{U_l(i)+U_l(i-1)}{2})^2 - H_l(i+1)\frac{R_s(i+1)}{B_o(i+1)}\rho_{gsc}(\frac{U_l(i)+U_l(i+1)}{2})^2] \\
& + dt[AH_l(i)P(i) - AH_l(i+1)P(i+1) - Adz(\frac{H_l(i)+H_l(i+1)}{2})(\frac{\rho_l(i)+\rho_l(i+1)}{2})g \sin(\theta) \\
& - S_l dz \tau_{wl} + Adz F_{lg}] = 0.
\end{aligned} \tag{3.37}$$

In the above equation, since liquid velocity was calculated in the segment sides we used interpolation to obtain the velocity in the center of the segment. In addition, we assumed that the fluid influx from/to the reservoir is perpendicular to the flow stream and we neglected the momentum transfer from fluid influx.

After rearranging the coefficients and converting the units to psi and ft/sec we obtain:

$$\begin{aligned}
& (\frac{1}{dz})[H_l(i+1)\rho_l(i+1)(\frac{U_l(i)+U_l(i+1)}{2})^2 - H_l(i)\rho_l(i)(\frac{U_l(i)+U_l(i-1)}{2})^2] + \\
& (\frac{1}{dz})[H_l(i+1)\frac{R_s(i+1)}{B_o(i+1)}\rho_{gsc}(\frac{U_l(i)+U_l(i+1)}{2})^2 - H_l(i)\frac{R_s(i)}{B_o(i)}\rho_{gsc}(\frac{U_l(i)+U_l(i-1)}{2})^2] \\
& + 144gc(\frac{1}{dz})[H_l(i+1)P(i+1) - H_l(i)P(i)] \\
& + (\frac{H_l(i)+H_l(i+1)}{2})(\frac{\rho_l(i)+\rho_l(i+1)}{2})g \sin(\theta) + \frac{\tau_{wl}S_l}{A} - F_{lg} = 0.
\end{aligned} \tag{3.38}$$

The final partial differential equation for liquid momentum conservation can be written as:

$$144gc \frac{\partial(H_l P)}{\partial z} + \frac{\partial(H_l \rho_l U_l^2 + H_l \frac{R_s}{B_o} \rho_{gsc} U_l^2)}{\partial z} + H_l \rho_l g \sin(\theta) + \frac{\tau_{wl} S_l}{A} - F_{lg} = 0. \quad (3.39)$$

In Equation (3.39), S_l is the wetted perimeter by liquid phase and τ_{wl} is the shear stress between liquid and wall. Depending on the flow regime, S_l can be the perimeter of the pipe or a portion of that. For bubbly flow, intermittent flow, and annular flow, we assume that $S_l = \pi d$. However, for stratified flow we use following equation, as can be seen in Figure 3.8:

$$S_l \approx D(\pi - \cos^{-1}(2H_l - 1)) \quad (3.40)$$

Wall friction loss is obtained from the following equation in which f_{wl} is a function of the Reynolds numbers (R_{el}, R_{ew}) and the wall roughness (ε),

$$\tau_{wl} = \frac{1}{2} f_{wl} \rho_l U_l |U_l| \quad (3.41)$$

$$f_{wl} = f_{wl0} F(R_{el}, R_{ew}) \quad (3.42)$$

f_{wl0} is the no-wall-flow Fanning friction factor which is calculated by Colebrook and White (1937) correlation:

$$f_{wl0}^{-0.5} = -4.0 \log \left[\frac{\varepsilon}{3.7D} + \frac{1.255}{f_{wl0}^{0.5} R_e} \right] \quad (3.43)$$

$F(R_{el}, R_{ew})$ is calculated from Ouyang (1998) correlation which is based on single phase flow. For turbulent axial flow Ouyang (1998) showed following equation for $F(R_{el}, R_{ew})$:

$$F(R_{el}, R_{ew}) = \begin{cases} 1 - 0.0153 R_{ew}^{0.3978} & \text{Perforated Wellbore} \\ 1 - 29.03 \left(\frac{R_{ew}}{R_e}\right)^{0.8003} & \text{Open-Hole Wellbore} \end{cases} \quad (3.44)$$

F_{lg} is also inter-phase friction force per unite bulk volume. This term is highly dependent on the flow regimes. Richter (1983) and Schwellnus and Shoukri (1991), explained that F_{lg} has two parts as virtual mass force and drag force. The drag force is due to shear stress between the phases and the virtual mass force is due to the relative acceleration between the phases. To simplify the numerical computation, we can neglect the virtual mass force, F_{VM} , term. This term is not usually shown in the two-fluid models (Pourafashry 2007, Shoham, 2005).

Thus, the equation for inter-phase force calculation is presented as follow:

$$F_{lg} = F_{VM} + F_D \approx F_D \quad (3.45)$$

Schwellnus and Shoukri (1991) showed that the drag force for bubbly flow is calculated as:

$$F_D = \frac{3CD_{H_l}}{4D} (1 - H_l) H_l \rho_l |U_g - U_l| (U_g - U_l), \quad (3.46)$$

$$\text{where, } CD_{H_l} = CD(H_l)^{-4.7} \quad (3.47)$$

$$\begin{aligned}
CD &= \frac{24}{Re} (1 + 0.15 Re^{0.007}) & Re < 1000 \\
CD &= 0.44 & Re \geq 1000
\end{aligned} \tag{4.48}$$

and for annular flow as:

$$F_D = \frac{2C_{fi}}{D} \sqrt{(1-H_l)} \rho_g |U_g - U_l| (U_g - U_l), \tag{3.49}$$

where $C_{fi} = 0.005(1 + 75H_l)$.

Schwellnus and Shoukri (1991) also discussed that drag force coefficient for slug flow can be obtained by interpolation between bubbly flow and annular flow. However we interpolate the entire drag force equation between these two flow regimes for slug flow. Hence we introduce slug flow drag force as

$$F_D = \frac{H_l - H_{l-annular}}{H_{l-bubbly} - H_{l-annular}} F_{D-bubbly} + \frac{H_{l-bubbly} - H_l}{H_{l-bubbly} - H_{l-annular}} F_{D-annular}. \tag{3.50}$$

For inter-phase drag force in stratified flow we used Petalas and Aziz (2000) correlation as follow:

$$F_D = \frac{f_i S_i}{2A} \rho_g |U_g - U_l| (U_g - U_l). \tag{3.51}$$

In Equation (3.51) S_i is the inter-phase perimeter and can be obtained as $S_i = D\sqrt{1 - (2H_l - 1)^2}$ and f_i is the inter-phase friction factor which is related to the

Reynolds number, the Froude number, liquid and gas velocity, and liquid and gas density as below:

$$f_i = (0.004 + 0.5 \times 10^{-6} R_{esL}) F_{rL}^{1.335} \left(\frac{\rho_l g D}{\rho_g U_g^2} \right) \quad (3.52)$$

$$F_{rL} = \frac{U_l}{\sqrt{g h_l}}, \quad (3.53)$$

$$R_{esL} = \frac{\rho_l U S_l D}{\mu_l}. \quad (3.54)$$

3.4.4 Gas Momentum Balance

Likewise, for gas momentum equation we have:

$$(Momentum_{in} - Momentum_{out}) + (Forces) = 0. \quad (3.55)$$

In this equation momentum equation is applied for free gas phase,

$$\begin{aligned} & A[(1 - H_l(i))\rho_g(i)\left(\frac{U_g(i) + U_g(i-1)}{2}\right)^2 - (1 - H_l(i+1))\rho_g(i+1)\left(\frac{U_g(i) + U_g(i+1)}{2}\right)^2] \\ & + A[(1 - H_l(i))P(i) - (1 - H_l(i+1))P(i+1) - dz(1 - \left(\frac{H_l(i) + H_l(i+1)}{2}\right))\left(\frac{\rho_g(i) + \rho_g(i+1)}{2}\right)g \sin(\theta) \\ & - \frac{\tau_{wg} S_g dz}{A} - dz F_{lg}] = 0. \end{aligned} \quad (3.56)$$

After rearranging the coefficients and converting the units to psi, ft/sec we obtain:

$$\left(\frac{1}{dz}\right)[(1 - H_l(i+1))\rho_g(i+1)\left(\frac{U_g(i) + U_g(i+1)}{2}\right)^2 - (1 - H_l(i))\rho_g(i)\left(\frac{U_g(i) + U_g(i-1)}{2}\right)^2]$$

$$+144gc\left(\frac{1}{dz}\right)[(1-H_l(i+1))P(i+1)-(1-H_l(i))P(i)]+(1-\frac{H_l(i)+H_l(i+1)}{2})\left(\frac{\rho_g(i)+\rho_g(i+1)}{2}\right)g\sin(\theta)+\frac{\tau_{wg}S_g}{A}+F_{lg}=0. \quad (3.57)$$

The final partial differential equation for gas mass conservation can be written as:

$$144gc\frac{\partial((1-H_l)P)}{\partial z}+\frac{\partial((1-H_l)\rho_g U_g^2)}{\partial z}+(1-H_l)\rho_g g\sin(\theta)+\frac{\tau_{wg}S_g}{A}+F_{lg}=0, \quad (3.58)$$

where S_g is the wetted perimeter by gas phase and τ_{wg} is the shear stress between gas and wall. Depending on the flow regime, S_g can be zero or a portion of the pipe perimeter. For bubbly flow, intermittent flow, and annular flow we assume that $S_g = 0$. In case we have stratified flow, we use the following relation:

$$S_g \approx D \cos^{-1}(2H_l - 1). \quad (3.59)$$

It should be noted that F_{lg} and τ_{wg} are calculated similarly as in Equations (3.46), (3.49), (3.50), and (3.51) in the liquid momentum section.

3.4.5 Total Energy Balance

Although in reality the flowing liquid and gas temperatures are not equal, for the sake of simplicity we assume they are identical. Accordingly, the following equation is used to calculate the total energy conservation:

$$(Energy_{in} - Energy_{out}) + (W_{Force}) \pm (Source / Sink) = 0. \quad (3.60)$$

Substituting the input/output energy, gravity potential energy and heat loss (as sink term) in the segment i , we obtain:

$$\begin{aligned}
& Adt \left[\frac{H_l(i-1) + H_l(i)}{2} \frac{\rho_l(i-1) + \rho_l(i)}{2} (\bar{h}_l(i-1) + \frac{U_l^2(i-1)}{2}) U_l(i-1) \right] - \\
& Adt \left[\frac{H_l(i) + H_l(i+1)}{2} \frac{\rho_l(i) + \rho_l(i+1)}{2} (\bar{h}_l(i) + \frac{U_l^2(i)}{2}) U_l(i) \right] + \\
& Adt \left[\left(1 - \frac{H_l(i-1) + H_l(i)}{2}\right) \frac{\rho_g(i-1) + \rho_g(i)}{2} (\bar{h}_g(i-1) + \frac{U_g^2(i-1)}{2}) U_g(i-1) \right] - \\
& Adt \left[\left(1 - \frac{H_l(i) + H_l(i+1)}{2}\right) \frac{\rho_g(i) + \rho_g(i+1)}{2} (\bar{h}_g(i) + \frac{U_g^2(i)}{2}) U_g(i) \right] \\
& + dzdt [PI_o \rho_{ores}] (P_{res} - P(i)) (\bar{h}_{lres}(i) + \frac{U_{lres}^2(i)}{2}) \\
& + dzdt [PI_g \rho_{gres}] (P_{res} - P(i)) (\bar{h}_{gres}(i) + \frac{U_{gres}^2(i)}{2}) \\
& - Adzdt H_l(i) \rho_l(i) \frac{U_l(i) + U_l(i-1)}{2} g \sin(\theta) - \\
& Adzdt (1 - H_l(i)) \rho_g(i) \frac{U_g(i) + U_g(i-1)}{2} g \sin(\theta) \\
& - Q_{total} dt = 0.
\end{aligned} \tag{3.61}$$

In the above equation, the oil and gas phase total density is used instead of separating the solution gas from free oil. The terms, \bar{h}_l and \bar{h}_g , are the liquid and gas enthalpy at the segment sides. Hence, we calculate the temperature in the segment sides in the energy equation. To obtain the temperature in the segment center, we use interpolation.

After rearranging the coefficients and using the unit conversion factors (Appendix B), we obtain the final energy conservation equation:

$$\begin{aligned}
& \frac{1}{dz} \left[\frac{H_l(i-1) + H_l(i)}{2} \frac{\rho_l(i-1) + \rho_l(i)}{2} \left(\bar{h}_l(i-1) + \frac{U_l^2(i-1)}{2} \right) U_l(i-1) \right] - \\
& \frac{1}{dz} \left[\frac{H_l(i) + H_l(i+1)}{2} \frac{\rho_l(i) + \rho_l(i+1)}{2} \left(\bar{h}_l(i) + \frac{U_l^2(i)}{2} \right) U_l(i) \right] + \\
& \frac{1}{dz} \left[\left(1 - \frac{H_l(i-1) + H_l(i)}{2} \right) \frac{\rho_g(i-1) + \rho_g(i)}{2} \left(\bar{h}_g(i-1) + \frac{U_g^2(i-1)}{2} \right) U_g(i-1) \right] - \\
& \frac{1}{dz} \left[\left(1 - \frac{H_l(i) + H_l(i+1)}{2} \right) \frac{\rho_g(i) + \rho_g(i+1)}{2} \left(\bar{h}_g(i) + \frac{U_g^2(i)}{2} \right) U_g(i) \right] \\
& + \left[\frac{PI_o \rho_{ores}}{A} \right] (P_{res} - P(i)) \left(\bar{h}_{lres}(i) + \frac{U_{lres}^2(i)}{2} \right) \\
& + \left[\frac{PI_g \rho_{gres}}{A} \right] (P_{res} - P(i)) \left(\bar{h}_{gres}(i) + \frac{U_{gres}^2(i)}{2} \right) \\
& - H_l(i) \rho_l(i) \frac{U_l(i) + U_l(i-1)}{2} g \sin(\theta) - (1 - H_l(i)) \rho_g(i) \frac{U_g(i) + U_g(i-1)}{2} g \sin(\theta) \\
& - \frac{Q_{total}}{Adz} = 0.
\end{aligned} \tag{3.62}$$

The enthalpy can be related to the pressure and temperature via the heat capacity (C_p ($\frac{Btu}{Flbm}$)) and Joule Thomson coefficient, (η ($\frac{^{\circ}F}{Btu}$)):

$$d\bar{h}_l = C_{pl} dT_l - \left(\frac{144}{J_c} \right) \eta_l C_{pl} dP, \tag{3.63}$$

$$d\bar{h}_g = C_{pg} dT_g - \left(\frac{144}{J_c} \right) \eta_g C_{pg} dP. \tag{3.64}$$

Hence, for any specific pressure and temperature, the liquid and gas enthalpies can be calculated from the above equations with respect to a reference pressure and temperature. The enthalpy calculation is explained in Appendix A.

Q_{total} is also the heat exchange between the fluid and the formation, according to Equation (3.65):

$$Q_{total} = 2\pi r_{to} dz U_{to} (T(i) - T_{res}(i)), \quad (3.65)$$

where

$$\frac{1}{U_{to}} = \frac{r_{to}}{r_{ti} h_{to}} + \frac{r_{to} \ln(r_{to} / r_{ti})}{k_t} + \frac{r_{to} \ln(r_{ins} / r_{to})}{k_{ins}} + \frac{r_{to}}{r_{ins} (h_c + h_r)} + \frac{r_{to} \ln(r_{co} / r_{ci})}{k_{cas}} + \frac{r_{to} \ln(r_{wb} / r_{co})}{k_{cem}},$$

and

$$T_{res} = T_{ebh} - g_T z_h.$$

The fluid heat coefficients can be calculated by Dittus–Boelter (1930) correlation:

$$hc = \frac{k_w}{D_H} Nu, \quad (3.66)$$

$$Nu = 0.023 Re^{0.8} Pr^n, \quad (3.67)$$

where n is 0.4 for heating and 0.33 for cooling.

3.5 SOLUTION PROCEDURE

After arranging the final equations we obtain system of non-linear equations which are solved to achieve the primary variables (pressure, holdup, liquid velocity, gas velocity and temperature). There are two methods to solve the system of equations. One procedure is to solve the equations, simultaneously, using Newton method. In this method, we solve the mass and momentum balance equations by constructing a jacobian

matrix and a residual vector. The equations that we solve are, f_1 , as liquid momentum balance, f_2 , as gas momentum balance, f_3 , as the summation of gas and liquid mass balance, and f_4 , as liquid mass balance. Since pressure is calculated from total mass conservation equation we used the summation of gas and liquid mass balance as f_3 . The jacobian matrix and residual vector are presented as follows:

$$\text{Jacobian} = \begin{bmatrix}
 \frac{\partial f_{1,1}}{\partial U_{l,1}} & \frac{\partial f_{1,1}}{\partial U_{g,1}} & \frac{\partial f_{1,1}}{\partial P_1} & \frac{\partial f_{1,1}}{\partial H_1} & \dots & \frac{\partial f_{1,1}}{\partial U_{l,N}} & \frac{\partial f_{1,1}}{\partial U_{g,N}} & \frac{\partial f_{1,1}}{\partial P_N} & \frac{\partial f_{1,1}}{\partial H_N} \\
 \frac{\partial f_{2,1}}{\partial U_{l,1}} & \frac{\partial f_{2,1}}{\partial U_{g,1}} & \frac{\partial f_{2,1}}{\partial P_1} & \frac{\partial f_{2,1}}{\partial H_1} & \dots & \frac{\partial f_{2,1}}{\partial U_{l,N}} & \frac{\partial f_{2,1}}{\partial U_{g,N}} & \frac{\partial f_{2,1}}{\partial P_N} & \frac{\partial f_{2,1}}{\partial H_N} \\
 \frac{\partial f_{3,1}}{\partial U_{l,1}} & \frac{\partial f_{3,1}}{\partial U_{g,1}} & \frac{\partial f_{3,1}}{\partial P_1} & \frac{\partial f_{3,1}}{\partial H_1} & \dots & \frac{\partial f_{3,1}}{\partial U_{l,N}} & \frac{\partial f_{3,1}}{\partial U_{g,N}} & \frac{\partial f_{3,1}}{\partial P_N} & \frac{\partial f_{3,1}}{\partial H_N} \\
 \frac{\partial f_{4,1}}{\partial U_{l,1}} & \frac{\partial f_{4,1}}{\partial U_{g,1}} & \frac{\partial f_{4,1}}{\partial P_1} & \frac{\partial f_{4,1}}{\partial H_1} & \dots & \frac{\partial f_{4,1}}{\partial U_{l,N}} & \frac{\partial f_{4,1}}{\partial U_{g,N}} & \frac{\partial f_{4,1}}{\partial P_N} & \frac{\partial f_{4,1}}{\partial H_N} \\
 \dots & \dots & \dots & \dots & \dots & \dots & \dots & \dots & \dots \\
 \frac{\partial f_{1,N}}{\partial U_{l,1}} & \frac{\partial f_{1,N}}{\partial U_{g,1}} & \frac{\partial f_{1,N}}{\partial P_1} & \frac{\partial f_{1,N}}{\partial H_1} & \dots & \frac{\partial f_{1,N}}{\partial U_{l,N}} & \frac{\partial f_{1,N}}{\partial U_{g,N}} & \frac{\partial f_{1,N}}{\partial P_N} & \frac{\partial f_{1,N}}{\partial H_N} \\
 \frac{\partial f_{2,N}}{\partial U_{l,1}} & \frac{\partial f_{2,N}}{\partial U_{g,1}} & \frac{\partial f_{2,N}}{\partial P_1} & \frac{\partial f_{2,N}}{\partial H_1} & \dots & \frac{\partial f_{2,N}}{\partial U_{l,N}} & \frac{\partial f_{2,N}}{\partial U_{g,N}} & \frac{\partial f_{2,N}}{\partial P_N} & \frac{\partial f_{2,N}}{\partial H_N} \\
 \frac{\partial f_{3,N}}{\partial U_{l,1}} & \frac{\partial f_{3,N}}{\partial U_{g,1}} & \frac{\partial f_{3,N}}{\partial P_1} & \frac{\partial f_{3,N}}{\partial H_1} & \dots & \frac{\partial f_{3,N}}{\partial U_{l,N}} & \frac{\partial f_{3,N}}{\partial U_{g,N}} & \frac{\partial f_{3,N}}{\partial P_N} & \frac{\partial f_{3,N}}{\partial H_N} \\
 \frac{\partial f_{4,N}}{\partial U_{l,1}} & \frac{\partial f_{4,N}}{\partial U_{g,1}} & \frac{\partial f_{4,N}}{\partial P_1} & \frac{\partial f_{4,N}}{\partial H_1} & \dots & \frac{\partial f_{4,N}}{\partial U_{l,N}} & \frac{\partial f_{4,N}}{\partial U_{g,N}} & \frac{\partial f_{4,N}}{\partial P_N} & \frac{\partial f_{4,N}}{\partial H_N}
 \end{bmatrix}$$

$$Residual = \begin{bmatrix} f_{1,1} \\ f_{2,1} \\ f_{3,1} \\ f_{4,1} \\ \dots \\ f_{1,N} \\ f_{2,N} \\ f_{3,N} \\ f_{4,N} \end{bmatrix} \quad Dxvar = \begin{bmatrix} \Delta U_{l,1} \\ \Delta U_{g,1} \\ \Delta P_1 \\ \Delta H_1 \\ \dots \\ \Delta U_{l,N} \\ \Delta U_{g,N} \\ \Delta P_N \\ \Delta H_N \end{bmatrix}$$

where, 1 is node one, and N is node N in the wellbore.

After solving for the pressure, holdup and velocity of the gas and liquid, the energy equation is solved. We can solve the energy equation either analytically or numerically. If we assume f_5 to be the total energy equation, then the jacobian matrix, residual vector and temperature variation vector for energy equation becomes:

$$Jacobian = \begin{bmatrix} \frac{\partial f_{5,1}}{\partial T_1} & \dots & \frac{\partial f_{5,1}}{\partial T_N} \\ \dots & \dots & \dots \\ \frac{\partial f_{5,N}}{\partial T_1} & \dots & \frac{\partial f_{5,N}}{\partial T_N} \end{bmatrix} \quad Residual = \begin{bmatrix} f_{5,1} \\ \dots \\ f_{5,N} \end{bmatrix} \quad Dxvar = \begin{bmatrix} \Delta T_1 \\ \dots \\ \Delta T_N \end{bmatrix}$$

Temperature is obtained by Newton method separately and then fluid properties are updated. Figure (3.9) shows the calculation procedures.

The other calculation procedure is to solve the equations explicitly and marching the nodes orderly (Shoham 2005). In this method, mass balance equation is solved in the boundary node, which the wellbore and reservoir pressure values are known and the liquid and gas velocity are obtained. From the velocity values and pressure at boundary

of the wellbore, pressure and holdup in the next node are calculated from the liquid and gas momentum equations. In Chapter 4, we use this calculation procedure for the compositional coupled wellbore-reservoir model. The marching method is more robust than solving the equations simultaneously, and it is not very dependent to initial guesses.

3.6 RESULTS

In order to solve the flow equations we need to assign appropriate boundary conditions. Different boundary conditions can be implemented for the wellbore model. In Appendix C we explain these boundary conditions and the corresponding discretized equations. In the following sections we study two kinds of problems: i) constant pressure at outlet and ii) constant liquid/gas injection flow rate at inlet.

For fluid properties calculation we used the pseudo-compositional approach. Hence, we calculated the liquid density, liquid viscosity, solution gas ratio, liquid formation volume factor, gas density, gas formation volume factor, oil enthalpy, and gas enthalpy from multiphase flash calculations. We used a fluid compound with 6 components, as explained in Tables 3.1 and 3.2.

Figure 3.10 through 3.12 show the oil formation volume factor (B_o), oil viscosity (μ_o) and oil enthalpy (H_o) versus pressure for different temperatures. Figure 3.13 through Figure 3.16 show solution gas ratio (R_s), gas formation volume factor (B_g), gas viscosity (μ_g) and gas enthalpy (H_g) versus pressure for different temperatures respectively. These parameters were calculated by compositional flash calculation approach.

3.6.1 Case 1: Constant Pressure at Outlet, No Flow at Inlet

Figure 3.17 shows the clear representation of flow domain that we study in this section. We assume a horizontal pipe with a surrounding reservoir with constant temperature of 100 °F and constant pressure of 800 psi. Since fluid bubble point pressure is 2,175 psi, we have a two-phase system at this condition. We assume that the perforation is all the way along the pipe and the reservoir can influx liquid and gas through these perforated zones. However we neglect the pressure drop through the perforations. We also assume that there is no flow in the inlet of the pipe and the outlet pressure is held at 500 psi. Figure 3.18 shows the schematic view of the pipe. The input data file for this case is available in Appendix D.1.

Figures 3.19 through 3.21 show the pressure, temperature, velocities and liquid holdup distribution along the well. As can be observed, we have non-linear pressure and temperature drop in the pipe and, correspondingly, we have non-uniform fluid influx into the pipe. Since in this case the heat transfer coefficient was chosen to be a large value ($U_{to} = 100 \text{ (Btu/ft}^2\text{sec)}$), the temperature drop is not significant. In Figure 3.19 there is a small temperature oscillation in the inlet. This behavior corresponds to numerical error.

As it can be observed in the simulation results, the code could impose the outlet pressure and the no-flow boundary conditions as assigned and the variables behavior was physically consistent.

3.6.2 Case 2: Constant Pressure at Outlet, Constant Flow Rate at Inlet

In this case, we have the same condition as case 1; however, we change the boundary node condition from no flow at the inlet to constant flow and assume there is no reservoir influx around the pipe. We assume that the pressure is constant (500 psi) at the outlet and that liquid velocity is 20 ft/sec, and gas velocity is 15 ft/sec with an inlet holdup of 0.6. We also assume that there is an insulator around the pipe ($U_{to} = 0$).

Figures 3.22 through 3.24 show the pressure, temperature, velocities and liquid holdup distribution along the well. As can be seen we observe about a 80 psi pressure drop and 2.5 °F temperature drop along the pipe. Comparing these results with the previous case, we obtain less pressure drop and more temperature variation. In fact, due to the large fluid influx, velocities are increased and yield more pressure drop.

Again this boundary condition setup is well-honored in the code and the results are physically correct.

3.6.3 Case 3: Constant Pressure at Outlet, Cold Fluid Influx

To verify the temperature calculation we set up a case with cold/hot fluid influx detection in the well. We assume discontinues formation temperature in which the fluid contents have different temperatures. Consequently, hot or cold fluid invades the well at different points.

In this section, we assume similar geometry and conditions as in case 1 plus cold gas and oil invasion from a distance of 500 ft to 600 ft from the inlet. We assume that the reservoir temperature is 100 °F, the cold section temperature is 90 °F and overall heat transfer coefficient U_{to} is 1 ($Btu/ft^2 \text{ sec}$). From this study we would like to find the flow behavior as the consequence of the cold fluid injection. This information is useful for inverse modeling of formation properties. Figures 3.25 though 3.27 show pressure, temperature, fluid velocities, holdup distributions and flow regime variation. As can be seen in Figure 3.25, around 500 ft distance from the toe, the temperature declines sharply and reaches 90 °F at about 600 ft distance from the toe. Afterwards, temperature builds up to 99 °F. The significance of the temperature decline depends on the overall heat loss coefficient (U_{to}). For large U_{to} the temperature sharply declines and builds up. Hence, depending on the casing and formation materials, temperature variation profile will change.

Another observation regarding the cold fluid influx is the liquid holdup increment in the interval that temperature declines, according to Figure 3.27. In fact, fluid property variation and gas condensation cause the liquid holdup to increase. From this observation we conclude that the holdup distribution is extensively correlated to temperature. On the other hand, we see that the fluid velocities are not significantly influenced by the temperature. In fact, this is due to our assumption that well index is constant along the well and formation properties do not vary. However, in case the well index value was not the same in the cold zone, we would observe fluid velocities change in this interval. Consequently, we could relate the velocity variation mostly to well index change, rather than only to temperature effect.

Table 3.1 Hydrocarbon fluid components data

Component	Composition (mole fraction)	Pc(atm)	Tc(K)	Acentric factor	Mol Weight
C1	0.5	45.4	190.6	0.008	16.043
C3	0.03	41.9	369.8	0.152	44.097
C6	0.07	32.46	507.5	0.27504	86
C10	0.2	25.01	622.1	0.443774	134
C15	0.15	18.25	718.6	0.651235	206
C20	0.05	14.36	782.9	0.816053	275

Table 3.2 Hydrocarbon fluid components enthalpy coefficient data (Appendix A)

Component	A	B	C	D	E	F
C1	-5.58E+00	5.65E-01	-2.83E-04	4.17E-07	-1.53E-10	1.96E-14
C3	-1.22E+00	1.80E-01	6.65E-05	2.51E-07	-1.25E-10	1.89E-14
C6	0.00E+00	-1.65E-02	4.12E-04	-5.77E-08	0.00E+00	0.00E+00
C10	0.00E+00	-4.49E-02	4.26E-04	-6.41E-08	0.00E+00	0.00E+00
C15	0.00E+00	-3.66E-02	4.16E-04	-6.18E-08	0.00E+00	0.00E+00
C20	0.00E+00	-2.78E-02	4.09E-04	-5.96E-08	0.00E+00	0.00E+00

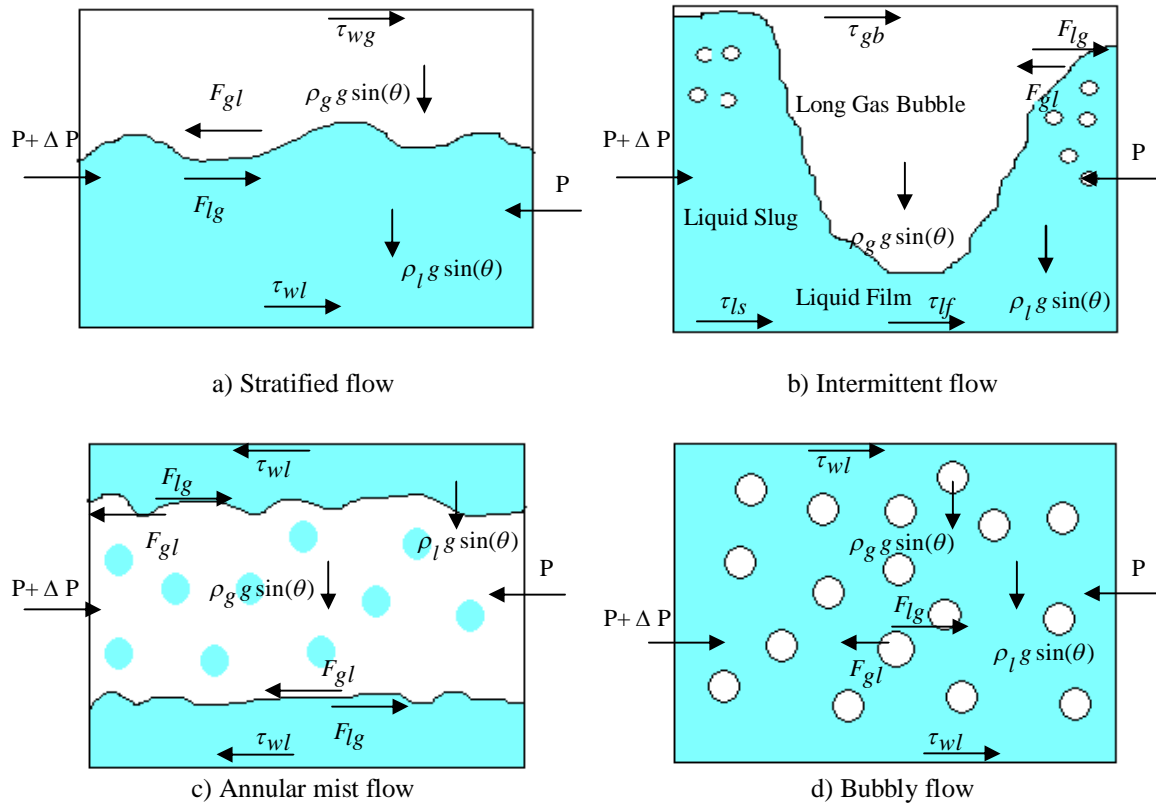


Figure 3.1 Dominant flow regimes and acting forces in horizontal tubular sections

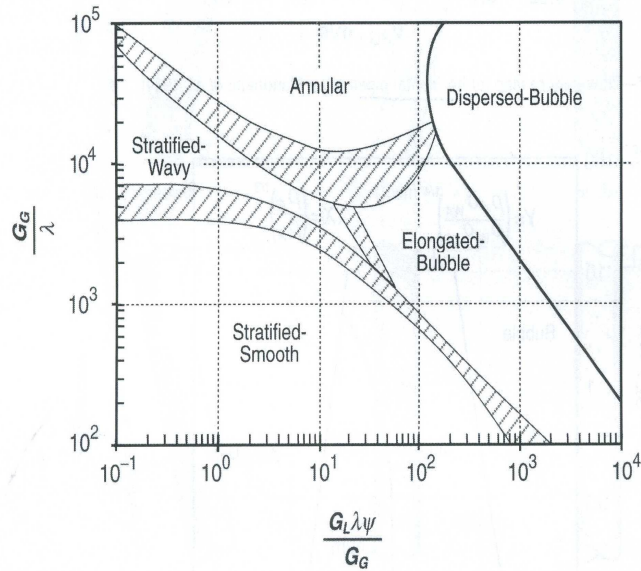


Figure 3.2 Flow pattern map in horizontal pipes (Baker, 1954)

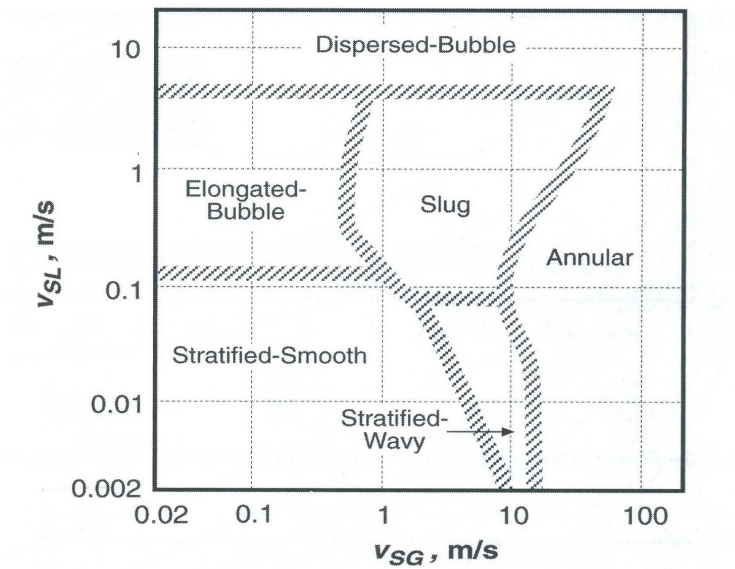


Figure 3.3 Flow pattern map in horizontal pipes (Mandhane et al., 1974)

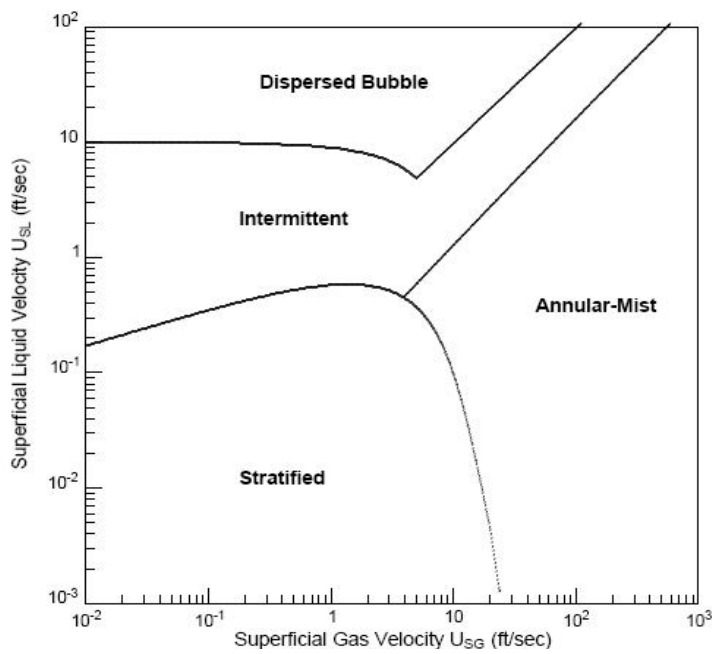


Figure 3.4 Flow pattern map in horizontal pipes, gas/oil system (Ouyang, 1998)

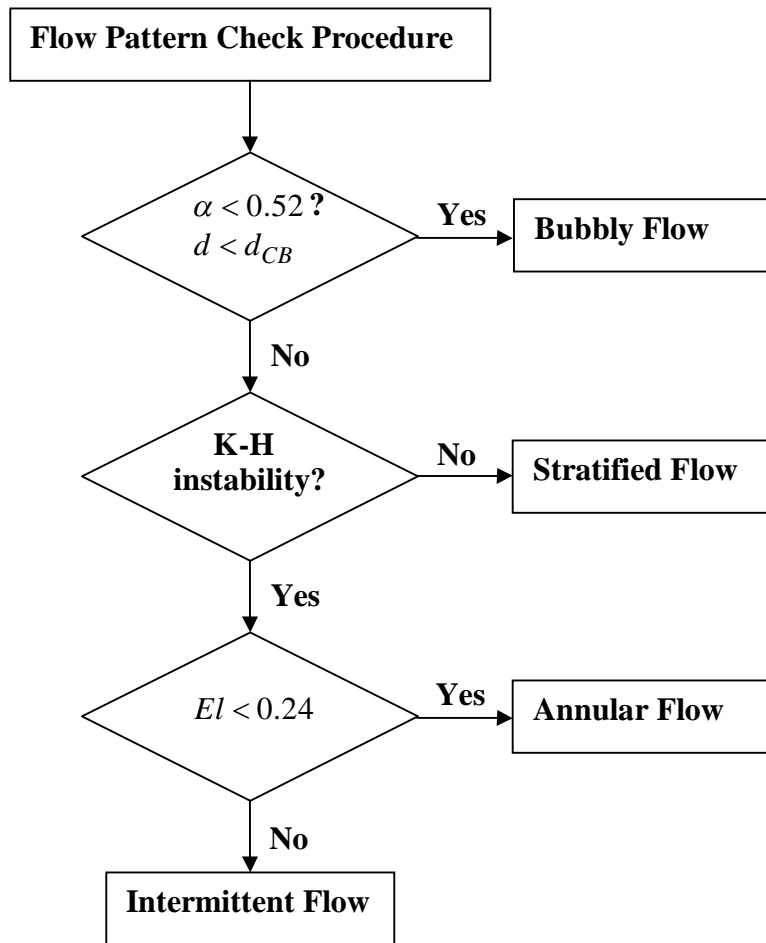


Figure 3.5 Procedure to select appropriate flow regimes (Ouyang, 1998)

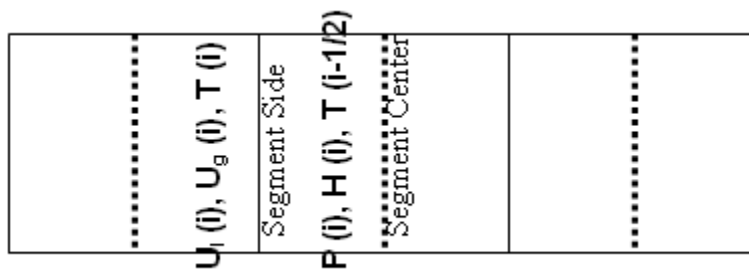


Figure 3.6 Schematic view of wellbore segments for nodal calculation

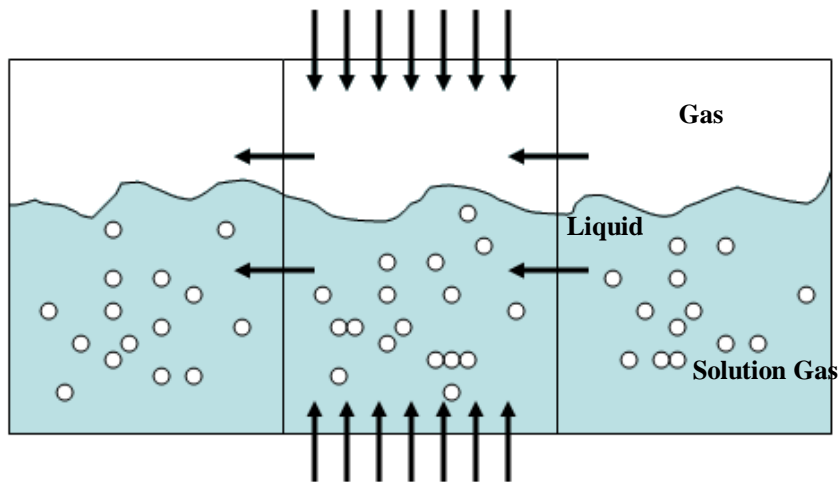


Figure 3.7 Schematic view of wellbore segments for fluid transfer

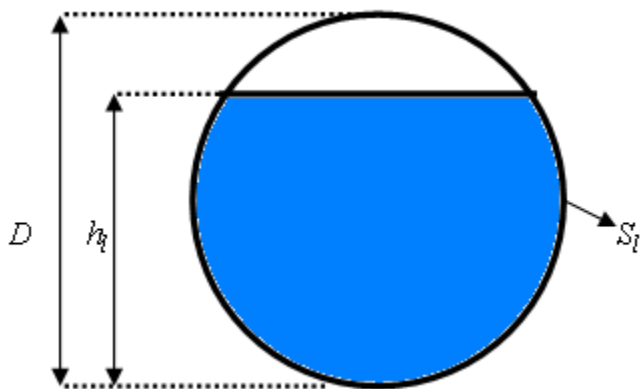


Figure 3.8 Schematic view of flow cross section in the pipe for stratified flow

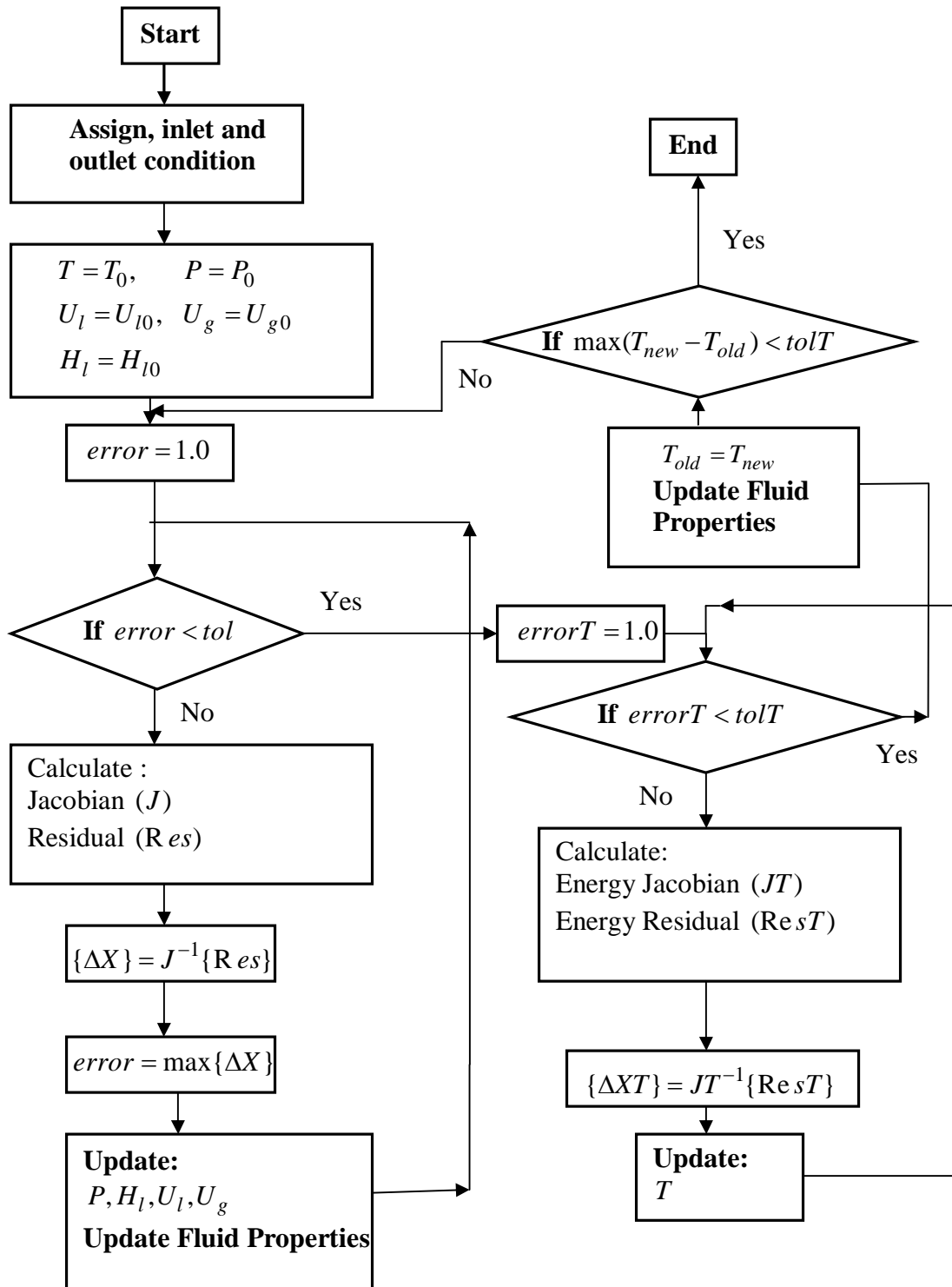


Figure 3.9 Numerical calculation procedure, using Newton method

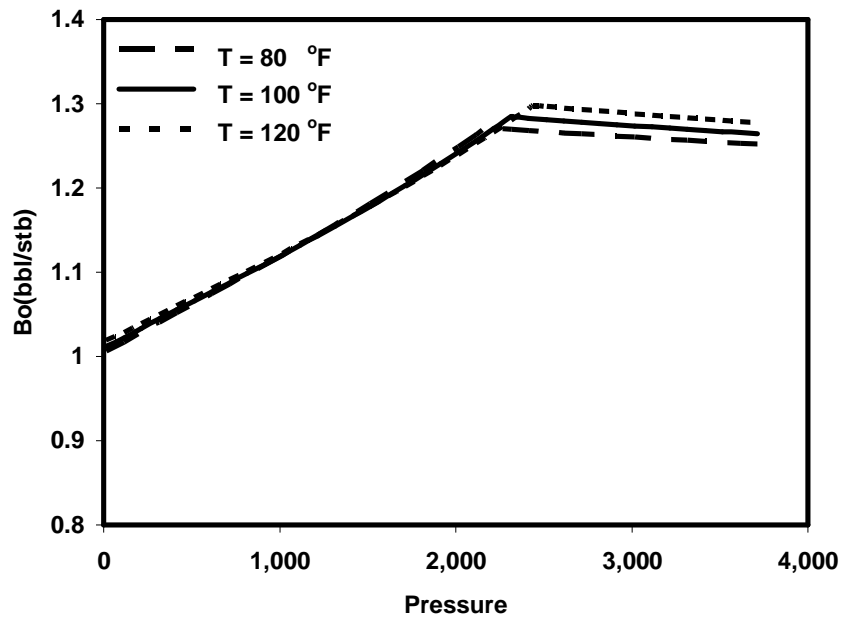


Figure 3.10 Oil formation volume factor for six-component fluid *versus* pressure for different temperatures

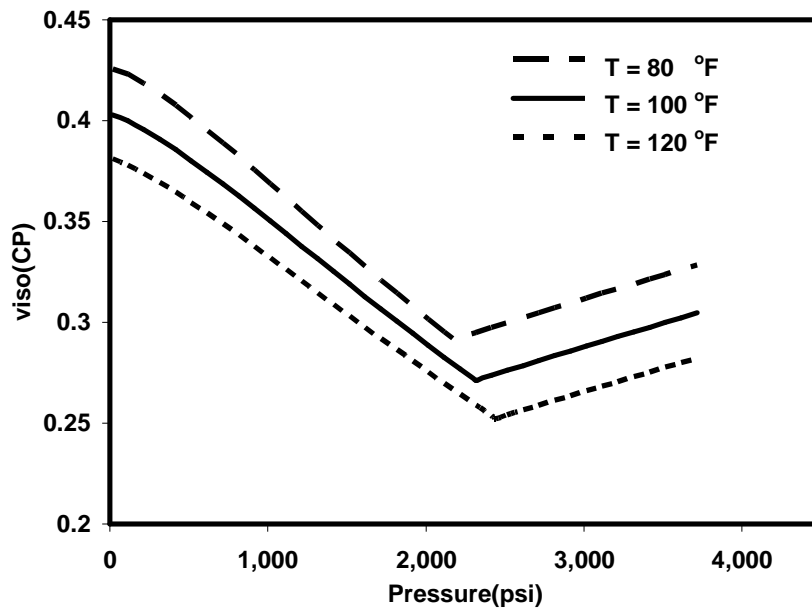


Figure 3.11 Oil viscosity for six-component fluid *versus* pressure for different temperatures

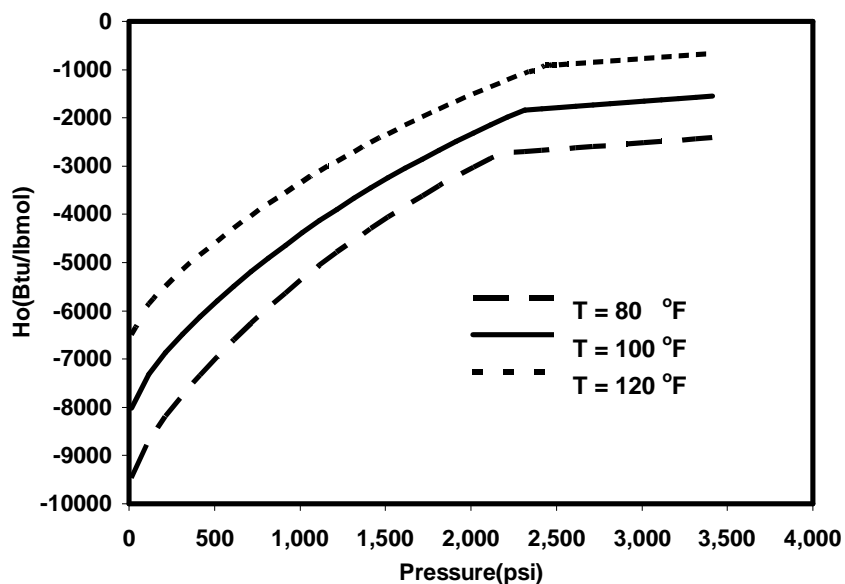


Figure 3.12 Oil enthalpy for six-component fluid *versus* pressure for different temperatures

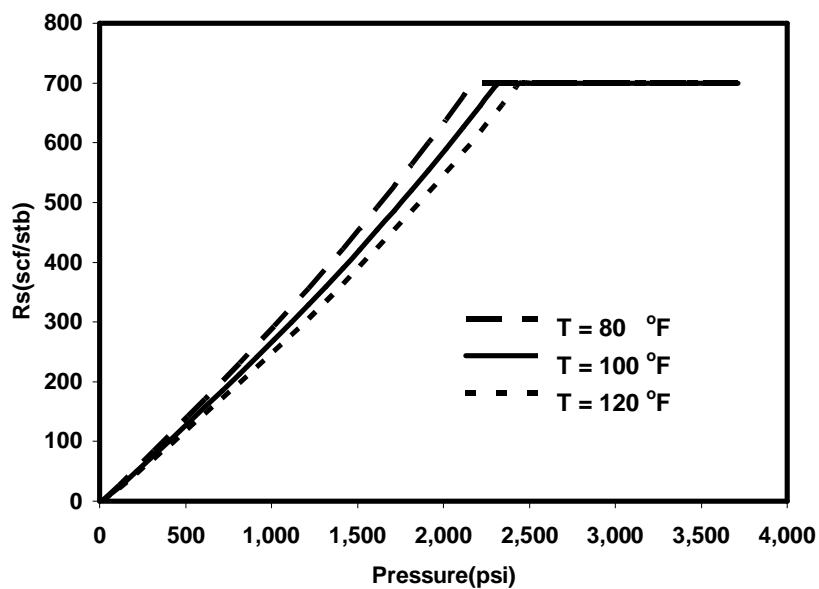


Figure 3.13 Solution gas ratio for six-component fluid *versus* pressure for different temperatures

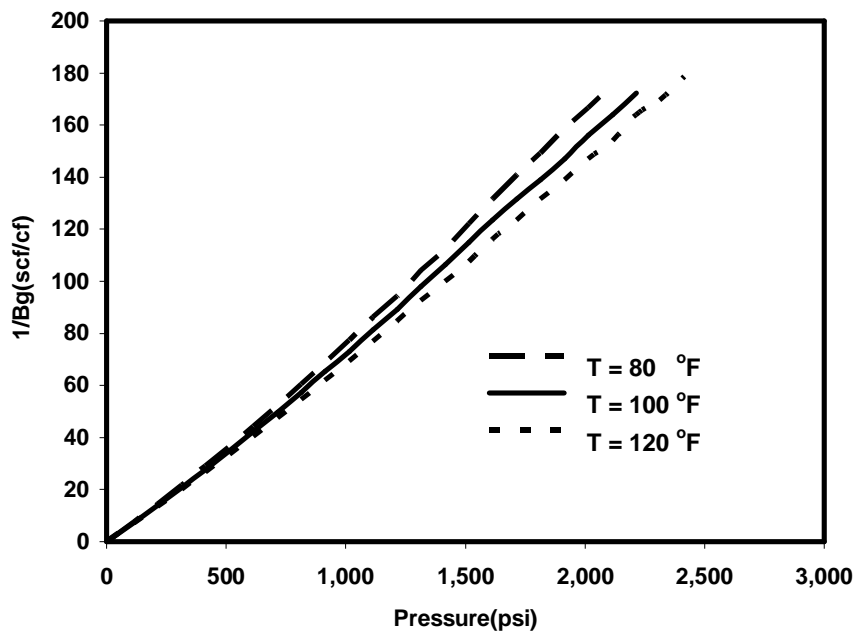


Figure 3.14 Gas formation volume factor for six-component fluid *versus* pressure for different temperatures

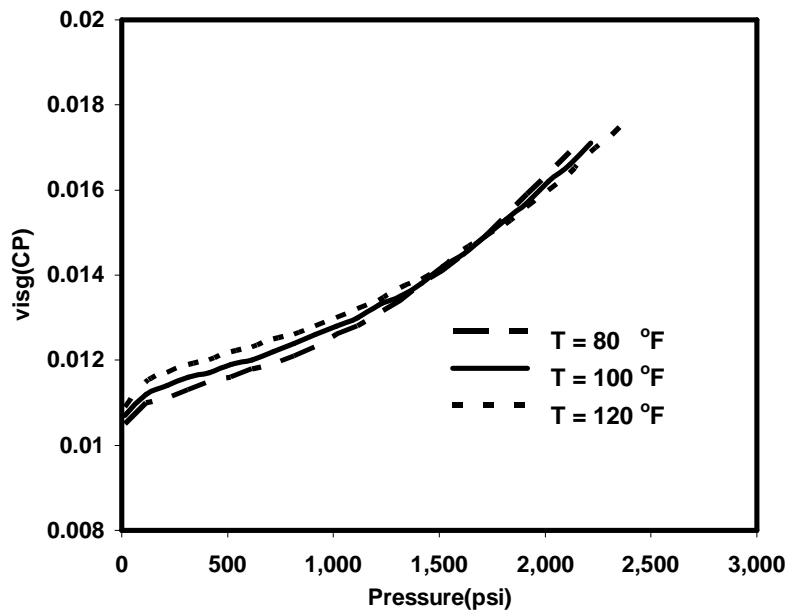


Figure 3.15 Gas viscosity for six-component fluid *versus* pressure for different temperatures

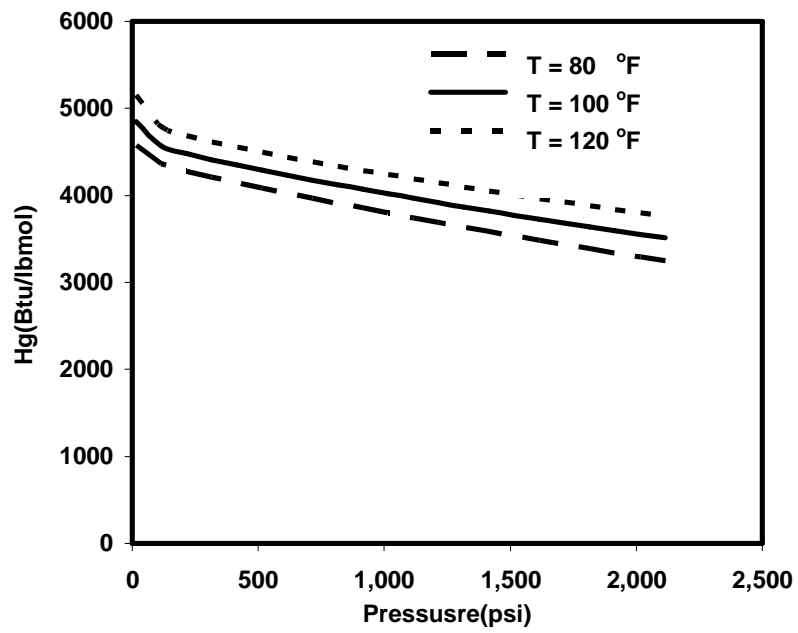


Figure 3.16 Gas enthalpy for six-component fluid *versus* pressure for different temperatures

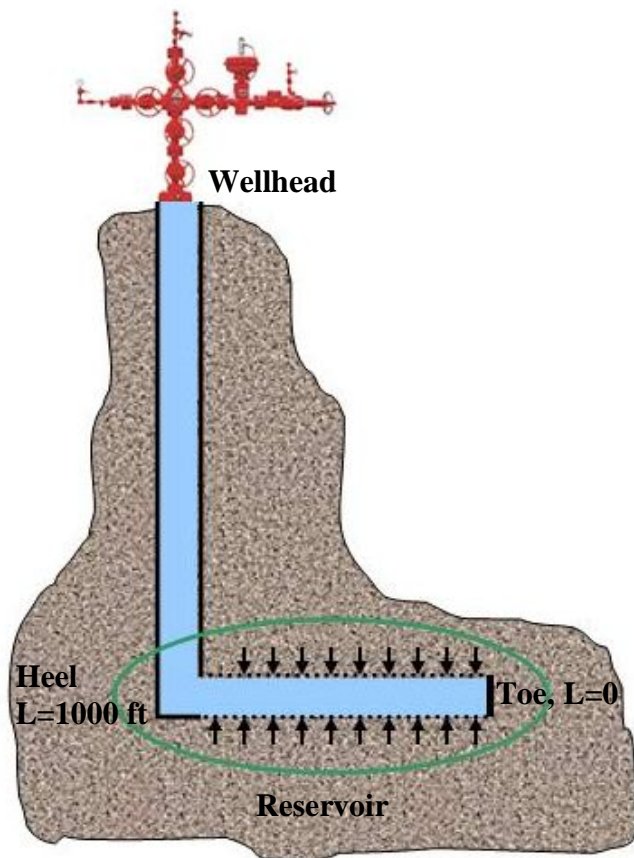


Figure 3.17 Schematic view of wellbore, reservoir and surface facility connection

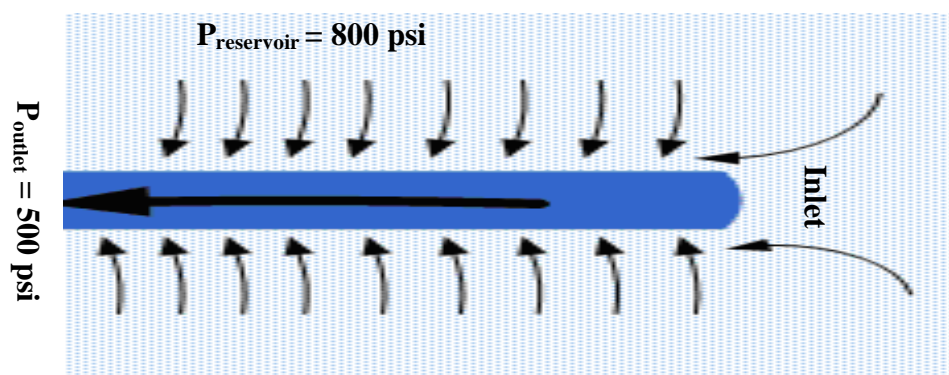


Figure 3.18 Schematic view of pipe and the setup in Case1

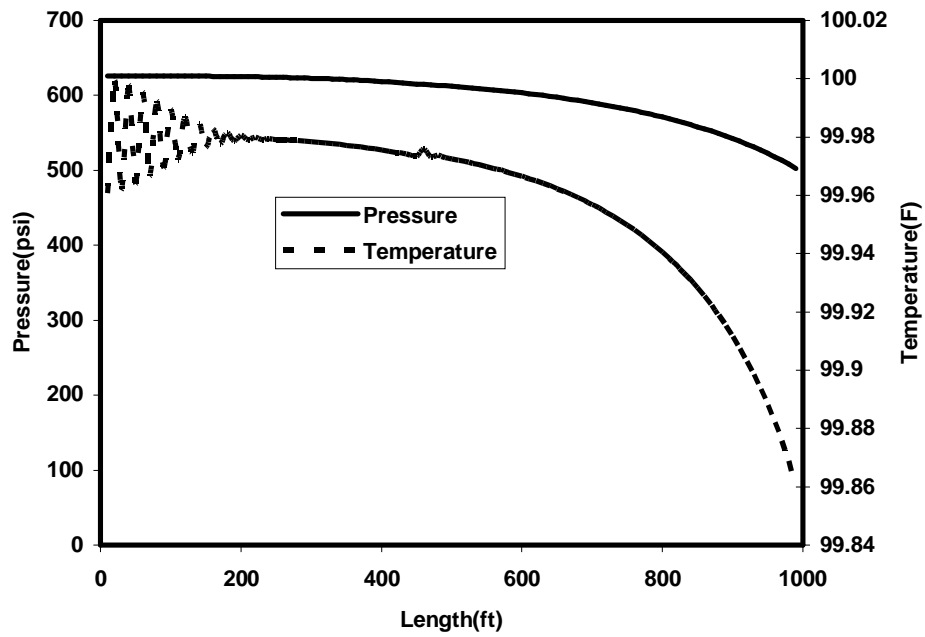


Figure 3.19 Pressure and temperature distributions along the well, Case 1

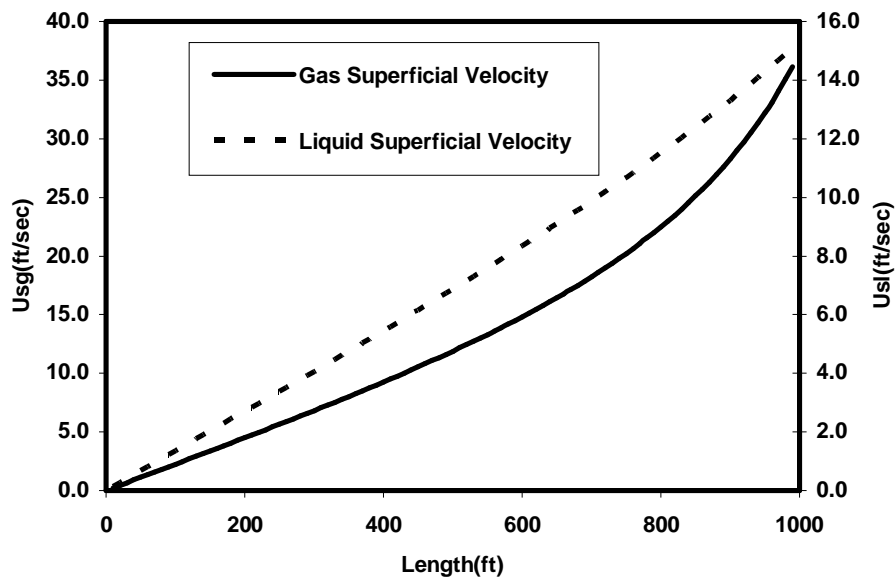


Figure 3.20 liquid and gas superficial velocity distribution, Case 1

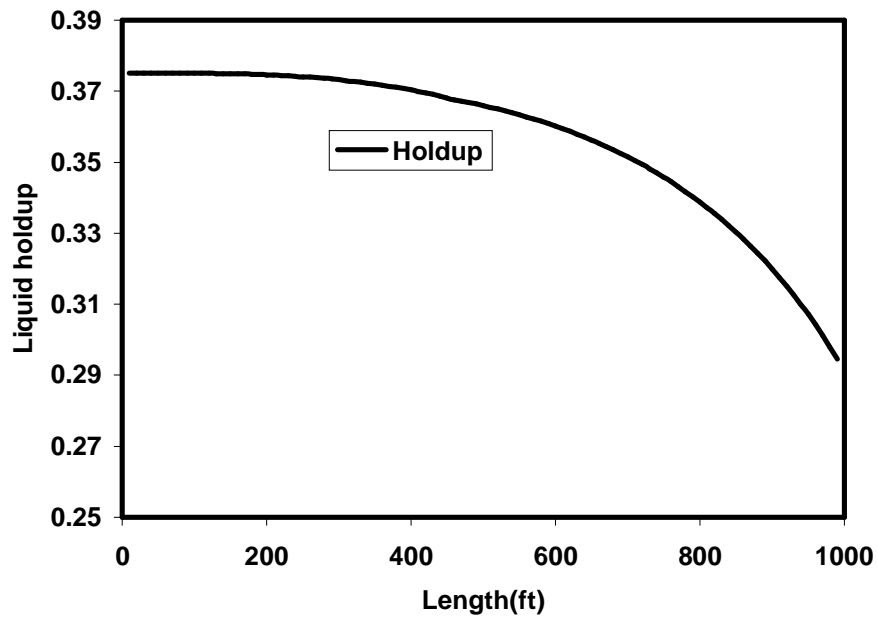


Figure 3.21 Liquid holdup distribution, Case 1

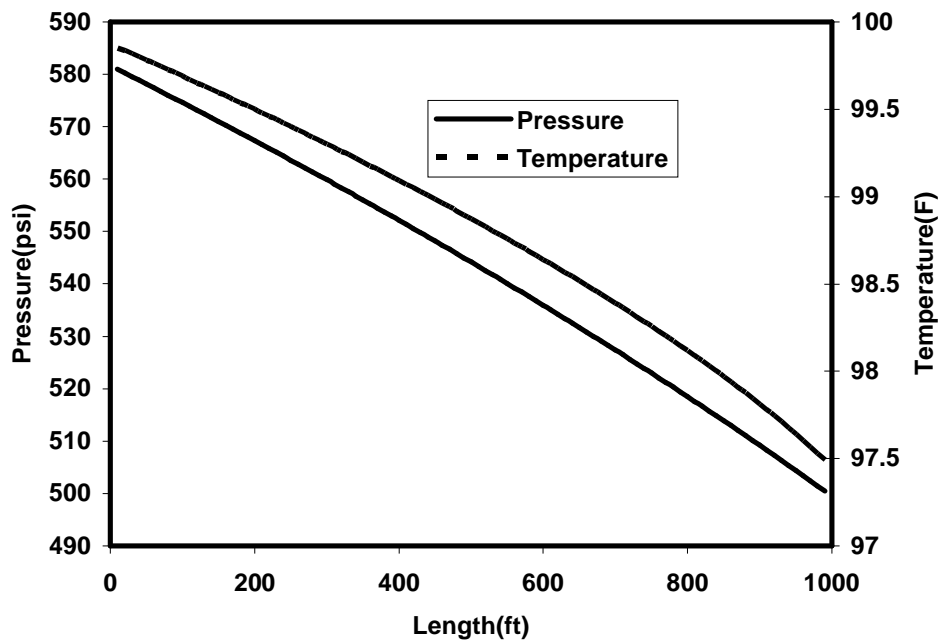


Figure 3.22 Pressure and temperature distribution along the well, Case 2

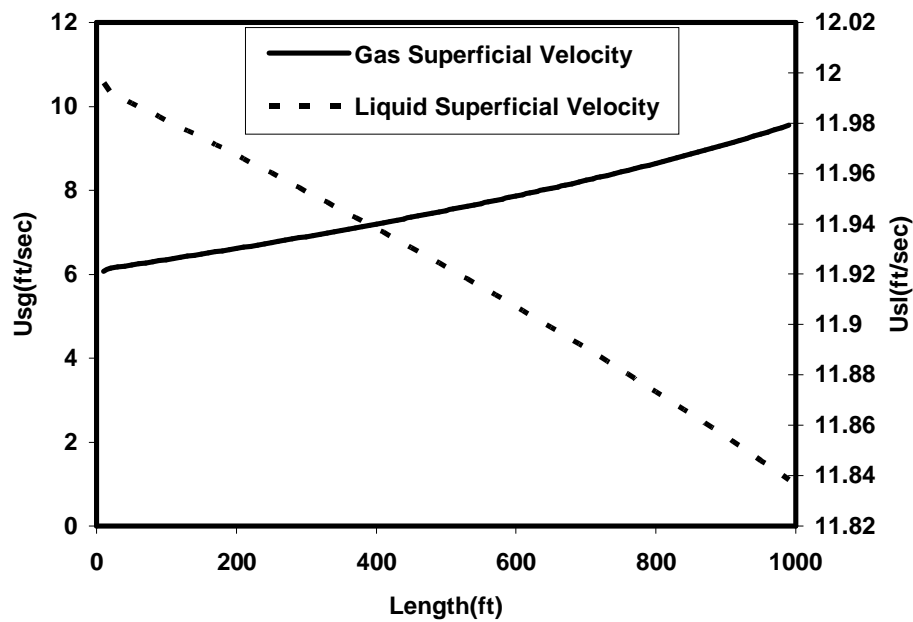


Figure 3.23 Liquid and gas superficial velocity distribution, Case 2

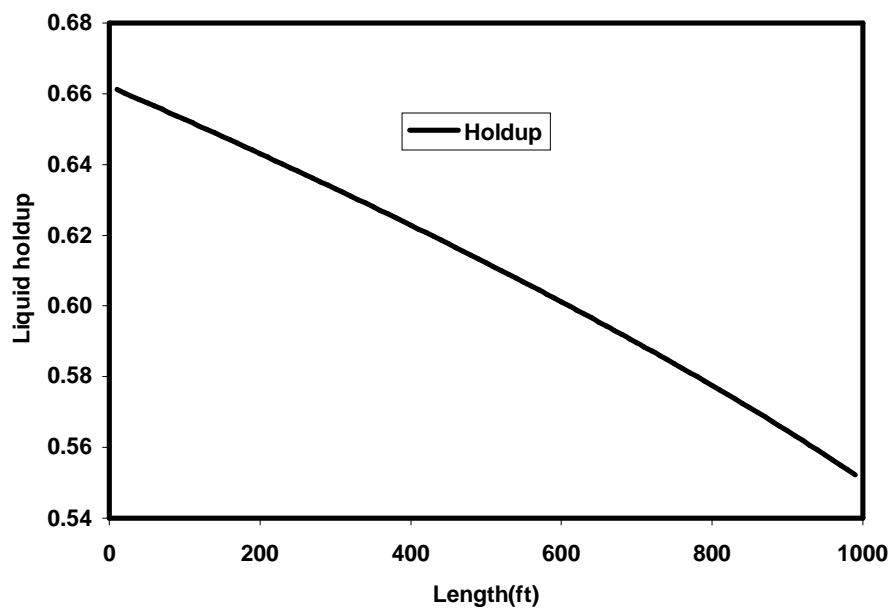


Figure 3.24 Holdup distribution, Case 2

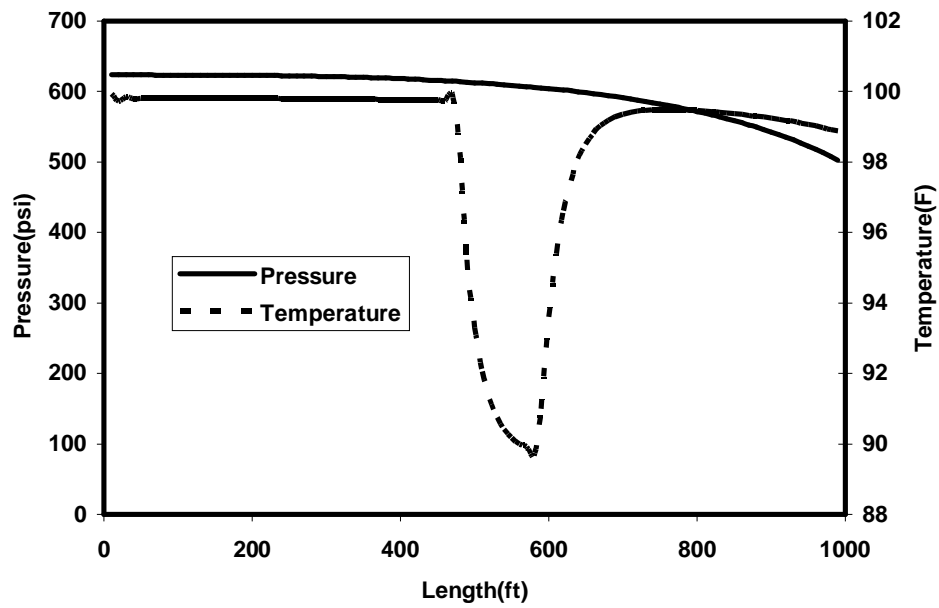


Figure 3.25 Pressure and temperature distribution, Case 3

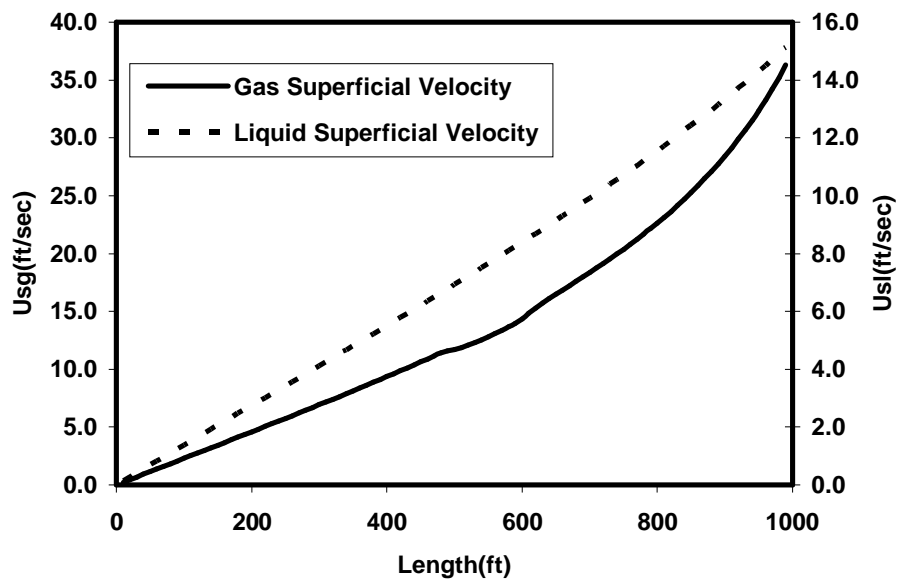


Figure 3.26 Liquid and gas superficial velocities, Case 3

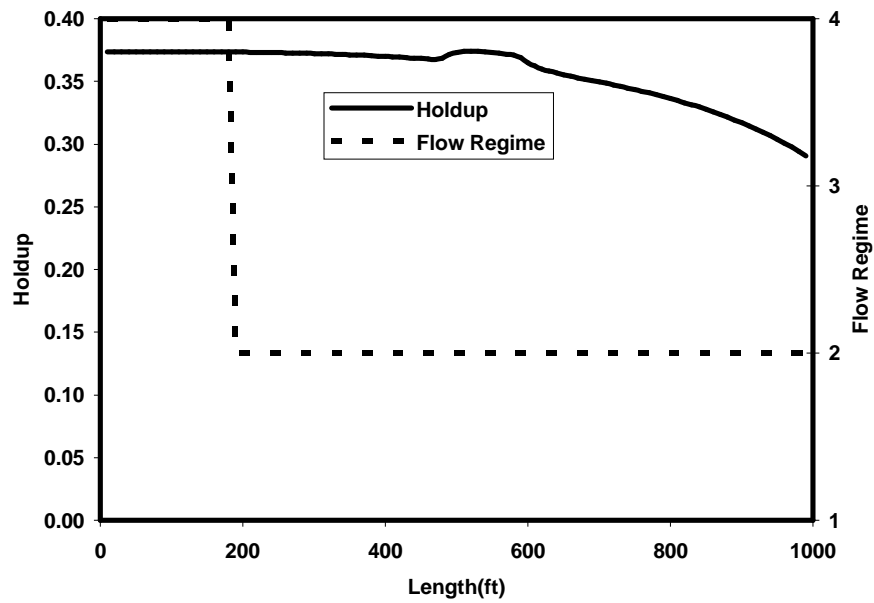


Figure 3.27 Holdup and flow regimes variations in the pipe, (1: bubbly, 2: intermittent, 3: annular, 4: stratified flow)

Chapter 4: Coupled Wellbore-Reservoir Compositional Model

In this chapter we introduce a compositional, simplified, mechanistic two-fluid model for the wellbore which is coupled to a compositional reservoir simulator. In Chapter 3, we introduced a pseudo-compositional standalone wellbore model. However, in this chapter we consider the hydrocarbon components tracking in the wellbore by a component based material balance equation.

In the following sections, we present the flow patterns in vertical inclination as well as horizontal inclination, governing equations, the methods for fluid properties calculation and the solution procedure for coupling the wellbore to the reservoir.

4.1 FLOW PATTERNS

In Chapter 3 we explained flow patterns map for horizontal inclination and we presented a mechanistic approach to predict the flow regimes in horizontal flow. Since in this chapter we have vertical and horizontal well connection we define the flow regimes in the vertical section in the following sections (Shoham, 2005).

4.1.1 *Bubble Flow*

At relatively low liquid rates and large holdup values bubbly flow exist in the two-phase flow system. In this flow regime bubbles are approximately homogeneously distributed in the liquid phase. Figure 4.1.a shows the schematic view of this flow regime.

4.1.2 *Slug Flow*

By increasing gas velocity small bubbles are agglomerated and generate larger bubbles which are called “Taylor-bubble”. These large Taylor bubbles can become almost equal to the entire pipe cross-section area. In addition to large gas bubbles liquid

slugs are generated which flow with the bubbles. Figure 4.1.b shows the schematic view of slug flow.

4.1.3 Churn Flow

Churn flow is very similar to slug flow but it occurs at higher gas velocity and is more chaotic. Figure 4.1.c shows the schematic view of churn flow.

4.1.4 Annular Flow

Likewise in horizontal flow, annular flow may also exist in vertical flow. At very high gas velocity a gas core in the middle of the pipe with an approximately uniform liquid film is generated around it. Figure 4.1.d shows the schematic view of annular flow.

4.1.5 Dispersed-Bubble Flow

At relatively high liquid rate discrete bubbles are generated which disperse in the liquid phase. For this flow pattern liquid phase is the continuous phase and bubbles are carried by liquid with no slippage. Hence, in this condition homogenous flow takes place. Figure 4.1.e shows the schematic view of the dispersed –bubble flow.

4.1.6 Flow regimes transition

In Chapter 3 we introduced a mechanistic model for flow patterns transition in different conditions. Similarly, in vertical flow there are mechanistic approaches to predict the flow patterns transitions. Figure 4.2 shows the flow regime identification procedure for vertical inclination.

As explained in section 4.1.1 at low gas velocity bubble flow exists. By increasing gas velocity bubbles are agglomerated and generate larger bubbles. In this condition, slug flow occurs. Taitel et al. (1980) showed that in transition from bubble to slug, gas fraction is approximately 0.25. Hence considering slip velocity, at transition condition it can be shown that:

$$v_s < \frac{v_{sg}}{0.25} - \frac{v_{sl}}{0.75} \quad (4.1)$$

Rearranging the variables and substituting the slip velocity based on bubble-rise velocity (Harmathy, 1960) following expression is obtained for transition from bubble to slug:

$$v_{sg} > 0.38 \left\{ \frac{g \sigma_s (\rho_l - \rho_g)}{\rho_l^2} \right\}^{1/4} + 0.333 v_{sl} \quad (4.2)$$

However by increasing liquid rates, large gas bubbles are broken down into small bubbles and dispersed-bubbly flow is occurred. Barnea (1987) showed that at this condition following expression is satisfied:

$$2 \left(\frac{0.4 \sigma_s}{(\rho_l - \rho_g) g} \right)^{0.5} \left(\frac{\rho_l}{\sigma_s} \right)^{0.6} \left(\frac{f}{2d} \right)^{0.4} (v_{sl} + v_{sg})^{1.2} > 0.725 + 4.15 \left(\frac{v_{sg}}{v_{sl} + v_{sg}} \right)^{0.5} \quad (4.3)$$

In the slug flow condition Taylor-bubbles and liquid slugs move together in the system. As the gas velocity increases, more chaotic flow is occurred where churn flow is appeared. Ansari et al. (1994), showed Equation 4.4 for transition from slug flow to churn flow:

$$v_{sg} > 3.17 v_{sl} \quad (4.4)$$

When gas velocity is very large annular flow occurs. Taitel et al. (1980) showed Equation as the critical gas superficial velocity for annular flow.

$$v_{sg} > 3.1 \left\{ \frac{g \sigma_s (\rho_l - \rho_g)}{\rho_g^2} \right\}^{1/4} \quad (4.5)$$

4.2 FLOW EQUATIONS FOR THE WELLBORE

Governing equations for the coupled wellbore-reservoir system encompass two sets of transport equations plus an equation-of-state-based flash calculation to obtain phase properties and compositions. One set of flow equations calculates pressure, velocity, temperature, and composition in the wellbore segments and the other calculates the fluid flow equations in the reservoir gridblocks. Figure 4.3 shows the reservoir and wellbore flow domains. In this section, we introduce the governing equations for the wellbore and describe the reservoir governing equations in Appendix D.

For the wellbore transport equations we make the following assumptions:

- the wellbore has two sections, a horizontal and a vertical;
- a one-dimensional flow is considered in the wellbore;
- the wellbore is explicitly coupled to the reservoir;
- the source or sink term are coupled in the wellbore by well indices values for each phase;
- the steady-state condition in the wellbore is considered since the transient time in the producer well is much smaller than in the reservoir; (In Chapter 5 we will show that transient period for wellbore is in the order of minutes. However, in general, reservoir time-step sizes are much greater than an hour)

- the liquid phase is the oil/water mixture in case that water exists in the flow;
- the liquid properties are calculated by volumetric averaging between water and oil;
- the compositional approach (Peng Robinson Equation of State) is applied to calculate the fluid properties;
- interface shear force, wall shear force, and body forces are modified for different flow regimes;
- the momentum equation is applied to a bulk of continuous phases flowing in the wellbore;
- the separate flow is considered for stratified and annular flow regimes;
- liquid droplet entrainment to the gas core is also considered in annular flow;
- both gas and liquid phases have identical pressure and temperature;
- pressure, holdup, and temperature are calculated in the center of the wellbore segments and liquid and gas velocities and mixture velocity are calculated in the edges of the wellbore segments.

4.2.1 Components Mass Balance

As Equation (4.6) shows, for any hydrocarbon component, the output mass flow rate to wellbore or reservoir blocks is equal to the input mass flow rate from adjacent wellbore or reservoir blocks,

$$(Mass_{in} - Mass_{out}) \pm (Source / Sink) = 0 \quad (4.6)$$

Substituting the input mass rate, output mass rate and the source and sink terms, we obtain:

$$dt(\dot{m}_{ic}(i) - \dot{m}_{ic}(i-1)) - \sum_{j=1}^{n_p} PI_j dx dt \rho_j \frac{Mw_{ic}}{Mw_j} x_{icj} (P_{res} - P(i)) = 0. \quad (4.7)$$

In the above equation, i is the segment number, ic is the component number ($1 \dots n_c + 1$), and PI_j is the well index of water, oil, and gas phases. Since the solubility of the hydrocarbon components in water and the solubility of water in hydrocarbon phases are neglected, the water productivity index only appears for component $n_c + 1$, which is water.

The well index for each fluid can be calculated by Equation (4.8). In this equation, we have two options to obtain the equivalent wellbore radius, r_o . It can be obtained by either Peaceman (1983) or Babu and Odeh's (1989) approaches,

$$PI_j = \frac{2\pi \sqrt{k_y k_z} \Delta x}{0.15802 [\ln(\frac{r_o}{r_w}) + Skin]} \lambda_{rj}. \quad (4.8)$$

Assuming small dx and dt values and dividing Equation (4.7) by $dx dt$, we obtain the partial differential form of this equation:

$$\frac{d\dot{m}_{ic}}{dx} - \sum_{j=1}^{n_p} PI_j \rho_j \frac{Mw_{ic}}{Mw_j} x_{icj} (P_{res} - P_{well}) = 0. \quad (4.9)$$

In the above equation, the first term is the convection term for mass flow rate of the component ic and the second term is the mass flux from the reservoir for component ic .

4.2.2 Momentum Balance

In the following sections we present the momentum equations for different flow regimes in vertical and horizontal inclinations. In general, we introduce the input/output momentum flux, body gravity force, and wall shear forces in the momentum equation for different flow regimes. In Chapter 3, Figure 3.1 shows these forces that can act on the phases.

4.2.2.1 Stratified and Annular-Mist Flow Momentum Equation

Equation (4.10) shows the momentum conservation for liquid phase in the segment i where stratified and annular-mist flows exist.

$$\begin{aligned} & \Delta t [\rho_l(i-1)U_l^2(i-1) - \rho_l(i)U_l^2(i)] - (AH_l(i)dx)dt \rho_l(i)g \sin \theta + \\ & \Delta t [H_l(i-1)P(i-1) - H_l(i)P(i)] - S_l dx dt \tau_{wl} - S_i dx dt \tau_i = 0. \end{aligned} \quad (4.10)$$

In the above equation, S_l is the wall-wetted perimeter by the liquid phase and S_i is the inter-phase perimeter. Depending on the type of flow regime, S_l and S_i vary. S_l can be the perimeter of the pipe or a portion of that. For bubbly flow, intermittent flow, and annular flow, we assume that $S_l = \pi D$. However, for stratified flow we use the following equation:

$$S_l \approx D(\pi - \cos^{-1}(2H_l - 1)). \quad (4.11)$$

S_i also depends on flow regime. For stratified flow regime we have:

$$S_i = D\sqrt{1 - (2H_l - 1)^2}, \quad (4.12)$$

and for the annular flow regime, we have :

$$S_i = \pi D \sqrt{1 - H_l} . \quad (4.13)$$

In Equation (4.10), τ_{wl} and τ_i are the wall shear stress and the inter-phase shear stress, respectively. The wall shear stress and inter-phase shear stress are calculated as follows:

$$\tau_{wl} = \frac{1}{2} f_{wl} \rho_l U_l^2 , \quad (4.14)$$

$$\tau_i = \frac{1}{2} f_i \rho_g |U_g - U_l| (U_g - U_l) . \quad (4.15)$$

As explained in Chapter 3, f_{wl} can be calculated by Equation (3.42) and f_i for stratified flow can be calculated by Equation (3.52).

For annular flow inter-phase shear factor, f_i , Petalas and Aziz (2000) showed another equation as below:

$$f_i = 0.24 f_c \left(\frac{\sigma}{\rho_c U_c D_c} \right)^{0.085} \text{Re}_{ef}^{0.305} , \quad (4.16)$$

where f_c is the Fanning friction factor based on the gas core Reynolds number and core hydraulic diameter, D_c .

After rearranging the coefficients and converting the units to psi and ft/sec in Equation (4.10) we obtain:

$$\begin{aligned} & \left[\frac{\rho_l(i)U_l^2(i) - \rho_l(i-1)U_l^2(i-1)}{dx} \right] + H_l(i)\rho_l(i)g \sin \theta + 144gc \left[\frac{H_l(i)P(i) - H_l(i-1)P(i-1)}{dx} \right] \\ & + \frac{S_l\tau_{wl}}{A} + \frac{S_i\tau_i}{A} = 0. \end{aligned} \quad (4.17)$$

Writing Equation (4.17) in partial differential form, we have:

$$\frac{\partial \rho_l U_l^2}{\partial x} + H_l \rho_l g \sin \theta + 144gc \left(\frac{\partial H_l P}{\partial x} \right) + \frac{S_l \tau_{wl}}{A} + \frac{S_i \tau_i}{A} = 0. \quad (4.18)$$

In the above equation, ρ_l is the liquid density, which consists of water and oil densities and U_l is the liquid phase velocity. The oil phase density is calculated by classical flash calculation and U_l is calculated by mass flow rate of each component that is transported by the liquid,

$$U_l = \frac{\sum_{i=1}^{n_c+1} \dot{m}_{il}}{A\rho_l}. \quad (4.19)$$

Changing the indices from l to g in Equation (4.18), we achieve the momentum equation for the gas phase in stratified and annular flow regimes:

$$\frac{\partial \rho_g U_g^2}{\partial x} + \alpha \rho_g g \sin \theta + 144gc \left(\frac{\partial P}{\partial x} \right) \alpha + \frac{S_g \tau_{wg}}{A} - \frac{S_i \tau_i}{A} = 0. \quad (4.20)$$

Likewise, we can calculate the wetted perimeter by the gas phase, S_g , for different flow regimes. In the stratified flow we approximately have:

$$S_g \approx D(\cos^{-1}(2H_l - 1)) . \quad (4.21)$$

Combining Equations (4.18) and (4.20), we obtain a system of nonlinear equations for separated flows that are solved to calculate the pressure and the holdup.

4.2.2.2 Bubbly Flow Momentum Equation

In bubbly flow regime we apply momentum equation for fluids mixture. Considering two-phase mixture velocity as

$$U_{tp} = \frac{\rho_l}{\rho_{tp}} U S_l + \frac{\rho_g}{\rho_{tp}} U S_g , \quad (4.22)$$

and two-phase density as

$$\rho_{tp} = \rho_l H_l + \rho_g (1 - H_l) . \quad (4.23)$$

Momentum equation becomes

$$\begin{aligned} & A dt [\rho_{tp} (i-1) U_{tp}^2 (i-1) - \rho_{tp} (i) U_{tp}^2 (i)] - (A dx) dt \rho_{tp} (i) g \sin \theta + A dt [P(i-1) - P(i)] \\ & - \pi D dx dt \tau_w = 0 . \end{aligned} \quad (4.24)$$

Rearranging the coefficients and converting the units to psi and ft/sec in equation (4.24) we obtain

$$\begin{aligned} & \left[\frac{\rho_{tp}(i)U_{tp}^2(i) - \rho_{tp}(i-1)U_{tp}^2(i-1)}{dx} \right] + \rho_{tp}(i)g \sin \theta + 144gc \left[\frac{P(i) - P(i-1)}{dx} \right] \\ & + \frac{\pi D \tau_w}{A} = 0. \end{aligned} \quad (4.25)$$

Writing Equation (4.25) in partial differential form, we have:

$$\frac{\partial \rho_{tp} U_{tp}^2}{\partial x} + \rho_{tp} g \sin \theta + 144gc \left(\frac{\partial P}{\partial x} \right) + \frac{\pi D \tau_w}{A} = 0. \quad (4.26)$$

To calculate liquid holdup in bubbly flow regime we can make no-slip assumption and use

$$H_l = \frac{US_l}{US_l + US_g}, \quad (4.25)$$

or we can apply drift flux model. Using drift flux model (Mishima and Ishii, 1984) to consider slippage in bubbly flow we obtain

$$U_g = C_0 U_m + U_0, \quad (4.26)$$

where

$$C_0 = C_w - 0.2 \left(\frac{\rho_g}{\rho_l} \right)^{0.5}, \quad (4.27)$$

$$U_0 = 1.53 \left(\frac{g(\rho_l - \rho_g)\sigma}{\rho_l^2} \right)^{0.25} \sin(\theta), \quad (4.28)$$

Usually $C_0 = 1.2$ is used in the Equation (4.26). Thus, liquid holdup is calculated as

$$H_l = 1 - \frac{US_g}{C_0 U_m + U_0}. \quad (4.29)$$

4.2.2.3 Intermittent Flow Momentum Equation

Likewise, considering momentum equation for the mixture of fluids we obtain following equation for intermittent flow:

$$\begin{aligned} & Adt[\rho_{tp}(i-1)U_{tp}^2(i-1) - \rho_{tp}(i)U_{tp}^2(i)] - (Adx)dt\rho_{tp}(i)g \sin \theta + Adt[P(i-1) - P(i)] \\ & - \bar{S}dxdt \bar{\tau}_w = 0. \end{aligned} \quad (4.30)$$

As can be seen in Figure 4.4, considering a slug unit, total friction force can be written as

$$\bar{S}dx\bar{\tau}_w = L_s\pi D\tau_{ls} + L_f(S_{lf}\tau_{lf} + S_{gb}\tau_{gb}). \quad (4.31)$$

In Equation (4.31) L_s is slug length, L_f is liquid film length, S_{lf} is wetted perimeter by liquid film, S_{gb} is wetted perimeter by gas bubble, τ_{ls} is liquid slug shear stress, τ_{lf} is liquid film shear stress and τ_{gb} is gas bubble shear stress. Tatiel and Barnea (1990) showed a slug model which addresses these parameters.

However we can simplify equation (4.30) by assuming shear stress as a homogenous model. Hence, by writing two-phase shear stress we obtain

$$Adt[\rho_{tp}(i-1)U_{tp}^2(i-1) - \rho_{tp}(i)U_{tp}^2(i)] - (Adx)dt\rho_{tp}(i)g \sin \theta + Adt[P(i-1) - P(i)]$$

$$-\pi D dx dt \tau_{tp} = 0. \quad (4.32)$$

For intermittent flow, liquid holdup also can be calculated as below:

$$H_l = \frac{H_{ls} U_{tp} + U_{gdb} (1 - H_{ls}) - U S_g}{U_{tp}}. \quad (4.33)$$

Gregory et al. (1978) showed that using U_m in m/sec H_{ls} is calculated as

$$H_{ls} = \frac{1}{1 + (U_m / 8.66)^{1.39}}. \quad (4.34)$$

Harmathy (1960) also showed that

$$U_{gdb} = C_0 U_m + U_b, \quad (4.35)$$

$$\text{where } U_b = 1.53 \left(\frac{g(\rho_l - \rho_g)\sigma}{\rho_l^2} \right)^{0.25} \sin(\theta).$$

4.2.3 Energy Balance

The energy equation was applied to the mixture of fluids, as shown in Equation (4.36):

$$\rho_l U_l \frac{\partial}{\partial x} \left(\bar{h}_l + \frac{U_l^2}{2} + g z_h \sin \theta \right) + \rho_g U_g \frac{\partial}{\partial x} \left(\bar{h}_g + \frac{U_g^2}{2} + g z_h \sin \theta \right) + Q_{exchange} = 0, \quad (4.36)$$

Rewriting Equation (4.36) in a simplified form for the mixture of liquid and gas, we obtain:

$$\rho_m U_m \frac{\partial}{\partial x} (\bar{h}_m + \frac{U_m^2}{2} + gz_h \sin \theta) + Q_{exchange} = 0 \quad (4.37)$$

where the subscript, m , represents the average mixture value. The first term in Equation (4.37), $\rho_m U_m \frac{\partial}{\partial x} (\bar{h}_m + \frac{U_m^2}{2} + gz_h \sin \theta)$, is the energy convection in the x direction due to the enthalpy exchange, acceleration and gravity. The second term, $Q_{exchange}$, is heat exchange from the surrounding formation to the wellbore. $Q_{exchange}$ consists of two terms as conduction heat exchange and materials influx heat exchange from the reservoir to the wellbore. Hence,

$$Q_{exchange} = 2\pi r_{to} U_{to} (T(i) - T_{res}(i)) - [\frac{PI_l \rho_{lres}}{A}] (P_{res} - P(i)) h_{lres}(i) - [\frac{PI_g \rho_{gres}}{A}] (P_{res} - P(i)) h_{gres}(i). \quad (4.38)$$

The enthalpy is related to the pressure and temperature, via the heat capacity, $(C_p(\frac{Btu}{Flbm}))$, and the Joule-Thomson coefficient, $(\eta(\frac{^{\circ}F}{ft^2}))$:

$$d\bar{h}_l = C_{pl} dT_l - (\frac{144}{J_c}) \eta_l C_{pl} dP, \quad (4.39)$$

$$d\bar{h}_g = C_{pg} dT_g - (\frac{144}{J_c}) \eta_g C_{pg} dP, \quad (4.40)$$

$$d\bar{h}_m = C_{pm}dT - \left(\frac{144}{J_c}\right)\eta_m C_{pm}dP, \quad (4.41)$$

C_{pm} and η_m are mixture parameters:

$$C_{pm} = C_{pg}(1 - H_l)\frac{\rho_g}{\rho_m} + C_{pl}H_l\frac{\rho_l}{\rho_m}, \quad (4.42)$$

$$\eta_m = \frac{1}{C_{pm}\rho_m} \left\{ (1 - H_l)\left(\frac{-T}{Z}\right)\left(\frac{dZ}{dT}\right)_P + H_l \right\}, \quad (4.43)$$

where, Z is the compressibility factor. Hence, we can calculate the liquid and gas enthalpies at the reservoir condition, as well as the enthalpy gradient in the wellbore, by using Equations (4.39), (4.40), and (4.41). Substituting the enthalpy difference from Equation (4.41), and $Q_{exchange}$ from Equation (4.38) into the energy Equation (4.37), we obtain:

$$\begin{aligned} & C_{pm} \frac{\partial T}{\partial x} - \eta_m C_{pm} \frac{\partial P}{\partial x} + U_m \frac{\partial U_m}{\partial x} + \frac{2\pi r_{to} U_{to} (T(i) - T_{res}(i))}{\rho_m U_m} \\ & - \frac{\left[\frac{PI_l \rho_{lres}}{A}\right](P_{res} - P(i))\bar{h}_{lres}(i) \left[\frac{PI_g \rho_{gres}}{A}\right](P_{res} - P(i))\bar{h}_{gres}(i)}{\rho_m U_m} = 0. \end{aligned} \quad (4.44)$$

Rearranging Equation (4.44) we have

$$\frac{\partial T}{\partial x} + \frac{2\pi r_{to} U_{to} T}{C_{pm} \rho_m U_m} = \eta_m \frac{\partial P}{\partial x} - \frac{U_m}{C_{pm}} \frac{\partial U_m}{\partial x} + \frac{2\pi r_{to} U_{to} T_{res}}{\rho_m U_m} + \frac{F(T_{res}, P_{res})}{C_{pm} \rho_m U_m}, \quad (4.45)$$

where $F(T_{res}, P_{res})$ is a function of the reservoir temperature and pressure and corresponds to the enthalpy influx from the reservoir to the wellbore. Equation (4.45) can be discretized and solved, numerically, or can be solved, analytically.

Alves et al. (1987) showed that the analytical solution for the temperature in a vertical well is given by:

$$T = (T_{ebh} - g_T L) + (T_i - T_{ebh}) \exp\left(-\frac{L}{A}\right) + g_T A [1 - \exp\left(-\frac{L}{A}\right)] + \frac{1}{\rho_m C_{pm}} \frac{dP}{dL} \phi A [1 - \exp\left(-\frac{L}{A}\right)], \quad (4.46)$$

where T_{ebh} is the reservoir bottom-hole temperature, T_i is temperature at depth L , and g_T is the thermal gradient. A and ϕ parameters are defined as follows:

$$A = \frac{C_{pm} \rho_m U_m}{2\pi r_o U_{to}}, \quad (4.47)$$

$$\phi = (\rho_m \eta_m C_{pm} \frac{dP}{dL} - \rho_m g \sin(\theta) - \rho_m U_m \frac{dU_m}{dL}) / \frac{dP}{dL}. \quad (4.48)$$

Modifying ϕ and g_T in Equation (4.46), we can obtain an analogous equation for horizontal wells. If we neglect the gravity and the thermal gradient by assuming $\theta = 0$ and $g_T = 0$ in the horizontal section, and if we add enthalpy influx to the equation we obtain:

$$T = (T_{ebh}) + (T_i - T_{ebh}) \exp\left(-\frac{L}{A}\right) + \frac{1}{\rho_m C_{pm}} \frac{dP}{dL} \phi A [1 - \exp\left(-\frac{L}{A}\right)]. \quad (4.49)$$

where

$$\phi = (\rho_m \eta_m C_{pm} \frac{dP}{dL} - \rho_m U_m \frac{dU_m}{dL} + \frac{F(T_{res}, P_{res})}{C_{pm} \rho_m U_m}) / \frac{dP}{dL}. \quad (4.50)$$

Thus, by introducing T_i as the boundary condition at the edge of the bottom segment with length L , and using the pressure and average mixture velocity gradient along the segment, we can obtain the temperature at the other edge of the segment.

4.2.4 Phase-Equilibrium Equation

The phase equilibrium in a wellbore segment consists of fugacity (the equality of each components fugacity in liquid and gas phases) and Rachford-Rice equations, according to Pedersen and Christensen (2007):

$$f_{ic}^o = f_{ic}^g, \quad ic = 1, \dots, nc, \quad (4.51)$$

$$r(v) = \sum_{ic=1}^{n_c} \frac{(K_{ic} - 1)z_{ic}}{1 + v(K_{ic} - 1)} = 0, \quad (4.52)$$

where v is the mole fraction of gas in the absence of water, K_{ic} is the equilibrium ratio, z_{ic} is the overall mole fraction of component ic in the feed, and $r(v)$ is the residual of the Rachford-Rice equation. Equations (4.51) and (4.52) are solved iteratively to obtain the phase fractions and phase composition. Since in the wellbore segments the phase velocities are much larger than the fluid flow in the reservoir, phase-bypass can occur in the wellbore system. Hence, we have local equilibrium and slip velocity between the phases. Non-equilibrium portions of the moving phases should be calculated; otherwise, in those cases where velocities are large, holdup and phase fractions obtained by flash calculations are not consistent. For this reason, the portion of the liquid or the gas phase

that is not in equilibrium with the other phase is defined as L_{ne} or G_{ne} , Figure 4.5. We assume that the compositions of non-equilibrium and equilibrium portions are the same. Thus,

$$H_l = \frac{(L_e + L_{ne})(1 + WOR)Z_o}{(L_e + L_{ne})(1 + WOR)Z_o + Z_g G} = \frac{(1 + L_{ne}/L_e)(1 + WOR)Z_o}{(1 + L_{ne}/L_e)(1 + WOR)Z_o + Z_g (G/L_e)}, \quad (4.53)$$

where Z_o and Z_g are oil and gas compressibility factors, respectively. G is the amount of gas moles, $L_e + L_{ne}$ is the total oil moles, and WOR is the water-oil ratio. If we assume G/L_e to be the gas-oil molar ratio at equilibrium, which is obtained from Equations (4.51) and (4.52), then L_{ne}/L_e is calculated as follows:

$$L_{ne}/L_e = \frac{(1 + WOR)Z_o H_l + Z_g (G/L_e) H_l - (1 + WOR)Z_o}{Z_o (1 + WOR)(1 - H_l)}. \quad (4.54)$$

Equation (4.54) is iteratively solved for convergence to both L_{ne}/L_e and holdup values. Consequently, it should be noted that L_{ne}/L_e affects the liquid flow rate and the holdup values.

4.3 COUPLING OF THE WELLBORE TO THE RESERVOIR

Figure 4.6 shows the schematic view of the wellbore segments and the reservoir grid blocks. As can be seen, we have two separate flow domains which are coupled via the perforated zone. In the reservoir, the governing equations for the wellbore are treated as a source/sink terms and vice versa. Hence, having the solution for one system (for pressure and flow rates) the other system's boundary condition as source and sink is also obtained.

There are different methods for coupling the wellbore to the reservoir. Behie et al. (1985) solved both reservoir and wellbore equations, simultaneously. Pourafshary et al. (2007) used an iterative substitution method. In this study, we used an iterative method for the coupled wellbore-reservoir simulation. Wellbore equations are solved separately and then the results are passed to the reservoir boundary condition via the source/sink terms in the transport equation. The reservoir simulator that we used was the General Purpose Adaptive Simulator which is a multi-component multiphase reservoir simulator (Wang et al., 1997; 1999; Han et al., 2006). The governing equations and the description are presented in Appendix E.

4.4 SOLUTION PROCEDURE

Since the flowing stream from reservoir up to the wellhead can change from single phase to two-phase and vice versa a robust wellbore model should be employed. In marching algorithm since each node is solved separately the singularity problem due to phase change can be resolved easily. Hence, in this chapter we use the marching method to solve the flow variables in the wellbore. In Chapter 3 we solved the wellbore equations fully implicitly. We used the liquid momentum equation to obtain liquid velocity, the gas momentum equation for gas velocity, the mixture of gas and liquid mass equation to calculate pressure, and the liquid mass conservation to calculate liquid holdup. However, in this chapter we solve the transport equations, differently. We apply the components mass conservations to calculate the mass flow rate of each component and then calculate the phase velocities based on Equation (4.19). We use the momentum equations to calculate pressure drop and holdup value.

Figure 4.7 shows the solution procedure. We first define the bottom-hole pressure in the boundary segment and solve the components mass flow rate from the continuity

equation in this segment. Subsequently, we perform a flow regime transition analysis, to identify the dominant flow regime in the segment. Considering the dominant flow regime, we solve the liquid and gas momentum equations iteratively to obtain the holdup and pressure. For bubbly flow and intermittent flow, we calculate the pressure drop by the momentum equation. From Equation (4.54), the slippage term L_{ne} / L_e is updated. After convergence is achieved for the mass flow rate, holdup, and pressure values in continuity and momentum equations, the energy equation is solved to update the temperature distribution. Energy equation is also solved iteratively since it is coupled to pressure and velocity. Reservoir temperature in the horizontal part and formation temperature in the vertical part of the wellbore are used as initial guesses for wellbore temperature.

4.5 RESULTS

In this section we describe the production from a horizontal well to illustrate the implementation of our coupled wellbore-reservoir simulator. This example shows that the inclusion of a wellbore model is crucial for the comprehensive reservoir simulation and wellbore monitoring.

Tables 4.1 and 4.2 show the input parameters for the base case and Appendix D.2 shows the input data file. In this case, a 1,000 ft long open-hole horizontal well is completed in a $2500 \times 2500 \times 300 \text{ ft}^3$ reservoir (Figure 4.1). Pressure at the heel is maintained at 2,130 psi.

Firstly, a comprehensive calculation from the toe to the surface is conducted to verify whether or not the physical condition setup is possible. In the initial monitoring, pressure, flow rates, temperature distributions and phase compositions along the well were calculated, according to Figures 4.2 through 4.7. Initially, the pressure drop in the

horizontal well section is 109.57 psi and the temperature variation is less than 0.1 °F. In fact, the pressure drop in the horizontal section is in the order of pressure drawdown, which means that neglecting its effect is not acceptable in the well flow performance. Figures 4.8 and 4.9 show that the pressure drop (1,415 psi) in the vertical section is more pronounced due to gravity effects. Temperature variation from the bottom-hole to the wellhead is 13.7 °F. Since flow rates are high, the heat transfer rate is low; thus, temperature variation is not high along the wellbore. Figure 4.10 shows the liquid fraction and shows that in the horizontal section, stratified flow is developed first at the toe where flow rates are small. Then one detects intermittent flow in the middle and bubbly flow in the vicinity of the heel. It can also be seen that holdup increases at the junction point of horizontal and vertical wells. This indicates that liquid accumulates at the crossing and blocks the flow.

Table 4.3 and Figures 4.14 and 4.15 illustrate the composition variation along the well. As can be observed, the light-component compositions in the liquid phase are greater at the bottom-hole than at the surface, and they decrease drastically in the liquid at the surface condition. According to the bubble point pressure (P_b) calculations, the P_b of this fluid is 2,700 psi, which means that the fluid is a light oil. Consequently, both the wellbore and the reservoir systems are below the P_b .

Second, after monitoring the system and investigating the flow streams, we open up the well and maintain the bottom-hole pressure at 2,130 psi. Figures 4.16 through 4.18 show the water, oil, and gas flow rates and compare the results with the case where the pressure drop is neglected in the horizontal section. Initially, there is up to a 30% difference between the flow rate predictions (Figures 4.19 through 4.21). These comparisons illustrate that for reservoir flow prediction and well performance, accurate wellbore simulation is mandatory.

In fact, the behavior seen in Figures 4.16 through 4.18 is justified by the results obtained in Figure 4.22, which shows the pressure profile as a function of time. This graph indicates that, initially, the pressure drop is in the order of draw-down pressure, but as time elapses and the reservoir is depleted, pressure profile in horizontal well becomes flatter. Although the pressure drop is negligible at late-stage production, estimated fluid flow rates between the cases which consider wellbore simulation and neglect wellbore simulation are not still identical. The initial pressure gradient in the horizontal well affects the initial depletion of the reservoir and, consequently, influences the potential of the reservoir to flow. In other words, neglecting the wellbore simulation in the course of reservoir simulation gives an over-estimation at the early stage of production and an under-estimation at the late stage.

Figures 4.21 and 4.22 show the liquid holdup and flow regimes, respectively. As can be seen, the liquid holdup initially decreases along the wellbore. Then it increases, starting from the flow upstream, at the late stage. This implies that at the early stage, because of the pressure drop, more gas is released in the wellbore, and thus, the liquid fraction decreases. However, at the late stage of production, when the flow rates diminish and a stratified flow is established, the liquid is entirely accumulated in the well. Figure 4.19 shows that after well production and reservoir depletion, bubbly flow disappears and stratified flow extends toward the heel. Annular mist flow is also developed at near the junction of vertical and horizontal wells. Our simulation results show that at late stages of production, in most of the cases, only stratified and intermittent flows remain in horizontal well. However, in this particular study, stratified flow and annular mist flow exist at late time production. In addition, annular flow is entirely captured in the vertical section.

Table 4.1 Input parameters for the base case

Reservoir dimension, ft ³	2500X2500X300
Reservoir gridblock number	50X50X3
Reservoir initial pressure, psi	2300
Reservoir initial water saturation	0.5
Reservoir initial temperature, °F	140
Reservoir permeability (kx=ky=kz), md	350
Well Depth, ft	5700
Wellbore diameter, ft	0.4
Wall roughness, ft/ft	0.0008
Horizontal well length , ft	1000
Well condition	Open-hole
Bottomhole pressure, psi	2130
Geothermal gradient, °F/ft	0.006976
Thermal conductivity of the earth, Btu/(hr-ft °F)	1.3
Formation density, lbm/ft ³	132
Heat capacity of earth, Btu/(lbm °F)	0.21
Thermal conductivity of the cement, Btu/(hr-ft °F)	4.021
Overall composition of reservoir fluid	
C1	0.6
C3	0.1
C6	0.1
C10	0.1
C15	0.05
C20	0.05

Table 4.2 Components critical values and pertinent data

Component	Tc (°F)	Pc (psi)	Vc (ft ³ /lbmole)	Mw (lbm/lbmol)	Acen
C1	343.0	667.8	1.599	16.0	0.013
C3	665.7	616.3	3.211	44.1	0.152
C6	913.4	436.9	5.923	86.2	0.301
C10	1111.8	304.0	10.087	142.3	0.488
C15	1270.0	200.0	16.696	206.0	0.650
C20	1380.0	162.0	21.484	282.0	0.850

Table 4.3 Gas and liquid phase compositions at different places for the base case

<i>Gas</i>				
<u>Component</u>	<u>(1) Toe</u>	<u>(2) Heel</u>	<u>(3) Wellhead</u>	<u>(4) Standard</u>
C1	0.9293	0.9300	0.9256	0.8648
C3	0.0544	0.0546	0.0658	0.1006
C6	0.0135	0.0130	0.0081	0.0341
C10	0.0023	0.00216	3.47E-04	4.37E-04
C15	2.36E-04	1.89E-04	5.77E-06	1.08E-06
C20	3.70E-05	2.70E-05	1.62E-07	4.36E-09
<i>Oil</i>				
<u>Component</u>	<u>(1) Toe</u>	<u>(2) Heel</u>	<u>(3) Wellhead</u>	<u>(4) Standard</u>
C1	0.5282	0.5101	0.2122	0.0059
C3	0.1098	0.1121	0.1288	0.0153
C6	0.1189	0.1240	0.2163	0.2400
C10	0.1212	0.1266	0.2221	0.3703
C15	0.0608	0.0635	0.1103	0.1843
C20	0.0609	0.0635	0.1101	0.1839

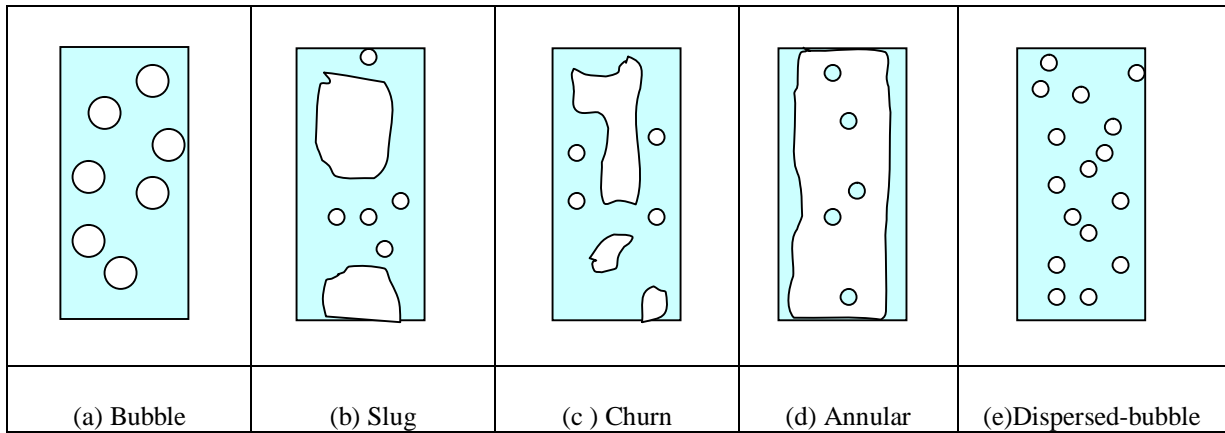


Figure 4.1 Different flow regimes in vertical flow

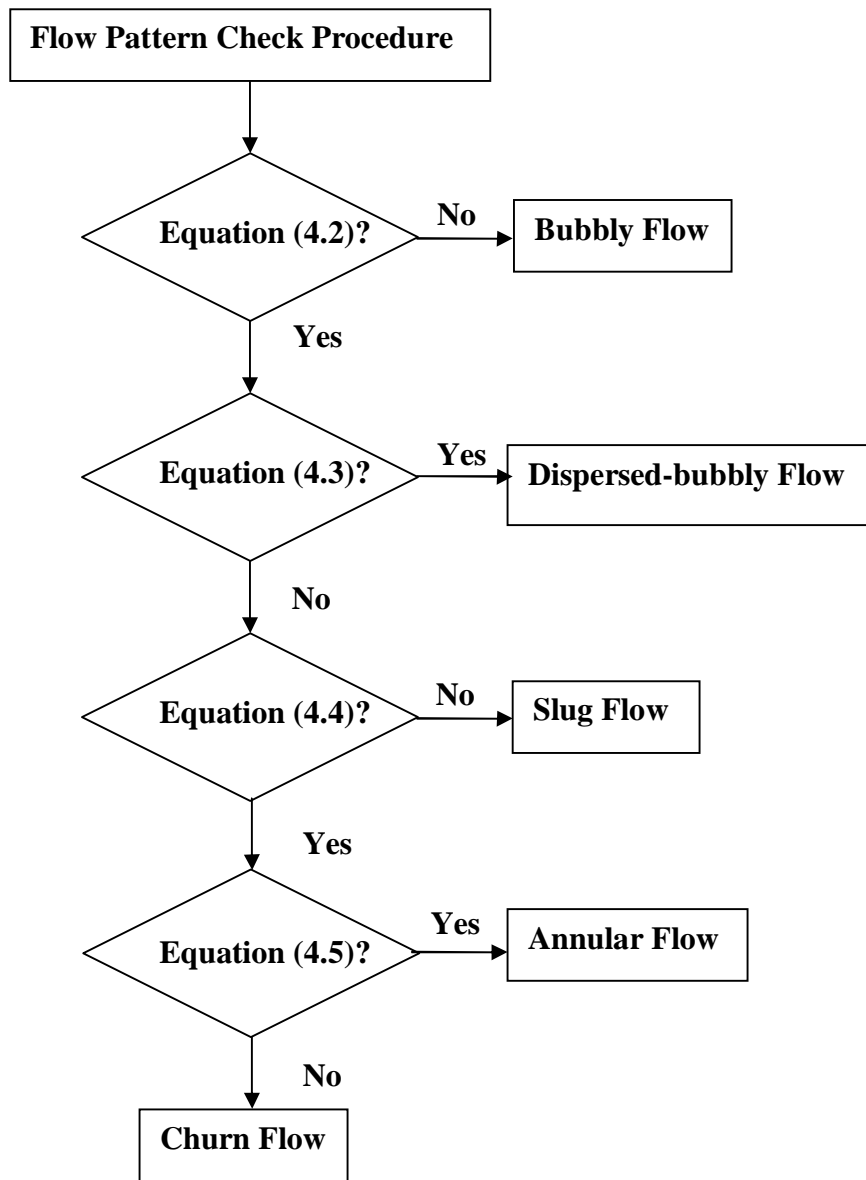


Figure 4.2 Procedure to select appropriate flow regimes for vertical inclination

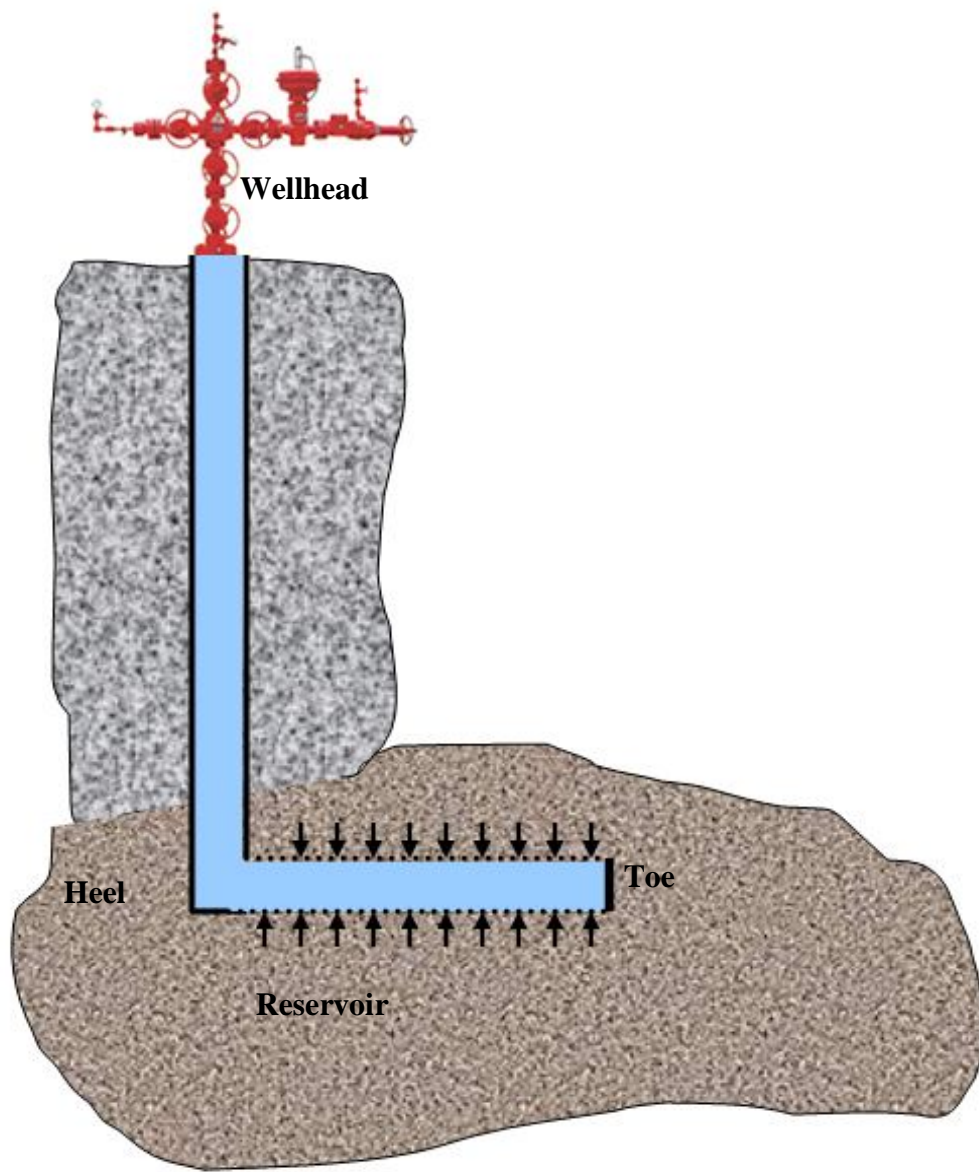


Figure 4.3 Schematic views of wellbore, reservoir and surface wellhead connection and flow domains

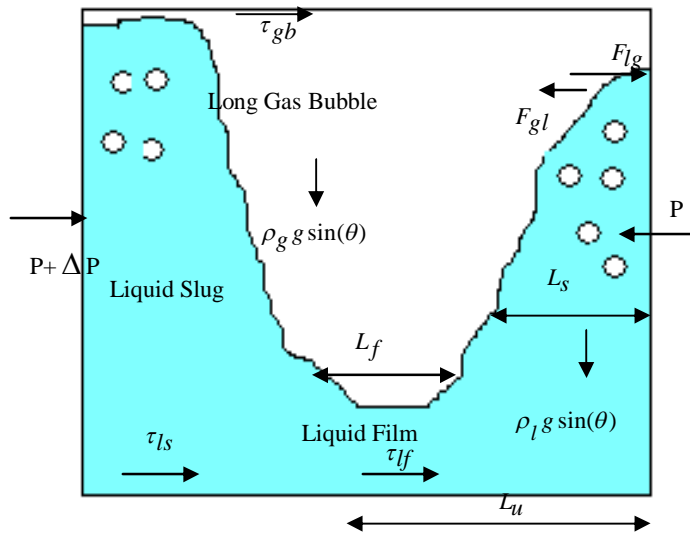


Figure 4.4 Intermittent flow regime

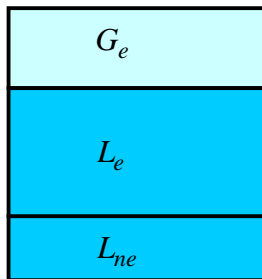


Figure 4.5 Schematic views of phases equilibrium

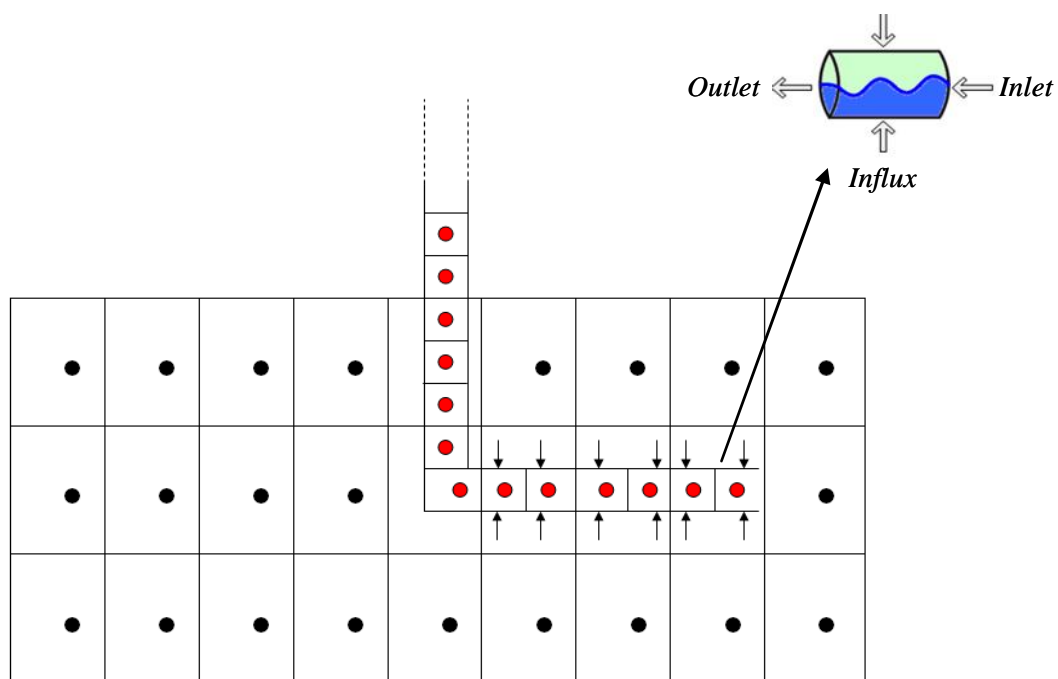


Figure 4.6 Schematic view of wellbore segments and reservoir gridblocks

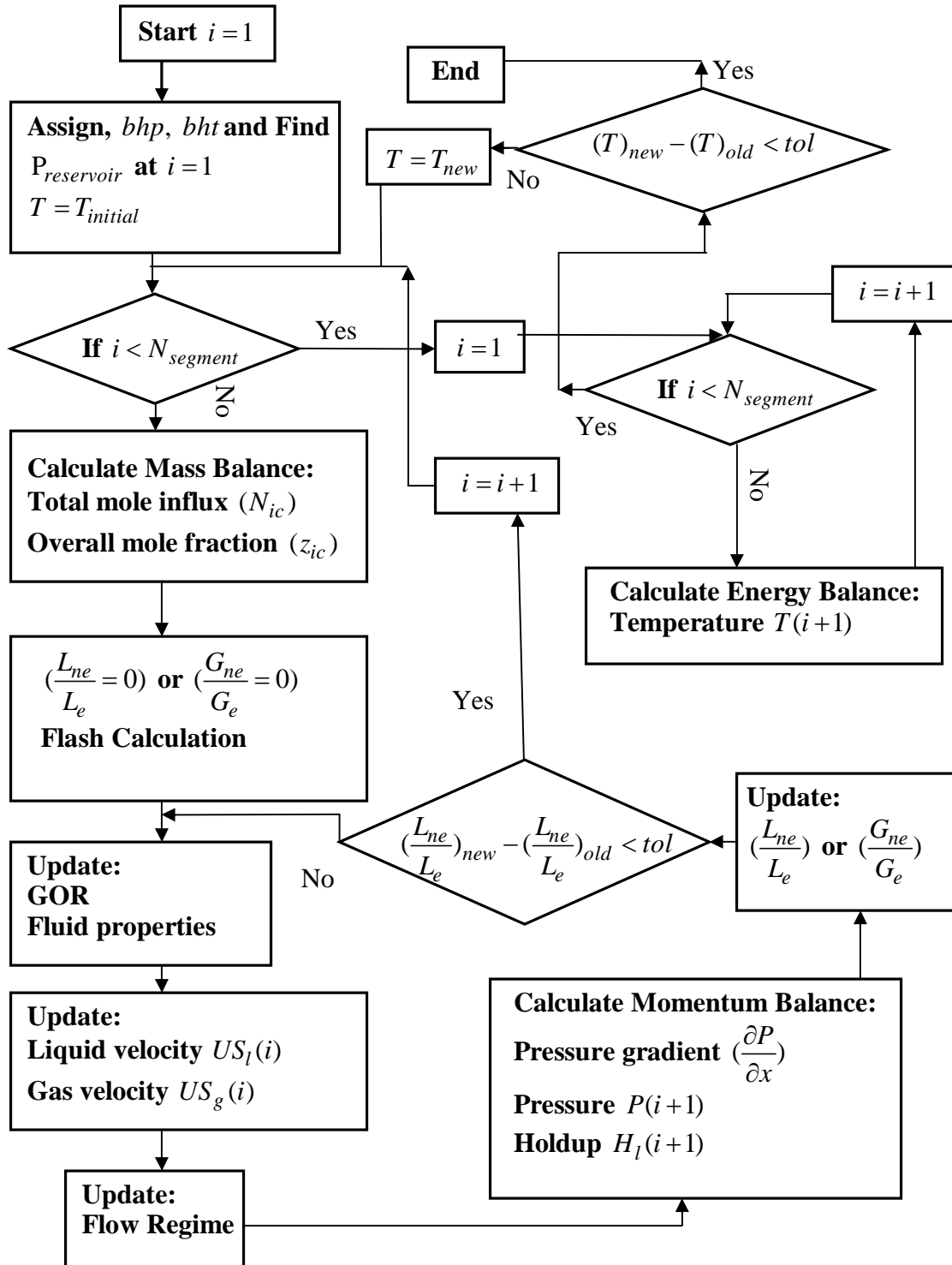


Figure 4.7 Solution procedure by marching algorithm

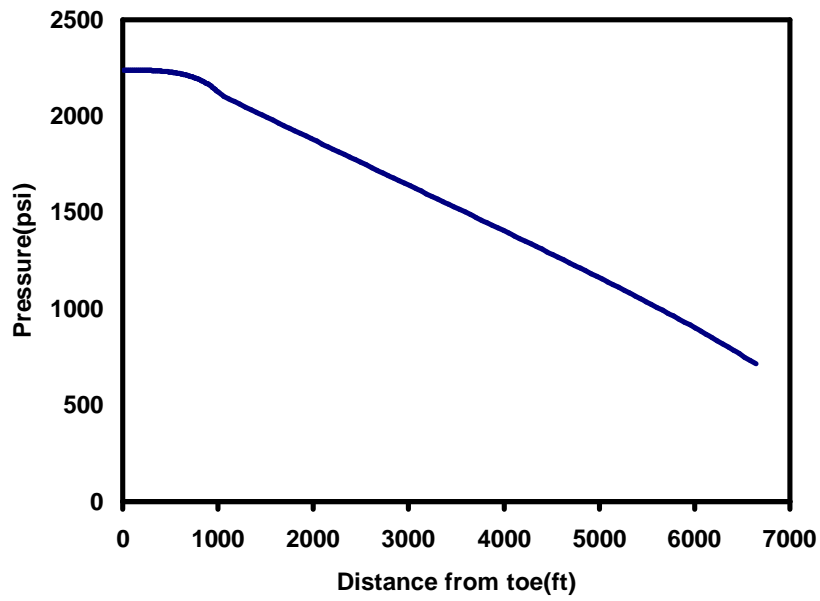


Figure 4.8 Pressure distribution from the toe to the surface

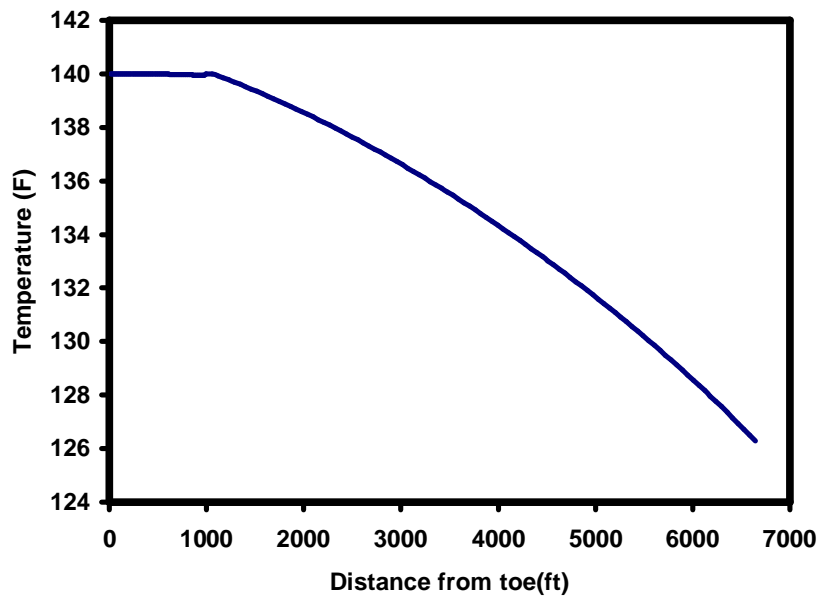


Figure 4.9 Temperature distribution from the toe to the surface

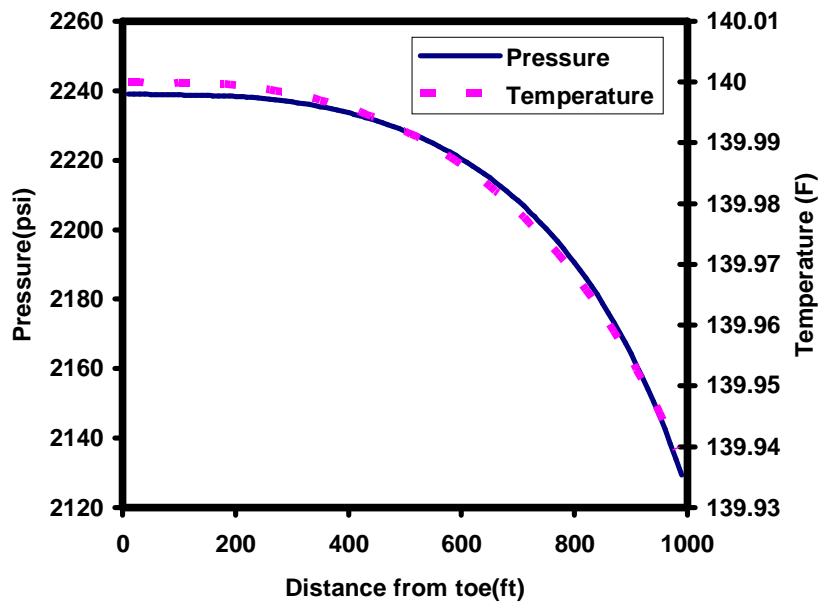


Figure 4.10 Temperature and pressure distribution in the horizontal section

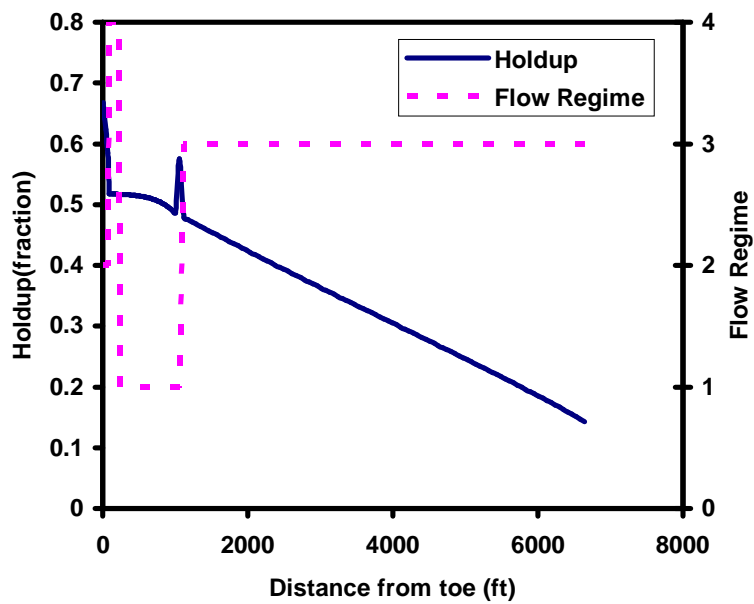


Figure 4.11 Holdup distribution and flow regime changes from the toe to the surface (1: bubbly, 2: stratified, 3: annular mist, 4: intermittent flow)

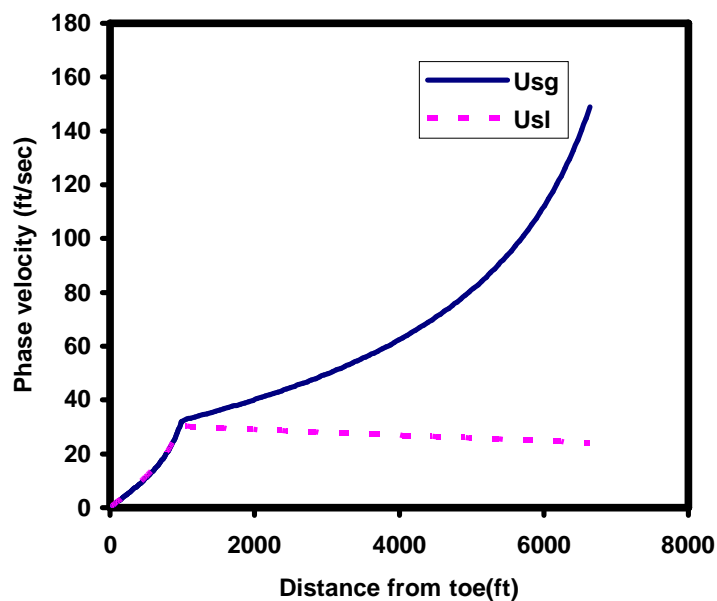


Figure 4.12 Phase velocity distribution from the toe to the surface

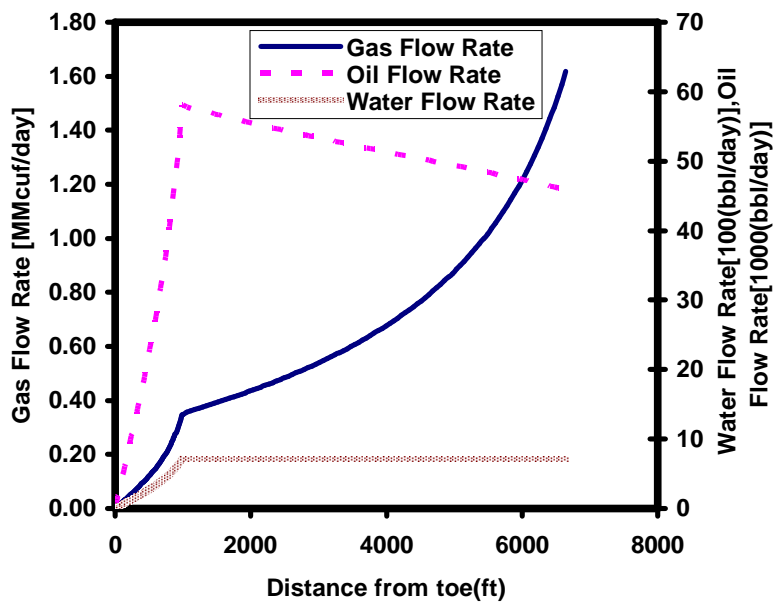


Figure 4.13 Flow rates from toe to the surface

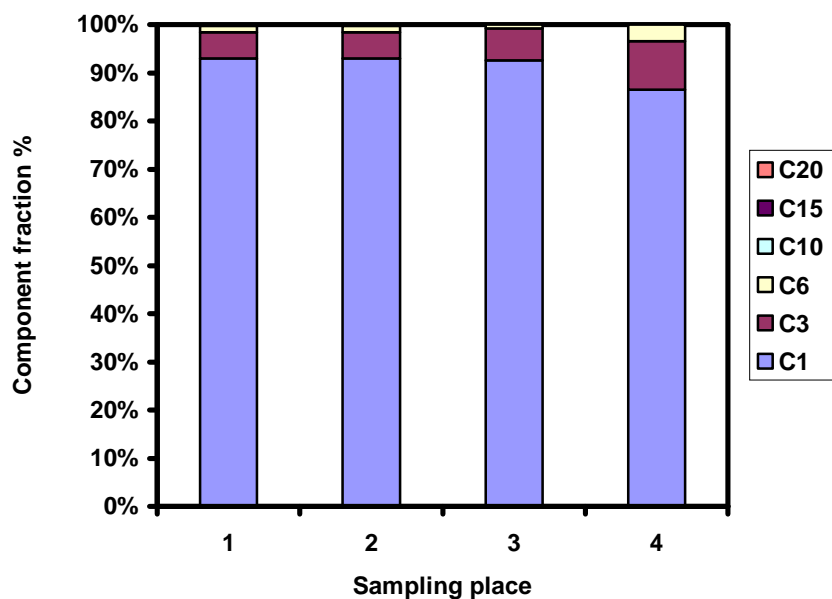


Figure 4.14 Gas phase composition at different sections of the wellbore (1: toe, 2: heel, 3: wellhead, 4: standard condition)

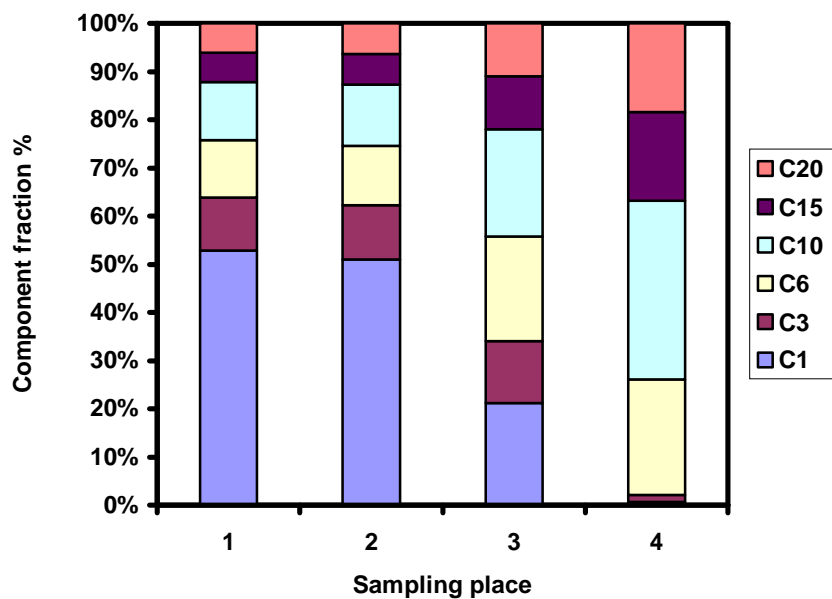


Figure 4.15 Oil phase composition at different sections of the wellbore (1: toe, 2: heel, 3: wellhead, 4: standard condition)

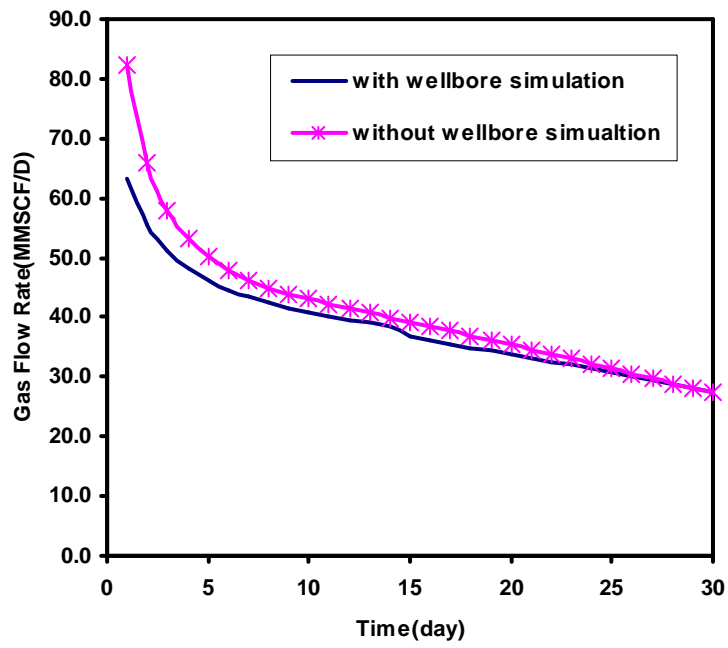


Figure 4.16 Comparison of gas flow rate with/without the wellbore simulation

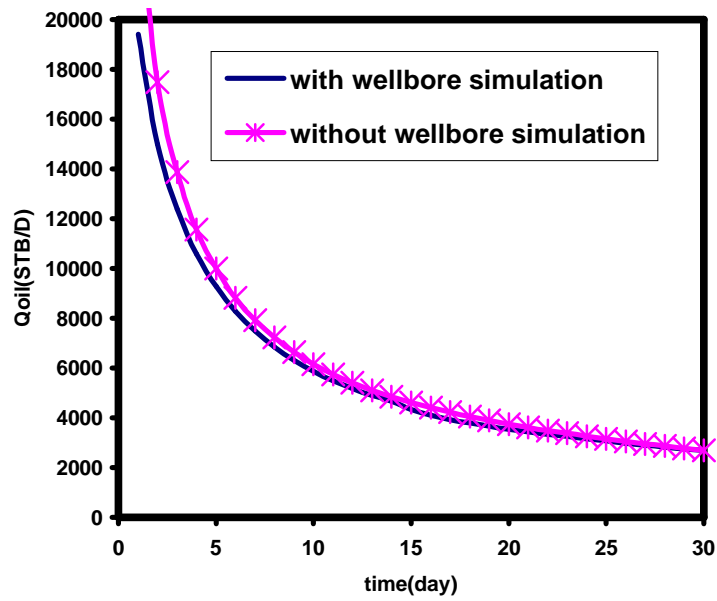


Figure 4.17 Comparison of oil flow rate with/without the wellbore simulation

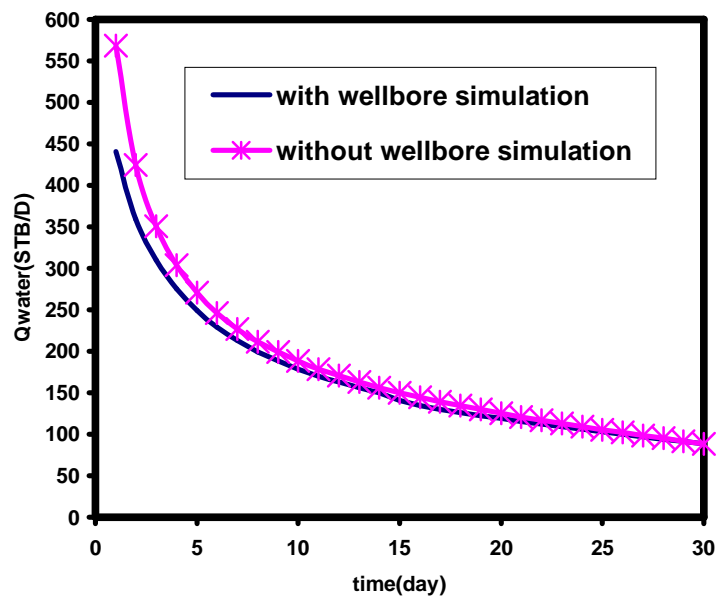


Figure 4.18 Comparison of water flow rate with/without the wellbore simulation

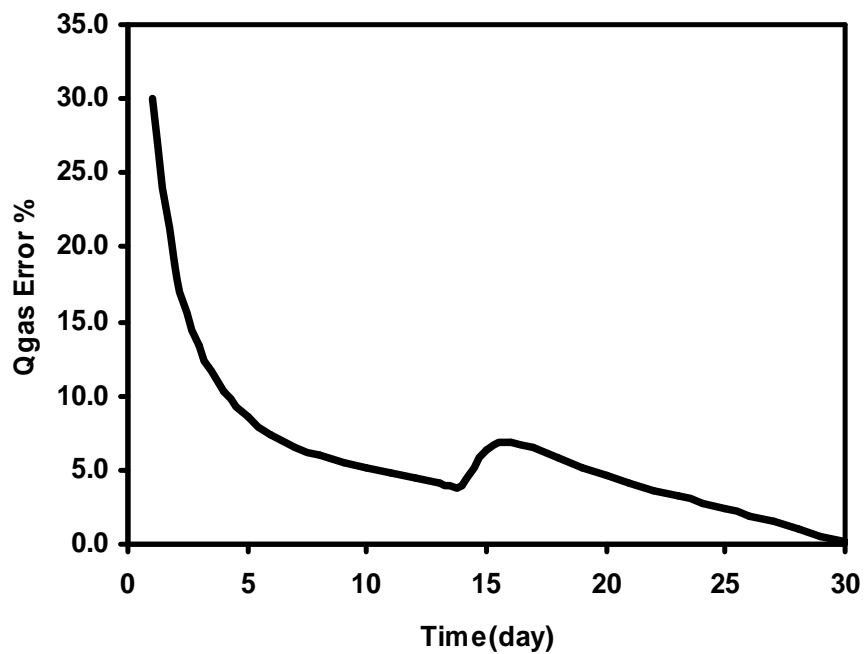


Figure 4.19 Gas flow rate estimation error

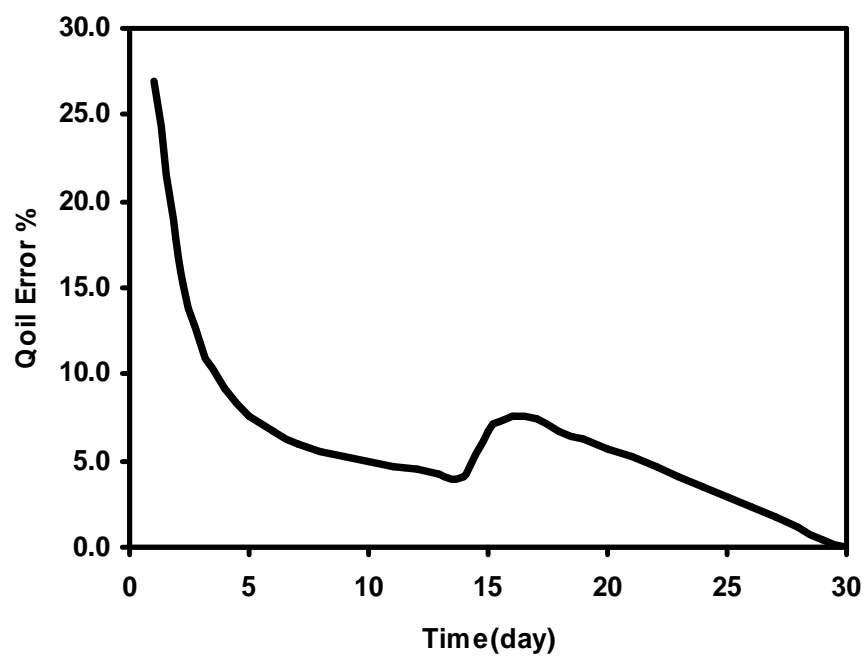


Figure 4.20 Oil flow rate estimation error

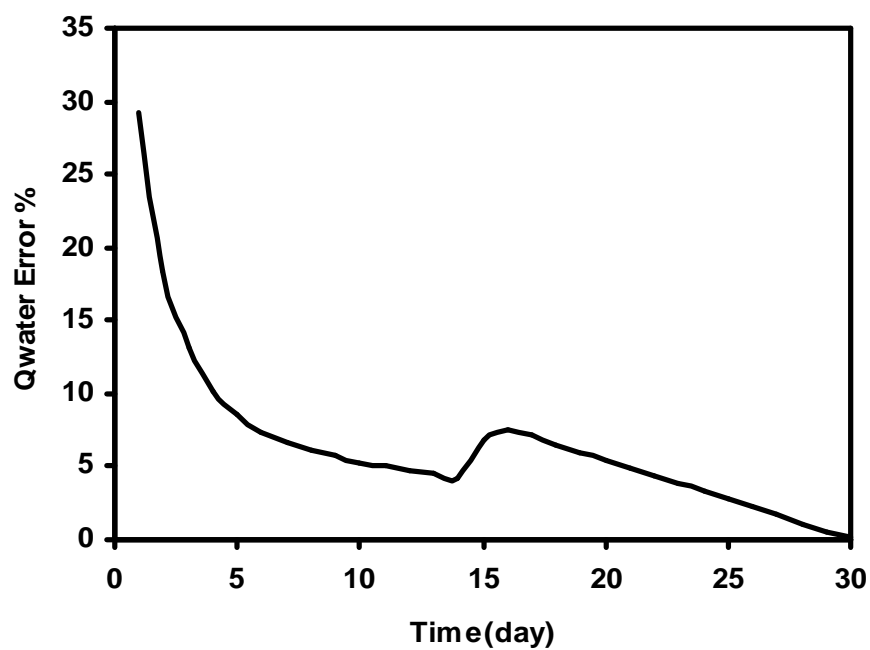


Figure 4.21 Water flow rate estimation error

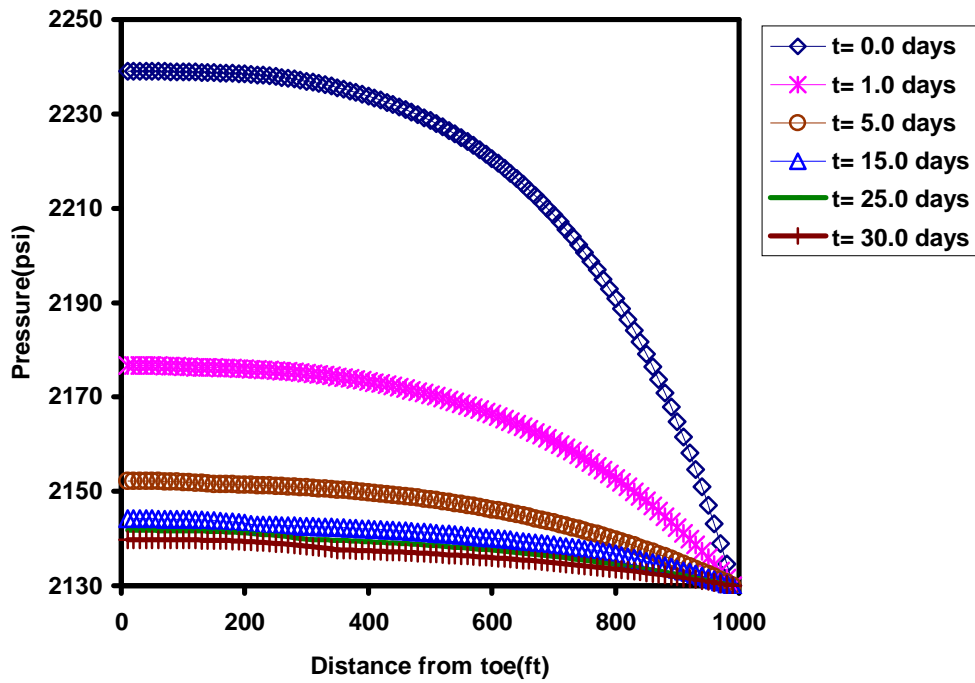


Figure 4.22 Pressure profile as a function of time for the horizontal section

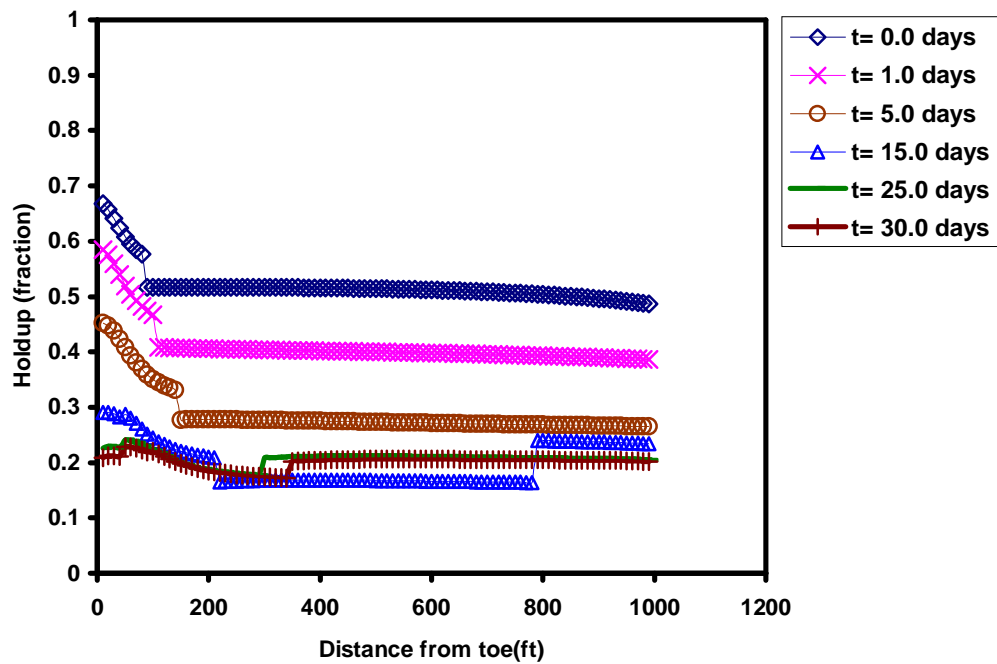


Figure 4.23 Holdup profile as a function of time for the horizontal section

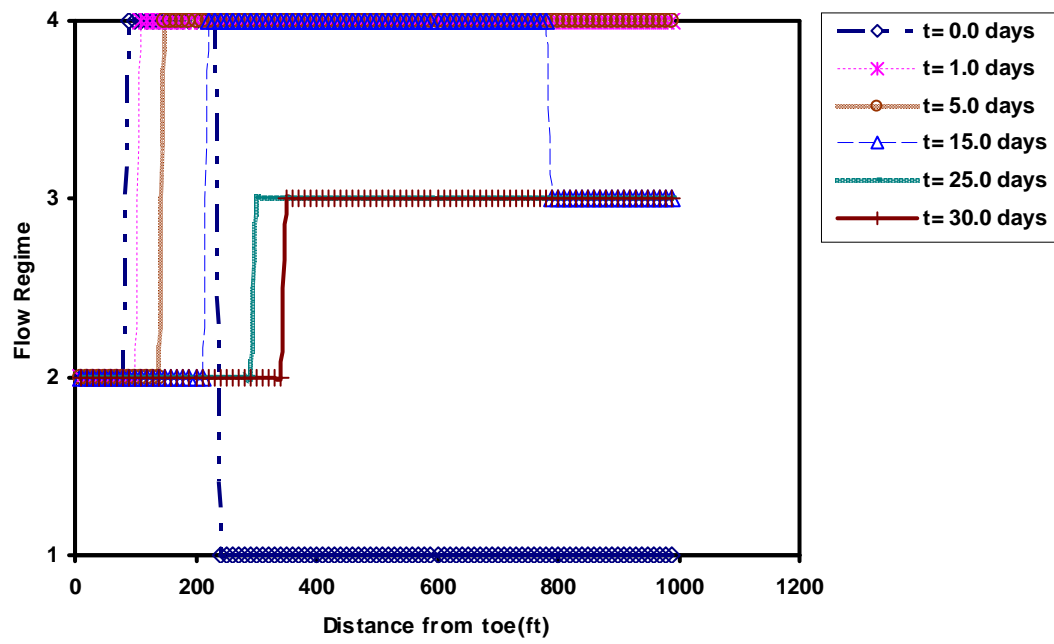


Figure 4.24 Flow regimes variation as a function of time for the horizontal section (1: bubbly, 2: stratified, 3: annular mist, 4: intermittent flow)

Chapter 5: Transient Pseudo-Compositional Thermal Wellbore Model

A great deal of research has been conducted to study transient two-phase flow in pipes. The development of this model is necessary in various industry applications. Researchers in different areas (*i.e.*, chemical and mechanical engineering processes) have developed elaborate programs to study the transient two-phase flow. For instance, some of these well-known codes are COBRA, CATHARE, and RELAP4 (Shoham, 2005). Those programs are used for complex problems in transient two-phase flow. In the petroleum industry some commercial codes such as OLGA (Bendiksen et al., 1986, 1991) are also available. This commercial software was developed by a consortium at SINTEF, Norway (Bendiksen et al., 1986).

In this chapter, we present an implementation of a pseudo-compositional, thermal, fully-implicit, transient, two-fluid model for wellbores. The simulator can be used as a standalone code or can be used in conjunction with reservoir simulator to mimic wellbore-reservoir dynamic interactions. For coupling wellbore to the reservoir we use productivity index values as explained in Chapter 4.

In our simulation, we compared different flow regimes effects on pressure and temperature distributions in a transient mode. We observed that the spatial distribution of fluids in different regimes can significantly affect the results. In fact different flow regimes effect is reflected in the closure relations for inter-phase and wall shear stresses.

5.1 FLOW EQUATIONS IN THE WELLBORE

The flow equations in this chapter are similar to the steady-state equations in Chapter 3. However, an accumulation term is added to the equations to consider transient

effect. We also apply the same assumptions as in Chapter 3 for mass conservation, momentum conservation, and energy equations.

The primary variables that are considered in the flow equations depend on the model and solution procedure used. Usually liquid and gas velocities, holdup, pressure, and liquid and gas temperatures are the primary variables in the model. However, in some of the models, such as drift-flux model, the mixture velocity, holdup, pressure and temperature are considered as primary variables. In our development, we assume five primary variables: liquid velocity, gas velocity, pressure, holdup, and temperature. We solve the gas/liquid mass balance, gas/liquid momentum balance, and two-phase energy equations to obtain these variables.

5.1.1 Liquid Mass Balance

For liquid mass balance we have:

$$(Mass_{in} - Mass_{out}) \pm (Source / Sink) = Accumulation . \quad (5.1)$$

Substituting the input/output mass flow rate, source and sink terms and mass accumulation we obtain Equation (5.2) for the liquid mass balance,

$$\begin{aligned} & Adt[H_l(i-1)\rho_l(i-1)U_l(i-1)] - Adt[H_l(i)\rho_l(i)U_l(i)] \\ & + dzdt[PI_o\rho_{ores}](P_{res} - P(i)) \pm dz\dot{m}_l dt = Adz[H_l(i)^{n+1}\rho_l(i)^{n+1} - H_l(i)^n\rho_l(i)^n] . \end{aligned} \quad (5.2)$$

i , represents spatial discretization and n represents the time discretization indexing. In Equation (5.2) source/sink terms are considered as $dz[PI_o\rho_{ores}](P_{res} - P(i))$ and $\pm\dot{m}_l dz$. The first term is used to account coupling wellbore to reservoir and the second term is

used for injection or production to the wellbore from other sources. We define PI and \dot{m}_l as productivity index per unit length and liquid mass flow rate per unit length.

Rearranging the coefficients and applying the upstream weighting (as explained in Chapter 3) for the coefficients we obtain:

$$\begin{aligned} & \left(\frac{dt}{dz}\right)[H_l(i)\rho_l(i) \times \max(U_l(i), 0) - H_l(i+1)\rho_l(i+1) \times \max(-U_l(i), 0)] \\ & - \left(\frac{dt}{dz}\right)[H_l(i-1)\rho_l(i-1) \times \max(U_l(i-1), 0) - H_l(i)\rho_l(i) \times \max(-U_l(i-1), 0)] \\ & + \left(\frac{dt}{A}\right)[PI_o \rho_{ores}](P(i) - P_{res}) \pm \left(\frac{\dot{m}_l dt}{A dz}\right) + [H_l(i)^{n+1} \rho_l(i)^{n+1} - H_l(i)^n \rho_l(i)^n] = 0. \end{aligned} \quad (5.3)$$

Dividing Equation (5.1) to $A dt dx$ we obtain

$$\begin{aligned} & \left[\frac{H_l(i-1)\rho_l(i-1)U_l(i-1) - H_l(i)\rho_l(i)U_l(i)}{dx} \right] \\ & + \frac{PI_o \rho_{ores} (P_{res} - P(i))}{A} \pm \frac{\dot{m}_l}{A} = \left[\frac{H_l(i)^{n+1} \rho_l(i)^{n+1} - H_l(i)^n \rho_l(i)^n}{dt} \right]. \end{aligned} \quad (5.4)$$

Assuming small values for dt and dx we obtain the partial differential equation for liquid mass conservation as follows:

$$\frac{\partial[H_l \rho_l U_l]}{\partial z} + \left[\frac{PI_o \rho_{ores}}{A} \right] (P_{well} - P_{res}) \pm \frac{\dot{m}_l}{A} + \frac{\partial[H_l \rho_l]}{\partial t} = 0 \quad (5.5)$$

5.1.2 Gas Mass Balance

Likewise, for the gas mass conservation we have:

$$\begin{aligned}
& \text{Adt}[(1-H_l(i-1))\rho_g(i-1)U_g(i-1) + \frac{R_s(i-1)}{B_o(i-1)}\rho_{gsc}H_l(i-1)U_l(i-1)] \\
& - \text{Adt}[(1-H_l(i))\rho_g(i)U_g(i) + \frac{R_s(i)}{B_o(i)}\rho_{gsc}H_l(i)U_l(i)] \\
& + dzdt[PI_g(i)\rho_{gres}(i) + PI_o(i)\frac{R_{sres}(i)}{B_{ores}(i)}\rho_{gsc}](P_{res}-P(i)) \pm \dot{m}_g dzdt = \\
& \text{Adz}[(1-H_l(i))^{n+1}\rho_g(i)^{n+1} - (1-H_l(i))^n\rho_g(i)^n] \\
& + \text{Adz}[(\frac{R_s(i)}{B_o(i)})^{n+1}\rho_{gsc}H_l(i)^{n+1} - (\frac{R_s(i)}{B_o(i)})^n\rho_{gsc}H_l(i)^n]. \tag{5.6}
\end{aligned}$$

After rearranging the coefficients and applying the upstream weighting (as explained in Chapter 3) we obtain:

$$\begin{aligned}
& (\frac{dt}{dz})[(1-H_l(i))\rho_g(i) \times \max(U_g(i), 0) - (1-H_l(i+1))\rho_g(i+1) \times \max(-U_g(i), 0) \\
& + \frac{R_s(i)}{B_o(i)}\rho_{gsc}H_l(i) \times \max(U_l(i), 0) - \frac{R_s(i+1)}{B_o(i+1)}\rho_{gsc}H_l(i+1) \times \max(-U_l(i), 0)] \\
& - (\frac{dt}{dz})[(1-H_l(i-1))\rho_g(i-1) \times \max(U_g(i-1), 0) - (1-H_l(i))\rho_g(i) \times \max(-U_g(i-1), 0) \\
& + \frac{R_s(i-1)}{B_o(i-1)}\rho_{gsc}H_l(i-1) \times \max(U_l(i-1), 0) - \frac{R_s(i)}{B_o(i)}\rho_{gsc}H_l(i) \times \max(-U_l(i-1), 0)] \\
& + (\frac{dt}{A})[PI_g(i)\rho_{gres}(i) + PI_o(i)\frac{R_{sres}(i)}{B_{ores}(i)}\rho_{gsc}](P(i) - P_{res}) \pm (\frac{\dot{m}_g dt}{A}) \\
& + [(1-H_l(i))^{n+1}\rho_g(i)^{n+1} - (1-H_l(i))^n\rho_g(i)^n] + [(\frac{R_s(i)}{B_o(i)})^{n+1}\rho_{gsc}H_l(i)^{n+1} \\
& - (\frac{R_s(i)}{B_o(i)})^n\rho_{gsc}H_l(i)^n] = 0 \tag{5.7}
\end{aligned}$$

Rearranging Equation (5.6) and assuming small dz and dt values we can obtain the partial differential equation for the gas mass conservation as follows:

$$\begin{aligned}
& \frac{\partial[(1-H_l)\rho_g U_g + \frac{R_s}{B_o}\rho_{gsc}H_l U_l]}{\partial z} + \left[\frac{PI_g \rho_{gres} + PI_o \frac{R_{sres}}{B_{ores}}\rho_{gsc}}{A} \right] (P_{well} - P_{res}) \pm \frac{\dot{m}_g}{A} \\
& + \frac{\partial[(1-H_l)\rho_g + (\frac{R_s}{B_o})\rho_{gsc}H_l]}{\partial t} = 0.
\end{aligned} \tag{5.8}$$

5.1.3 Liquid Momentum Balance

Adding the accumulation term to Equation (3.29), we obtain the liquid momentum equation for the transient flow:

$$(Momentum_{in} - Momentum_{out}) + (Forces) = Accumulation. \tag{5.9}$$

In fact this equation comes from Newton's 2nd law which states that total force acting on a body will give rise to a rate of change of momentum according to

$$F = \left(\frac{1}{g_c}\right) \frac{dM}{dt} \tag{5.10}$$

where M is momentum which is defined as

$$M = mU. \tag{5.11}$$

This rate of change in momentum arises from all the forces acting on the control volume plus to that from convective momentum transport as shown in Equation (5.9).

Substituting the inlet/outlet momentum, body forces and accumulation term in Equation (5.9) we obtain:

$$\begin{aligned}
& Adt[H_l(i)\rho_l(i)(\frac{U_l(i)+U_l(i-1)}{2})^2 - H_l(i+1)\rho_l(i+1)(\frac{U_l(i)+U_l(i+1)}{2})^2] \\
& + Adt[H_l(i)\frac{R_s(i)}{B_o(i)}\rho_{gsc}(\frac{U_l(i)+U_l(i-1)}{2})^2 - H_l(i+1)\frac{R_s(i+1)}{B_o(i+1)}\rho_{gsc}(\frac{U_l(i)+U_l(i+1)}{2})^2] \\
& + dt[AH_l(i)P(i) - H_l(i+1)P(i+1) - \\
& Adz(\frac{H_l(i)+H_l(i+1)}{2})(\frac{\rho_l(i)+\rho_l(i+1)}{2})g \sin(\theta) - S_l dz F_{wl} + Adz F_{lg}] = \\
& Adz[(\frac{H_l(i)+H_l(i+1)}{2})^{n+1}(\frac{\rho_l(i)+\rho_l(i+1)}{2})^{n+1}U_l(i)^{n+1} - \\
& (\frac{H_l(i)+H_l(i+1)}{2})^n(\frac{\rho_l(i)+\rho_l(i+1)}{2})^n U_l(i)^n]. \tag{5.12}
\end{aligned}$$

where, F_{wl} and F_{lg} are liquid wall shear stress and inter-phase force per bulk volume, respectively, as explained in Chapter 3.

Assuming small dz and dt in Equation (5.12) and dividing to $Adtdz$ the final partial differential equation for the liquid momentum equation can be written as follows:

$$144gc \frac{\partial(H_l P)}{\partial z} + \frac{\partial(H_l \rho_l U_l^2)}{\partial z} + H_l \rho_l g \sin(\theta) + \frac{F_{wl} S_l}{A} - F_{lg} + \frac{\partial(H_l \rho_l U_l)}{\partial t} = 0. \tag{5.13}$$

where $144gc$ is used for unit conversion.

5.1.4 Gas Momentum Balance

Likewise, for the gas phase we can write momentum equation as follows:

$$\begin{aligned}
& Adt[(1-H_l(i))\rho_g(i)(\frac{U_g(i)+U_g(i-1)}{2})^2 - (1-H_l(i+1))\rho_g(i+1)(\frac{U_g(i)+U_g(i+1)}{2})^2] \\
& + Adt[(1-H_l(i))P(i) - (1-H_l(i+1))P(i+1) - dz(1-(\frac{H_l(i)+H_l(i+1)}{2}))(\frac{\rho_g(i)+\rho_g(i+1)}{2})g \sin(\theta) \\
& - \frac{F_{wg}S_g dz}{A} - dzF_{lg}] = Adz[(1-\frac{H_l(i)+H_l(i+1)}{2})^{n+1}(\frac{\rho_g(i)+\rho_g(i+1)}{2})^{n+1}U_g(i)^{n+1} - \\
& (1-\frac{H_l(i)+H_l(i+1)}{2})^n(\frac{\rho_g(i)+\rho_g(i+1)}{2})^nU_g(i)^n]. \tag{5.14}
\end{aligned}$$

After rearranging the coefficients and converting the units (to psi and ft/sec) we obtain:

$$\begin{aligned}
& (\frac{dt}{dz})[(1-H_l(i+1))\rho_g(i+1)(\frac{U_g(i)+U_g(i+1)}{2})^2 - (1-H_l(i))\rho_g(i)(\frac{U_g(i)+U_g(i-1)}{2})^2] \\
& + 144gc(\frac{dt}{dz})[(1-H_l(i+1))P(i+1) - (1-H_l(i))P(i)] \\
& + dt(1-\frac{H_l(i)+H_l(i+1)}{2})(\frac{\rho_g(i)+\rho_g(i+1)}{2})g \sin(\theta) \\
& + \frac{F_{wg}S_g dt}{A} + F_{lg}dt + [(1-\frac{H_l(i)+H_l(i+1)}{2})^{n+1}(\frac{\rho_g(i)+\rho_g(i+1)}{2})^{n+1}U_g(i)^{n+1} \\
& - (1-\frac{H_l(i)+H_l(i+1)}{2})^n(\frac{\rho_g(i)+\rho_g(i+1)}{2})^nU_g(i)^n] = 0. \tag{5.15}
\end{aligned}$$

The final partial differential equation for the gas momentum conservation can be written as follows:

$$\begin{aligned}
& 144gc \frac{\partial((1-H_l)P)}{\partial z} + \frac{\partial((1-H_l)\rho_g U_g^2)}{\partial z} + (1-H_l)\rho_g g \sin(\theta) + \frac{F_{wg}S_g}{A} + F_{lg} \\
& + \frac{\partial((1-H_l)\rho_g U_g)}{\partial t} = 0. \tag{5.16}
\end{aligned}$$

5.1.5 Mixture Momentum Balance

For transient two-phase flow modeling momentum equation for mixture of fluid can also be used. Livescu et al. (2009) used mixture momentum equation to calculate the mixture velocity U_m , instead of the liquid and gas velocities, separately.

Equation (5.17) shows the mixture momentum equation:

$$\begin{aligned}
 & Adt[\rho_m(i)(\frac{U_m(i)+U_m(i-1)}{2})^2 - \rho_m(i+1)(\frac{U_m(i)+U_m(i+1)}{2})^2] \\
 & + Adt[P(i) - P(i+1) - dz(\frac{\rho_m(i)+\rho_m(i+1)}{2})g \sin(\theta) - \\
 & \frac{1}{2} f_{wtp}(\frac{\rho_m(i)+\rho_m(i+1)}{2})U_m(i)|U_m(i)|(\pi D)dz = \\
 & Adz[(\frac{\rho_m(i)+\rho_m(i+1)}{2})^{n+1}U_m(i)^{n+1} - (\frac{\rho_m(i)+\rho_m(i+1)}{2})^n U_m(i)^n]. \tag{5.17}
 \end{aligned}$$

Assuming small dt and dz the final partial differential equation for mixture momentum conservation can be written as follows:

$$144gc \frac{\partial(P)}{\partial z} + \frac{\partial(\rho_m U_m^2)}{\partial z} + \rho_m g \sin(\theta) + \frac{f_{wtp} \rho_m U_m |U_m| (\pi D)}{2A} + \frac{\partial(\rho_m U_m)}{\partial t} = 0. \tag{5.18}$$

In the case the mixture momentum equation is used to calculate the liquid and gas velocities an auxiliary equation is required. Equation (5.19) shows the empirical equation (Mishima and Ishii, 1984) which relates the gas velocity to mixture velocity:

$$U_g = C_0 U_m + V_d, \tag{5.19}$$

$$\text{where } C_0 = C_w - 0.2(\frac{\rho_g}{\rho_l})^{0.5} \tag{5.20}$$

$$U_0 = 1.53 \left(\frac{g(\rho_l - \rho_g)\sigma}{\rho_l^2} \right)^{0.25} \sin(\theta) \quad (5.21)$$

This calculation method for momentum equation is called drift-flux model. Although this model simplifies the equations and makes the problem computationally less expensive, it is not able to capture the inter-phase momentum transfer phenomena accurately.

5.1.6 Total Energy Balance

Although in reality the liquid and gas temperatures are not equal in the pipe flow, to simplify the computational procedure we assume they are identical. Accordingly, Equation (5.22) shows the total energy conservation by adding liquid and gas energy balance to solve bulk temperature. It should be mentioned that the inter-phase effects are eliminated in the overall energy equation,

$$\begin{aligned} & Adt[H_l(i-1)\rho_l(i-1)(\bar{h}_l(i-1) + \frac{U_l^2(i-1)}{2})U_l(i-1)] \\ & - Adt[H_l(i)\rho_l(i)(\bar{h}_l(i) + \frac{U_l^2(i)}{2})U_l(i)] + \\ & + Adt[H_l(i-1)\frac{R_s(i-1)}{B_o(i-1)}\rho_{gsc}(\bar{h}_g(i-1) + \frac{U_l^2(i-1)}{2})U_l(i-1)] \\ & - Adt[H_l(i)\frac{R_s(i)}{B_o(i)}\rho_{gsc}(\bar{h}_g(i) + \frac{U_l^2(i)}{2})U_l(i)] \\ & + Adt[(1-H_l(i-1))\rho_g(i-1)(\bar{h}_g(i-1) + \frac{U_g^2(i-1)}{2})U_g(i-1)] \end{aligned}$$

$$\begin{aligned}
& -Adt[(1-H_l(i))\rho_g(i)(\bar{h}_g(i) + \frac{U_g^2(i)}{2})U_g(i)] \\
& +dzdt[PI_o\rho_{ores}](P_{res}-P(i))(\bar{h}_{lres}(i) + \frac{U_{lres}^2(i)}{2}) \\
& +dzdt[PI_g\rho_{gres} + PI_o(\frac{R_{sres}}{B_{ores}})\rho_{gsc}](P_{res}-P(i))(\bar{h}_{gres}(i) + \frac{U_{gres}^2(i)}{2}) \\
& -AdzH_l(i)\rho_l(i)(\frac{U_l(i-1)+U_l(i)}{2})g\sin(\theta)dt \\
& -Adz(1-H_l(i))\rho_g(i)(\frac{U_g(i-1)+U_g(i)}{2})g\sin(\theta)dt \\
& -Q_g dz(\frac{S_g}{\pi D})dt - Q_l dz(\frac{S_l}{\pi D})dt = Adz[H_l(i)^{n+1}\rho_l(i)^{n+1}(\bar{e}_l(i) + \frac{U_l^2(i)}{2})^{n+1} - \\
& H_l(i)^n\rho_l(i)^n(\bar{e}_l(i) + \frac{U_l^2(i)}{2})^n] + Adz[(1-H_l(i)^{n+1})\rho_g(i)^{n+1}(\bar{e}_g(i) + \frac{U_g^2(i)}{2})^{n+1} - \\
& (1-H_l(i)^n)\rho_g(i)^n(\bar{e}_g(i) + \frac{U_g^2(i)}{2})^n]. \tag{5.22}
\end{aligned}$$

Assuming $T_l = T_g = T$ and substituting the internal energy and unit conversion factors,

we can obtain the partial differential form of the total energy equation as follows:

$$\begin{aligned}
& \frac{\partial[H_l\rho_l(\bar{h}_l + \frac{U_l^2}{2g_cJ_c})U_l]}{\partial z} + \frac{\partial[H_l\frac{R_s}{B_o}\rho_{gsc}(\bar{h}_g + \frac{U_l^2}{2g_cJ_c})U_l]}{\partial z} \\
& + \frac{\partial[(1-H_l)\rho_g(\bar{h}_g + \frac{U_g^2}{2g_cJ_c})U_g]}{\partial z} + [\frac{PI_o\rho_{ores}}{A}](P_{res}-P)(\bar{h}_{lres} + \frac{U_{lres}^2}{2g_cJ_c}) \\
& + [\frac{PI_g\rho_{gres} + PI_o(\frac{R_{sres}}{B_{ores}})\rho_{gsc}}{A}](P_{res}-P)(\bar{h}_{gres} + \frac{U_{gres}^2}{2g_cJ_c}) \\
& + H_l\rho_l U_l g \sin(\theta) + (1-H_l)\rho_g U_g g \sin(\theta) + Q_g(\frac{S_g}{A\pi D}) + Q_l(\frac{S_l}{A\pi D})
\end{aligned}$$

$$+ \frac{\partial [H_l \rho_l (\bar{h}_l - (\frac{144}{J_c}) \frac{P}{\rho_g} + \frac{U_l^2}{2g_c J_c})]}{\partial t} + \frac{\partial [(1-H_l) \rho_g (\bar{h}_g - (\frac{144}{J_c}) \frac{P}{\rho_g} + \frac{U_g^2}{2g_c J_c})]}{\partial t} = 0. \quad (5.23)$$

5.2 SOLUTION PROCEDURE

We solved the mass balance and momentum balance equations by constructing a jacobian matrix, J and a residual vector, R with the primary variables such as liquid velocity, gas velocity, liquid holdup, and pressure. As explained in Chapter 3 the equations that we solve are, f_1 as liquid momentum balance, f_2 as gas momentum balance, f_3 as the summation of gas and liquid mass balance, and f_4 as liquid mass balance. After solving for pressure, holdup and velocity of the gas and liquid, the energy equation is solved. We can solve the energy equation either analytically or numerically. If we assume f_5 is the total energy equation, then the jacobian matrix, JT residual vector, RT and temperature variation vector are generated to solve the non-linear equation. Figure 5.1 shows the calculation procedure steps as a flow chart.

5.3 RESULTS

To demonstrate what we have developed, we considered the two following case studies: i) startup and injection rate variation in the pipe and ii) thermal transient problem. In Chapter 6 we discuss the transient model against experimental data and other simple analytical solutions.

5.3.1 Case 1: Constant Flow Rate Injection, Constant Outlet Pressure

In this case, we assume that a mixture of oil and gas is injected into a pipe initially filled with 50% oil and 50% gas. Initial velocities of fluids are considered to be zero. We impose a constant pressure at 1,000 psi in the outlet, a constant liquid flow rate of $0.314 \text{ ft}^3/\text{sec}$, and constant gas flow rate of $0.157 \text{ ft}^3/\text{sec}$ in the inlet. We also assume that the injected gas is associated gas with the oil at the injection pressure condition. The overall composition of the injected fluid and other pertinent data is presented in Table 5.1.

In this case, we perform the oil and gas injection for 500 seconds and then increase the gas flow rate to $0.471 \text{ ft}^3/\text{sec}$. We run the simulation for additional 500 seconds.

Figures 5.2 through 5.5 show the liquid and gas superficial velocities, pressure, and holdup variation by time in the middle point (length=500 ft). These figures demonstrate how the transient flow occurs along the pipe. It is seen that after about 200 sec, after beginning the injection, the system reaches to steady-state condition and in the second injection, after 500 sec, again it takes about 200 sec. to reach to a steady-state condition. Figure 5.7 also shows the liquid velocity response. It is seen that in each injection period liquid velocity increases. The reason for this behavior is the inter-phase drag force exerted by the gas phase. In fact, in the second injection which we increase only gas flow rate, we observe liquid velocity increment as well.

Figures 5.6 through 5.9 also show the liquid and gas superficial velocities, pressure, and holdup profiles for different times. As can be observed, for the first injection we observe about 11 psi pressure drop along the pipe and for the second injection we obtain 19 psi.

5.3.2 Case 2: Cold Fluid Injection in the Inlet and Middle of Pipe

In this case, we have a similar assembly as Case 1. However we inject fluids with a lower temperature to investigate the transient thermal effect. We assume a mixture of gas and oil is injected into the wellbore at 100 °F, where the initial fluid temperature and surrounding temperature is 120 °F. We consider the outlet pressure to be 500 psi, the inlet liquid flow rate to be $0.314 \text{ ft}^3/\text{sec}$, and the gas flow rate to be $0.251 \text{ ft}^3/\text{sec}$.

In this case, we perform the oil and gas injection for 500 seconds and then open the perforation at intervals 500-600 ft from the inlet after 500 sec. We inject cold fluid with 110 °F and 1,100 psi from the perforation zone. We assume the productivity index value in the perforation zone for both gas and liquid as equal to $10^{-5} (\text{ft}^3/\text{sec.psi.ft})$. We ran the simulation for a total of 1,000 seconds. By this example we would like to test a transient thermal process with our code.

Figures 5.10 through 5.14 show that the liquid and gas superficial velocities, pressure, holdup and temperature in the middle segment in the pipe. The initial injection pulse causes pressure to jump from 500 psi to about 505 psi and temperature reduction from 120 °F to about 118 °F. In fact, the cool fluid mixing and heat exchange with the surrounding area occur and lead to the final temperature of about 118 °F, in the middle section of pipe. After 500 sec., we open a 100 ft interval in the middle of the pipe. Pressure in the perforation zone was 1,100 psi, and fluid was injected from this position to the pipe. As Figures 5.15 and 5.20 show that we have non-uniform gas and liquid influx in this zone. We have also embedded the perforation zone with cold fluid at 110 °F. Hence, after opening this zone we see a significant temperature reduction is occurred. Figure 5.19 shows that temperature is reduced to about 104 °F at 600 ft from the inlet. After this point temperature is increased and reaches to about 113 °F at outlet.

The results that we observe from our thermal code are reasonable. We obtain the same physical behavior that we expected from this problem.

Table 5.1 Wellbore geometry and fluid data

Wellbore diameter	0.4 ft
Wellbore roughness	0.0008 ft
Wellbore inclination	0 rad
Number of segments	100
Segments length	10 ft
Surrounding temperature	120 °F
Inlet temperature	120 °F
Overall heat transfer coefficient	0.1 Btu/sec. °F.ft ²
Injection fluid overall composition	C1=0.25
	C3=0.25
	C6=0.1
	C10=0.1
	C15=0.15
	C20=0.15

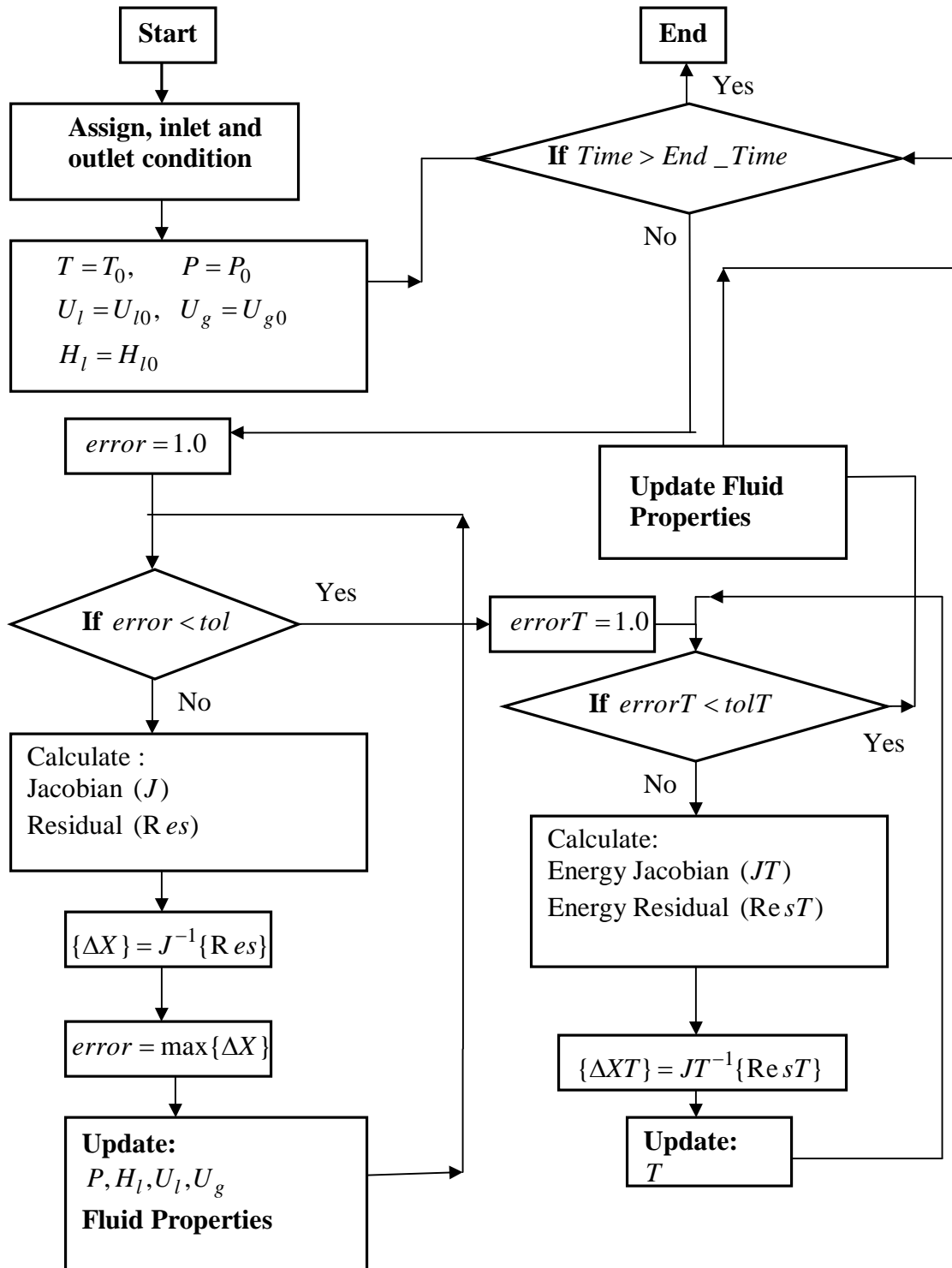


Figure 5.1 Numerical calculation procedure, using Newton method

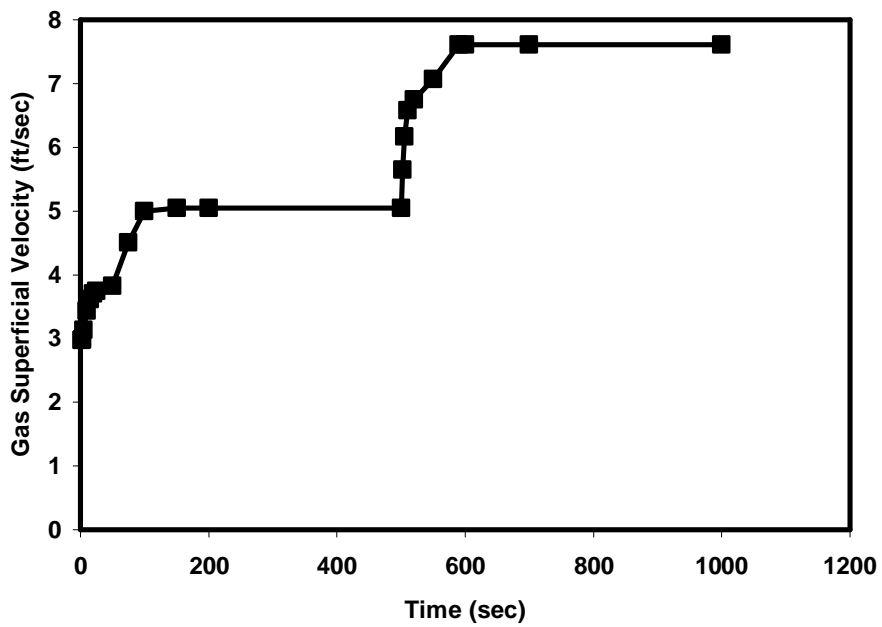


Figure 5.2 Gas superficial velocity in the middle of the pipe *versus* time for Case 1

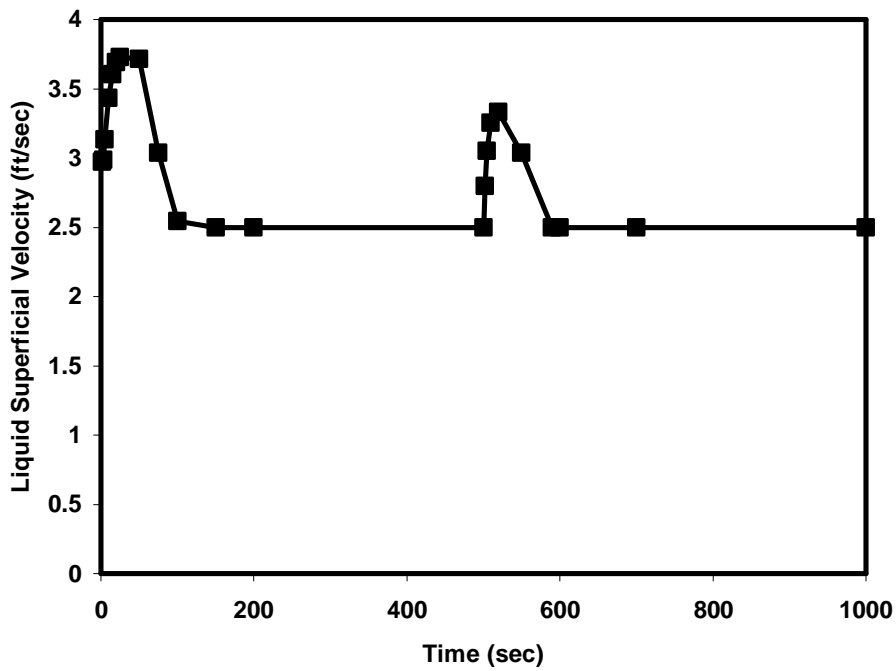


Figure 5.3 Liquid superficial velocity in the middle of the pipe *versus* time for Case 1

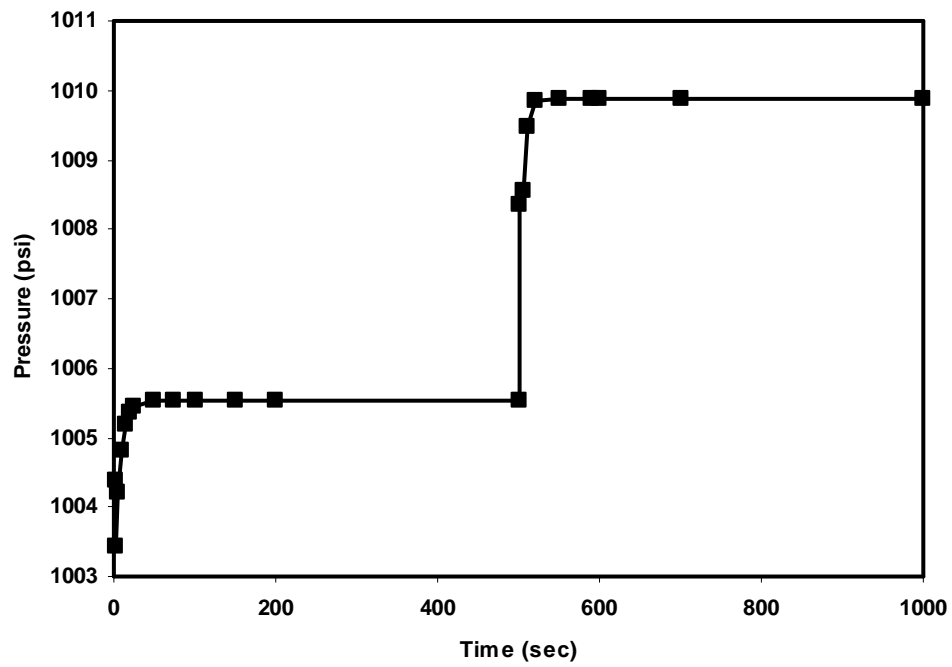


Figure 5.4 Pressure in the middle of the pipe *versus* time for Case 1

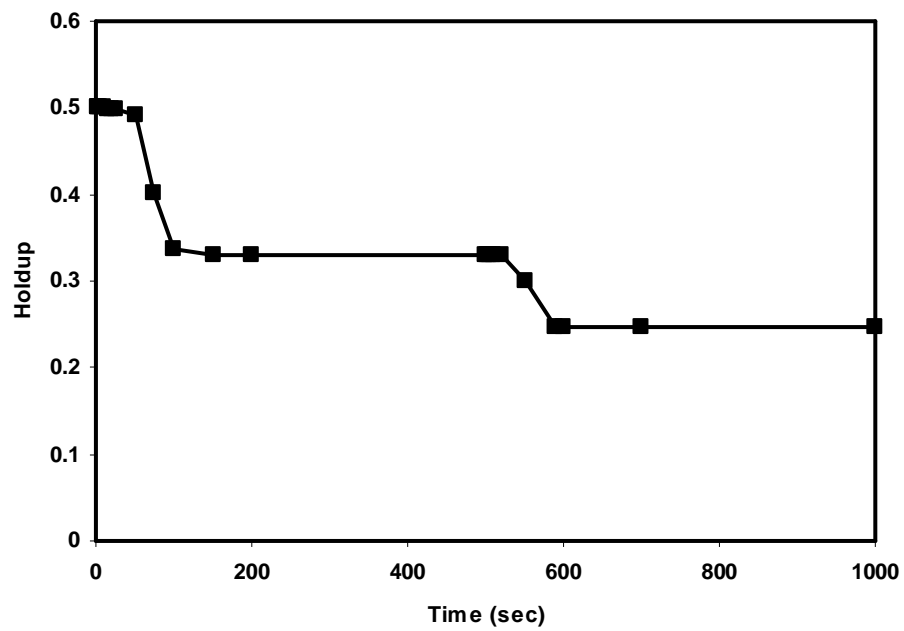


Figure 5.5 Holdup in the middle of the pipe *versus* time for Case 1

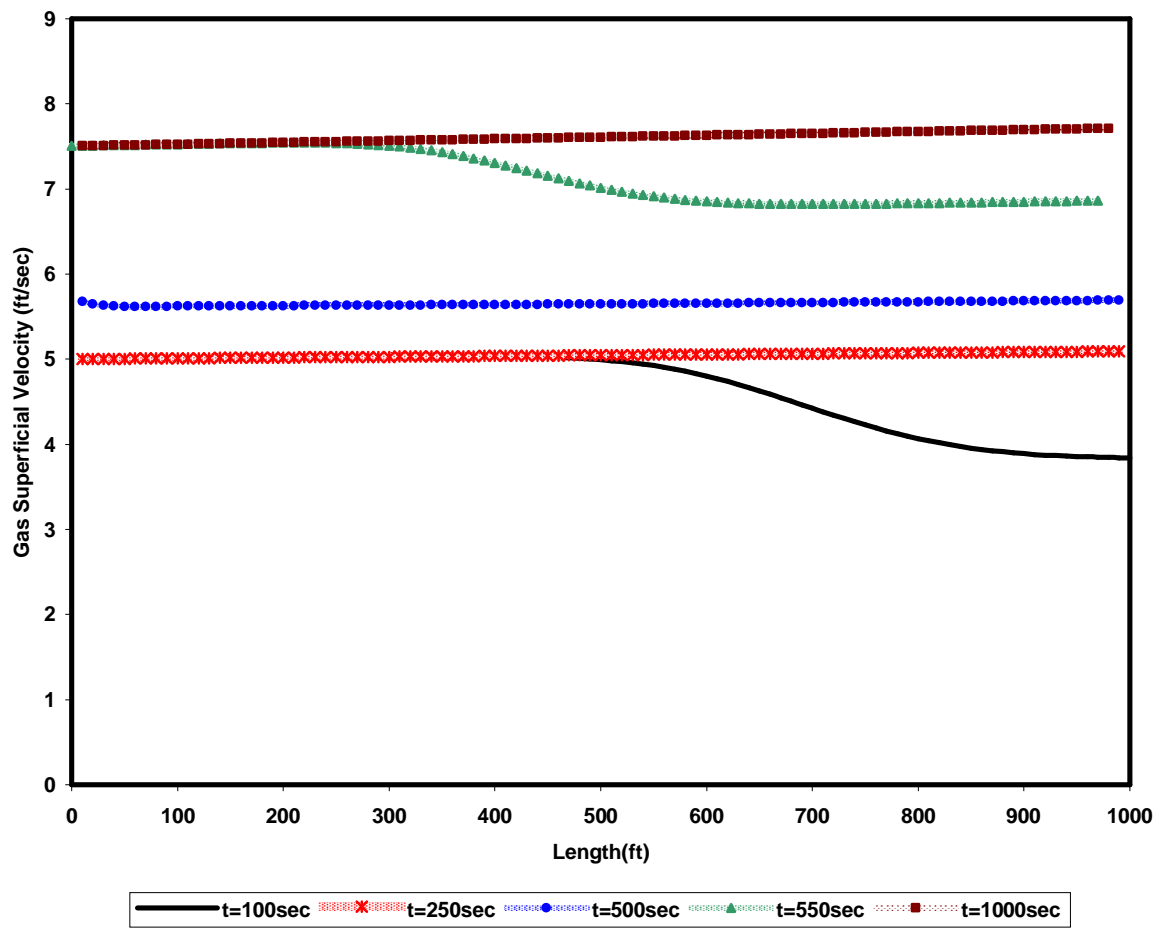


Figure 5.6 Gas superficial velocity profile for different times for Case 1

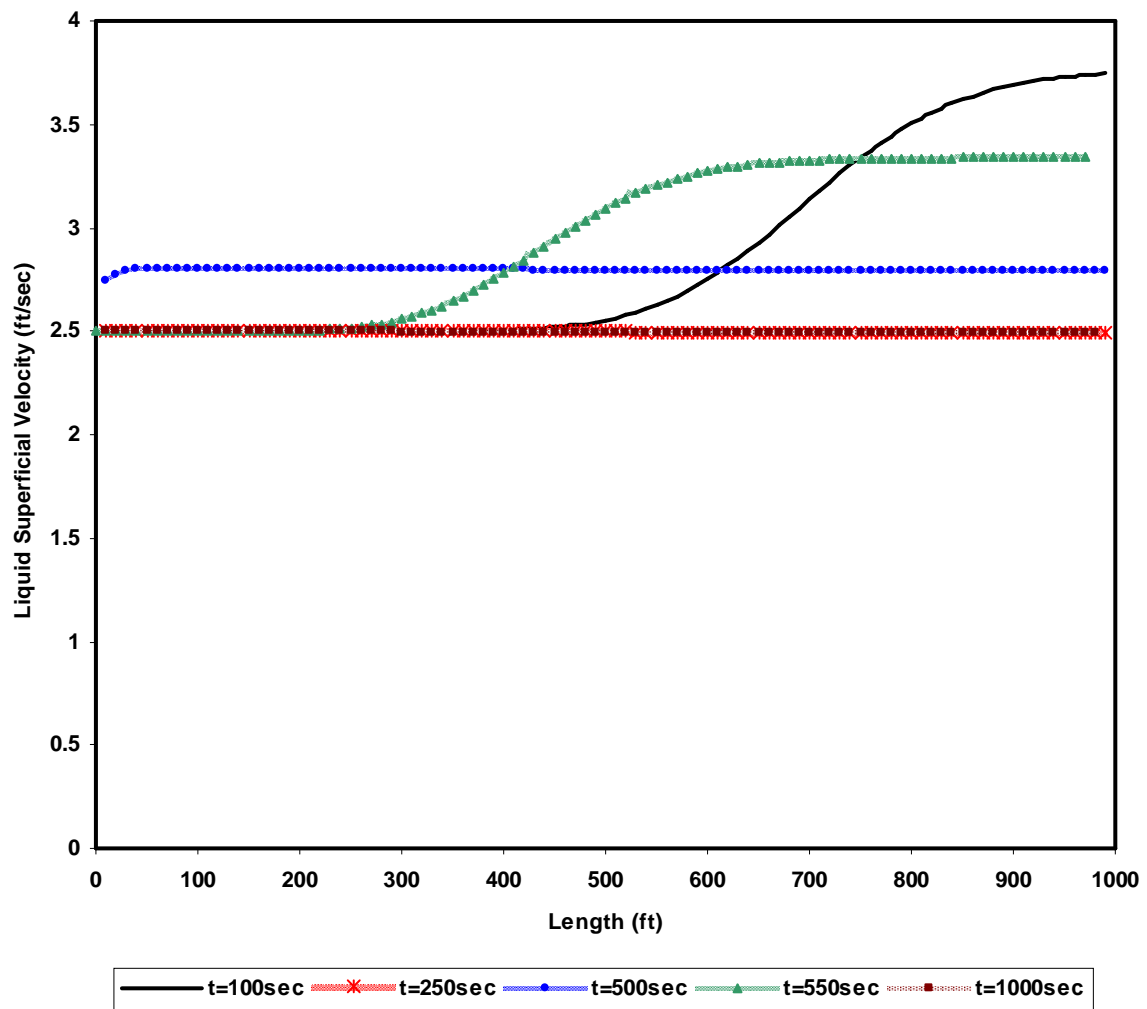


Figure 5.7 Liquid superficial velocity profile for different times for Case 1

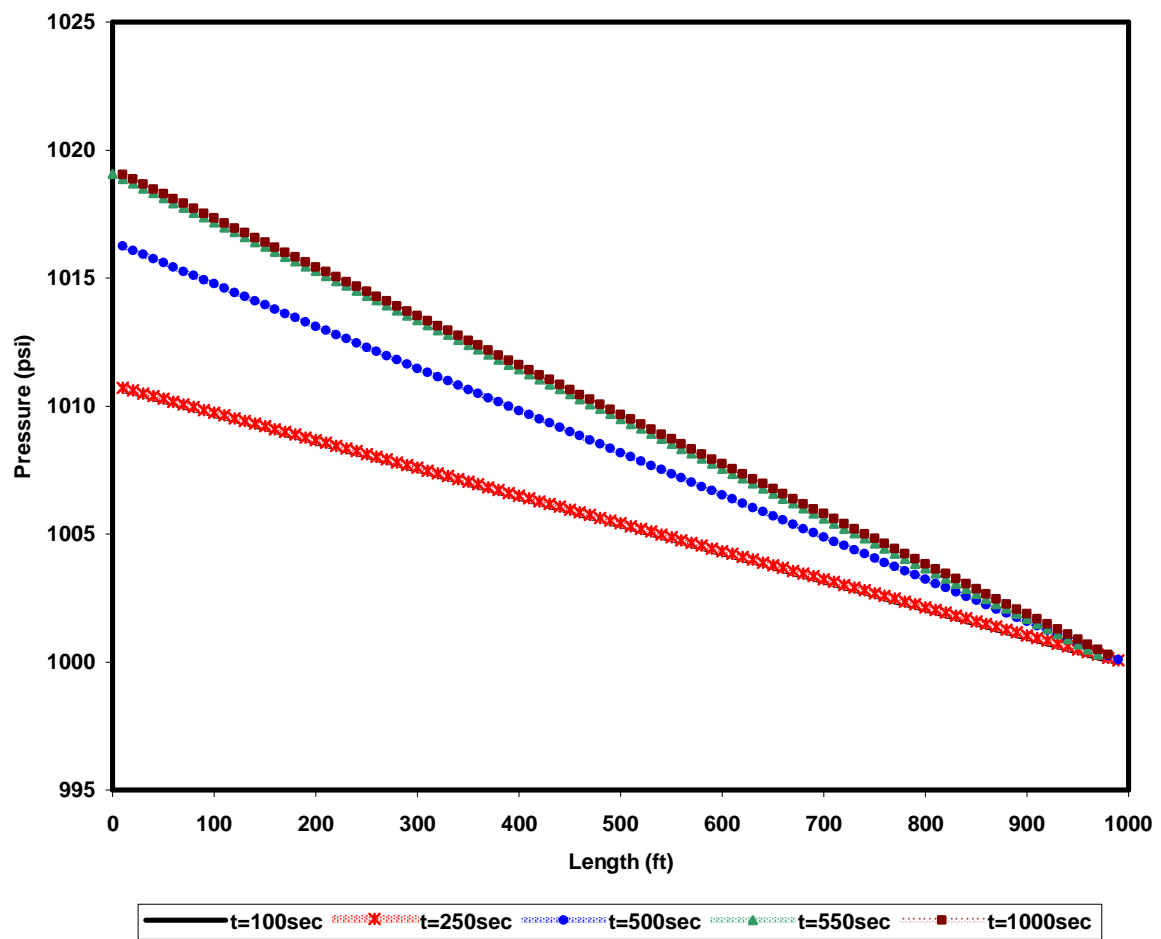


Figure 5.8 Pressure profile for different times for Case 1

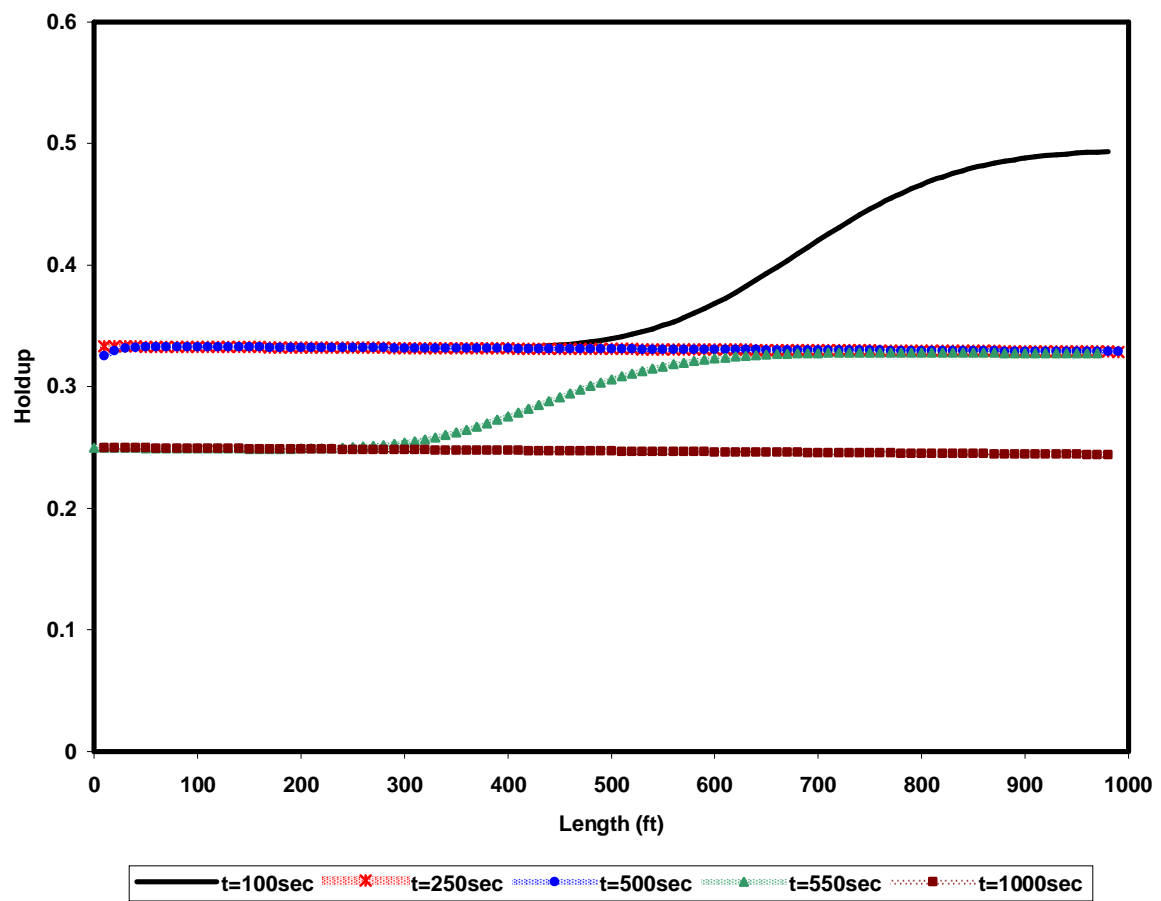


Figure 5.9 Holdup profile for different times for Case 1

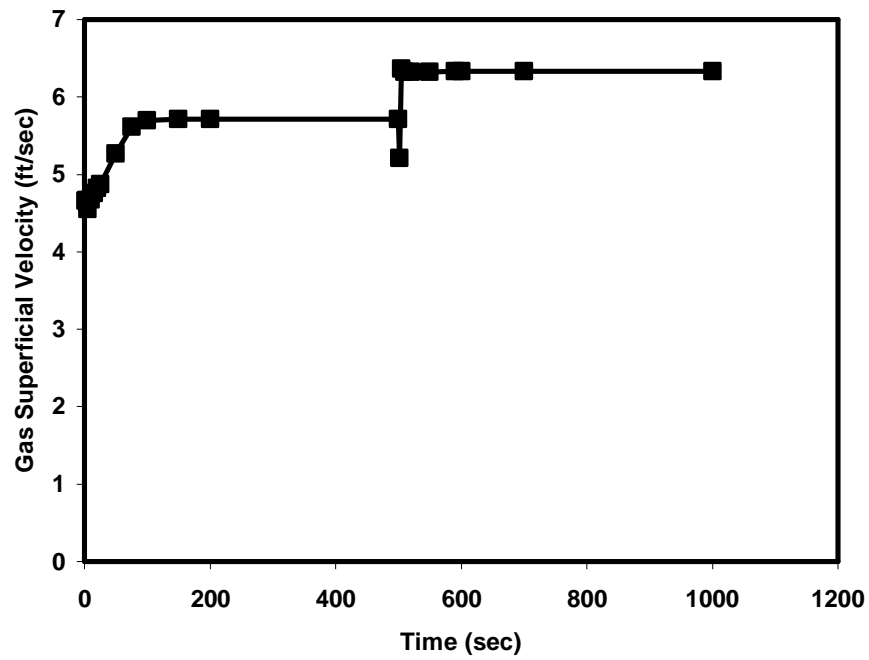


Figure 5.10 Gas superficial velocity in the middle of the pipe *versus* time for Case 2

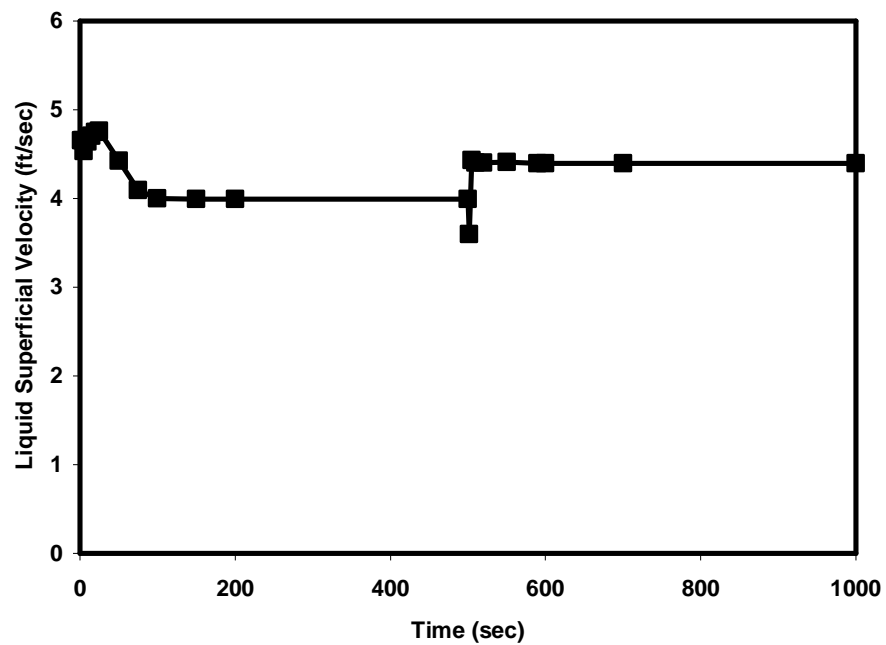


Figure 5.11 Liquid superficial velocity in the middle of the pipe *versus* time for Case 2

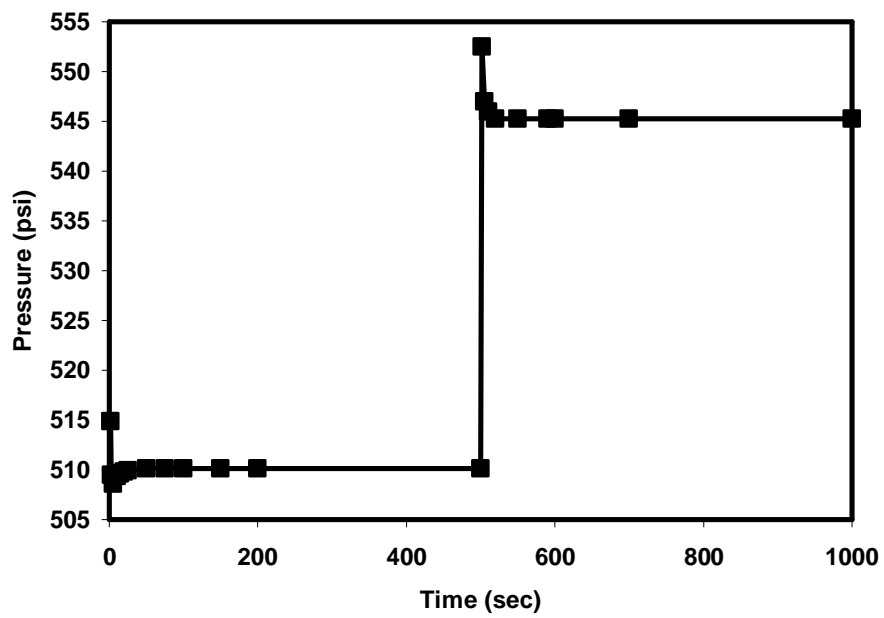


Figure 5.12 Pressure in the middle of the pipe *versus* time for Case 2

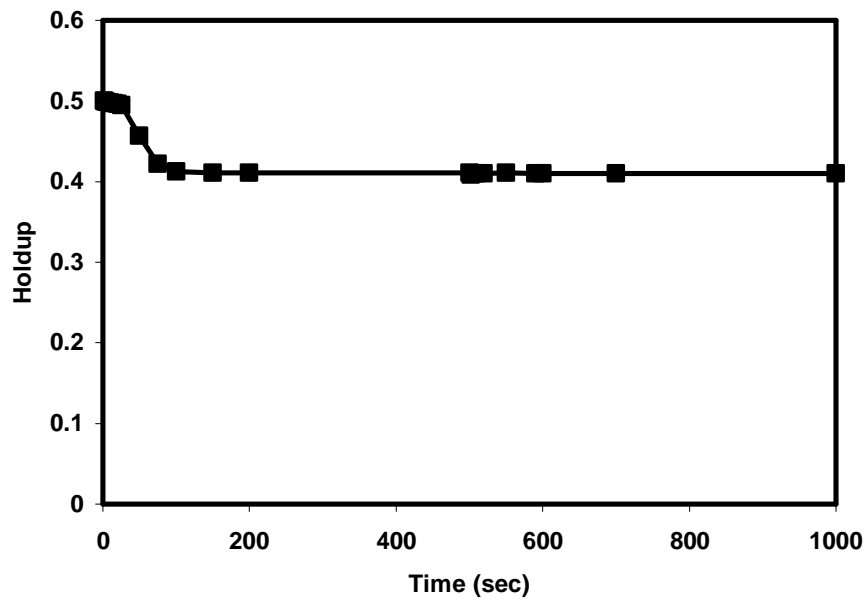


Figure 5.13 Holdup in the middle of the pipe *versus* time for Case 2

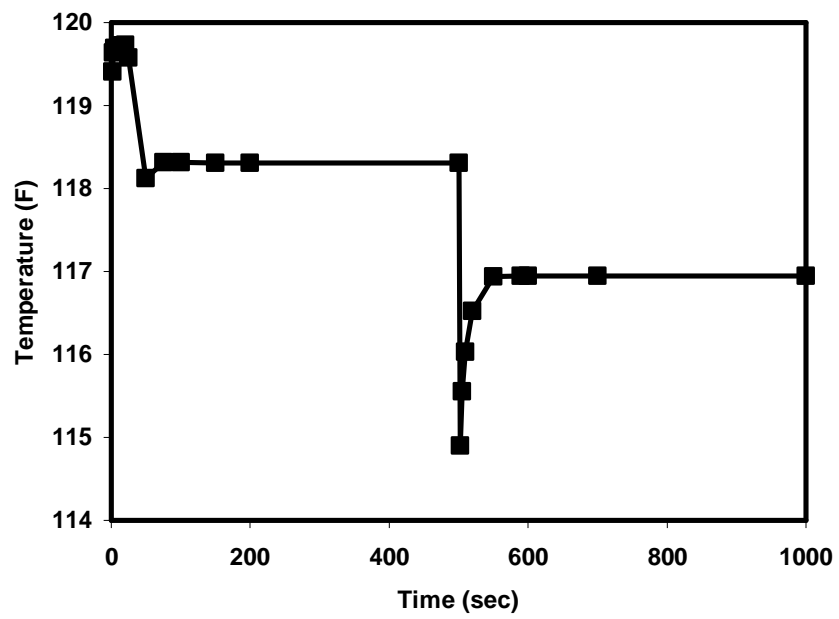


Figure 5.14 Temperature in the middle of the pipe *versus* time for Case 2

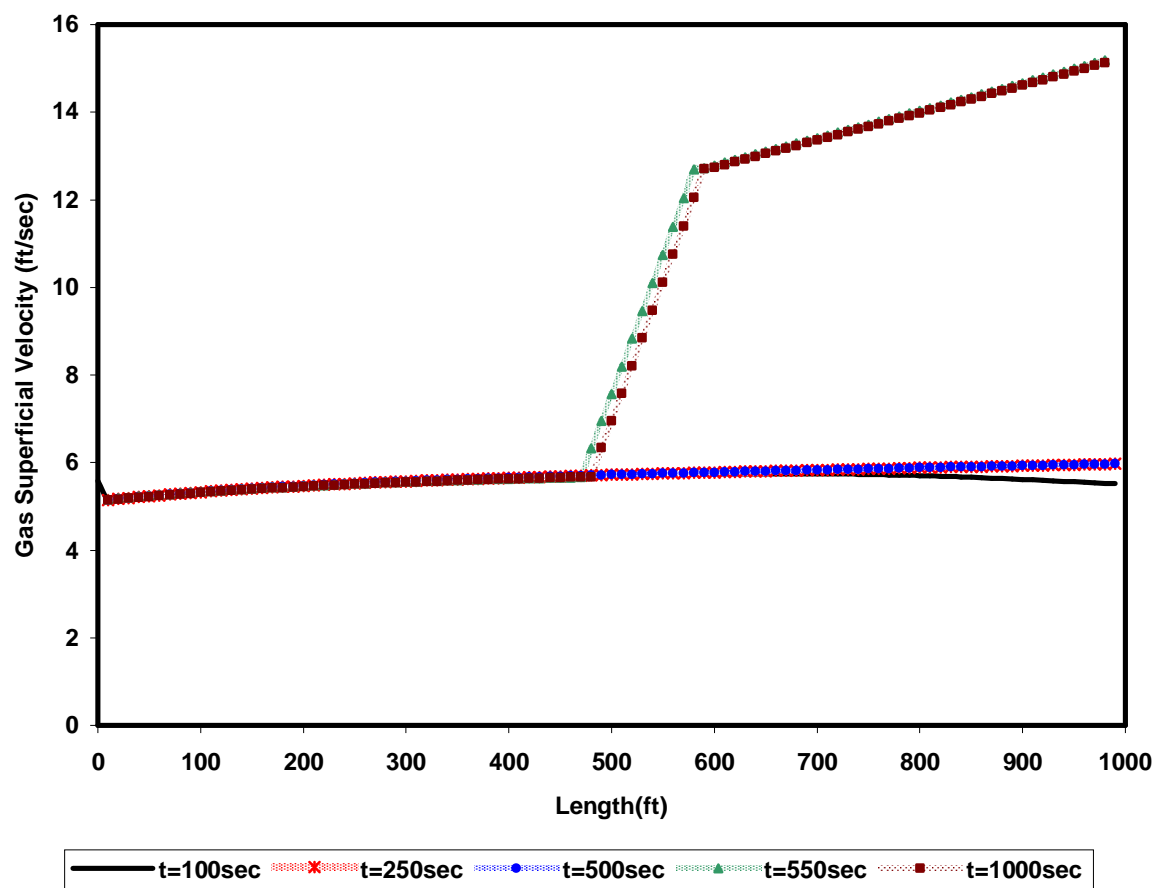


Figure 5.15 Gas superficial velocity profile for different times for Case 2

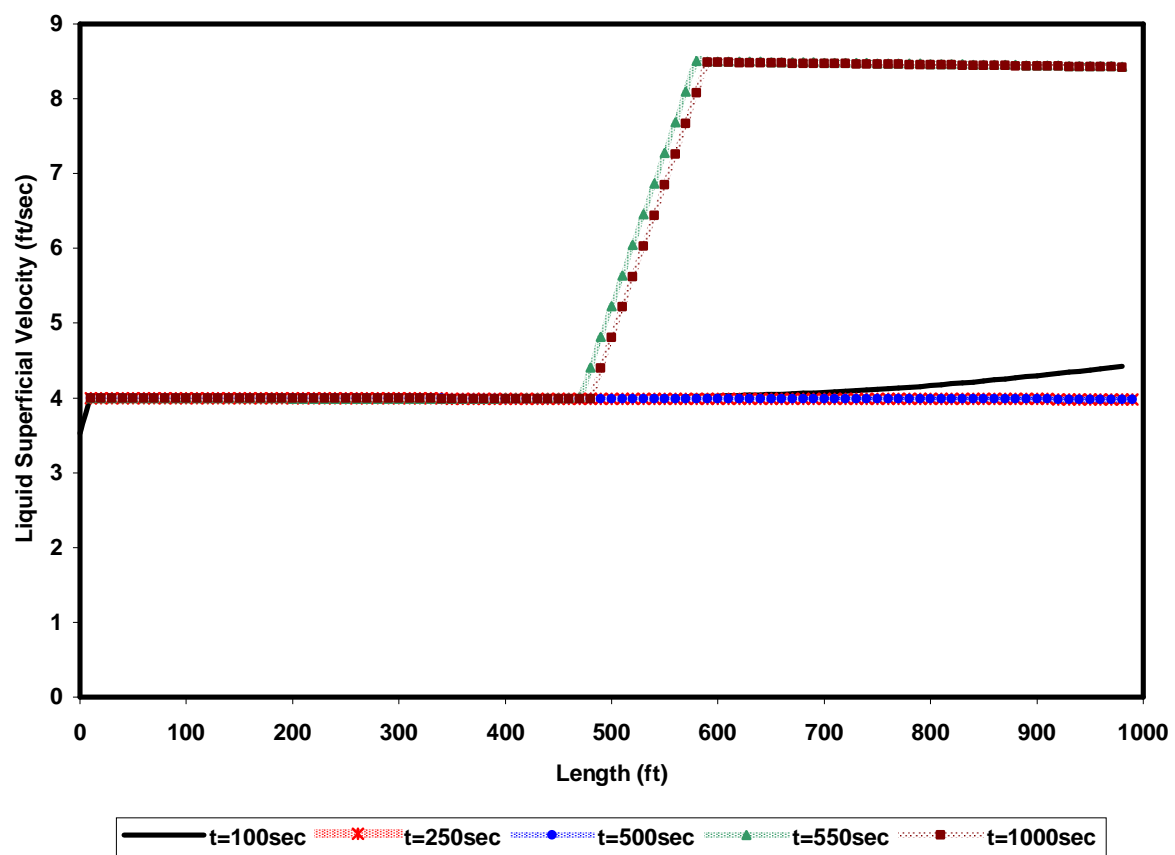


Figure 5.16 Liquid superficial velocity profile for different times for Case 2

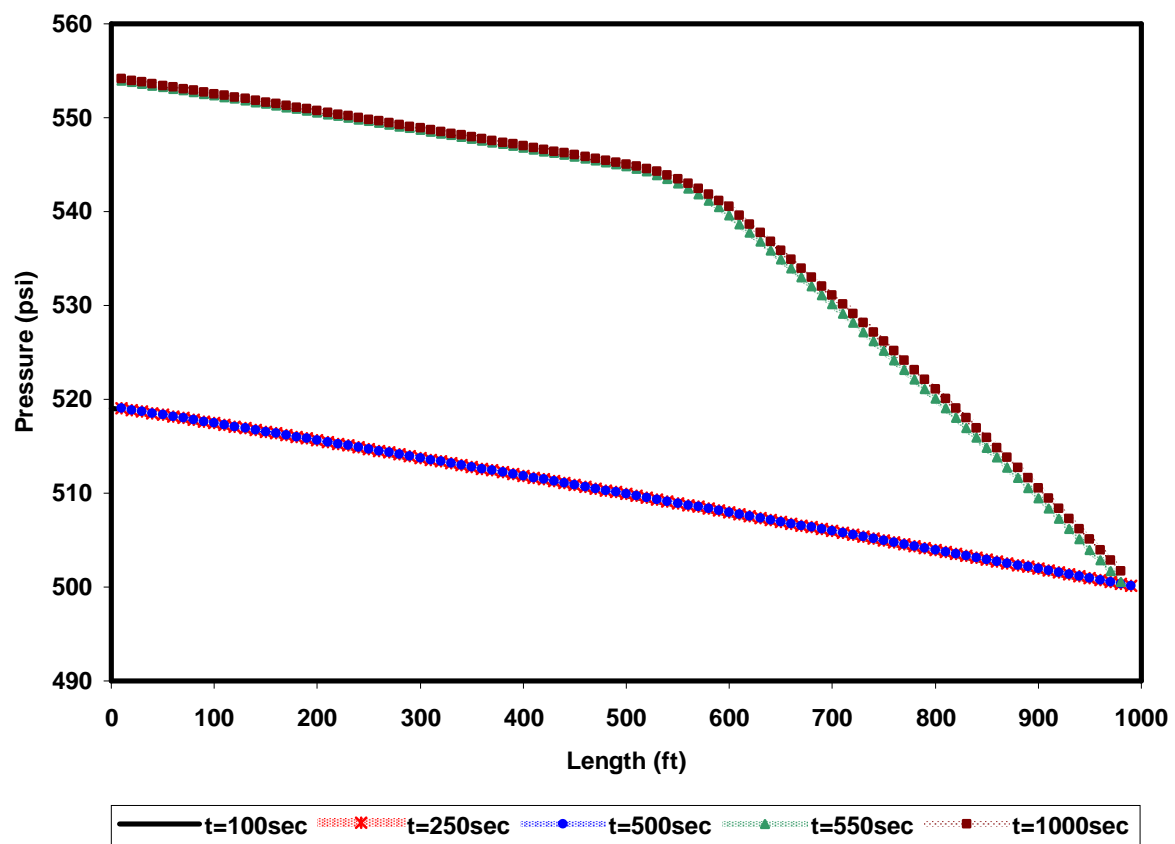


Figure 5.17 Pressure profile for different times for Case 2

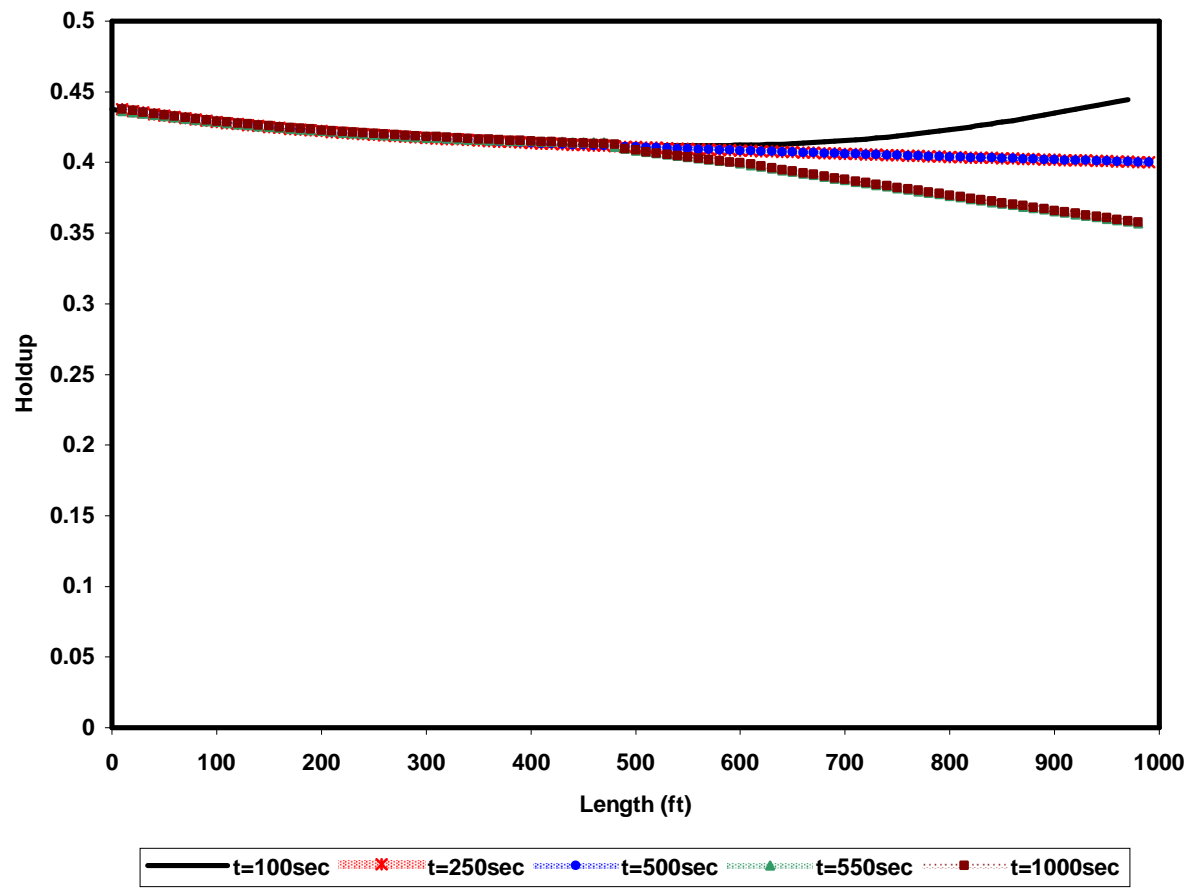


Figure 5.18 Holdup profile for different times for Case 2

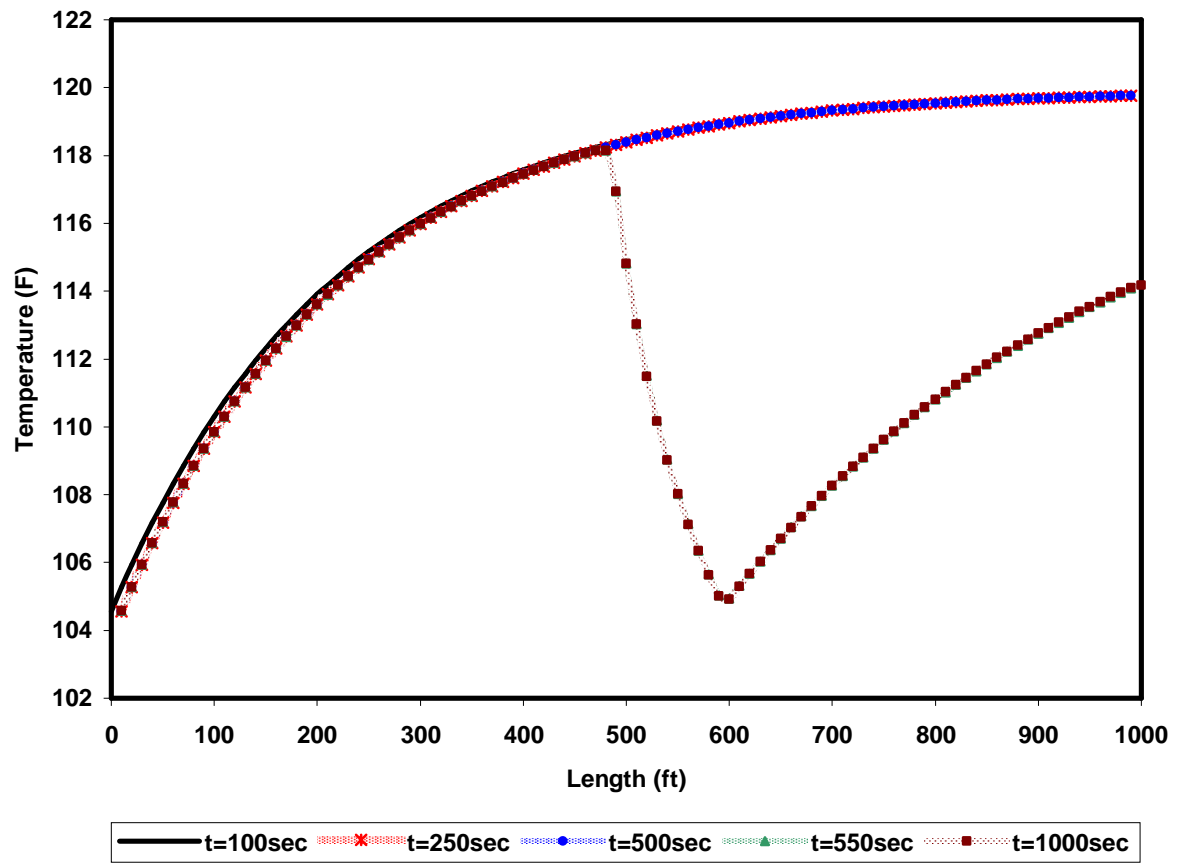


Figure 5.19 Temperature profile for different times for Case 2

Chapter 6: Comparisons of Models and the Investigation of the Sensitivity of Model Parameters

In this chapter, we compare the numerical schemes for the mathematical models that we developed for two-phase flow models. We vary the spatial discretization and time-step size to examine the sensitivity of the results and computational CPU time for various parameters. In addition, we compare the compositional explicit model with the pseudo-compositional fully-implicit model to investigate how the solution procedure can affect the results. Eventually, we also compared the model results with experimental data reported by Minami and Shoham (1994) to investigate flow regimes effect and a real picture of the accuracy of the model.

In Section 6.1 we present the spatial discretization effect on the numerical results and in Section 6.2 we investigate the time-step size effect. In Section 6.3 we compare the steady-state simulation results with long time transient simulation results. In Section 6.4 we compare the compositional explicit solution procedure with the pseudo-compositional implicit method. For validation of the results, in Section 6.5 we compare the numerical results with analytical solutions, and in Section 6.6 we compare our simulation results with experimental data.

6.1 SPATIAL DISCRETIZATION

Table 6.1 shows the input parameters for the cases that we used in this section. We apply water and air as the fluids that are flowing in the system. In fact, we adopt this simple two-phase flow system to eliminate the phase behavior calculations.

To verify the spatial discretization effect, we performed the cases with 20, 50, 100 and 200 segments. Figures 6.1 through 6.4 show the pressure, holdup, liquid, and gas superficial velocities comparison. As can be seen, the results are very close to each other

and they merge almost to the same value after $N=100$. The corresponding mesh size for $N=100$ is 10 ft . The results show that mesh refinement smaller than 10 ft does not improve the accuracy. Table 6.2 shows the maximum difference between the results respect to finest mesh size that we used.

Table 6.3 shows the computation times for different mesh sizes. It can be observed that for the 200 segments case a significant computation time is required. However, the difference between 100 segments case and 200 segments case is very small. Hence, for the simulation purpose, 100 segments with six times faster computation time is more cost effective.

6.2 TIME-STEP SIZE

To investigate the time-step size effect on the solutions, we performed simulations for water/air flow considering time-step sizes of 0.1sec, 1 sec and 10 sec. We applied the 100 segments case as discussed in the previous section and ran the cases for a 4,000 sec simulation time.

Table 6.4 shows the CPU time required for different time-step sizes (The computer property is 1.8 GHz processor and 2038 MB of RAM). As can be observed for $dt = 0.1\text{ sec}$, a significant computation time is needed. However, as Figures 6.5 through 6.8 show the difference between the results is not notable. Table 6.5 shows the difference between the results.

Although selecting small time-step improves the results and the convergence but it takes significant run time. In fact for small time-step less number of iterations is needed in the Newton method. However, larger number of calculation steps is required to reach the end of the simulation time.

Hence, for simulation purpose adopting appropriate time-step size is crucial. The best approach for time-step selection is using adaptive time-stepping. In this approach small time-step is chosen in the early time and large time-step size is chosen in the late transient time. Equation (6.1) shows the calculation of time-step by using relative mass error value (rme).

$$dt_{\min} = 2rme \times \frac{1}{\frac{1}{S} \frac{dS}{dt}} \quad (6.1)$$

where S is the total mass in the segment.

It should also be noted that there is another limitation for time-step size. The time-step size should satisfy the Courant–Friedrichs–Lewy (CFL) condition (Courant et al., 1967). For one-dimensional case, the CFL condition is given by

$$\frac{U \cdot dt}{dx} \leq C \quad (6.2)$$

where C is constant and depends on the numerical problem that we solve.

For our numerical problem the CFL condition is reflected to time-step size that constrains it to a value less than the time for the flow to travel adjacent grid point. Hence from this constraint the maximum time-step size can be obtained as

$$dt_{\max} = \frac{dx_{\min}}{U_{j \max}} \quad (6.3)$$

6.3 COMPARISON OF STEADY-STATE AND TRANSIENT SOLUTIONS

In Chapter 3, we introduced the fully-implicit, steady-state two-phase model. In Chapter 5, we presented the corresponding transient model. To verify the outcome of the transient model for a long simulation time we set up a water/air flow case in this section. We assume a 1000 *ft* long well with the liquid inlet velocity of 10 *ft*/sec, the gas inlet velocity of 8 *ft*/sec and the gas-oil ratio of 50%. We also consider similar fluid data and wellbore geometry to what was reported in Table 6.1. The objective of this test was to verify how the final outcome of the transient model approaches the steady-state solution.

Figures 6.9 through 6.12 show the pressure, holdup, liquid superficial velocity and gas superficial velocity profiles for the transient model after 4,000 sec. and also steady-state model solution. As can be observed, there is a good agreement between the solutions.

6.4 COMPARISON BETWEEN THE PSEUDO-COMPOSITIONAL AND THE COMPOSITIONAL MODELS

In Chapter 4, we developed a compositional wellbore model which was coupled to the reservoir simulator. An explicit solution procedure was adopted to solve the wellbore equations in that model. In this chapter, we compare that solution procedure with the fully-implicit procedure reported in Chapter 5.

In Table 6.6, the wellbore geometry, reservoir properties and fluid compositions are reported. The bubble point pressure for the 6-component fluid was computed as 2,814 psi. Thus, the simulating condition is below bubble point pressure for the reservoir and for the wellbore.

Figures 6.13 through 6.17 show the results for the compositional explicit model and for the pseudo-compositional fully-implicit model for pressure, holdup, liquid

velocity, gas velocity profiles, and flow regime identification. Although the solution procedures as well as the fluid properties calculation in those models were completely different, we obtained a good agreement between the results. In addition, the flow regime identification in both models was similar, only the holdup values were different for the two models, near the toe zone.

One reason for the difference in the holdup values can be the multiple solutions that exist for a non-linear set of equations. Since in our explicit model in Chapter 4 we use a steady-state model and solve holdup from the summation of the liquid and gas momentum equations, depending on the initial guess, we might obtain different results for holdup. However, since we start from an initial condition which is established in the system, we obtain the most correct answer for holdup in the transient model. Another reason would be the closure relationships that we used in the two models. In the explicit model, we simplified the inter-phase closure relations; however more comprehensive models were applied in the fully-implicit model.

6.5 COMPARISON BETWEEN THE NUMERICAL AND THE ANALYTICAL SOLUTIONS

We performed single phase incompressible water injection with low velocity (0.1 ft/sec) into a very smooth vertical pipe with 0.4 ft diameter. In this case, we had an ideal single phase flow with no friction loss. Hence, we expect to obtain only a pressure gradient due to gravity and the same fluid velocity as in the inlet. Figure 6.18 shows the results obtained from the numerical and analytical pressure calculation along the well. As can be seen there is good agreement between the numerical and analytical solutions. The difference between the results is less than 0.2 psi .

6.6 VALIDATION OF THE TRANSIENT MODEL WITH EXPERIMENTAL DATA

In this section, we compare the transient model results to experimental data reported by Minami and Shoham (1994), discussing the flow regime effect on the model results. Figure 6.19 shows the schematic diagram of the flow loop used by Minami and Shoham. The flow loop is a 420 m steel pipe and there are 4 measurement stations in the flow path as shown in figure. Each station is comprised by a 3 m PVC pipe located at 63.7 m, 202.7 m, 230.8 m and 398 m from the inlet mixing tee. In each station appropriate equipments are placed to measure pressure and holdup.

Compressed air and kerosene are used as the two-phase mixture in the experiment. Initially, a steady-state condition is set by $0.065 \frac{m^3}{sec}$ gas flow rate and $0.00085 \frac{m^3}{sec}$ liquid flow rate at the inlet and 205 kPa pressure at the outlet (separator). After about 87 sec, the gas flow rate in the inlet is increased to $0.105 \frac{m^3}{sec}$ and then transient behavior is recorded in the stations and outlet.

Minami and Shoham (1994) reported that slug flow was observed through the pipe in their experiment. We used two different flow regimes in our simulation to investigate the transient results against the experimental data. Since slug flow in higher frequency is close to the stratified flow, we used the stratified flow with some modification in the inter-phase friction factor coefficient as our main model. In addition, we used the bubbly flow model to compare the results with modified stratified flow and to show the importance of flow regime on the results. Figures 6.20 through 6.22 show the comparison between modified stratified flow and experimental data, and Figures 6.23 through 6.25 shows the bubbly flow results. As can be observed in the figures, there was good agreement among the models and the experimental data. However, the holdup values in the bubbly flow were different from the experimental data. In fact, the flow

regime model and closure relations for wall friction and inter-phase friction have a significant role on holdup value.

Table 6.1 Wellbore geometry and fluid data for water and air flow in horizontal pipe

Wellbore diameter	0.4 ft
Wellbore roughness	0.008 ft
Wellbore inclination	0 rad
Number of segments	200, 100, 50, 10
Segments length	5, 10, 20, 100 ft
Surrounding temperature	120 °F
Inlet temperature	120 °F
Overall heat transfer coefficient	0.1 Btu/sec. °F.ft ²
Inlet liquid flow rate	0.9425 ft ³ /sec
Inlet gas flow rate	0.314 ft ³ /sec
Liquid density	62.4 lbm/ ft ³
Gas density	0.07 lbm/ ft ³
Simulation time	4000 sec

Table 6.2 Comparison between the results for different mesh sizes, maximum difference respect to fine mesh size (dz = 5 ft)

Mesh size (ft)	Pressure(psi)	Holdup	Gas Velocity (ft/sec)	Liquid Velocity (ft/sec)
50	1.25	1.26e-3	2.05e-1	4.58e-3
20	8.5e-1	1.52e-3	2.36e-2	1.31e-3
10	3.5e-1	4.72e-5	7.02e-4	7.76e-5

Table 6.3 CPU time comparison for the segments variation study (1.8 GHz processor and 2038 MB of RAM)

Case 1 (N=200, dt=10 sec)	495.14 sec
Case 2 (N=100, dt=10 sec)	86.0 sec
Case 3 (N=50, dt=10 sec)	16.4 sec
Case 4 (N=20, dt=10 sec)	3.2 sec

Table 6.4 CPU time comparison for the time-step variation study
(1.8 GHz processor and 2038 MB of RAM)

Case 1 (N=100, dt=10 sec)	86.0 sec
Case 2 (N=100, dt=1 sec)	531.8 sec
Case 3 (N=100, dt=0.1 sec)	2862.6 sec

Table 6.5 Comparison between the results for different time-step sizes,
maximum difference respect to smallest time-step size (dt = 0.1
sec)

Time-step(sec)	Pressure(psi)	Holdup	Gas Velocity (ft/sec)	Liquid Velocity (ft/sec)
1	3.95e-4	2.84e-6	4.23e-5	4.68e-6
10	8.73e-5	6.30e-7	9.35e-6	1.03e-6

Table 6.6 Wellbore geometry and fluid data for the compositional model

Wellbore diameter	0.4 ft
Wellbore roughness	0.008 ft
Wellbore inclination	0 rad
Number of segments	100
Segments length	10 ft
Surrounding temperature	140 °F
Inlet temperature	140 °F
Overall heat transfer coefficient	0.1 Btu/sec. °F.ft ²
Oil productivity index	10 ⁻⁵ ft ³ /(sec.psi.ft)
Gas productivity index	10 ⁻⁵ ft ³ /(sec.psi.ft)
Water productivity index	0 ft ³ /(sec.psi.ft)
Reservoir pressure	2000 psi
Pressure at heel	1800 psi
	C1=0.6
	C3=0.1
Fluid composition (mole fraction)	C6=0.1
	C10=0.1
	C15=0.05
	C20=0.05

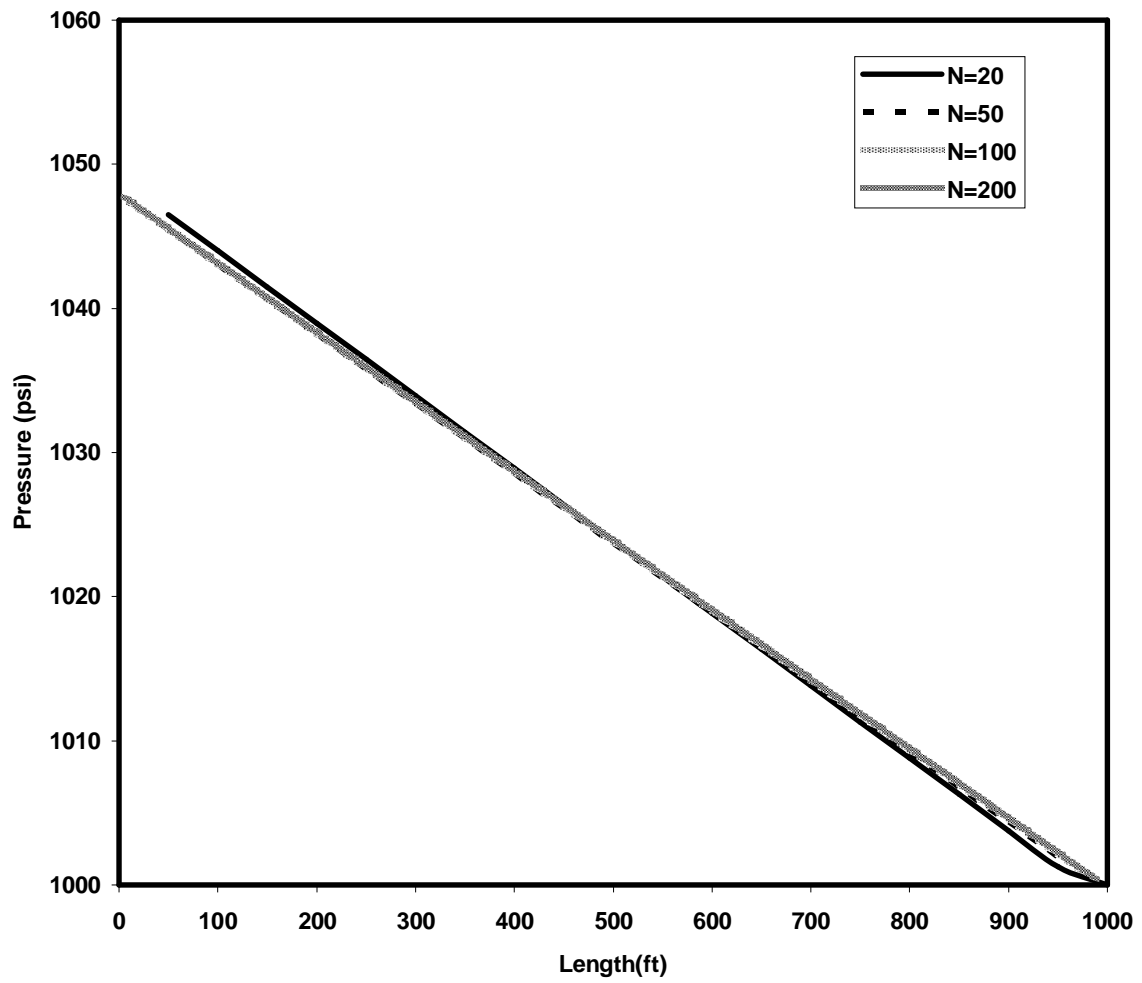


Figure 6.1 Pressure profile for different mesh sizes after 4000 sec

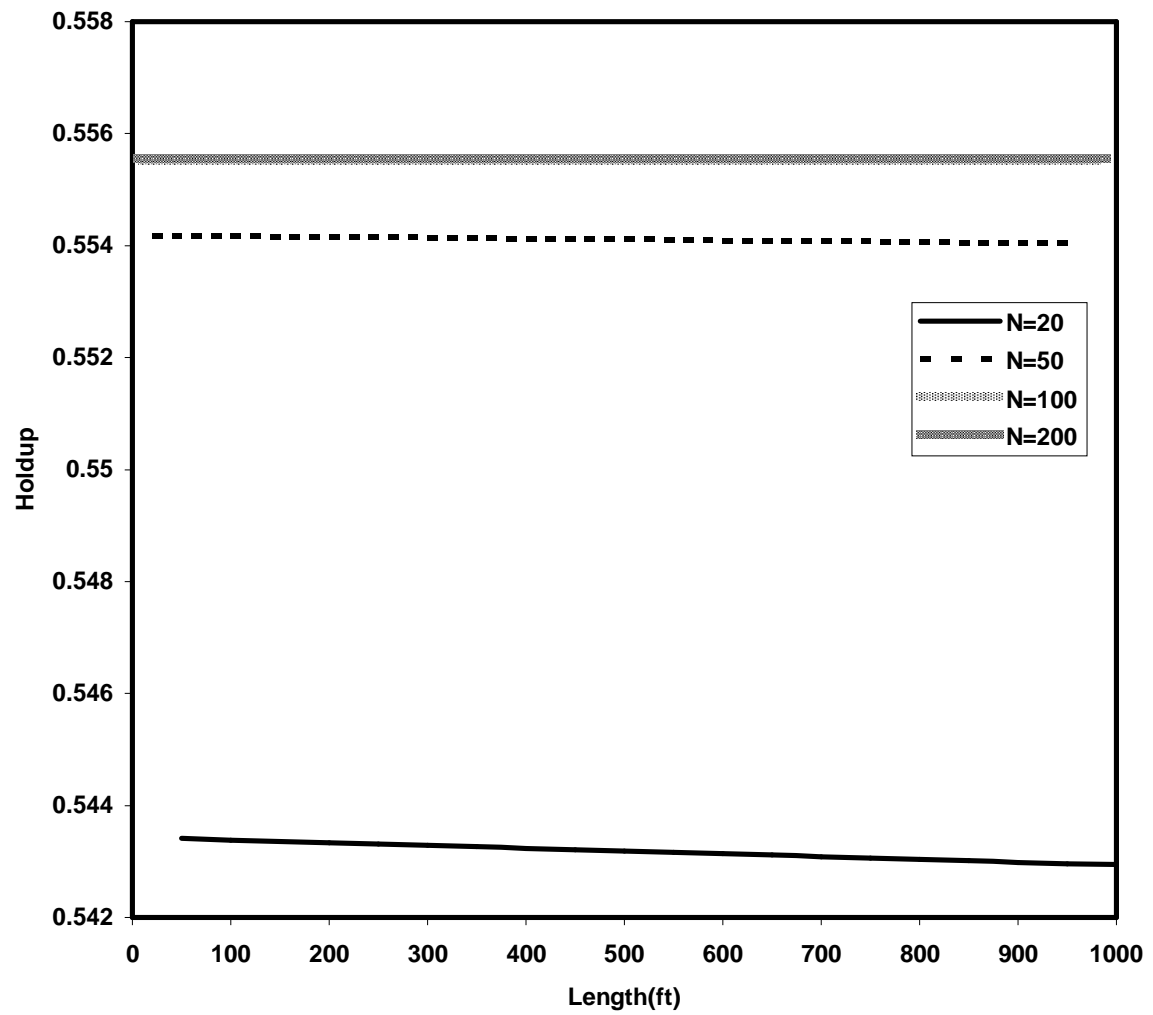


Figure 6.2 Holdup profile for different mesh sizes after 4000 sec

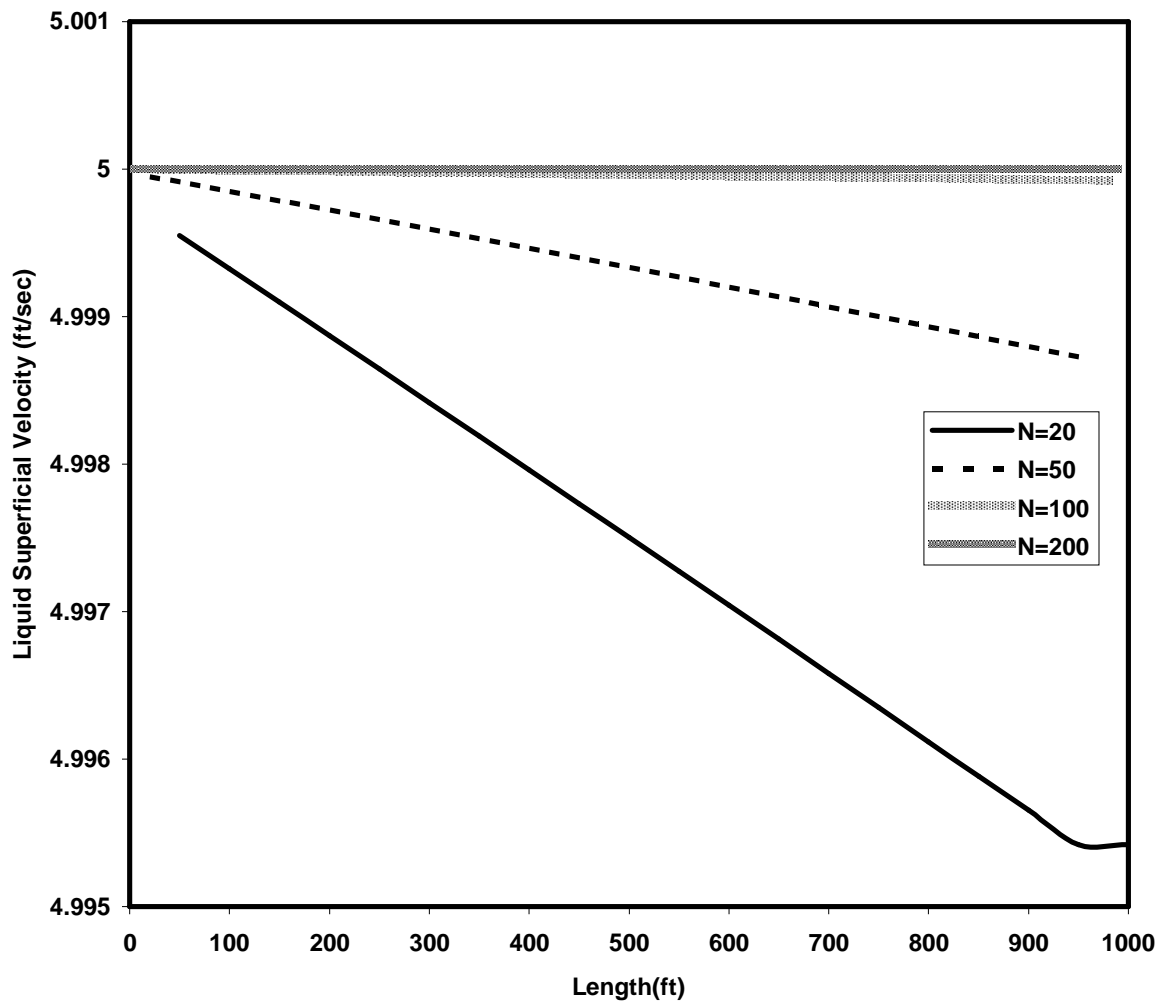


Figure 6.3 Liquid superficial velocity profile for different mesh sizes after 4000 sec

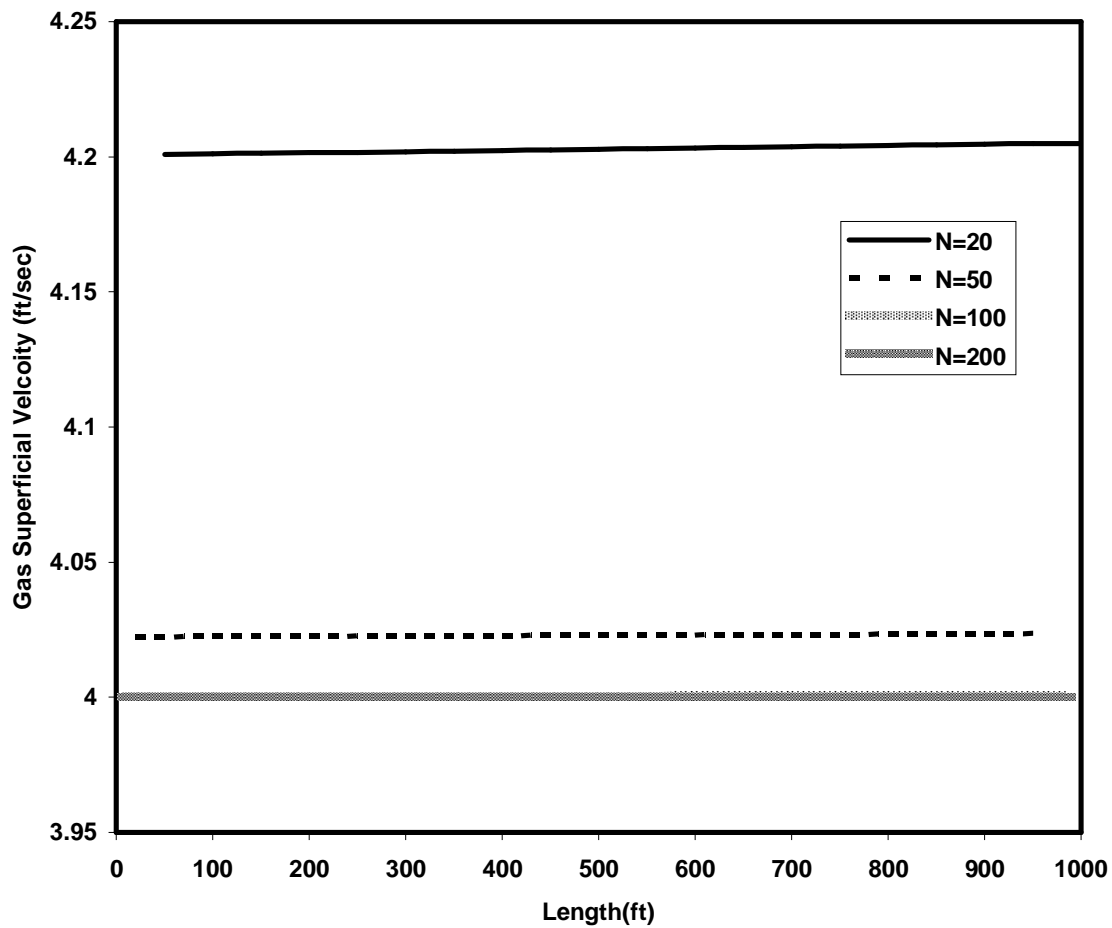


Figure 6.4 Gas superficial velocity profile for different mesh sizes after 4000 sec

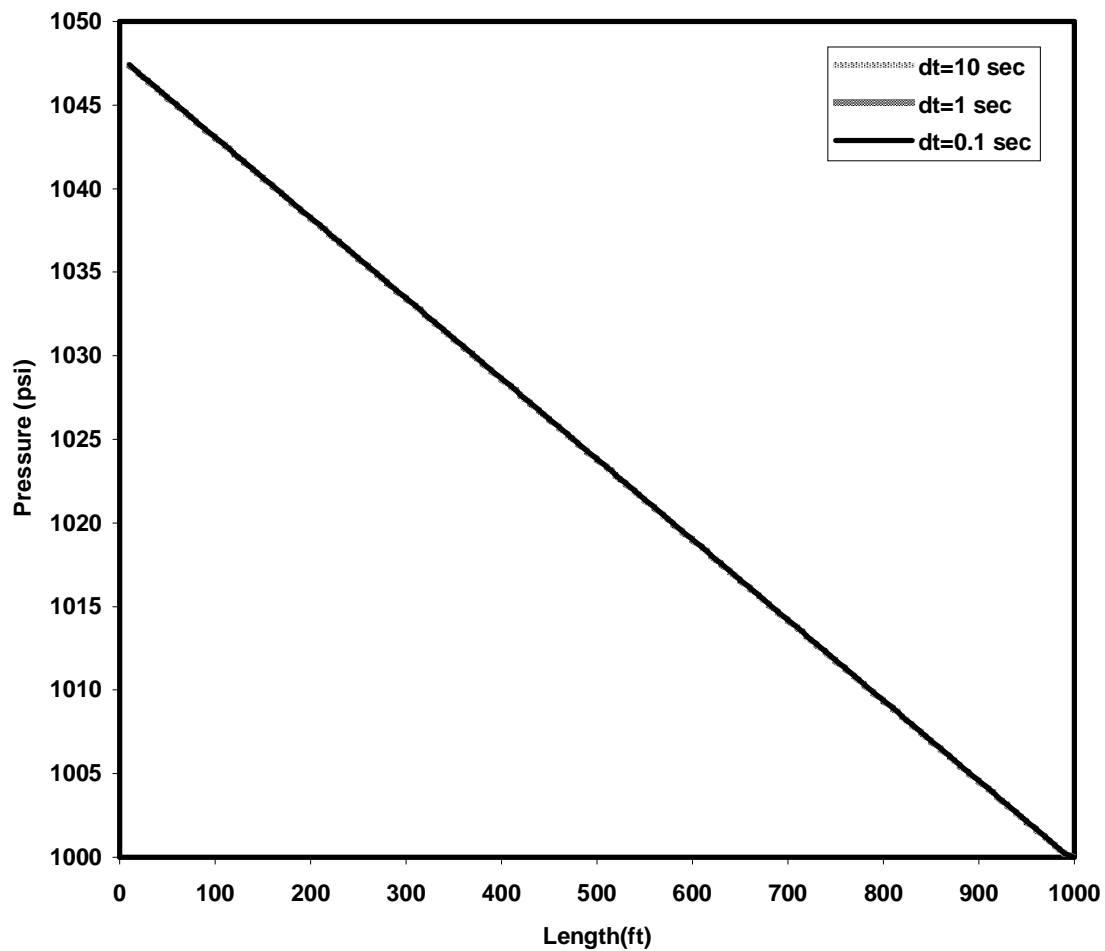


Figure 6.5 Pressure profile for different time-step sizes after 4000 sec

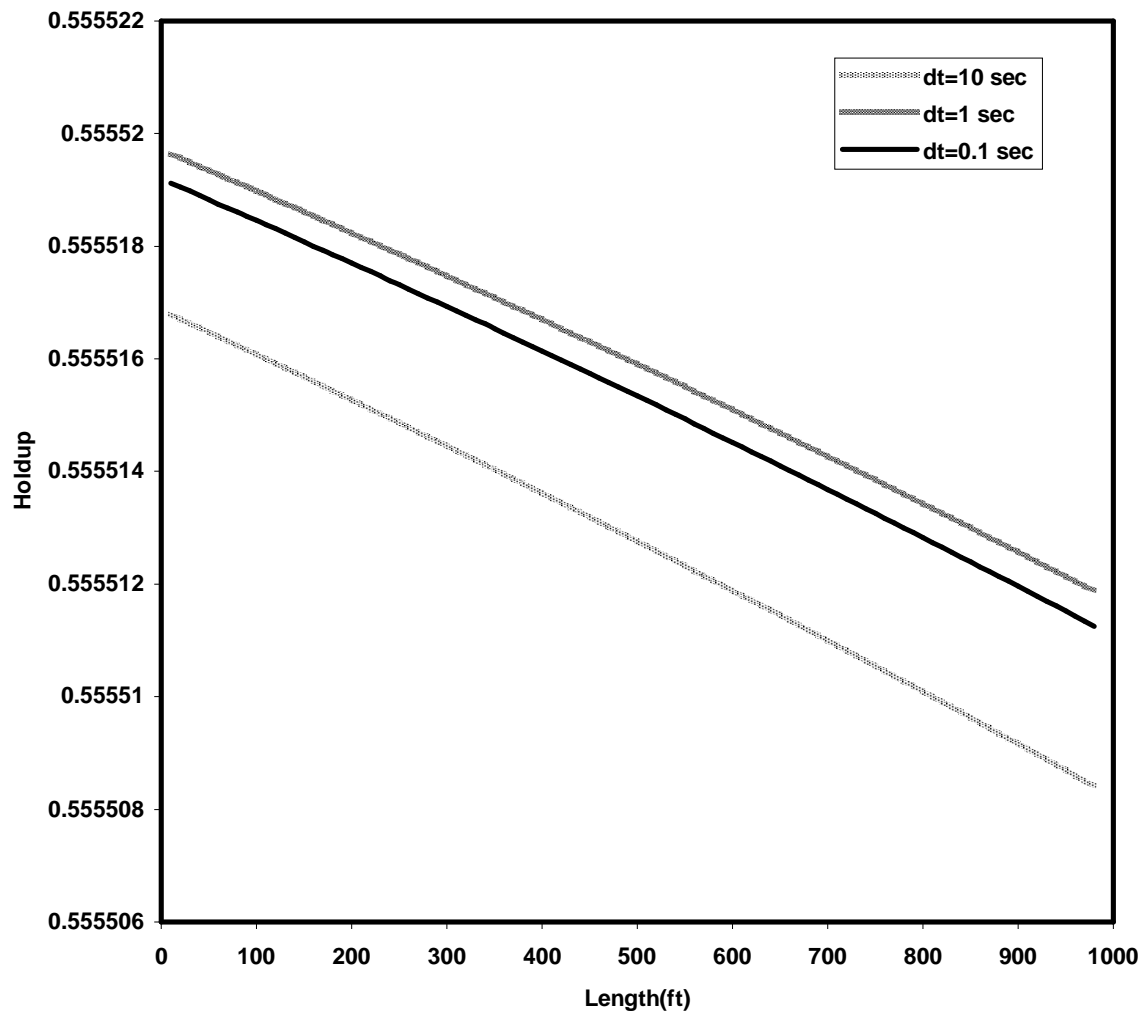


Figure 6.6 Holdup profile for different time-step sizes after 4000 sec

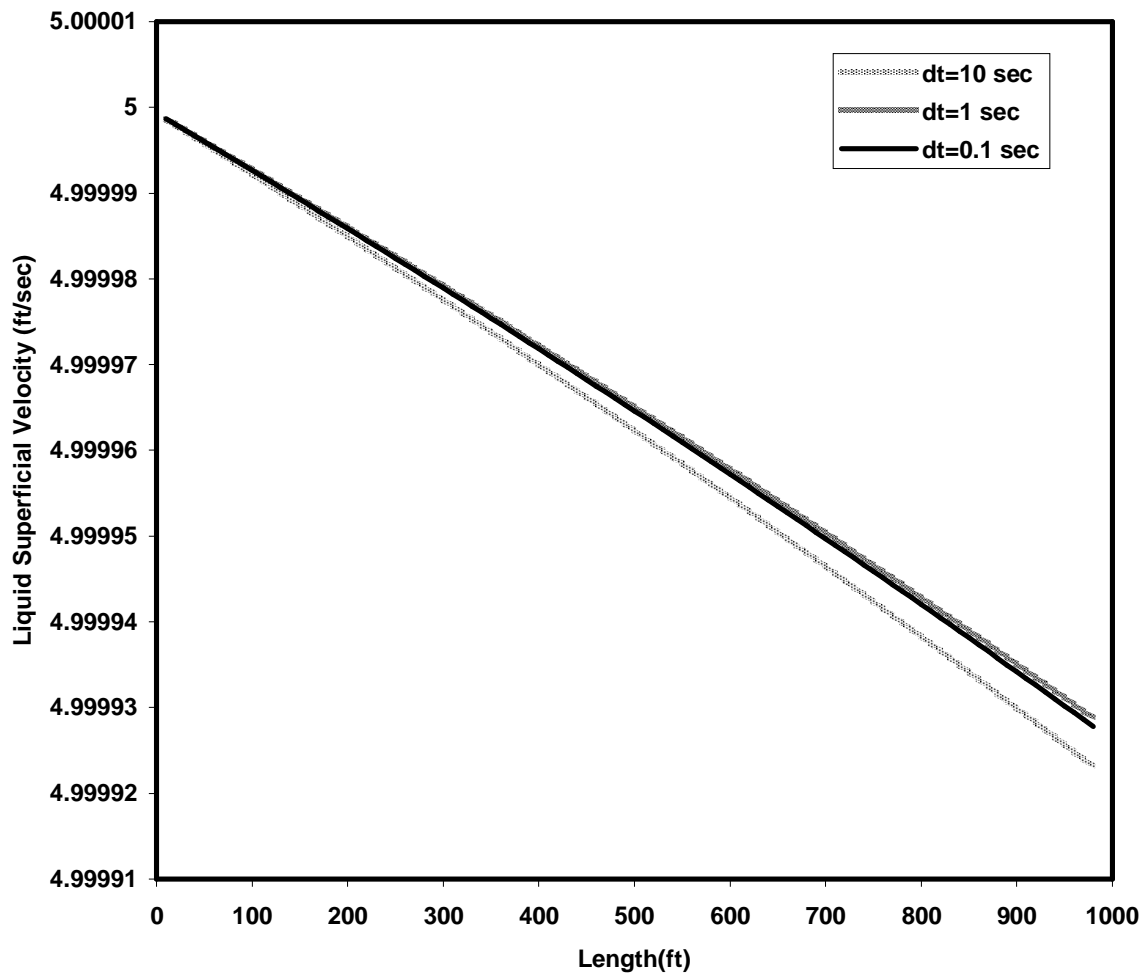


Figure 6.7 Liquid superficial velocity profile for different time-step sizes after 4000 sec

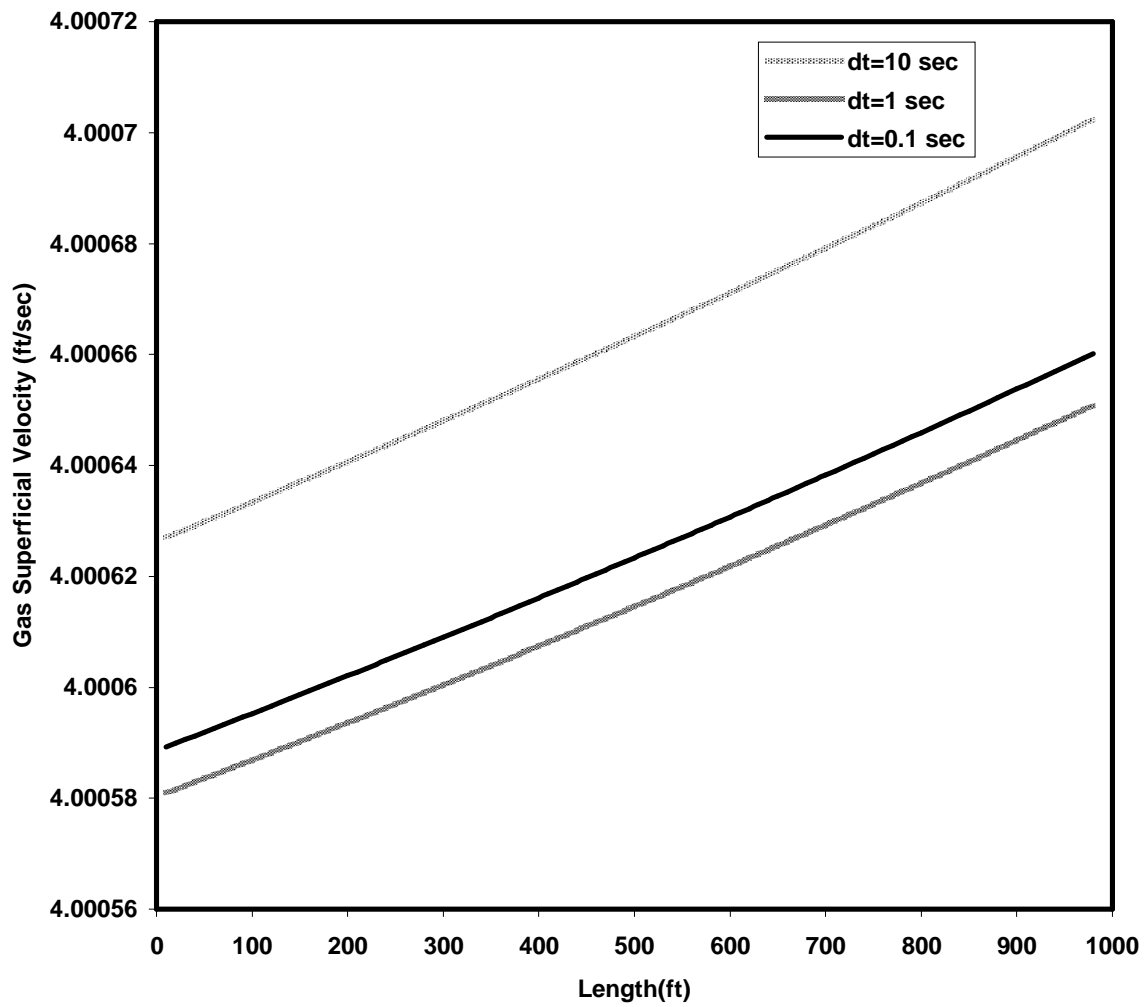


Figure 6.8 Gas superficial velocity for different time-step sizes after 4000 sec

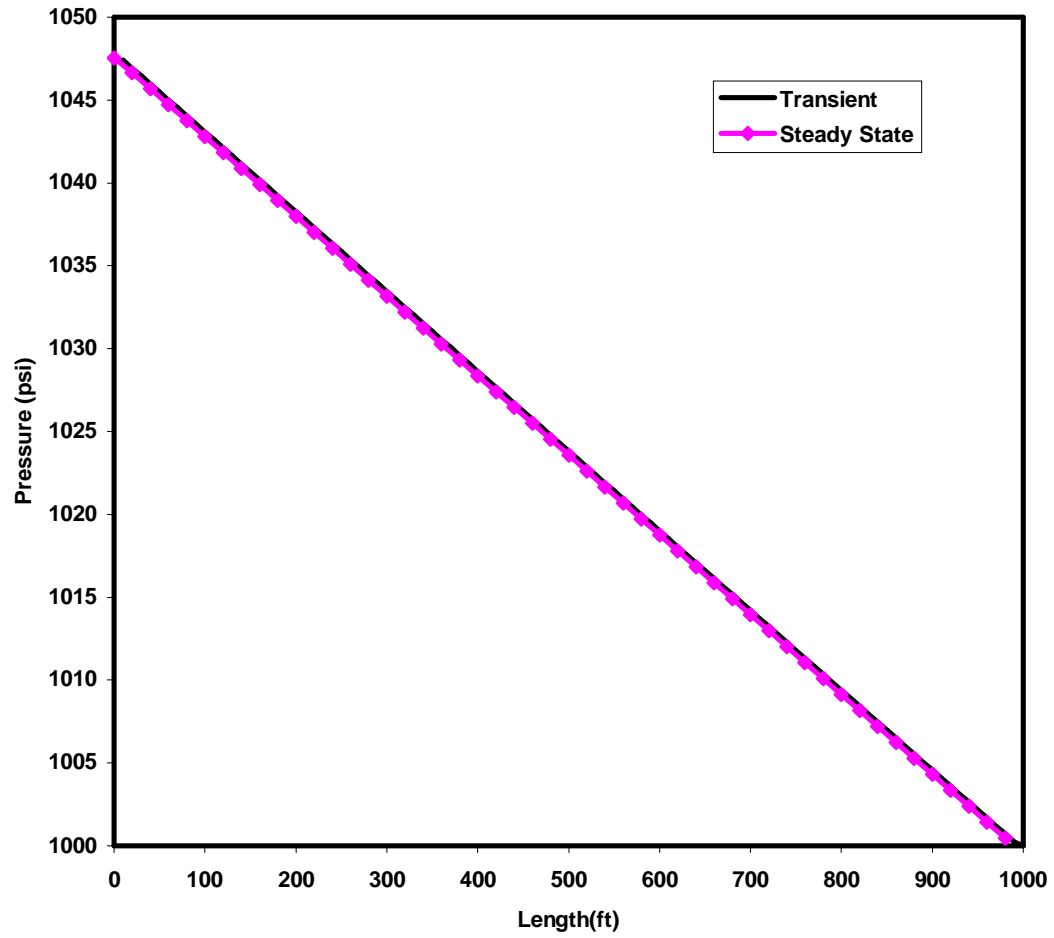


Figure 6.9 Pressure profile comparison between transient and steady-state solutions

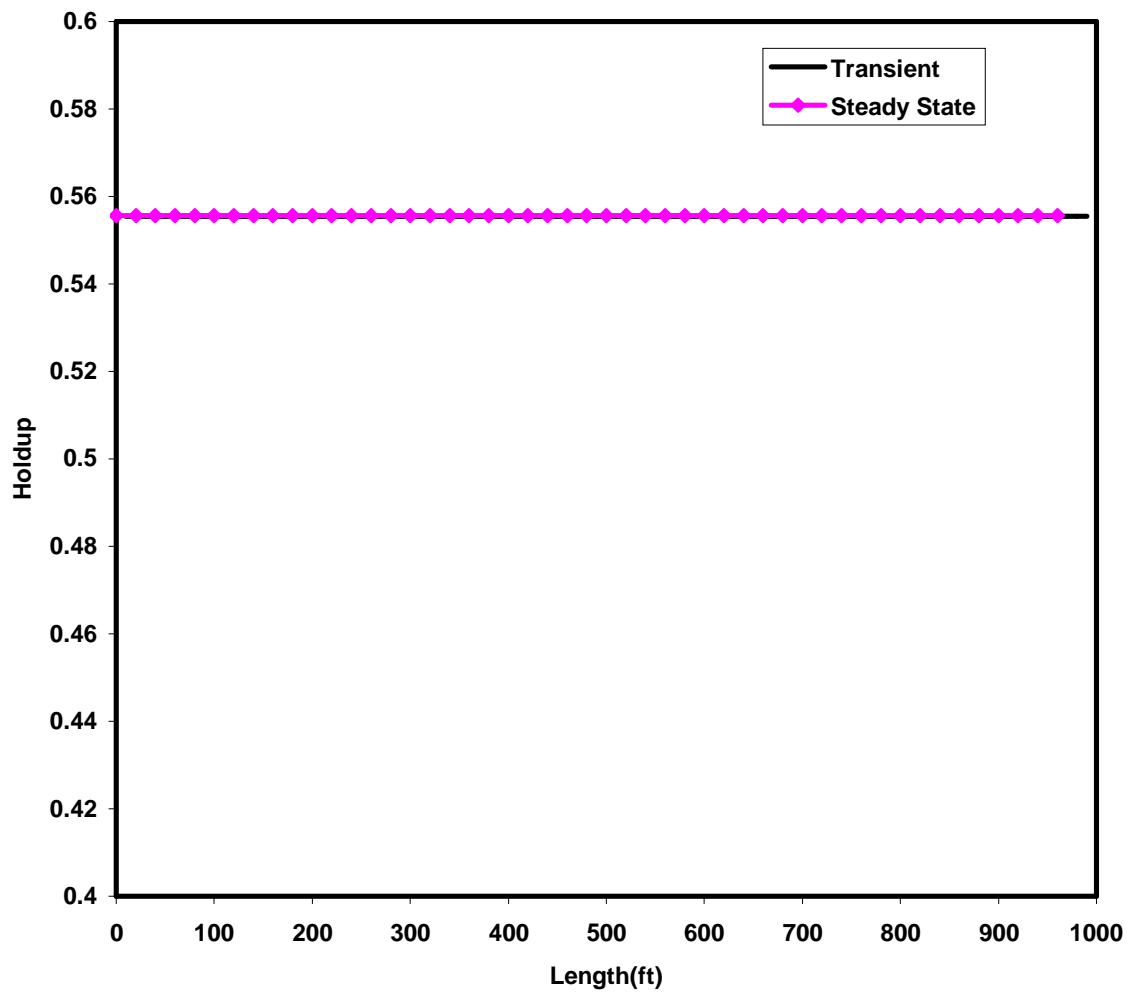


Figure 6.10 Holdup profile comparison between transient and steady-state solutions

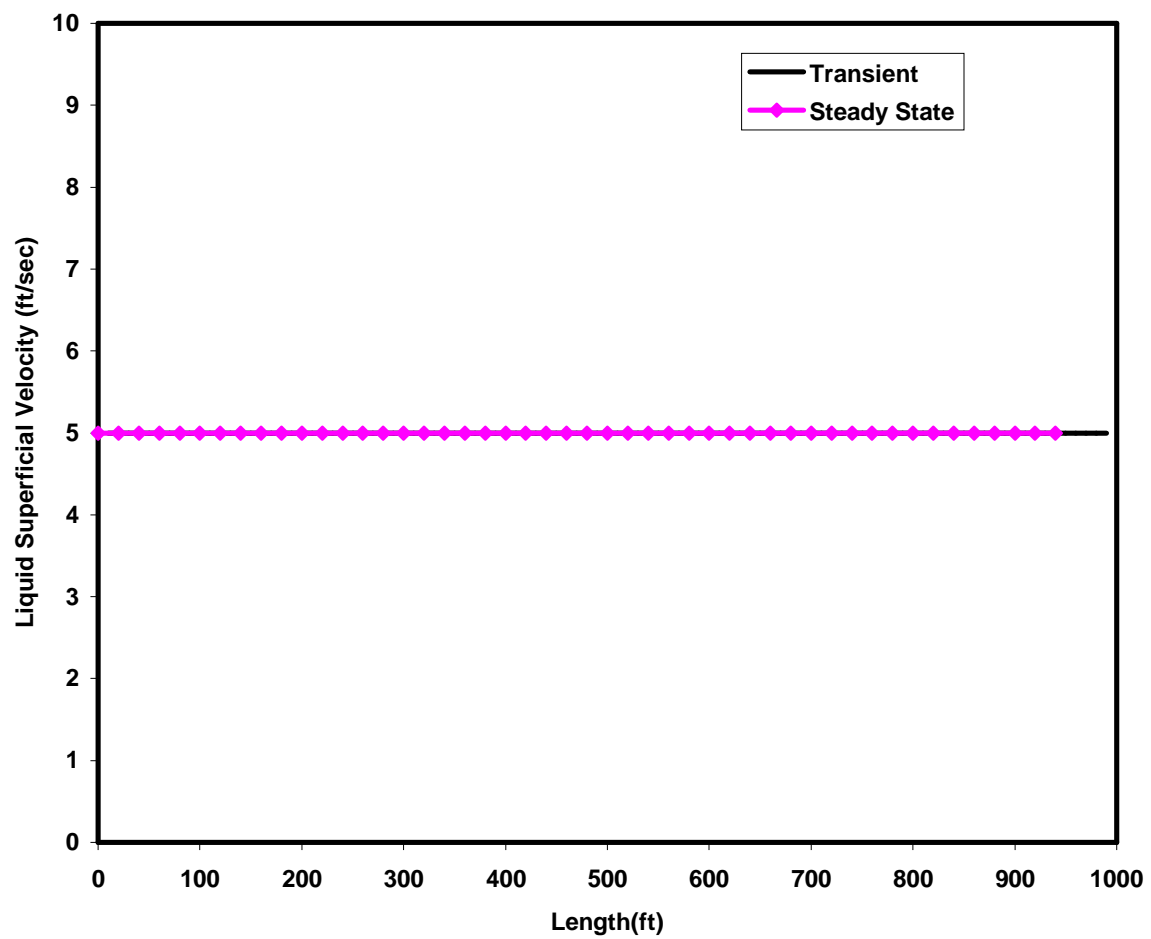


Figure 6.11 Liquid superficial velocity profile comparison between transient and steady-state solutions

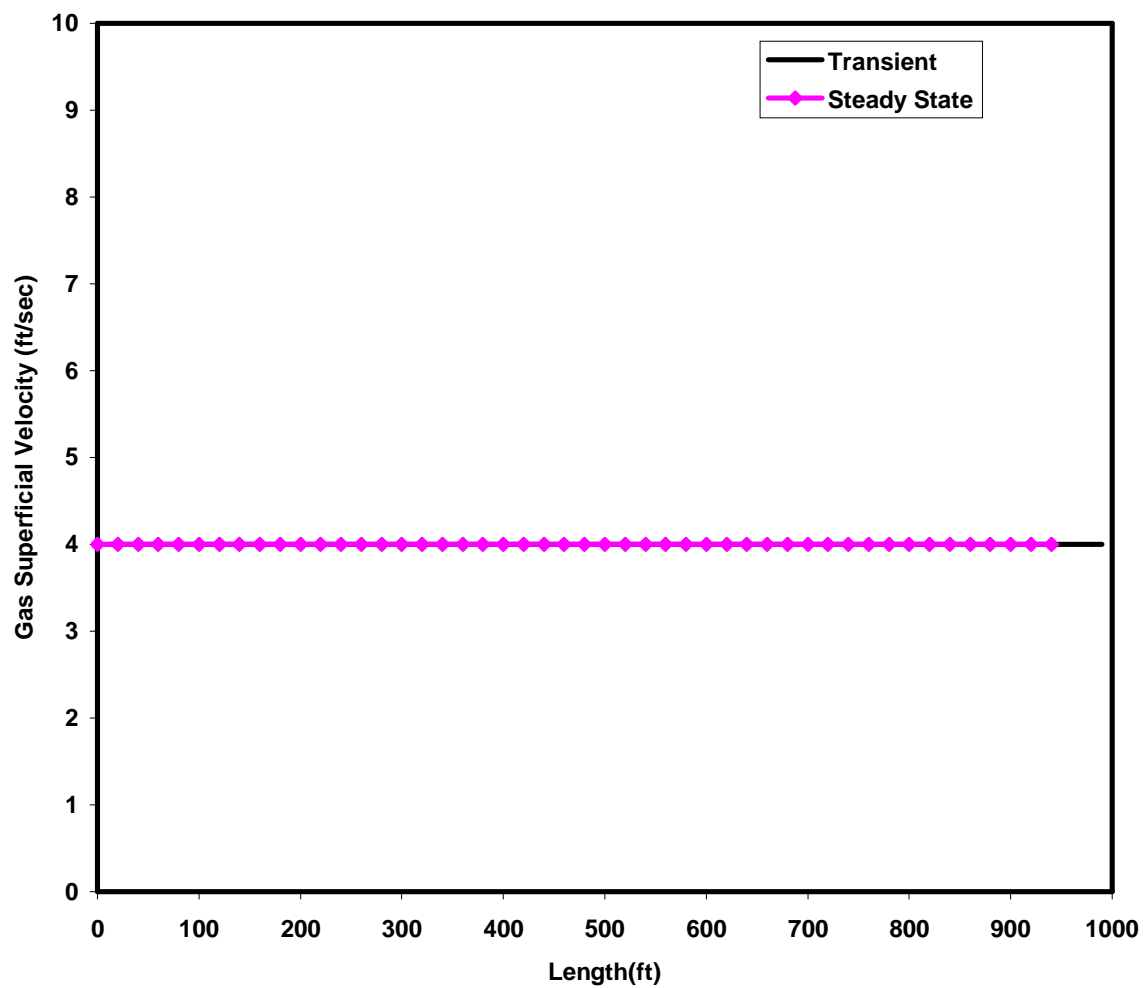


Figure 6.12 Gas superficial velocity profile comparison between transient and steady-state solutions

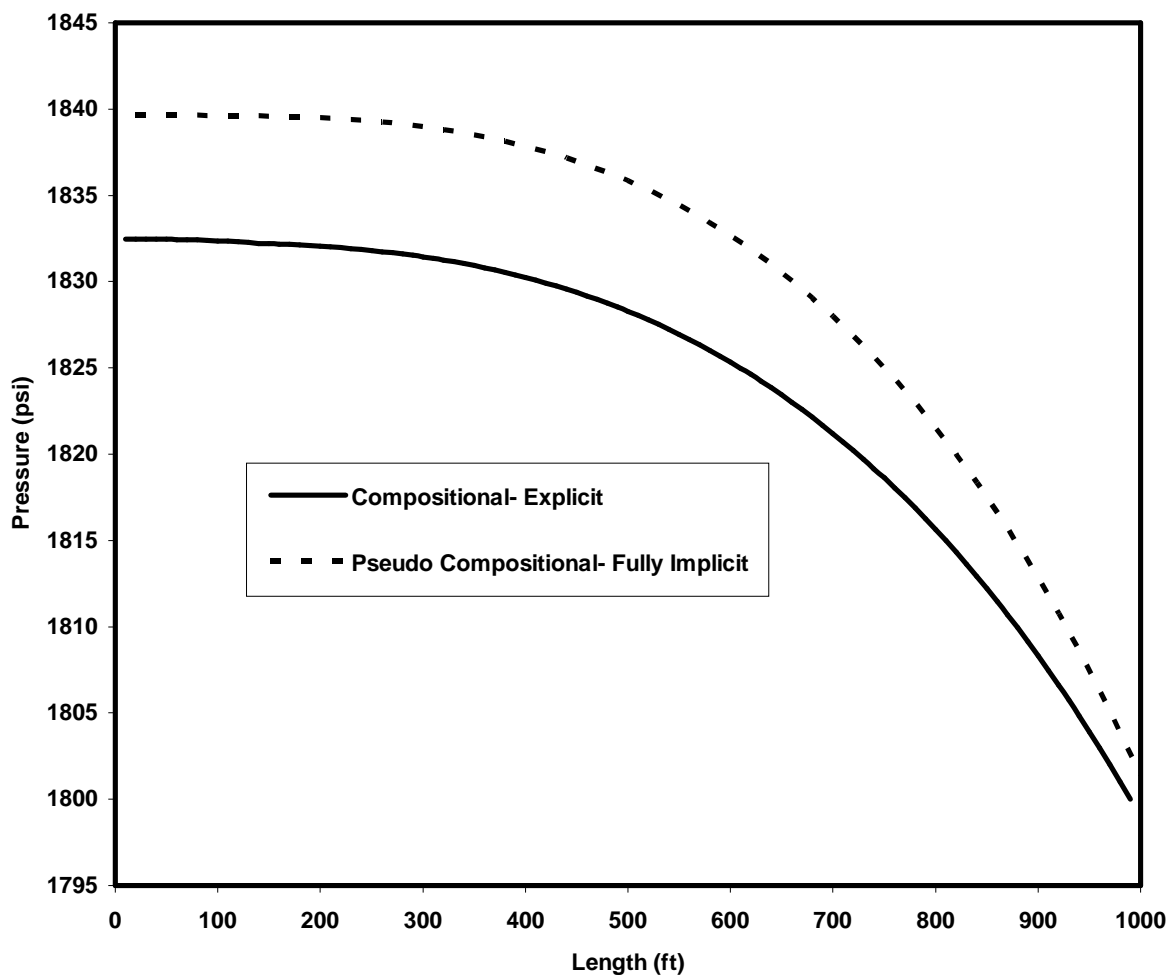


Figure 6.13 Pressure profile comparison between the compositional/explicit and pseudo-compositional/fully implicit calculation methods

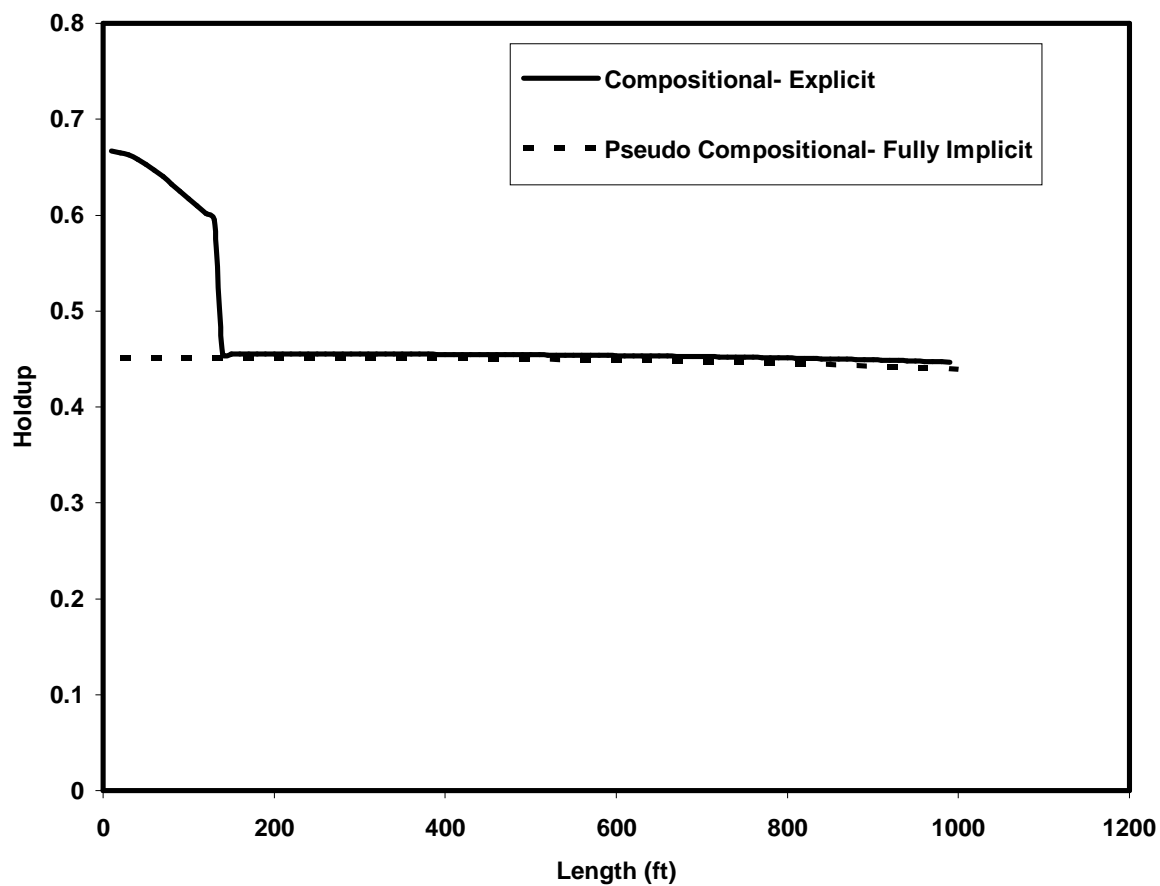


Figure 6.14 Holdup profile comparison between the compositional/explicit and pseudo-compositional/fully implicit calculation methods

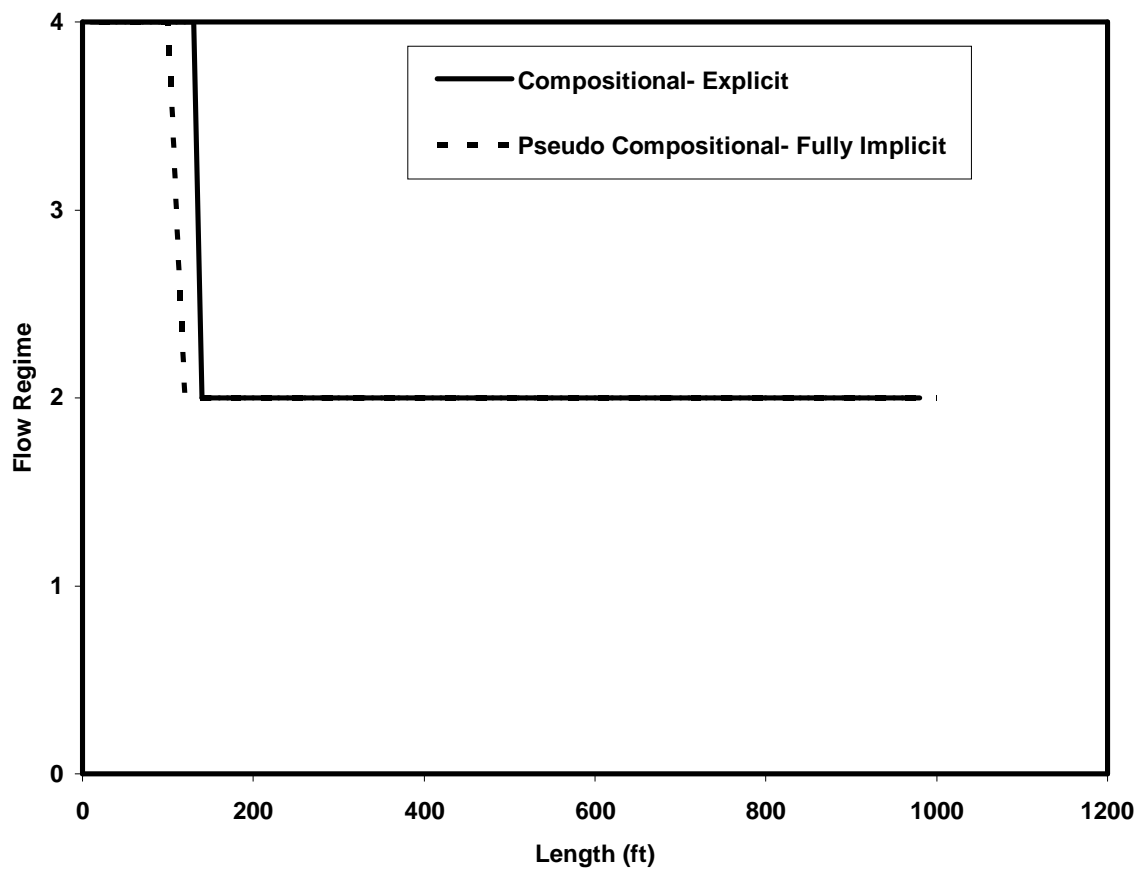


Figure 6.15 Flow Regimes profile comparison between the compositional/explicit and pseudo-compositional/fully implicit calculation methods (1: bubbly, 2: intermittent, 3: annular, 4: stratified flow)

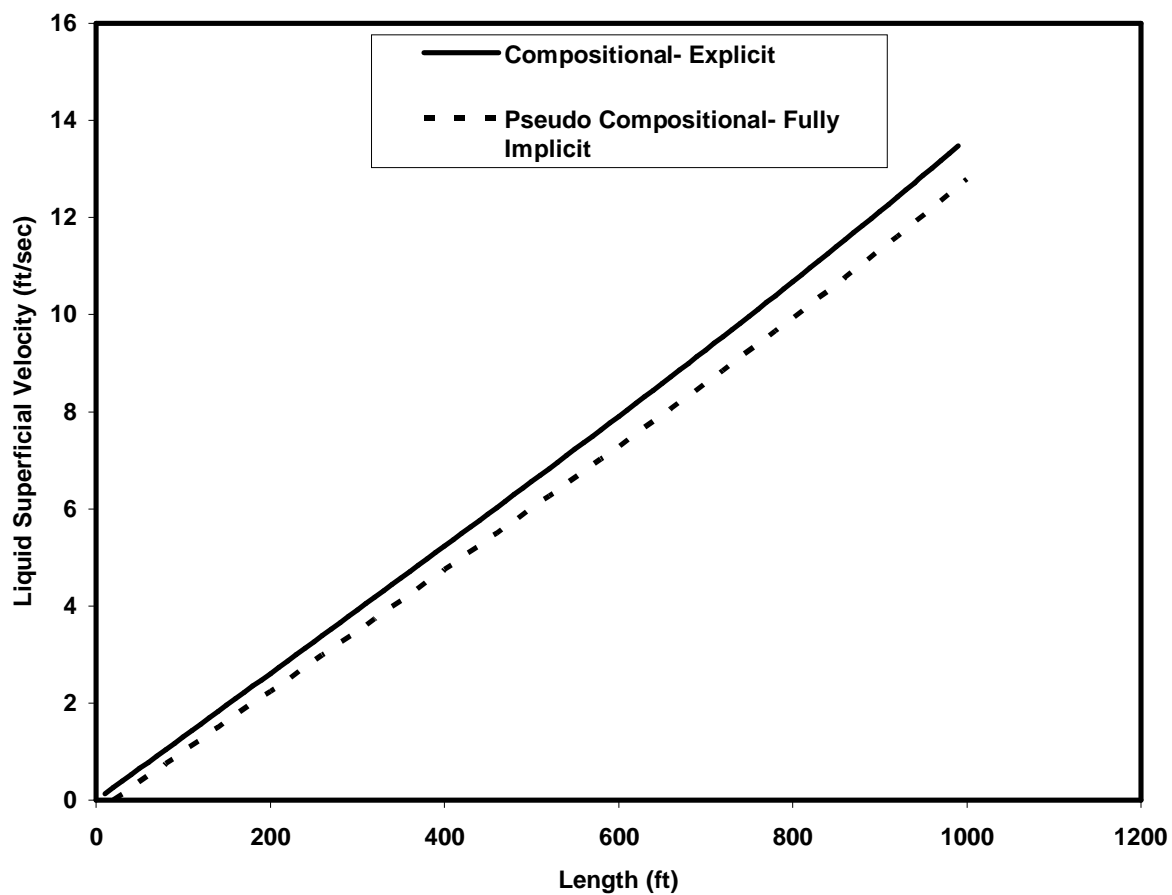


Figure 6.16 Liquid superficial velocity profile comparison between the compositional/explicit and pseudo-compositional/fully implicit calculation methods

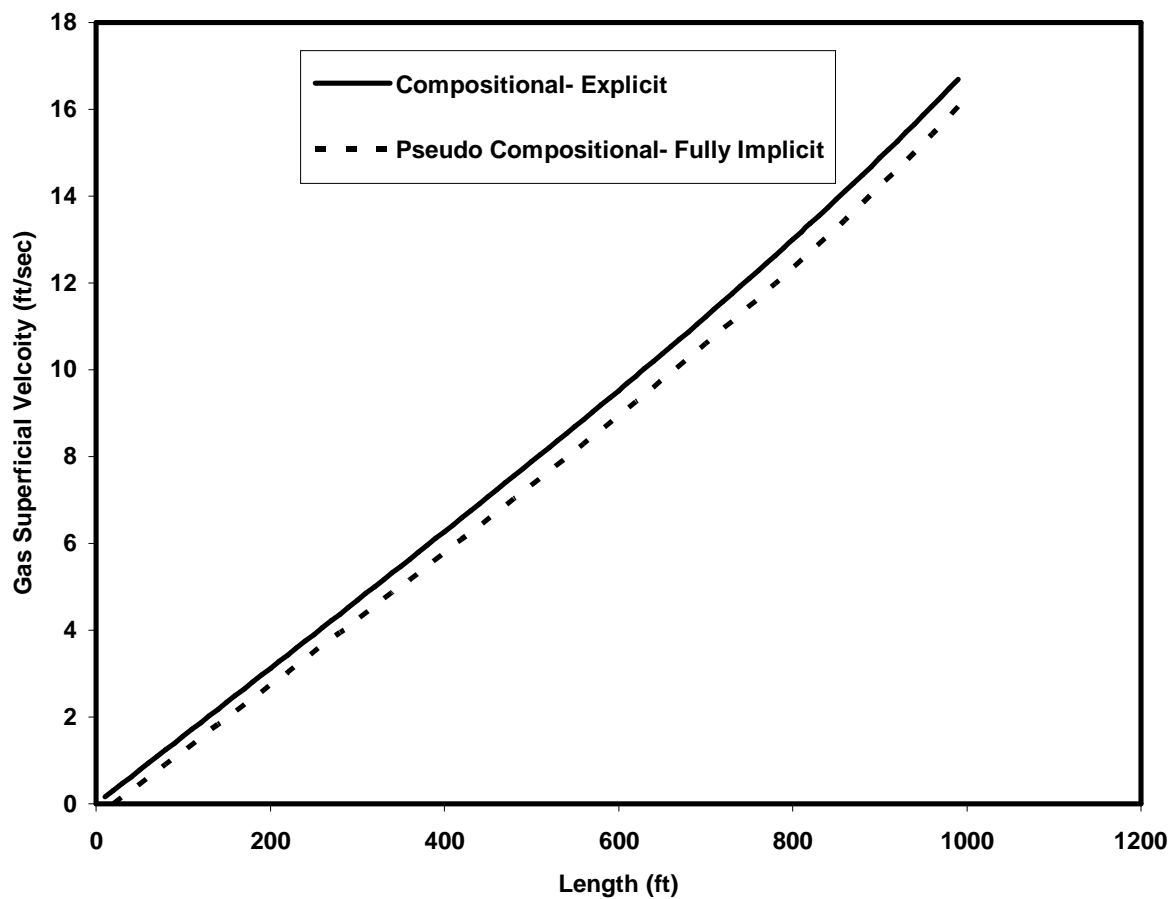


Figure 6.17 Liquid superficial velocity profile comparison between the compositional /explicit and pseudo-compositional/fully implicit calculation methods

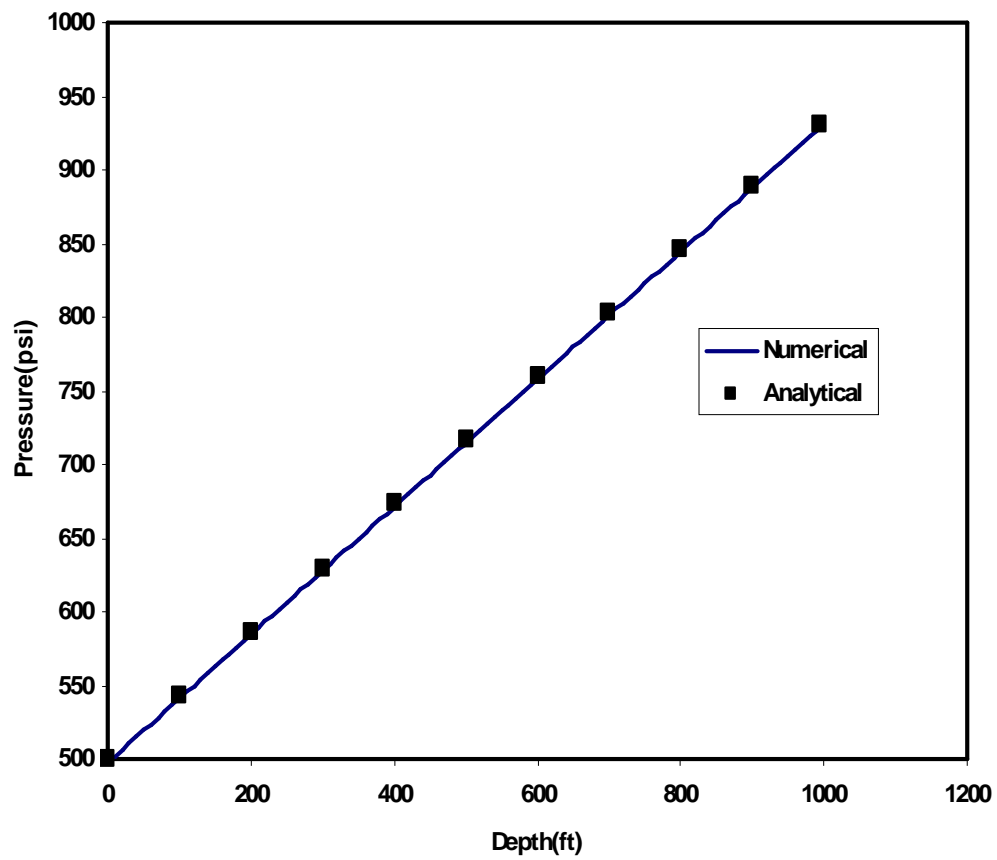


Figure 6.18 Pressure profile comparison between the numerical and analytical calculations

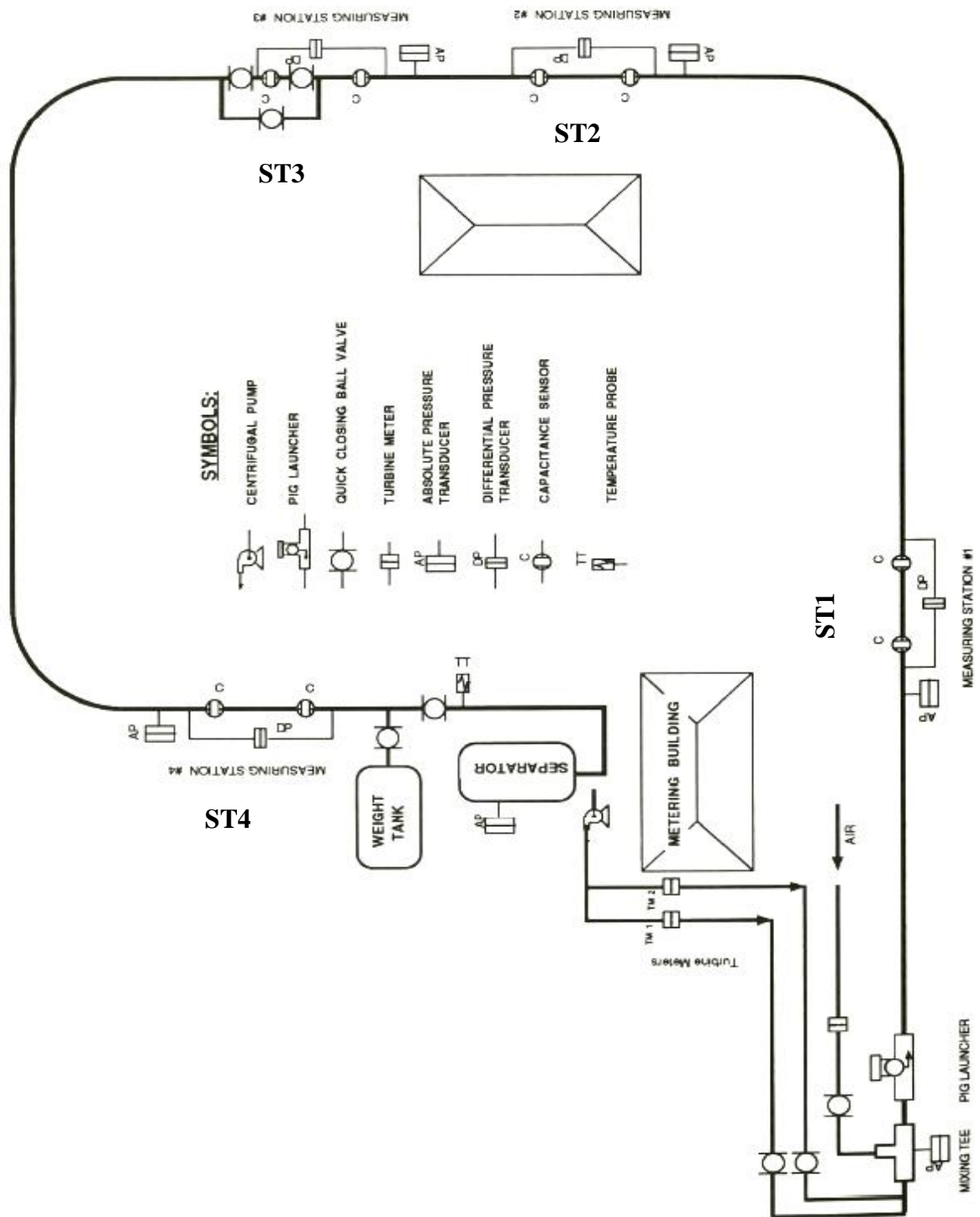


Figure 6.19 Schematic view of experimental setup, Minami and Shoham (1994)

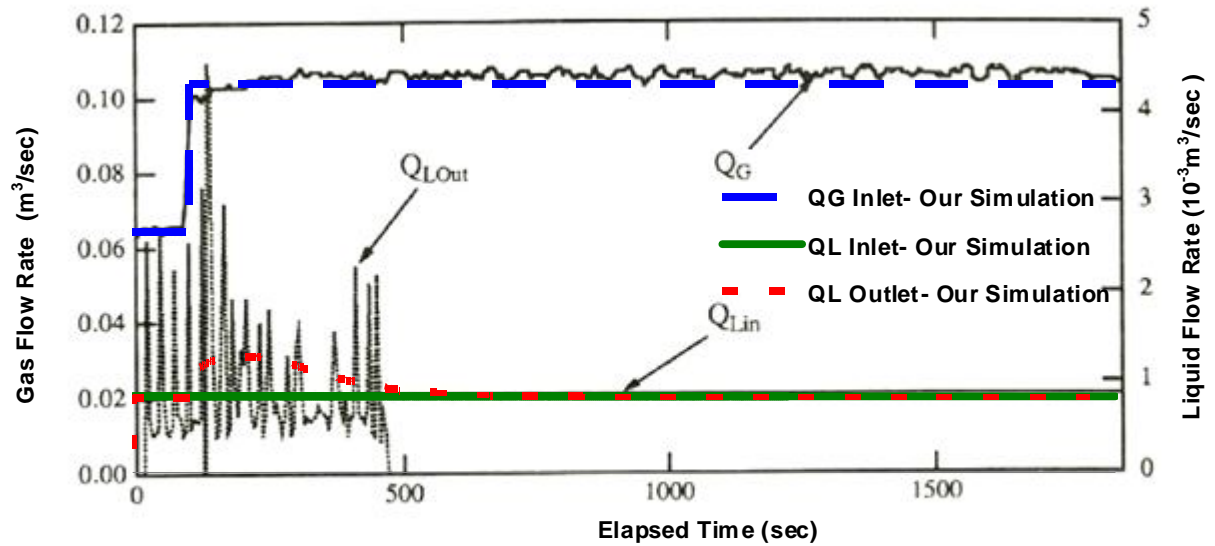


Figure 6.20 Comparison between experimental data (Minami and Shoham, 1994) and the stratified flow regime model results for gas/liquid inlet and outlet flow rates *versus* time

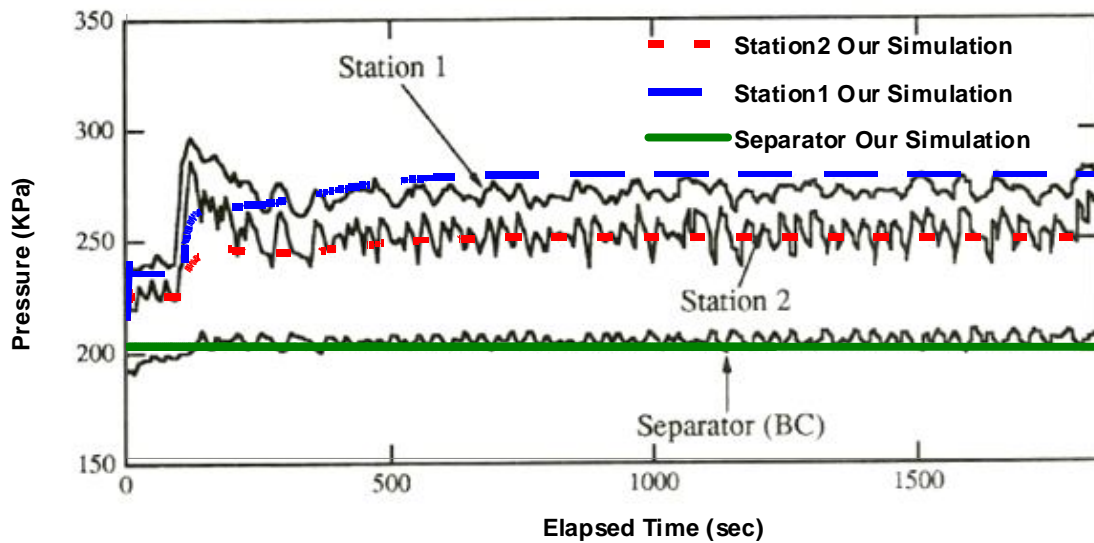


Figure 6.21 Comparison between experimental data (Minami and Shoham, 1994) and the stratified flow regime model results for pressure *versus* time in station 1 and station 2

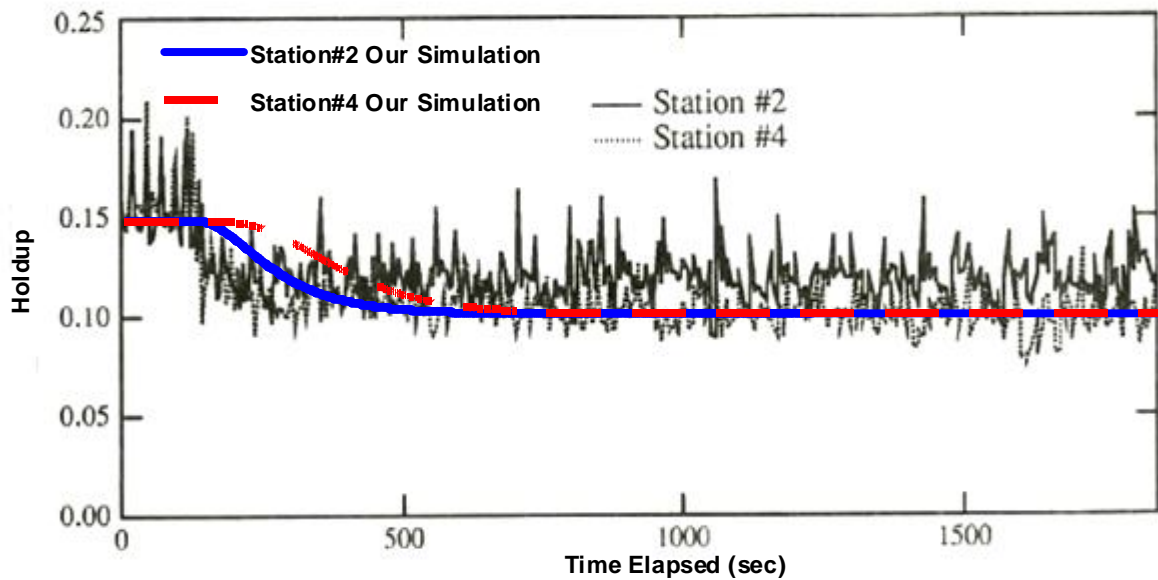


Figure 6.22 Comparison between experimental data (Minami and Shoham, 1994) and the stratified flow regime model results for holdup in station 2 and station 4

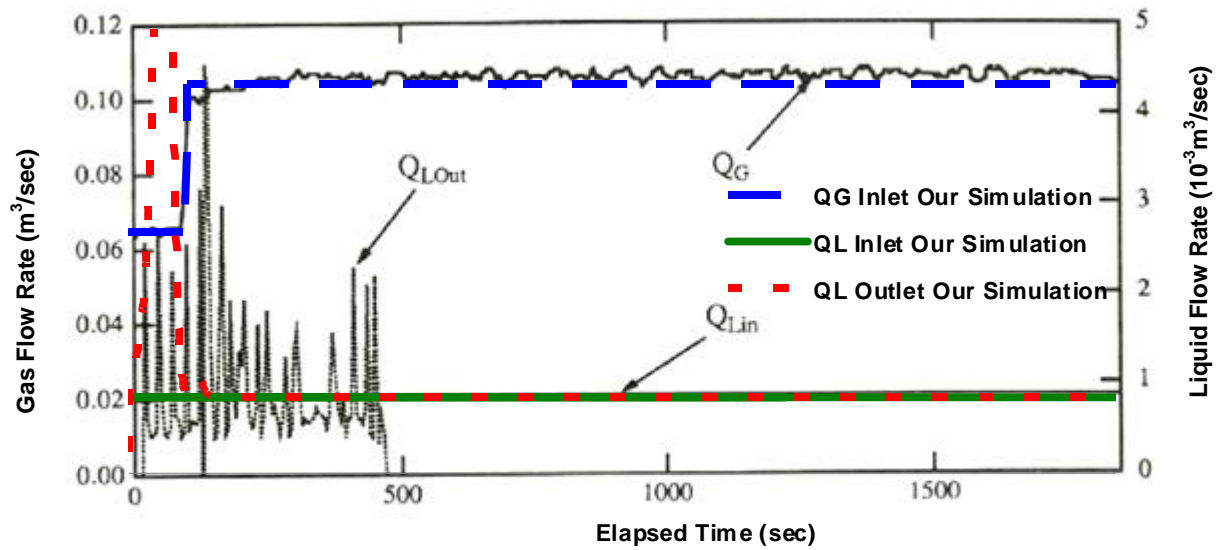


Figure 6.23 Comparison between experimental data (Minami and Shoham, 1994) and the bubbly flow regime model results for gas/liquid inlet and outlet flow rates *versus* time

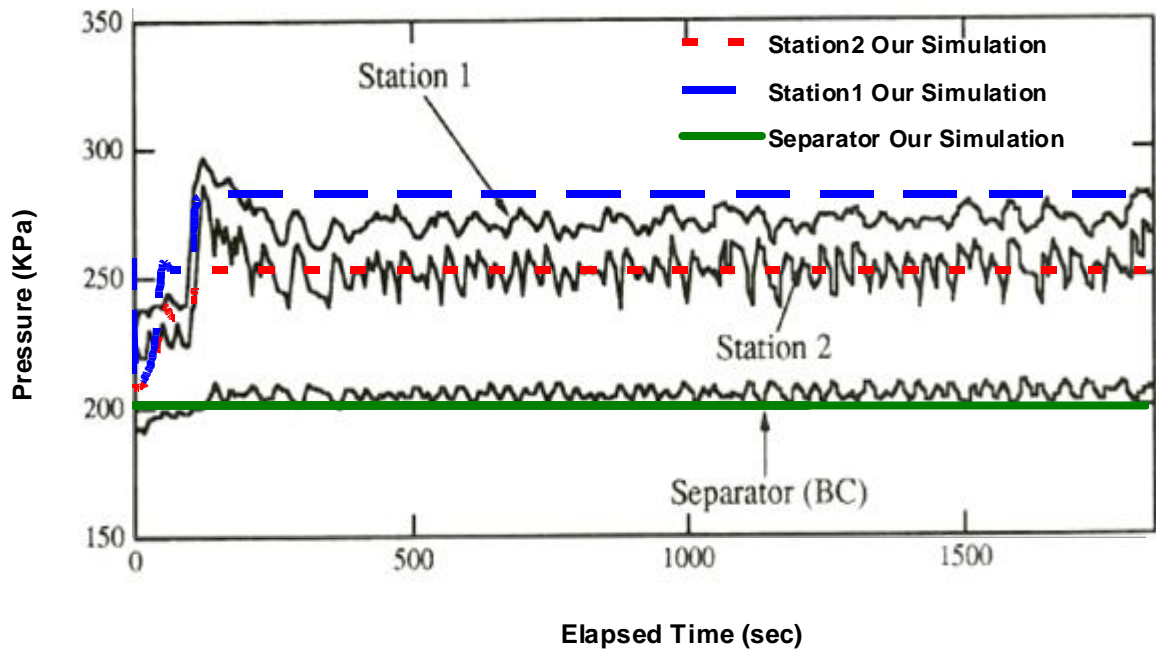


Figure 6.24 Comparison between experimental data (Minami and Shoham, 1994) and the bubbly flow regime model results for pressure *versus* time in station 1 and station 2

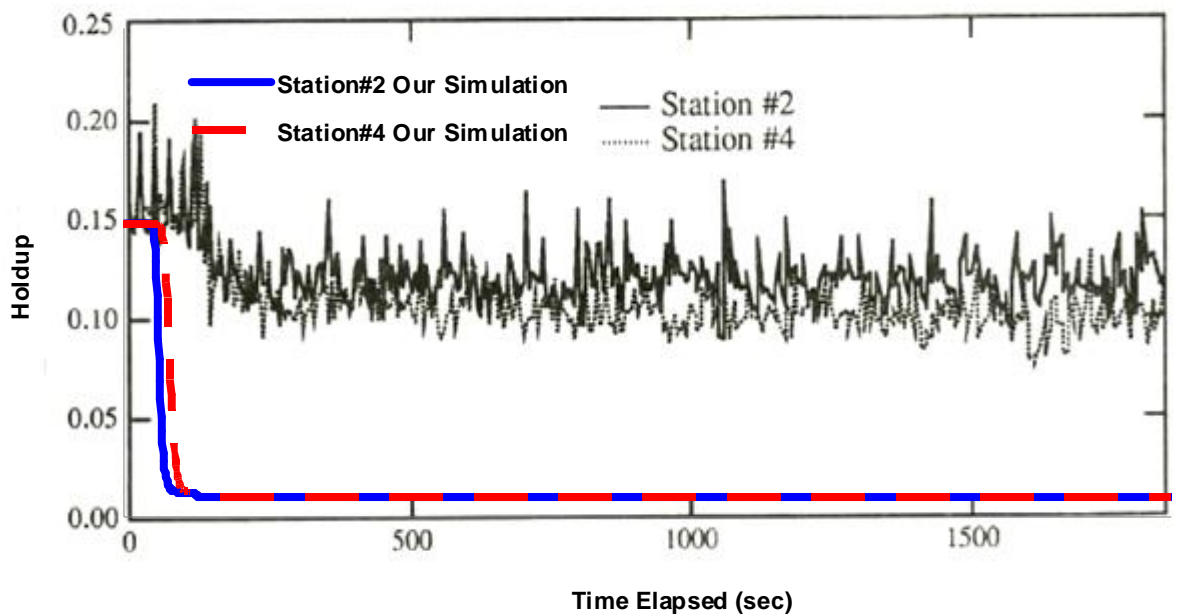


Figure 6.25 Comparison between experimental data (Minami and Shoham, 1994) and the bubbly flow regime model results for holdup in station 2 and station 4

Chapter 7: Summary, Conclusions and Recommendations

This chapter presents the summary, conclusions of this research and gives recommendations for further extensions of this work.

7.1 SUMMARY

In the following, we summarize the work presented in this study.

- A steady-state, fully-implicit, pseudo-compositional, thermal two-fluid mechanistic model was developed to model two-phase flow in the wellbore;
- The model was applied to calculate the pressure, holdup, temperature, liquid and gas velocity in the wellbore;
- Drag force and inter-phase momentum transfer models were implemented in the momentum equations to mimic the effect of different flow regimes;
- A steady-state, compositional, thermal, simplified two-fluid mechanistic wellbore model coupled to a compositional reservoir simulator was developed;
- The compositional wellbore simulator is able to compute the pressure, holdup, temperature, and components mass flow rates;
- This wellbore model is capable of simulating multiple-zone production from horizontal and vertical wells;
- Different types of wellbore-reservoir coupling were discussed and an explicit coupling was implemented;
- An equation-of-state (EOS), compositional, fully-implicit simulator (GPAS) was used as the reservoir simulator to couple to the wellbore simulator;
- A coupled horizontal and vertical wellbore model was also developed in which the boundary condition could be assigned in the wellhead, heel or toe;

- Analytical temperature calculation was implemented in the coupled wellbore-reservoir simulator;
- A transient, pseudo-compositional, thermal, two-fluid mechanistic wellbore model was implemented;
- Mass transfer between phases was considered by EOS compositional models in the pseudo-compositional model;
- The energy equation was solved based on the enthalpy calculation for the pseudo-compositional wellbore model;
- Time and space discretization sensitivity analysis were performed for the transient model. In addition, the CPU time was compared for different time-steps and mesh sizes;
- The implemented numerical models were compared to analytical solutions and the transient simulator results were successfully confronted with published experimental data.

7.2 CONCLUSIONS

The conclusions from this study can be listed as follows

- For accurate and more realistic representation of the production well flow behavior and also for the reservoir simulation considering an appropriate wellbore model is crucial. It is shown that a horizontal wellbore simulator is important for flow-rate predictions in the event that multiphase flow exists in the system.
- In the two-fluid model, we were able to observe the effect of the inter-phase momentum transfer, where phase 1 flow affects phase 2 flow, and vice-versa.
- In the two-fluid implicit model using an appropriate closure relationship for inter-phase momentum transfer is important for holdup calculation. As the comparison

between different flow regimes with experimental data showed for instance by using bubbly flow regime, with corresponding inter-phase and wall shear stress relationships, we obtained inaccurate results for holdup. However, for this system the pressure and velocity response had good agreement with experimental data.

- In the cases where the two-phase flow system was converted to a single phase and vice-versa, singularity is occurred in the equations. In some of the cases, singularity cause to stop the computations due to the unstable results. Simplified two-fluid model with considering compositional calculation resolves the singularity issue in the events that two-phase is converted to single phase and vice versa.

7.3 RECOMMENDATIONS

The recommendations for further study in this area are presented in the following:

- In this study, we considered transient model for liquid and gas phases. However, it is recommended to consider the compositional transient simulation as well. In fact, by adding N_c+1 mass balance equations for N_c hydrocarbon components and water to liquid and gas momentum equations we can solve the system of equations for our transient compositional model.
- The investigation of different inter-phase momentum equations for the flow regimes to handle the slippage between the phases, as well as the improvement in the drag force calculation for slug flow should be investigated;
- The comparison of a drift flux model and a two-fluid model in terms of holdup calculation and convergence should be carried out;
- One of the shortcomings in two-fluid model is instability in high velocity and density contrast between the liquid and gas phases. This issue is raised when the system of equations become ill-conditioned. For this purpose conducting research on stability of

the equations and characteristic analysis of partial differential equations is recommended to clarify in what conditions the equations are not well-posed.

- The implementation of a compositional transient coupled wellbore-reservoir simulator is recommended to model transient wellbore-reservoir dynamic interaction.
- The compositional transient wellbore model should be extended to include wellbore damage simulations, such as wax, asphaltene and scale deposition, after adequate upgrading.

Appendix A: Fluid Properties Calculation

A.1 COMPRESSIBILITY FACTOR CALCULATION

The compressibility factor can be calculated by compositional methods or blackoil correlations. In the compositional approach, a cubic EOS model is used to calculate pressure, temperature, and volume relation as follows:

$$p = \frac{RT}{V-b} - \frac{a}{V^2 + Vb(1+c) - cb^2}, \quad (\text{A.1})$$

or,

$$p = \frac{RT}{V-b} - \frac{a}{(V + \delta_1 b)(V + \delta_2 b)}, \quad (\text{A.2})$$

$$\text{where } 2\delta_1 = (1+c) - \sqrt{(1+c)^2 + 4c}, \quad (\text{A.3})$$

$$\text{and } \delta_1 \delta_2 = -c. \quad (\text{A.4})$$

Using $c = 1$, Equation (A.2) becomes the Peng-Robinson Equation of State and using $c = 0$, it becomes the Soave-Redlich-Kwong Equation-of-State.

The Peng-Robinson Equation-of-State (Peng and Robinson, 1976) is given as follows:

$$P = \frac{RT}{V-b} - \frac{a(T)}{V(V+b) + b(V-b)}. \quad (\text{A.5})$$

The parameters, a and, b for a pure component are computed from:

$$a(T) = 0.45724 \frac{R^2 T_c^2}{P_c} \alpha(T) \quad (\text{A.6})$$

$$b = 0.07780 \frac{RT_c}{P_c} \quad (\text{A.7})$$

$$\sqrt{\alpha} = 1 + \kappa \left(1 - \sqrt{\frac{T}{T_c}} \right) \quad (\text{A.8})$$

$$\kappa = 0.37464 + 1.54226\omega - 0.26992\omega^2 \text{ if } \omega < 0.49 \quad (\text{A.9})$$

$$\kappa = 0.379640 + 1.485030 \omega - 0.164423 \omega^2 + 0.016666 \omega^3 \text{ if } \omega \geq 0.49 \quad (\text{A.10})$$

For a multi-component mixture, a and b are obtained by mixing rules as follows:

$$a = \sum_{i=1}^{N_c} \sum_{j=1}^{N_c} x_i x_j \sqrt{a_i a_j} (1 - k_{ij}), \quad (\text{A.11})$$

$$b = \sum_{i=1}^{N_c} x_i b_i, \quad (\text{A.12})$$

where a_i and b_i are for pure components. The constant, k_{ij} is the binary interaction coefficient between components i and j .

Considering that $Z = \frac{PV}{RT}$, the Peng-Robinson Equation-of-State can be written in the form:

$$Z^3 + \alpha Z^2 + \beta Z + \gamma = 0. \quad (\text{A.13})$$

In Equation (A.13), α , β , and γ are calculated as

$$\alpha = -1 + B, \quad (\text{A.14})$$

$$\beta = A - 3B^2 - 2B, \quad (\text{A.15})$$

$$\gamma = -AB + B^2 + B^3, \quad (\text{A.16})$$

$$\text{where } A = \frac{aP}{(RT)^2} \text{ and } B = \frac{bP}{RT}.$$

Solving Equation (A.13), we obtain three roots which two of them are real. Hence we can calculate the z-factors for gas and oil phases.

For the blackoil model we use another approach for gas z-factor calculation. Dranchuk and Abou-Kassem (1975) introduced the expression:

$$\begin{aligned} Z = 1 + & \left(A_1 + \frac{A_2}{T_r} + \frac{A_3}{T_r^3} + \frac{A_4}{T_r^4} + \frac{A_5}{T_r^5} \right) \rho_r + \left(A_6 + \frac{A_7}{T_r} + \frac{A_8}{T_r^2} \right) \rho_r^2 \\ & - A_9 \left(\frac{A_7}{T_r} + \frac{A_8}{T_r^2} \right) \rho_r^5 + A_{10} \left(1 + A_{11} \rho_r^2 \right) \frac{\rho_r^2}{T_r^3} \exp(-A_{11} \rho_r^2). \end{aligned} \quad (\text{A.17})$$

In Equation (A.17), the coefficients are defined as follows:

$$\begin{aligned} A_1 &= 0.3265 & A_2 &= -1.0700 & A_3 &= -0.5339 \\ A_4 &= 0.01569 & A_5 &= -0.05165 & A_6 &= 0.5475 \\ A_7 &= -0.7361 & A_8 &= 0.1844 & A_9 &= 0.1056 \\ A_{10} &= 0.6134 & A_{11} &= 0.7210 \end{aligned}$$

A.2 PHASE EQUILIBRIUM CALCULATION

One of the criteria for phase equilibrium is the equality of the partial molar Gibbs free energies, or the chemical potentials, which can be expressed as fugacity (Sandler, 1999). Hence, in the thermodynamic equilibrium between phases we have:

$$f_{ij} = f_{i\ell} \quad i = 1, \dots, n_c \text{ and } j = 2, \dots, n_p (j \neq \ell). \quad (\text{A.18})$$

f_{ij} , is the fugacity of component i in phase j , which is a function of pressure, temperature and phase composition, $f_{ij} = f_{ij}(P, T, x_{ij})$.

The fugacity equation, (A.18), is combined with the phase composition constraints and Rachford-Rice equation in order to solve for each phase composition (Pedersen and Christensen, 2007). Phase composition is used for density and other properties calculation of the phases.

A.3 DENSITY CALCULATION

After calculating the gas compressibility factor, using the blackoil or compositional approach, the gas density ($\frac{lbm}{ft^3}$) can be obtained as follows:

$$\rho_g = \frac{MW_g P}{Z_g R T}. \quad (\text{A.19})$$

where, MW_g , is the gas molecular weight in ($\frac{lbm}{lbmol}$), P is pressure in (psi), R the universal gas constant, 10.73, and T is the temperature ($^{\circ}R$).

Oil density, by using the oil specific gravity (γ_o), the oil formation volume factor (B_o) and dissolved solution gas-oil ratio (R_s) can also be calculated from blackoil models. The Standing's correlation (Standing, 1947) is used to estimate the dissolved gas-oil ratio for saturated oils as follows:

$$R_s = \gamma_g \left(\frac{P}{18 \times 10^{y_g}} \right)^{1.204}, \quad (\text{A.20})$$

where

γ_g = Gas gravity (air =1)

y_g = Gas mole fraction = $0.00091T - 0.0125\gamma_{API}$

T = Reservoir temperature, °F.

For the saturated oil formation volume factor (B_o ($\frac{bbl}{stb}$)), Standing (1947) presented:

$$B_o = 0.972 + 0.000147 F^{1.175} \quad (\text{A.21})$$

where ,

$$F = R_s \left(\frac{\gamma_g}{\gamma_{OSC}} \right) 0.5 + 1.25T. \quad (\text{A.22})$$

Using Equations (A.20) and (A.21), we can obtain the oil density as follows:

$$\rho_o = \frac{62.37\gamma_o + 0.0136R_s\gamma_g}{B_o} \quad (\text{A.23})$$

where, γ_o , is the oil gravity (for water equals to 1).

In a compositional approach, the oil density is obtained from compositional flash calculation. In fact at a given temperature, pressure and overall composition oil phase z-factor, oil molar weight are calculated and used in Equation (A.24) to obtain oil density.

$$\rho_o = \frac{MW_o P}{Z_o R T}. \quad (A.24)$$

In Equation (A.24), MW_o is the oil molecular weight in ($\frac{lbm}{lbmol}$), P is pressure in (psi), R is universal gas constant 10.73, and T is temperature in ($^{\circ}R$).

The dissolved gas-oil ratio (R_s) and the oil formation volume factor (B_o) are also obtained by performing flash calculation at standard conditions ($P = 14.7 psi$, $T = 520^{\circ}R$) and calculating the amount of oil and gas volume change from a given condition to standard condition.

A.4 VISCOSITY CALCULATION

Lohrenz et al. (1964) presented different correlations for compositional oil and gas viscosities calculation. Following are the equations.

$$\mu_{\beta} = \begin{cases} \mu_{\beta}^* + 0.000205 \frac{\xi_{\beta r}}{\eta_{\beta}} & \xi_{\beta r} \leq 0.18 \\ \mu_{\beta}^* + \frac{(\chi_{\beta}^4 - 1)}{10^4 \eta_{\beta}} & \xi_{\beta r} > 0.18 \end{cases} \quad (A.25)$$

where

$$\xi_{\beta r} = \rho_{\beta} \sum_{i=1}^{n_c} x_{i\beta} V_c(i) \quad (A.26)$$

$$\chi_{\beta} = 1.023 + 0.2336\xi_{\beta r} + 0.58533\xi_{\beta r}^2 - 0.40758\xi_{\beta r}^3 + 0.09332\xi_{\beta r}^4, \quad (\text{A.27})$$

$$\eta_{\beta} = \frac{5.44 \left[\sum_{i=1}^{n_c} x_{i\beta} T_{ci} \right]^{\frac{1}{6}}}{\left[\sum_{i=1}^{n_c} x_{i\beta} WM_i \right]^{\frac{1}{2}} \left[\sum_{i=1}^{n_c} x_{i\beta} P_{ci} \right]^{\frac{2}{3}}}, \quad (\text{A.28})$$

$$\mu_{\beta}^* = \frac{\sum_{i=1}^{n_c} x_{i\beta} \tilde{\mu}_i \sqrt{MW_i}}{\sum_{i=1}^{n_c} x_{i\beta} \sqrt{MW_i}}. \quad (\text{A.29})$$

The low-pressure pure component viscosity is calculated as follows:

$$\hat{\mu}_i = \frac{0.0001776(4.58T_{ri} - 1.67)^{5/8}}{\zeta_i}, \quad (\text{A.30})$$

where

$$\zeta_i = \frac{5.44T_{ci}^{1/6}}{MW_i^{1/2} P_{ci}^{2/3}}. \quad (\text{A.31})$$

For the blackoil model there are two steps to calculate the oil viscosity. First, the gas-free oil viscosity is obtained and then the gas-saturated oil viscosity is computed. For the first step, Egbugah and Ng (1983) correlations can be applied:

$$\log\{\log(\mu_{oD} + 1)\} = 1.8653 - 0.025086\gamma_{API} - 0.5644\log(T) \quad (\text{A.32})$$

In Equation (A.32), μ_{oD} , is the gas-free oil viscosity, at 14.7 psia. To calculate oil viscosity, μ_{oD} is used in the Beggs and Robinson (1975) correlation, such as:

$$\mu_o = A\mu_{oD}^B, \quad (\text{A.33})$$

$$A = 10.715(R_s + 100)^{-0.515}, \quad (\text{A.34})$$

$$B = 5.44(R_s + 150)^{-0.338}. \quad (\text{A.35})$$

For the gas viscosity calculation, Lee et al (1966) introduced the following equations:

$$\mu_g = K \exp[X \rho_g^Y], \quad (\text{A.36})$$

$$\text{where, } K = \frac{(9.4 + 0.02MW_g)T^{1.5}}{209 + 19MW_g + T}, \quad (\text{A.37})$$

$$X = 3.5 + \frac{986}{T} + 0.01MW_g, \quad (\text{A.38})$$

$$Y = 2.4 - 0.2X. \quad (\text{A.39})$$

In Equations (A.36) through (A.39), μ_g is the gas viscosity (*micropois*), ρ_g is the gas density ($\frac{g}{cc}$), MW_g is the gas molecular weight and T is the temperature ($^{\circ}R$).

Table A.1 shows an example for fluid properties calculation for a mixture of 50% C1 and 50% NC10, at 100 $^{\circ}F$ and 1000 psi.

A.5 ENTHALPY CALCULATION

The enthalpy is a function of pressure and temperature, via the heat capacity (C_p ($\frac{Btu}{^{\circ}Flbm}$)) and Joule-Thomson coefficient (η ($\frac{^{\circ}F}{\frac{Btu}{ft^3}}$)), as shown in Equation (A.40).

$$d\bar{h}_j = C_{pj}dT_j - \left(\frac{144}{J_c}\right)\eta_j C_{pj}dP. \quad (\text{A.40})$$

Hence, enthalpy needs to be calculated with respect to a reference pressure and temperature.

$$\bar{h}_j(T, P) = \bar{h}_j(T_{ref}, P_{ref}) + \int_{T_{ref}}^T C_{pj}dT - \int_{P_{ref}}^P \left(\frac{144}{J_c}\right)\eta_j C_{pj}dP, \quad (\text{A.41})$$

$$\bar{h}_j(T, P) = \int_{T_{ref}}^T C_{pj}dT - \int_{P_{ref}}^P \left(\frac{144}{J_c}\right)\eta_j C_{pj}dP. \quad (\text{A.42})$$

In Equation (A.42) J_c is the conversion factor, η_j is the phase, j is the Joule - Thomson coefficient, and C_{pj} is phase j heat capacity. The Joule-Thomson coefficient can be calculated as follows:

$$\eta_j = \frac{1}{C_{pj}} \left\{ T \left[\frac{\partial}{\partial T} \left(\frac{1}{\rho_j} \right) \right]_p - \frac{1}{\rho_j} \right\}. \quad (\text{A.43})$$

The heat capacity can be calculated by different correlations for water, oil and gas. Holman (1958) has reported the following equation for specific heat capacity of water for the range of 20 °C to 290 °C.

$$C_{p_w} (J / kg.K) = \frac{4245 - 1.841T}{\rho_w}. \quad (\text{A.44})$$

Gambill (1957) has presented the following equation to calculate the specific heat capacity of oil as a function of temperature and oil-specific gravity:

$$C_{p_o} (J / kg.K) = \frac{1684 + 3.389T}{\sqrt{\gamma_{oil}}}. \quad (\text{A.45})$$

Waples D.W and Waples J.S (2004) presented the temperature dependence of the specific heat capacity for natural gas using a fourth-order polynomial:

$$C_{p_g} (Btu / lbm.^{\circ}F) = AT^4 + BT^3 + CT^2 + DT + E. \quad (\text{A.46})$$

The coefficients in Equation (A.46) are functions of pressure. For instance, the following polynomials are used for methane:

$$\begin{aligned}
 A(P) &= -2.52 \times 10^{-22} P^3 + 1.34 \times 10^{-18} P^2 + -9.15 \times 10^{-16} P + 1.62 \times 10^{-13} \\
 B(P) &= 5.37 \times 10^{-19} P^3 - 2.85 \times 10^{-15} P^2 + 1.37 \times 10^{-12} P - 4.67 \times 10^{-10} \\
 C(P) &= -3.47 \times 10^{-16} P^3 + 1.86 \times 10^{-12} P^2 + 2.01 \times 10^{-11} P + 3.95 \times 10^{-17} \\
 D(P) &= 7.70 \times 10^{-14} P^3 - 4.21 \times 10^{-10} P^2 - 5.96 \times 10^{-7} P + 3.70 \times 10^{-4} \\
 E(P) &= -1.03 \times 10^{-11} P^3 + 5.24 \times 10^{-8} P^2 + 1.55 \times 10^{-4} P + 4.88 \times 10^{-1}.
 \end{aligned}$$

In the compositional calculation, the enthalpy is obtained from the excess enthalpy (h^E) as follows:

$$h^E = h - h^* = pv - RT + \frac{T(\partial a / \partial T) - a}{\delta_2 - \delta_1} \ln\left(\frac{v + \delta_2 b}{v + \delta_1 b}\right). \quad (\text{A.47})$$

where, h is the system enthalpy and h^* is the enthalpy at the ideal gas state. h^* is calculated from:

$$h^* = \sum_i x_i h_i^*, \quad (\text{A.48})$$

$$\text{where, } h_i^* = H_A + H_B T + H_C T^2 + H_D T^3 + H_E T^4 + H_F T^5. \quad (\text{A.49})$$

In Equation (A.49), h_i^* is only a function of temperature ($^{\circ}R$) and cannot be derived from an Equation-of-State. Passut and Danner (1972) have compiled the values of H_A through H_F for components commonly encountered in petroleum engineering. In most practical applications, the important variables are the enthalpy differences and not the absolute enthalpies. Thus, the reference point for H can be chosen, arbitrarily.

To validate the enthalpy calculation, we have compared our results with Computer Modeling Group software (CMG, WINPROP version 2008.10) for a fluid mixture of 50% C1 and 50% NC10, at $T = 100\text{ }^{\circ}\text{F}$. As it can be observed in Figure (A.1) and (A.2), there is a good agreement between our results and the CMG calculation.

Table A.1 Fluid properties calculation for a mixture of 50% C1 and 50% NC10 at $100\text{ }^{\circ}\text{F}$ and 1000 psi

Liquid z-factor Z_o	0.437
Gas z-factor Z_g	0.886
Oil mole fraction $V_o(lbmol/lbmol)$	0.280
Oil mole fraction at standard condition $V_{so}(lbmol/lbmol)$	0.301
Oil molecular weight $MW_o(lbm/lbmol)$	103.68
Gas molecular weight $MW_g(lbm/lbmol)$	16.13
Oil density $\rho_o(lbm/ft^3)$	39.51
Gas density $\rho_g(lbm/ft^3)$	3.01
Bubble point pressure $Pb(psi)$	1915
Solution gas oil ratio $R_s(scft/stb)$	273.94
Oil viscosity $\mu_o(cp)$	0.28
Gas viscosity $\mu_g(cp)$	0.00127
Oil formation volume factor $B_o(rbbl/stb)$	1.12
Gas formation volume factor $B_g(ft^3/scft)$	0.00140

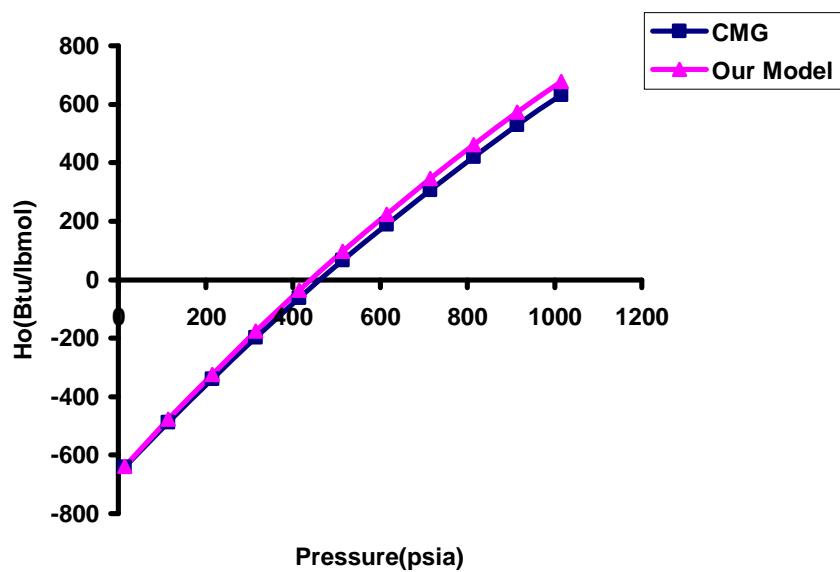


Figure A.1 Oil phase enthalpy calculation and comparison with CMG for the mixture of 50% C1 and 50% NC10, at 100 °F

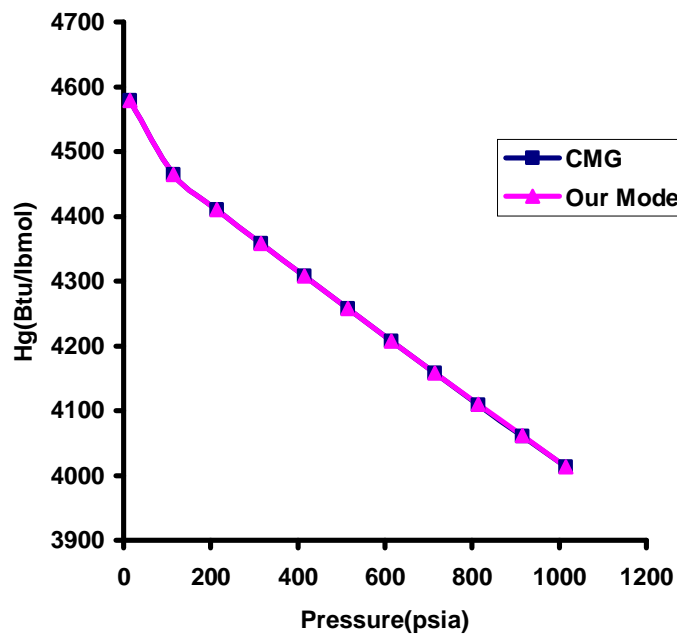


Figure A.2 Gas phase enthalpy calculation and comparison with CMG for the mixture of 50% C1 and 50% NC10, at 100 °F

Appendix B: Unit Conversion

$$1(psi) = 1\left(\frac{lbf}{in^2}\right)$$

$$144(in^2) = 1(ft^2)$$

$$J_c(ft-lbf) = 1(Btu), J_c = 778.77$$

$$g_c(ft/sec^2) = 1(lbf), g_c = 32.17$$

Appendix C: Wellbore Boundary Conditions

In the following sections, we explain how the different boundary conditions are applied to the numerical model. We apply the linear interpolation approach for the boundary nodes.

C.1 CONSTANT FLOW RATE INLET AND CONSTANT PRESSURE OUTLET

Inlet Node

$$U_l(0) = U_{linlet}$$

$$U_g(0) = U_{ginlet}$$

$$P(0) = 2P(1) - P(2)$$

$$H_l(0) = 2H_{linlet} - H_l(1)$$

$$T_l(0) = 2T_{linlet} - T_l(1)$$

$$T_g(0) = 2T_{ginlet} - T_g(1)$$

Outlet Node

$$U_l(N+1) = 2U_l(N) - U_l(N-1)$$

$$U_g(N+1) = 2U_g(N) - U_g(N-1)$$

$$P(N+1) = 2P_{wellhead} - P(N)$$

$$H_l(N+1) = 2H_l(N) - H_l(N-1)$$

$$T_l(N+1) = 2T_l(N) - T_l(N-1)$$

$$T_g(N+1) = 2T_g(N) - T_g(N-1)$$

C.2 NO FLOW INLET AND CONSTANT PRESSURE INLET

Inlet Node

$$U_l(0) = 0$$

$$U_g(0) = 0$$

$$P(0) = P(1) = P_{bh}$$

$$H_l(0) = H_l(1)$$

$$T_l(0) = 2T_{linlet} - T_l(1)$$

$$T_g(0) = 2T_{ginlet} - T_g(1)$$

Outlet Node

$$U_l(N+1) = 2U_l(N) - U_l(N-1)$$

$$U_g(N+1) = 2U_g(N) - U_g(N-1)$$

$$P(N+1) = 2P(N) - P(N-1)$$

$$H_l(N+1) = 2H_l(N) - H_l(N-1)$$

$$T_l(N+1) = 2T_l(N) - T_l(N-1)$$

$$T_g(N+1) = 2T_g(N) - T_g(N-1)$$

C.3 NO FLOW INLET AND CONSTANT PRESSURE OUTLET

Inlet Node

$$U_l(0) = 0$$

$$U_g(0) = 0$$

$$P(0) = P(1)$$

$$H_l(0) = H_l(1)$$

$$T_l(0) = 2T_{linlet} - T_l(1)$$

$$T_g(0) = 2T_{ginlet} - T_g(1)$$

Outlet Node

$$U_l(N+1) = 2U_l(N) - U_l(N-1)$$

$$U_g(N+1) = 2U_g(N) - U_g(N-1)$$

$$P(N+1) = 2P_{wellhead} - P(N)$$

$$H_l(N+1) = 2H_l(N) - H_l(N-1)$$

$$T_l(N+1) = 2T_l(N) - T_l(N-1)$$

$$T_g(N+1) = 2T_g(N) - T_g(N-1)$$

C.4 NO FLOW INLET AND CONSTANT FLOW RATE OUTLET

Inlet Node

$$U_l(0) = 0$$

$$U_g(0) = 0$$

$$P(0) = P(1)$$

$$H_l(0) = H_l(1)$$

$$T_l(0) = 2T_{linlet} - T_l(1)$$

$$T_g(0) = 2T_{ginlet} - T_g(1)$$

Outlet Node

$$U_l(N) = U_{lwellhead}$$

$$U_g(N) = U_{gwellhead}$$

$$P(N+1) = 2P(N) - P(N-1)$$

$$H_l(N+1) = 2H_{lwellhead} - H_l(N)$$

$$T_l(N+1) = 2T_l(N) - T_l(N-1)$$

$$T_g(N+1) = 2T_g(N) - T_g(N-1)$$

D.1 SAMPLE INPUT DATA FOR THE STANDALONE WELLBORE CASE

[illegible]

181

D.2 SAMPLE INPUT DATA FOR THE COUPLED WELLBORE/RESERVOIR CASE

The following is a sample input file that we used in Chapter 4. The program language is FORTRAN 90 and it is run on UNIX.

```
TITLE(2)="3-D SIX COMPONENT GAS/OIL PRODUCTION"
```

```
DESCRIPTION( )=  
"THICKNESS (FT) : 300"  
"LENGTH (FT) : 2500"  
"WIDTH (FT) : 2500"  
"GRID BLOCKS : 50x50x3"
```

```
COMPOSITIONAL_MODEL  
$DEBUGS  
TIMEEND = 30  
    $ I/O OPTIONS  
OUTLEVEL = 1  
$SPLINEOUT  
$GEOMOUT  
PROCOUT  
OUTPUT_PRE  
$OUTPUT_NPH  
OUTPUT_SAT  
OUTPUT_OIL  
OUTPUT_GAS  
$OUTPUT_DEN  
OUTPUT_WEL  
OUTPUT_HIS  
WELLFILE = "6COMP.WEL"
```

```
HISDATA_NUM = 100  
OUTPUT_TIME( ) = 100 1000 2000 3000 3650  
$NO_CRASH
```

```
$OUTPUT FREQUENCY  
ISTEP( , , )=1  
JSTEP( , , )=1  
KSTEP( , , )=1
```

```
$ FAULT BLOCK AND MESH DATA  
METHOD = 2  
DOWN( ) = 0 0 1  
NX(1) = 50  NY(1) = 50  NZ(1) = 3  
MES = "cart"  
DX( ) = 50  DY( ) = 50  DZ( ) = 100
```

```
$ COMPOUND NAMES  
COMPOUND(1) = "C1"          COMPOUND(2) = "C3"
```

```

COMPOUND(3) = "C6"          COMPOUND(4) = "C10"
COMPOUND(5) = "C15"         COMPOUND(6) = "C20"

$ COMPOUND CRITICAL TEMPERATURES
CRIT()  343.0 665.7 913.4 1111.8 1270.0 1380.0

$ COMPOUND CRITICAL PRESSURES
CRIP()  667.8 616.3 436.9 304.0 200.0 162.0

$ COMPOUND CRITICAL VOLUMES
CRIV()  1.599 3.211 5.923 10.087 16.696 21.484

$ COMPOUND ACEN
ACEN()  0.013 0.152 0.301 0.488 0.650 0.850

$ COMPOUND MOL WEIGHTS
MOLW()  16.0 44.1 86.2 142.3 206.0 282.0

$ COMPOUND PARA
PARA()  71.00 151.0 271.0 431.0 631.0 831.0

$ VSP
VSP()  -0.1538 -0.0733 -0.00499 0.0754 0.1451 0.1436
$ BINARY INTERACTION COEFFICIENTS
BINC(,) = 0.0    0.0    0.0    0.0    0.0    0.0
          0.0    0.0    0.0    0.0    0.00 0.0
          0.0    0.0    0.0    0.0    0.0    0.0
          0.0    0.0    0.0    0.0    0.0    0.0
          0.0    0.00 0.0    0.0    0.0    0.0
          0.0    0.00 0.0    0.0    0.0    0.0

$ MAX NUMBER OF PHASES
NPHASE = 3

$ MAXNEWT MAX NUMBER OF NEWTON ITERATION
MAXNEWT = 20

$ Initial rock & water properties
ROCKZ = 0.000001  ROCKP = 1500
H2OZ = 0.000003  H2OP = 14.696  H2OD = 3.468
SURTF = 60.0  SURPS = 14.696
RESTF = 140.0

$ TOLERANCE
CVGOPT = 2
TOL_FLASH = 0.0001
TOL_VOLUME = 0.0001
TOL_MASS = 0.0001
TOL_WATER = 0.0001

$ POROSITY
POROSITY1() = 0.3

```

```

$ PERMEABILITIES
XPERM1() = 350
YPERM1() = 350
ZPERM1() = 350
XYPERM1() = 0
XZPERM1() = 0
YZPERM1() = 0

$ INITIAL WATER SATURATION
SWINI1() = 0.5

$ INITIAL WATER CELL PRESSURE
PINI1() = 2300

$ INITIAL PHASE VISCOSITIES AT EACH CELL
VIS1() = 1.0

$ INITIAL COMPOSITIONS
ZXY1(,,,1) = .6
ZXY1(,,,2) = .1
ZXY1(,,,3) = .1
ZXY1(,,,4) = .1
ZXY1(,,,5) = .05
ZXY1(,,,6) = .05

$ RELPERM DATA
$ RELP 1 for table lookup, 2 for function based

RELP 2
$MODREL(1) = 3

$ NRELFUN 1 for corey, more to be added later
NRELFUN 1
$ data for each phase : water, phase 2 and phase 3
ENDPT() = 0.4 0.9 0.9
SR() = 0.3 0.1 0.0
EXPN() = 3.0 2.0 2.0

$ ===== WELL SPECIFICATIONS =====

NUMWELL = 1
WELLBOREMODEL = 1
TRANSIENTFLAG = 0
$ --- The first well ---

WELLNAME(1) = "PRODUCER 1"
WELL-INCLINATION(1) = "HORIZONTAL"
WELL-DIRECTION(1) = "X"
KINDWELL(1) = 3

$ --- Wellbore Paramers ---
DEPTH = 5700.
TETA = 1.5707

```

```

RTI = 0.098
RTO = 0.189
RWB = 0.425
RCI = 0.3243
RCO = 0.3654
EW = 0.0008
QWATER = 0.
GW = 1.
IFT = 31.6
TP = 158
TEARTH_REF = 84.
GE = 0.006976
KEARTH = 1.3
DENEARTH = 132
CEARTH = 0.21
KCEM = 4.021
SALINITY = 35000
BHT = 140
WP_FLAG = -1
W_SEGMENT = 10
$ --- End Wellbore Parameters ----

WELLTOP(1 TO 3,1,1) = 50 225 75
WELLBOTTOM(1 TO 3,1,1) = 1050 225 75
DIAMETER(1,1) = 0.4
WELLPQ(1) Block
    Interpolation Linear
    Extrapolation Constant
    Data 0. 2130
EndBlock

EndInitial

$ TRANSIENT DATA INPUT BLOCKS
BeginTime 0.0
TIME_CONTROL = 1
DELTIM = 1 DTIMMUL = 1.0 DTIMMAX = 30 DTIMMIN = 1
TUNE = 0.5 DCMAX = 0.5 DAQCMAX = 0.5 DPMAX = 0.5 DSMAX = 0.5
$MAXMOL = 1 MAXP = 10000 ERRLIMIT = 0.2
$ WZ() 0.77 0.20 0.01 0.01 0.005 0.005 0.0
EndTime

```

Appendix E: Reservoir Simulation Model (GPAS)

In our coupled wellbore-reservoir model we used a compositional reservoir simulator, called GPAS (Wang et al., 1997; 1999; Han et al., 2006). In this simulator, different modules such as unstructured gridding, chemical flooding, thermal flooding and asphaltene precipitation (Fazelipour, 2007) are available. This simulator has the capability to run in parallel mode. In this section, we explain the equations and the solution procedure that are used for the compositional reservoir simulation.

E.1 GOVERNING EQUATIONS

In GPAS, there are $2n_c+2$ governing equations to solve per control volume (n_c is number of hydrocarbon components). The main equations are presented as follows:

1) Phase equilibrium equations

$$\ln(f_i^g) - \ln(f_i^o) = 0 \rightarrow \ln K_i - \ln \Phi_i^o + \ln \Phi_i^g = 0, \quad i=1 \text{ to } n_c \quad (\text{E.1})$$

f_i^j : fugacity of component i in phase j
 K_i : equilibrium ratio of component i
 Φ_i^j : fugacity coefficient of component i in phase j
 n_c : number of components

2) Volumetric constraint equation

$$\sum_{i=1}^{n_c+1} N_i \sum_{j=1}^{n_p} L_j \bar{v}_j = 1 \rightarrow \frac{N_{aq}}{\xi_{aq}} + \frac{N_o}{\xi_o} + \frac{N_g}{\xi_g} - 1 = 0 \quad (\text{E.2})$$

N_i : moles of component i per pore volume
 N_j : moles of phase j per pore volume (j =aq:aqueous, o:oleic, g:gaseous)
 n_p : number of phases
 L_j : mole fraction of phase j
 \bar{v}_j : molar volume of phase j
 ξ_j : molar density of phase j

3) Material balance equations

$$V_b \frac{\partial}{\partial t} (\phi N_i) - V_b \bar{\nabla} \cdot \sum_{j=1}^{n_p} \frac{\bar{k} k_{rj}}{\mu_j} \xi_j x_{ij} (\bar{\nabla} P_j - \gamma_j \bar{\nabla} D) - q_i = 0, \quad i=1 \text{ to } n_c \quad (\text{E.3})$$

V_b : bulk volume

ϕ : porosity

\bar{k} : absolute permeability tensor

k_{rj} : relative permeability to phase j

μ_j : viscosity of phase j

x_{ij} : mole fraction of component i in phase j

P_j : pressure of phase j

γ_j : specific gravity of phase j

D : depth

q_i : molar rate of component i injected or produced

E.2 SOLUTION PROCEDURE

From the governing equations we obtain $(2n_c+2)n_b$ non-linear equations (n_b is the number of gridblocks). Hence we solve these equations to obtain the same number of unknowns:

$$\vec{x} = (\vec{x}_1, \vec{x}_2, \dots, \vec{x}_{n_b}), \text{ where } \vec{x}_I = (\ln K_1, \dots, \ln K_{n_c}, N_1, \dots, N_{n_c}, P_{aq}, N_{H_2O}).$$

To solve these non-linear equations, Newton method is applied. A residual vector (\vec{R}) and a jacobian matrix (J) are constructed to solve the linear system of equations.

$$J(\vec{x}^{\text{old}}) \Delta \vec{x} = -\vec{R}(\vec{x}^{\text{old}}) \quad (\text{E.4})$$

Expanding the matrices we have:

$$\begin{pmatrix} J_{1,1} & J_{1,2} & \dots & J_{1,n_b} \\ J_{2,1} & J_{2,2} & \dots & J_{2,n_b} \\ \vdots & & & \vdots \\ J_{n_b,1} & J_{n_b,2} & \dots & J_{n_b,n_b} \end{pmatrix} \begin{pmatrix} \Delta \bar{x}_1 \\ \Delta \bar{x}_2 \\ \vdots \\ \Delta \bar{x}_{n_b} \end{pmatrix} = - \begin{pmatrix} \bar{R}_1 \\ \bar{R}_2 \\ \vdots \\ \bar{R}_{n_b} \end{pmatrix}, \quad (E.5)$$

where,

$$J_{I,J} = \begin{pmatrix} \frac{\partial R_{f_1}|_I}{\partial \ln K_1|_J} & \dots & \frac{\partial R_{f_1}|_I}{\partial \ln K_{n_c}|_J} & \frac{\partial R_{f_1}|_I}{\partial N_1|_J} & \dots & \frac{\partial R_{f_1}|_I}{\partial N_{n_c}|_J} & \frac{\partial R_{f_1}|_I}{\partial P_{aq}|_J} & \frac{\partial R_{f_1}|_I}{\partial N_{H_2O}|_J} \\ \vdots & & \vdots & \vdots & & \vdots & \vdots & \vdots \\ \frac{\partial R_{f_{n_c}}|_I}{\partial \ln K_1|_J} & \dots & \frac{\partial R_{f_{n_c}}|_I}{\partial \ln K_{n_c}|_J} & \frac{\partial R_{f_{n_c}}|_I}{\partial N_1|_J} & \dots & \frac{\partial R_{f_{n_c}}|_I}{\partial N_{n_c}|_J} & \frac{\partial R_{f_{n_c}}|_I}{\partial P_{aq}|_J} & \frac{\partial R_{f_{n_c}}|_I}{\partial N_{H_2O}|_J} \\ \frac{\partial R_v|_I}{\partial \ln K_1|_J} & \dots & \frac{\partial R_v|_I}{\partial \ln K_{n_c}|_J} & \frac{\partial R_v|_I}{\partial N_1|_J} & \dots & \frac{\partial R_v|_I}{\partial N_{n_c}|_J} & \frac{\partial R_v|_I}{\partial P_{aq}|_J} & \frac{\partial R_v|_I}{\partial N_{H_2O}|_J} \\ \frac{\partial R_{m_1}|_I}{\partial \ln K_1|_J} & \dots & \frac{\partial R_{m_1}|_I}{\partial \ln K_{n_c}|_J} & \frac{\partial R_{m_1}|_I}{\partial N_1|_J} & \dots & \frac{\partial R_{m_1}|_I}{\partial N_{n_c}|_J} & \frac{\partial R_{m_1}|_I}{\partial P_{aq}|_J} & \frac{\partial R_{m_1}|_I}{\partial N_{H_2O}|_J} \\ \vdots & & \vdots & \vdots & & \vdots & \vdots & \vdots \\ \frac{\partial R_{m_{n_c}}|_I}{\partial \ln K_1|_J} & \dots & \frac{\partial R_{m_{n_c}}|_I}{\partial \ln K_{n_c}|_J} & \frac{\partial R_{m_{n_c}}|_I}{\partial N_1|_J} & \dots & \frac{\partial R_{m_{n_c}}|_I}{\partial N_{n_c}|_J} & \frac{\partial R_{m_{n_c}}|_I}{\partial P_{aq}|_J} & \frac{\partial R_{m_{n_c}}|_I}{\partial N_{H_2O}|_J} \\ \frac{\partial R_{m_{H_2O}}|_I}{\partial \ln K_1|_J} & \dots & \frac{\partial R_{m_{H_2O}}|_I}{\partial \ln K_{n_c}|_J} & \frac{\partial R_{m_{H_2O}}|_I}{\partial N_1|_J} & \dots & \frac{\partial R_{m_{H_2O}}|_I}{\partial N_{n_c}|_J} & \frac{\partial R_{m_{H_2O}}|_I}{\partial P_{aq}|_J} & \frac{\partial R_{m_{H_2O}}|_I}{\partial N_{H_2O}|_J} \end{pmatrix}$$

$$\Delta \bar{x}_I = (\Delta \ln K_1, \dots, \Delta \ln K_{n_c}, \Delta N_1, \dots, \Delta N_{n_c}, \Delta P_{aq}, \Delta N_{H_2O})$$

$$\bar{R}_I = (R_{f_1}, \dots, R_{f_{n_c}}, R_v, R_{m_1}, \dots, R_{m_{n_c}}, R_{m_{H_2O}}) \text{ for } I^{\text{th}} \text{ gridblock}$$

R_{f_i} : Residual of phase equilibrium equation for component i

R_v : Residual of volumetric constraint equation

R_{m_i} : Residual of material balance for component i

The number of linear equations to be solved for a loop of Newton iteration depends on the number of components and gridblocks, as shown in Equation (E.5). Therefore, if a large number of components and gridblocks are used in a simulation, computational time and memory usage will be substantial. However, this problem can be overcome by parallel computation using multiple processors, which is an important capability of GPAS.

Glossary

The following list of nomenclature includes only the generalized symbols used in the text. Symbols which have been used to represent different quantities have been defined as they were used in the text.

A	Wellbore/pipe cross section area (ft^2)
A_f	Bubble critical diameter calculation coefficient
B_f	Bubble critical diameter calculation coefficient
B_o	Oil formation volume factor ($\frac{rbbl}{stb}$)
CD	Drag force coefficient for bubbly flow
C_{fi}	Drag force coefficient for annular flow
d_{CB}	Bubble critical diameter (ft)
D	Pipe diameter (ft)
D_H	Hydrolytic diameter (ft)
dz	Segment length
dx	Segment length
\bar{e}	Internal energy ($\frac{Btu}{lbm}$)
F_{lg}	Liquid/gas inter-phase shear force per bulk volume ($\frac{lbforce}{ft^3}$)
F	Force ($lbforce$)
f	Friction factor
f_{ic}^j	Fugacity of component ic in phase j
G	Gas phase molar ratio
g	Acceleration owing to gravity ($\frac{ft}{sec}$)
g_T	Thermal gradient ($\frac{^{\circ}F}{ft}$)
H_l	Liquid holdup

h_L	Liquid height in stratified flow (ft)
\bar{h}	Enthalpy ($\frac{Btu}{lbm}$)
hc	Heat transfer coefficient ($\frac{Btu}{ft^2 \text{ sec}}$)
i	Segment index number
k_y	Y-permeability (md)
k_z	Z-permeability (md)
k_w	Thermal conductivity of the liquid ($\frac{Btu}{ft \text{ sec}}$)
k_t	Tubing heat conduction coefficient ($\frac{Btu}{ft \text{ sec}}$)
k_{ins}	Insulator heat conduction coefficient ($\frac{Btu}{ft \text{ sec}}$)
k_{cas}	Casing heat conduction coefficient ($\frac{Btu}{ft \text{ sec}}$)
k_{cem}	Cement heat conduction coefficient ($\frac{Btu}{ft \text{ sec}}$)
L_e	Fraction of liquid in equilibrium
L_{ne}	Non-equilibrium fraction of liquid
M_w	Molecular weight ($\frac{lbm}{lbmol}$)
\dot{m}	Mass flow rate ($\frac{lbm}{\text{sec}}$)
m	Bulk mass (lbm)
n_p	Number of phases
nc	Number of components
Nu	Nusselt number
PI	Productivity index ($\frac{ft^3}{psi \cdot \text{sec} \cdot ft}$)
P	Pressure (psi)
Pr	Prandtl number
q	Flow rate ($\frac{ft^3}{\text{sec}}$)

Q	Heat loss ($\frac{Btu}{sec}$)
R_s	Solution gas oil ration ($\frac{scf}{stb}$)
R_e	Reynolds number
r_{to}	Tubing outer radius (ft)
r_{ti}	Tubing inner radius (ft)
r_{ins}	Insulator outer radius (ft)
r_{ci}	casing inner radius (ft)
r_{co}	casing outer radius (ft)
r_{wb}	wellbore outer radius (ft)
$Skin$	skin factor
S	wetted perimeter (ft)
t	time (sec)
T	Temperature ($^{\circ}F$)
U_{to}	Overall heat transfer coefficient ($\frac{Btu}{ft^2 sec}$)
US	Superficial velocity ($\frac{ft}{sec}$)
U	Actual velocity ($\frac{ft}{sec}$)
UD	Drift velocity ($\frac{ft}{sec}$)
V	Bulk volume (ft^3)
W	Mass flow rate ($\frac{lbm}{sec}$)
WOR	Water oil ratio
x_{icj}	mole fraction of component ic in phase j
z_h	Elevation (ft)
Z	Compressibility factor

Greek Symbols

α	Gas volume fraction
ε	Wall roughness (<i>ft</i>)
λ_L	No-slip holdup
λ_r	Relative permeability mobility ratio (cP^{-1})
λ_v	Liquid over gas viscosity ratio ($\frac{CP}{CP}$)
μ	Viscosity (CP)
ρ	Density ($\frac{lbm}{ft^3}$)
τ	Shear stress (<i>psi</i>)

Subscripts

<i>C</i>	Core
<i>D</i>	Drag
<i>ebh</i>	Earth bottom-hole
<i>g</i>	Gas
<i>i</i>	Inter-phase
<i>ic</i>	Component index
<i>icj</i>	Component <i>ic</i> in phase <i>j</i>
<i>in</i>	Input
<i>Im</i>	Mixture of fluid influx
<i>j</i>	Phase index (water-oil-gas)
<i>l</i>	Liquid
<i>m</i>	Mixture
<i>o</i>	Oil
<i>out</i>	Output
<i>res</i>	Reservoir
<i>sc</i>	Standard condition
<i>tp</i>	Two-phase mixture
<i>VM</i>	Virtual mass
<i>w</i>	Water
<i>wg</i>	Wall and gas
<i>wl</i>	Wall and liquid
<i>wtp</i>	Wall and mixture

References

- Almehaideb, R.A., Aziz, K., and Pedrosa Jr., O.J.: "A Reservoir/Wellbore Model for Multiphase Injection and Pressure Transient Analysis," Paper SPE 17941, presented at 6th Middle East Oil Technical Conference and Exhibition, Manama, Bahrain, Mar. 11-14, 1989.
- Alves, G.E.: "Concurrent Liquid-Gas Flow in a Pipeline Contactor," Chemical Engineering. Progress, 1954, 50, 9, 449-456.
- Alves, I.N., Alhanati, F.J.S., and Shoham, O.: "A Unified Model for Predicting Flowing Temperature Distribution in Wellbores and Pipelines," SPE Production Engineering Journal, Nov 1992, 4, 363-367.
- Ansari, A.M., Sylvester, N.D., Sarica, C., Shoham, O., and Brill, J. P.: "A Comprehensive Mechanistic Model for Upward Two-Phase Flow in Wellbores," SPE Production & Facilities Journal, 1994, 143-151.
- Avelar, C.S. Ribeiro, P.R., and Sepehrnoori, K.: "Deepwater Gas Kick Simulation," Journal of Petroleum Science and Engineering, Jul 2009, 67, 13-22.
- Babu, D.K., and Odeh, A.S.: "Productivity of a Horizontal Well," Soc. Pet. Eng. Reservoir Eng., Nov 1989, 4, 417-421.
- Baker, O.: "Design of Pipeline for Simultaneous Flow of Oil and Gas," Oil & Gas Journal, Jul 1954, 53, 185.
- Barnea, D.: "A Unified Model for Predicting Flow-Pattern Transition for the Whole Range of Pipe Inclinations," International Journal of Multiphase Flow, 1987, 13, 1-12.
- Behie, A., Collins, D., Forsyth, P.A., and Sammon, P.H.: "Fully Coupled Multiblock Wells in Oil Simulation," Paper SPE 11877, Journal of Petroleum Technology, Aug 1985, 535-542.
- Beggs, H.D. and Brill, J.P.: "A Study of Two-Phase Flow in Inclined Pipes," Journal of Petroleum Technology, May 1973, 607-617.
- Beggs, H.D., and Robinson, J.R.: "Estimating the Viscosity of Crude Oil Systems," Journal of Petroleum Technology, Sep 1975, 27, 1140-1141.
- Bendiksen, K.H., Brandt, I., Fuchs, P., Linga, H., Malnes, D., and Moe, R.: "Two-Phase Flow Research at SINTEF and IFE: Some Experimental Results and a Demonstration

of the Dynamic Two-Phase Flow Simulator OLGA” Offshore Northern Seas Conference, Stavanger, Norway, Aug. 27-28, 1986.

Bendiksen, K.H., Malnes, D., Moe, R., and Nuland, S.: “The Dynamic Two-Fluid Model OLGA: Theory and Application,” SPE Production Engineering, May 1991, 6, 171-180.

Colebrook, C.F. and White C.M.: “Experiments with Fluid Friction in Roughened Pipes,” Proc. Roy. Soc, 1937, 161A, 367-381.

Courant, R., Friedrichs, K., and Lewy, H.: “On the partial difference equations of mathematical physics,” IBM Journal, Mar 1967, 215-234, English translation of the 1928 German original.

Dittus, F.W., and Boelter, L.M.K.: “Heat Transfer in Automobile Radiators of the Tubular Type,” University of California/Berkeley Publications in Engineering, 1930, 2, 13, 443.

Dranchuk, P.M. and Abou-Kassem, J.H.: “Calculation of Z-factor for Natural Gases Using Equations of State,” Journal of Canadian Petroleum Technology, Jul 1975, 34.

Dukler, A.E., Wicks. M. III., and Cleveland, R.G.: “Frictional Pressure Drop in Two-Phase Flow: An Approach Through Similarity Analysis,” AIChE Journal, 1964, 10, 44.

Duns, H.Jr. and Ros, N.C.J.: “Vertical Flow of Gas and Liquid Mixtures in Wells,” Paper 22-PD6 of the Sixth World Petroleum Congress, Frankfurt, Germany, Jun 1963.

Eaton, B.A., Andrews, D.E., Knowles, C.R., Silberberg, I.H., and Brown, K.E.: “The Prediction of Flow Patterns, Liquid Holdup and Pressure Losses Occurring During Continuous Two-Phase Flow in Horizontal Pipelines,” Journal of Petroleum Technology, Jun 1967, 815.

Egbogah, E.O. and Ng, J.T.: “An Improved Temperature-Viscosity Correlation for Crude Oil Systems,” Journal of Petroleum Science and Engineering, Jul 1990, 4, 197-200.

Fan, L., Lee, W.J., and Spivey, J.P.: “Semi-Analytical Model for Thermal Effect on Gas Well Pressure Buildup Tests,” Paper SPE 56612, presented at SPE Annual Technical Conference and Exhibition, Houston, Texas, Oct. 3-6, 2000.

Fazelipour, W.: “*Development of a Fully Implicit, Parallel, Equation-of-State Compositional Simulator to Model Asphaltene Precipitation in Petroleum Reservoirs*,” M.Sc. Thesis, the University of Texas at Austin, 2007.

- Gambill, W. R.: "You Can Predict Heat Capacities," Chemical Engineering, Jun 1957, 243–248.
- Gomez, L.E., Shoham, O., and Taitel, Y.: "Prediction of Slug Liquid Holdup-Horizontal to Upward Vertical Flow," International Journal of Multiphase Flow, Mar 2000, 26, 3, 517.
- Govier, G.W. and Aziz, K.: *"The Flow of Complex Mixture in Pipes,"* Van Nostrand, Reinhold, New York City, 1972.
- Gould, L.: "Compositional Two-Phase Flow in Pipelines," Paper SPE 5685, Journal of Petroleum Technology, Mar 1979, 373-384.
- Gregory, G.A., Nicholson, M.K. and Aziz, K.: "Correlation of Liquid Volume Fraction in the Slug for Horizontal Gas-Liquid Slug Flow" International Journal of Multiphase Flow, 1978, 4, 33-39.
- Gui, P., Cunha, L.B. and Cunha, J.C.: "A Numerical Two-Phase Flow Model Coupling Reservoir and Multisegment Horizontal Well," Paper SPE 107989, presented at SPE Rocky Mountain Oil & Gas Technology Symposium, Denver, Colorado, U.S.A., Apr. 16-18, 2007.
- Hagedorn, A.R. and Brown, K.E.: "Experimental Study of Pressure Gradients Occurring During Continuous Two-Phase Flow in Small-Diameter Vertical Conduits," Journal of Petroleum Technology, Apr.1965, 475.
- Han, C., Delshad, M., Sepehrnoori, K., and Pope, G.: "A Fully Implicit, Parallel, Compositional Chemical Flooding Simulator," Society of Petroleum Engineering Journal, 2007, 12, 3, 322-338.
- Harmathy, T.Z.: "Velocity of Large Drops and Bubbles in Media of Infinite or Restricted Extent," AIChE Journal, 1960, 6, 281-286.
- Hasan, A.R., and Kabir, C.S.: "A Study of Multiphase Flow Behavior in Vertical Wells," SPE Production Engineering Journal, May 1988, 263–272.
- Hasan, A.R., and Kabir, C.S.: "A Wellbore/Reservoir Simulator for Testing Gas Wells in High-Temperature Reservoirs," SPE Formation Evaluation Journal, Jun 1996, 128-135.
- Hasan, A.R., and Kabir, C.S., and Wang, X.: "Development and Application of a Wellbore/Reservoir Simulator for Testing Oil Wells," SPE Formation Evaluation Journal, Sep 1997, 182-188.

- Hasan, A.R., Kabir, C.S., and Wang, X.: "Wellbore Two-Phase Flow and Heat Transfer During Transient Testing," Society of Petroleum Engineering Journal, Jun 1998, 3, 2, 174-180.
- Holman, J.P.: "*Heat Transfer*," 4th ed., McGraw-Hill Book Co, New York, 1958.
- Islam, M.R., and Chakma, U.: "Comprehensive Physical and Numerical Modeling of a Horizontal Well," Paper SPE 20627, presented at SPE Annual Technical Conference and Exhibition, New Orleans, U.S.A., Sep. 23-26, 1990.
- Kutateladze S.S. and Borishanskii, V.M.: "*A Concise Encyclopedia of Heat Transfer*," Pergamon Press, 1966.
- Lee, A.L., Gonzalez, M.H., and Eakin, B.E.: "The Viscosity of Natural Gases" Journal of Petroleum Technology, Aug 1966, 997-1000.
- Livescu, S., Durlofsky, L.J., Aziz, K.: "A Semianalytical Thermal Multiphase Wellbore Flow Model for Use in Reservoir Simulation," Paper SPE 115796, presented at SPE Annual Technical Conference and Exhibition, Denver, Colorado, U.S.A., Sep. 21-24, 2008.
- Livescu, S., Durlofsky, L.J., Aziz, K.: "Development and Application of a Fully-coupled Thermal Compositional Wellbore Flow Model," Paper SPE 121306, presented at the SPE Western Regional Meeting, San Jose, California, U.S.A., Mar. 24-26, 2009.
- Lohrenz, J., Bray, B.G., and Clark, C.R.: "Calculation Viscosities of Reservoir Fluids From Their Composition," Trans., AIME, 1964, V.142, 159-172.
- Mandhane, J.M., Gregory, G.A., and Aziz, K.: "Flow-Pattern Map for Gas-Liquid Flow in Horizontal Pipes," International Journal of Multiphase Flow, 1974 1,537.
- Minami, K., and Shoham, O.: "Transient Two-Phase Behavior in Pipelines-Experimental and Modeling," International Journal of Multiphase Flow, 1994, 20, 4, 737.
- Mishima, K., and Ishii, M.: "Flow Regime Transition Criteria for Upward Two-Phase Flow in Vertical Tubes," International Journal of Heat and Mass Transfer, 1984, 27, 723-737.
- Mukherjee, H., and Brill, J.P.: "Liquid Holdup Correlations for Inclined Two-Phase Flow," Journal of Petroleum Technology, May 1983, 1003-1008.
- Nennie, E.D., Alberts, G.J.N., Belfroid, S.P.C., Peters, E., and Joosten, G.J.P.: "An Investigation into the Need of a Dynamic Coupled Well-Reservoir Simulator," Paper SPE 110316, presented at SPE Annual Technical Conference and Exhibition, Anaheim, California, U.S.A., Nov. 11-14, 2007.

- Orkiszewski, J.: "Predicting Two-Phase Pressure Drops in Vertical Pipe," *Journal of Petroleum Technology*, Jun 1967, 829-838.
- Ozon, P.M., Ferschneider, G., and Chwetzoff, A.: "A New Multiphase Flow Model Predicts Pressure and Temperature Profile," Paper SPE 16535, presented at the SPE Offshore Europe Conference, Aberdeen, Scotland, Sept. 8-11, 1987.
- Ouyang, L.B.: "*Single Phase and Multiphase Fluid Flow in Horizontal Wells*," Ph.D. Dissertation, Stanford University, 1998.
- Ouyang, L.B. and Aziz, K.: "A Mechanistic Model for Gas-Liquid Flow in Pipes with Radial Influx or Outflux," Paper SPE 56525, presented at the SPE Annual Technical Conference and Exhibition, Houston, Texas, U.S.A., Oct. 3-6, 1999.
- Passut, C.A. and Danner, R.P.: "Correlation of Ideal Gas Enthalpy, Heat Capacity, and Entropy," *Ind. Eng. Chem. Proc. Des. Development*, 1972, 11, 543-546.
- Peaceman, D.W.: "Interpretation of Well-Block Pressure in Numerical Reservoir Simulation with Non-square Grid Blocks and Anisotropic Permeability," *Journal of Petroleum Technology*, Jun 1983, 531-543.
- Pedersen, K.S., and Christensen, P.L.: "*Phase Behavior of Petroleum Reservoir Fluid*," Taylor & Francis Group, LLC, Florida, 2007.
- Peng, D.Y., and Robinson, D.B.: "A New Two-Constant Equation of State," *Industrial and Engineering Chemical: Fundamentals*, 1976, 15, 59-64.
- Petalas, N., and Aziz, K.: "A Mechanistic Model for Multiphase Flow in Pipes," *Journal of Canadian Petroleum Technology*, Jun 2000, 39, 43-55.
- Pourafshary, P.: "*A Coupled Wellbore/Reservoir Simulator to Model Multiphase Flow and Temperature Distribution*," Ph.D. Dissertation, the University of Texas at Austin, 2007.
- Pourafshary, P., Varavei, A., Sepehrnoori, K., and Podio, A.L.: "A Compositional Wellbore/Reservoir Simulator to Model Multiphase Flow and Temperature Distribution," *Journal of Petroleum Science and Engineering*, 2009, 69, 40-52.
- Richter, H.J.: "Separated Two-Phase Flow Model: Application to Critical Two-Phase Flow," *International Journal of Multiphase Flow*, 1983, 9.51, 1-530.
- Sandler, S.I.: "*Models for Thermodynamic and Phase Equilibrium Calculations*," Chemical Industries, v. 52. New York, Dekker, 1999.

- Schwellnus, C.F., and Shoukri, M.: "A Two-Fluid Model for Non-Equilibrium Two-Phase Critical Discharge," The Canadian Journal of Chemical Engineering, Feb 1991, 69,188-197.
- Shoham, O.: *"Mechanistic Modeling of Gas-Liquid Two-phase Flow in Pipes,"* Society of Petroleum Engineering, 2005.
- Simpson, H.C., Rooney, D.H., Grattan, E., and Al-Samarrae, F.: "Two-Phase Flow in Large Diameter Horizontal Lines," European Two-Phase Flow Meeting, Grenoble, France, Jun. 6-8, 1977.
- Standing, M.B.: "A Pressure-Volume-Temperature Correlation for Mixtures of California Oils and Gases," Drill. and Prod. Prac, API, 1947.
- Stone, T.W., Edmund, N.R., and Kristoff, B.J.: "A Comprehensive Wellbore/Reservoir Simulator," Paper SPE 18419, presented at the SPE Reservoir Simulation Symposium, Houston, Texas, U.S.A., Feb. 6-8, 1989.
- Taitel, Y. and Barnea, D.: "Two-Phase Slug Flow," Advances in Heat Transfer, Vol.20, Academic Press Inc., San Diego, CA, 1990, 83-132.
- Taitel, Y., and Dukler, A.E.: "A Model for Predicting Flow Regime Transition in Horizontal and Near Horizontal Gas-Liquid Flow," AIChE Journal, 1976, 22, 47-57.
- Taitel, Y., Barnea, D., and Dukler, A.E.: "Modeling Multi-Pattern Transitions for Steady Upward Gas-Liquid Flow in Vertical Tubes," AIChE Journal, 1980, 26, 345-354.
- Varavei, A.: *"Development of an Equation-of-State Thermal Flooding Simulator,"* Ph.D. Dissertation, the University of Texas at Austin, 2009.
- Vicente, R.: *"A Numerical Model Coupling Reservoir and Horizontal Well Flow Dynamics,"* Ph.D. Dissertation, the Pennsylvania State University, 2000.
- Vicente, R. and Ertekin, T.: "Modeling of Coupled Reservoir and Multifractured Horizontal Well Flow Dynamics," Paper SPE 101929, presented at the SPE Annual Technical Conference and Exhibition, San Antonio, Texas, U.S.A, Sep. 24-27, 2006.
- Waples, D.W. and Waples, J.S.: "A review and Evaluation of Specific Heat Capacities of Rocks, Minerals, and Subsurface Fluids. Part 2: Fluids and Porous Rocks," Natural Resources Research, Jun 2004, 131, 2, 123-130.
- Wang, P., Yotov, I., Wheeler, M., Arbogast, T., Dawson, C., Parashar, M., and Sepehrnoori, K.: "A New Generation EOS Compositional Reservoir Simulator: Part I

Formulation and Discretization,” Paper SPE 37979, SPE Reservoir Simulation Symposium, Dallas, Texas, U.S.A., Jun. 8-11, 1997.

Wang, P., Balay, S., Sepehrnoori, K., Wheeler, J., Abate, J., Smith, B., and Pope, G.: “A Fully Implicit Parallel EOS Compositional Simulator for Large Scale Reservoir Simulation,” Paper SPE 51885, SPE Reservoir Simulation Symposium, Houston, Texas, U.S.A, Feb. 14-17, 1999.

Winterfeld, P.H.: “Simulation of Pressure Buildup in a Multiphase Wellbore Reservoir System,” SPE Formation Evaluation Journal, Jun 1989, 4, 2, 247-252.

Yuan, M. and Zhou, D.: “Evaluation of Two-phase Flow Correlation and Mechanistic Models for Pipelines at Horizontal and Inclined Upward Flow,” Paper SPE 101929, SPE Production and Operation Symposium, Oklahoma city, Oklahoma, U.S.A., Apr. 4-8, 2009.

Vita

Mahdy Shirdel was born in 1984, in Tehran, Iran. He received two B.Sc. degrees: Mechanical Engineering and Petroleum Engineering, from Sharif University of Technology in 2007. Subsequently, he joined the Department of Petroleum and Geosystems Engineering of The University of Texas at Austin. Currently, he is a Ph.D. candidate working under the supervision of Dr. Kamy Sepehrnoori, focusing on the development of a thermal, compositional, fully implicit, wellbore-reservoir simulator to predict asphaltene, wax and scale deposition in the coupled system.

Permanent address: No. 14 East Kuhsar Alley, Moein Street, Pounak Square, Tehran, Iran

This thesis was typed by the author.